Experimental and Theoretical Studies of Proton Induced Nuclear Spallation

Habilitation dissertation

Krzysztof Pysz

Institute of Nuclear Physics
Polish Academy of Science
Cracow, Poland

Kraków, 2015

Wydano nakładem Instytutu Fizyki Jądrowej Polskiej Akademii Nauk w Krakowie

Recenzent: Prof. dr hab. Antoni Szczurek

ISBN: 978-83-6542-36-8

Abstract

Progress in the understanding of the proton induced disintegration of the atomic nuclei at the GeV incident energy range related to the achievements of the PISA (Proton Induced SpAllation) experiment is reported. The scientific motivation of the spallation research is given. Experimental technique as well as the measured distributions of the double differential cross section ($d^2\sigma/d\Omega dE$) for spallation products in broad range of bombarding energies and for target nuclei of various masses are presented. Interpretation of obtained results in the frame of a classical two step model utilizing the mechanism of intranuclear cascade for the first phase of the reaction and the statistical evaporation from the thermalized target-like remnant for a second step is described. Significant deficiencies of two step approach in reproducing of the experimental observables related to the dynamic stage of the reaction is indicated. Search for the features of alternatives scenarios of spallation process with the use of phenomenological models is undertaken and the conclusion indicating the need of inclusion to the theoretical description of the reaction the intermediate compound and excited fragments is derived. A new microscopical model (Spallation Model with Cascade++) of the first dynamical phase of a pA reaction is developed. Besides of the binary nuclear interactions a mechanism consisting in a Dynamic Clustering in Nuclear Medium (DCNM) is postulated. The resulting improvement in the theoretical description of the distributions of the Light Charged Particles (LCP) in comparison to the models where only binary interactions are considered is shown.

Streszczenie

Celem monografi jest zaprezentowanie postępu w badaniach nad spallacja jądrową dokonanego wskutek przeprowadzonych pomiarów podwójnie różniczkowych przekrojów czynnych ($d^2\sigma/d\Omega dE$) produktów reakcji proton-tarcza (pA) w eksperymancie PISA (Proton Induced SpAllation). Pomiary odbywały się z użyciem tarcz jądrowych o różnych masach i dla szerokiego zakresu energii padających protonów. Opisane są cele naukowe badań nad spallacją. Interpretacja uzyskanych wyników doświadczalnych przy pomocy klasycznego opisu reakcji spalacji za pomocą modelu dwustopniowego pokazała częściową, ale znaczną nieadekwatność modeli pierwszej, dynamicznej części reakcji opisywanej jako kaskadę dwuciałowych oddziaływań jądrowych. Przy pomocy modeli fenomenologicznych poszukiwano możliwych, alternatywnych scenariuszy przebiegu reakcji pA i stwierdzono konieczność włączenia do opisu modelowego pośrednich, wzbudzonych stanów wielonukleonowych. Skonstruowano nowy model mikroskopowy pierwszej fazy reakcji spalacji nazwany Modelem Spalacji z Kaskadą++ (Spallation Model with Cascade++ (SMC++)). Oprócz oddziaływań binarnych zastosowano w nim hipotetyczny mechanizm polegający na kreacji chwilowych klastrów wielonukleonowych we wzbudzonej materii jądrowej (Dynamic Clustering in Nuclear Medium (DCNM)). Uzyskano znaczne polepszenie opisu teoretycznego dla rozkładów lekkich cząstek naładowanych z reakcji spalacji w porównaniu do modeli zakładających wyłącznie oddziaływania dwuciałowe.

Contents

1 Introduction

The main aim of this work is to summarize the progress done in proton induced spallation physics due to successful experimental program of the PISA collaboration (Proton Induced SpAllation) [1]. The PISA experiment was performed in Research Center Jülich in Germany at the COller SYnchrotron COSY with the use of the proton beam at energies between 175 and 2500 MeV. Proton bombardment of variety of thin targets composed of elements from ^{12}C to ^{197}Au provided the precise distributions of double differential cross sections, $d\sigma^2/d\Omega dE$, for charged reaction products spanning from ^{1}H to composite particles up to Al emitted between 15° and 120° of the laboratory θ angle. Precise detection system allowed for isotopic separation of reaction products up to mass of B element. Careful analysis of the collected data benefited in creation of a vast data base, which significantly extend the available set of the observables related to the proton induced spallation reaction.

The collected experimental data became a benchmark for the relevant models of spallation processes. Performed comparison of the obtained data with the results of available models of spallation mechanisms indicated that complexity of mechanisms, which interplay in proton-nucleus interaction at GeV energy range is, with no doubt, higher than it is assumed and implemented in even the most successful theoretical approaches nowadays.

Performed by PISA collaboration the phenomenological interpretation of the data based on assumption of the competition of the processes embedded in traditional two step model (cascade of binary collisions and evaporation of particles from reaction remnant) and those based on the more thermodynamical nature like emission from a few exited moving sources gained a significant improvement in description of the experimental data. The assumed moving sources which are the fragments of the initial target nucleus, are an intermediate states in the disintegration of the bombarded nucleus and the observed in experiments distributions of particles would be the effect of their decomposition.

Since the phenomenological analysis of the PISA experimental data indicated the classes and conditions of alternative processes, which could contribute to the observed experimental spectra but are not regarded in the contemporary spallation models a natural next step in the spallation research was to try an implementation of suggested processes to the microscopical model. For this aim a new spallation model called Spallation Model with Cascade++ (SMC++) has been created. This model utilize the achievements of the most successful spallation codes available in literature but its structure and performance permits for the full control on the whole set of the reaction constituents during modeled process and simplicity in implementations of a new reaction mechanisms. The computer code which comprises the SMC++ model is written in C++ programing language and utilizes the contemporary tool used for data organization, analysis and visualization - the CERN ROOT package [2, 3].

A hypothetical process called Dynamical Clustering in Nuclear Medium (DCNM) has been proposed and implemented into the SMC++ model. This mechanism allows for the larger energy transfer from impinging particle to a target nucleus and the faster energy dissipation among the target nucleons than it is possible in the classical description of the initial spallation reaction phase regarded as a sequence of binary hadronic collisions. In effect a significant improvement in model description of the yield and distributions of both the single as well as the composite Light Charged Particles (LCP) observed in experiments was achieved.

The PISA experiment, the collected data, their analysis and interpretation is a subject of five PhD theses [4, 5, 6, 7, 8]. Two additional PhD theses are under preparation. The following publications which are related to the results of PISA experiment have been published up to now: [1, 9, 10, 11, 12, 13, 14]. The outline of the new spallation model SMC++ and the DCNM mechanism its presented in [15].

The author of the present dissertation has been engaged to the PISA experiment from the most early phase, contributing to the development of the experimental program as well as to the concept of PISA apparatus as the internal beam experiment installed at the accumulation ring COSY. He was committed to the design of experimental chamber, the detectors, the advanced vacuum and gas flow system, electronic chain and the whole setup. During his stay in the Research Center Jülich as "postdoc" he was responsible for the production and installation of the PISA setup components their tests and commissioning, the planing and conducting of the experimental runs and the coordination of the work of PhD-students and technicians. Author contributed to the data analysis and their interpretation. He independently developed a new spallation model SMC++ where his idea about nuclear interaction by dynamical clustering in nuclear medium has been implemented.

In order to show the results of the PISA collaboration on the broader background and to present the contemporary status of the research on the spallation physics the present work recall not only the ideas and results of PISA but refers as well to the other important experimental and theoretical achievements contributing to the collected set of valuable observables and having influence on the significant progress in mathematical description of experimental facts. But also the still existing deficiencies in the understanding of all these complex phenomenons interplaying in the proton-nucleus interaction at high energy will be indicated.

In chapter 2 the motivation for the research on nuclear spallation will be given - both these having the pure scientific origin as well as such resulting from the need of practical utilization of knowledge about spallation phenomena. This chapter is supplemented by an outline of the experimental works having the greatest impact on the understanding of the spallation and being relevant to the subject of this dissertation. Two of them - these, which results are used as an additional benchmark for ideas presented in this dissertation are presented with more details.

Chapter 3 is devoted to present the technical aspects of the PISA experiment and the analysis applied in order to derived the valuable distributions of the double differential cross sections of reaction products. The PISA results will be there also confronted to the experimental data of other groups in these mass, energy and angular range where the comparison is possible.

In order to present the current status of the experimental research in proton induced spallation and to draw some general conclusion, in chapter 4 the extensive presentation of the results of the PISA experiment will be given.

In chapter 5 the most important contributions to the theoretical understanding and description of the spllation processes will be presented. The general idea of the so-called two step model will be presented together with the most successful theoretical approaches to the individual components of the two step model. Besides the theoretical approaches accounting for the statistical description of some aspect of observed spectra the special attention will be given for these models which deal with dynamics of the first part of the reaction.

Verification of the two step model with the use of results of the PISA experiment is done in chapter 6.

In chapter 7 the interpretation of the PISA results with the two step model is extended by a phenomenological analysis in the framework of moving sources model.

Chapter 8 gives the outline of the Spallation Model with Cascade++ (SMC++) and presents the assumptions of the dynamical clustering (DCNM) mechanism.

The description of the SMC++ model is followed in chapter 9 with the presentation of its results concerning the double differential cross section for the neutrons and the charged light particles in the broad range of proton impinging energies and the bombarded target materials. The resulting pion spectra are shown as well. The theoretical calculations are compared to the experimental results of PISA and other relevant data.

The whole work of the PISA collaboration and the induced with this experiment progress in the understanding of the proton induced spallation process are summarized in chapter 10.

Appendix containing the broad set of figures presenting the results of SMC++ results in the domains of neutron and LCP production have been added. The calculations are verified with the experimental data measured at SATURNE (for neutrons) and in the PISA experiments (for LCPs). The latter are compared as well to the relevant results of Intranuclear Cascade Liege (INCL) model.

Appendix is followed by acknowledgement and list of references used in this dissertation.

In order to facilitate the reading of this monograph the glossary of abbreviations used in the text is given at the end of the dissertation.

2 The importance of exploration of the proton induced spallation

This work gives a contribution to a broad field of nuclear physics where properties of exited nuclear matter are explored. Diverse motivations for studies undertaken on creation and decomposition of the unstable heavy nuclear systems exist. From purely scientific point of view demanded is identification of processes acting in nuclear spallation, understanding of their interplay and their reliable mathematical description. But since already long time ago the nuclear physics joined the world of applied science the aims of examination of various aspects of spallation may have also medical or technical origin.

2.1 Basic motivation

The purely mathematical description of the processes taking place in nuclear systems of even few nucleons are presently still not possible. The elementary processes related to the simplest in this respect nucleon-nucleon (NN) interaction were explored theoretically over decades. In order to provide the formulae of the NN potential the purely phenomenological approaches are used or the more advanced ones which utilize the meson exchange models and the effective field theories. In recent years there are attempts to describe the NN interaction from the first principles of quantum chromodynamics with the application of the chiral perturbation theory [16, 17]. Usually the energy application range of contemporary NN potentials is restricted to the elastic range (below the pion production threshold about T_{lab} = 300 MeV). But there are also models which try to account for the NN into NΔ coupling [18]. In general, nowadays the free nucleon-nucleon interaction is described with tolerable precision only for $T_{lab} < 500$ MeV [17].

The influence of the nuclear medium modifies the hadronic interactions making them even more complicated and difficult for mathematical formulation. But even with the satisfactory knowledge about the properties of the hadronic interaction in the nuclear matter the prediction of the behaviour of complicated many-body systems would be still not feasible. The time dependent microscopic description of the interacting quantum system consisting of many constituents would require solving of so many coupled equations that nowadays it is still out of reach.

In such circumstances instead of process description based on solutions of microscopic interactions more effective models of reactions have to be used. The research has to be based on conclusions drawn from observation of more general properties of nuclear matter. Often the macroscopic approach is used where nuclear matter is treated as a hydrodynamical or thermodynamical system, which can be described with the global parameters like temperature (T), density (ρ), pressure (p), energy (E) or the compressibility and viscosity. The adequate tool for description of the behavior of such a system should be the thermodynamical equation of state. The total energy of the system [19] can be given by the following components:

$$E(T, \rho) = E_T(T, \rho) + E_C(T_0, \rho) + E_0; \tag{2.1}$$

where:
$E_T(T, \rho)$ - thermal energy;
$E_C(T_0, \rho)$ - compression energy;

E_0 - ground state energy at $\rho = \rho_0$ and $T = T_0$;

There is a hope that with realistic time dependent equation of state the fate of the exited and decaying nuclear system can be described properly by a transition between the phases of the excited nuclear matter.

The issue of equation of state of nuclear matter is exploited experimentally with the collision of heavy ions of high energies up to several hundreds of MeV/A (see e.g. [20]). With collisions of two heavy nuclei the high densities and temperatures of the colliding system can be achieved. But success of this approach is still not satisfactory. The behaviour of the exited system created in the heavy ion collision is far from being determined only by the thermodynamical phenomenons. Beside the thermal excitation the system is biased by a large amount of introduced linear and angular momenta which lead to the dynamical distortions. Additional instabilities are created and unexpected decay modes are observed due to e.g. the shape variation of the colliding system.

In this view the philosophy behind the exploration of the in-medium hadronic interactions by means of the reactions induced by collisions of a nucleus with a simple projectile (where for this respect the nucleons, pions, electrons, antiprotons or even the light composite nuclei can be considered) is quite different. When reaction is induced by a single and light particle which posses even high energy then the changes in global parameters of the system like its density ρ, mass or the charge are still small. The angular and linear momenta introduced to the bombarded nucleus are much smaller than these in the case of heavy ion collision. Strong shape deviations and collective flows are avoided. The processes of energy transfer and dissipation have a more local nature and are by far less violent than in the case of tens or hundreds simultaneous interactions taking place when the two heavy nuclei are a subject of head-on collision.

The great advantage of research with the use of light projectile consists in a fact that the dynamical effects related to the initial phase of the reaction when momentum is transferred to the system and spreads among its constituents can be decoupled from the purely statistical phenomena showing up when afterward the system achieve a thermal equilibrium. Besides the exploration of the global properties of the nuclear matter imagined as a thermal system the possibility of the study of the individual hadronic interaction in the nuclear medium responsible for the energy dissipation is gained.

The spallation physics with the light impact particles is thus the natural laboratory where the still not well recognized high energy intranuclear hadronic interaction can be effectively studied.

2.2 Practical aspects of spallation studies

Motivations for studies on spallation processes originate also from beyond the need of the basic understanding of the mechanisms which govern the projectile-nucleus interaction. Since the spallative processes play already an important role in many aspects of the human's activity and will be crucial for the success of the important task of humankind planned for the future, their sufficient understanding and ability of quantitative and precise calculations of their effects is strongly demanded.

The following fields of the science, technology and medicine where the quantitative knowledge about the effects of spallation processes is needed are:

- astrophysics,
- nuclear power plant construction and operation,

- management of the nuclear waste,
- design and construction of spallation neutron sources,
- radiological safety on Earth as well as in space conditions,
- effectiveness and side-effects in hadron therapy of cancer.

Two examples of application of the knowledge about the nuclear spallation will be described below. First of them concern still our basic understanding of the physical world. It turned out that the spallation processes are to some extent responsible for the observed composition of the interstellar gas. The second example describes the idea of transmutation of nuclear waste.

2.2.1 Astrophysical origin of nuclides

The nuclear composition of the solar system is different than this of the cosmic rays. Isotopes of Li, Be, B, F, Cl, K, Sc, Ti, V, Cr, Mn observed in the solar system are less abundant than these observed in the cosmic rays by at least one order of magnitude. In case of Li, Be, B (so-called LiBeB) the discrepancy reaches even six orders of magnitude.

Observed differences concern the cosmic rays of the energies from 70 to 280 MeV/nucleon. The composition of comics rays of energies from outside this range is not known. Since the case of origins of the light element is very significant the most of efforts was put on explaining the LiBeB puzzle.

It was noticed that the cosmic ray interaction in the interstellar medium can play an important role in the origin of this observed excess of several elements in cosmic ray mass-spectrum. In 1970 H. Reeves proposed a scenario concerning the LiBeB nucleosynthesis [21] where - contrary to most of the nuclear species, LiBeB are formed by the spallative interaction between the energetic Galactic Cosmic Rays (GCR) and the Interstellar Medium (ISM). As opposed to "normal" nucleosynthesis taking place in the stars the spallative origin of elements is sometimes called "non thermal" nucleosynthesis.

In the first calculations by M. Meneguzzi et al. [22] it was assumed that protons and α-particles of GCR interact with nuclei of C, N, O of ISM producing the lighter nuclei of Li, Be, B. The authors took the local, presently known LiBeB and CNO (nuclei of Carbon, Nitrogen and Oxygen) abundances and extrapolated them over whole lifetime of galaxy assuming them to be constant. The calculations reproduced quite well the observed abundances of ^{6}Li, ^{9}Be and ^{10}B. The model, however, could not reproduce correctly the ^{7}Li/^{6}Li ratio (1.2 instead of 12.5 observed in meteorites). Also the estimated ^{11}B/^{10}B ratio was 2.5 when observed is 4.

In 1985 Walker and others [23] performed new calculations introducing freshly compiled set of spallation cross sections by Read and Viola [24]. They encountered, however, similar problems as Meneguzzi et al. [22]. In order to explain the observed ratio of B isotopes Walker et al. suggested an existence of low energy component of GCR flux responsible for additional ^{11}B production. They also put forward the idea that significant amount of ^{7}Li could have been produced still during the Big Bang nucleosynthesis.

In the end of 80-ties and over the first half of 90-ties of the last century the new measurements of relative abundances of Li, Be and B with respect to the H for stars of various metalicities (iron abundances) become possible (for compilation see [25]). The stellar metalicity [Fe/H] defined as log(Fe/H) - log(Fe/H)$_{solar}$, where log(Fe/H)$_{solar} = 3 \cdot 10^{-5}$ is the photospheric iron abundance, is the natural representation of the elapsed time since the formation of the Galaxy

[26]. Thus, these measurement allowed the observation of an increase of the LiBeB during the Galaxy evolution. The results were surprising to the astrophysicist since they found that the dependence of abundances of Be and B on the metalicity is linear instead of quadratic. The quadratic dependence was expected because if the origin of LiBeB is purely GCR spallation both the evolving CNO number as well as the bombarding flux should be proportional to the integrated number of supernova explosion up to the observation moment. It is believed that both ISM and GCR originate in the supernovae explosions where synthesized elements are released into the ISM increasing the metalicity.

The linear dependence of BeB abundances vs. stellar metalicity may suggested that BeB elements can be produced in reverse way that it was assumed earlier i.e. by energetic CNO components of the cosmic rays interacting with the protons and α-particles of the ISM. In such a case the metalicity of the ISM does not influence the production rate and the abundance-metalicity dependence remain linear [27]. This hypothesis created, however, a problem of the origin of the enough abundant and energetic fluxes of CNO nuclei which are so far not clearly identified.

In the case of ^{7}Li it turned out that over almost whole galactic life the amount of this isotope remained constant what was interpreted in the way that at least a part of the observed ^{7}Li was produced in Big Bang nucleosynthesis together with H and He isotopes.

The results of measurements of time dependent abundances of LiBeB showed that earlier believed theory of pure spallative origin of LiBeB must be verified. This induced a great debate among the astrophysicist about the possible sources and mechanisms of production of Li, Be and B isotopes and in general, about the origin, the energy spectrum and the possible ways of primary acceleration of the cosmic rays. The debate lasts up to now.

In 1997 Ramaty et al., [28] preformed a new calculations of LiBeB elements abundances taking into account various scenarios and processes which could contribute to the observed amounts of these isotopes. They [28] and also E. Vangioni-Flam et al. [25],[29] summarized the present status of studies on the productions of the LiBeB isotopes:

- about 10% of ^{7}Li is produced in the nucleosynthesis in the Big Bang. The remaining 90% is believed to be created in various galactic object including types II supernovae and giant stars,
- core collapse of types II supernovae can contribute to ^{11}B production via neutrino induced spallation of ^{12}C. This process can help to reproduce the measured ^{11}B/^{10}B ratio,
- bulk of ^{6}Li, ^{9}Be and ^{10}B must be produced by spallation process. Both processes where protons and α-particles bombard the CNO nuclei as well as reversal processes are taken into account. The relative contributions of these processes depend strongly on assumed mechanisms of creation and acceleration of the cosmic rays and on their mass- and energy spectra,
- one more important factor influencing the relative contribution of various processes in the LiBeB production is the still unknown relation between relative (to H) abundances of O and Fe elements.

In order to perform the calculation of the element abundances in the galaxy the following components are necessary:

- composition of the GCR,
- composition of ISM,

- energy spectrum of the GCR,
- relevant reaction cross sections.

The spallation physics can contribute to this interesting astrophysical problem supplying the precise set of demanded reaction cross sections in the energy range of about 50 to 3000 MeV.

As it was mentioned earlier in the simulation starting from 1985 (Walker et al. [23]) and later on (R. Ramaty et al. [28]) the cross sections tabulated by Read and Viola [24] has been used. For the quoted later simulation additionally the data obtained by Webber et al. [30] - [31] were utilized. Compilations of Read and Viola contains the excitation functions measured in various experiments for p and α reaction on α, C, N and O leading to various isobares mostly for low energies (up to 200 MeV) but there are exceptions where beam energies were even 300 GeV. The cross sections of Webber et al. come from big experimental campaign performed in Lawrence Berkeley Laboratory Bevelac over the period of 5 years, aimed especially on measurement of cross sections useful for astrophysical applications. The liquid hydrogen and helium targets were irradiated by about 30 separate beams of relativistic nuclei from ^{10}B to ^{55}Mn of the energy of about 600 MeV/nucleon.

Both the data of Read and Viola as well as those from Webber et al. are of good quality (the error bars are mostly small (about 5%)). For energy region where the both sets of the data overlap they are in agreement except for Li where discrepancies are of the factor of 2.

Precise nuclear spallation cross sections are needed in astrophysics also for other purposes [32]. It is believed that extinct radioisotopes like ^{26}Al, ^{41}Ca and ^{53}Mn that existed at the time of formation of the solar system and which have been found in meteorites were produced by interaction of low energy cosmic rays with ISM. In general, for better understanding of the radionuclide composition of meteorites found in recent years on Antarctic ice fields and in hot desert the plenty of new spallation cross section are needed. The study of interaction of protons and alphas with variety of target nuclei is needed for investigations of solar cosmic rays exposure of the lunar surface material as well as of the Earth atmosphere.

2.2.2 Nuclear waste transmutation

A great issue of the contemporary nuclear power industry, having significant political and social implication is the disposal of the long-living radio-toxical products of the nuclear power plants. Beside the transuranic elements the most danger are the long living fission fragments. Few of them have a half-life time of millions years (^{129}I - 15.7 million years, ^{135}Cs - 2.3 millions years, ^{93}Zr - 1.53 million years). Other have the half-life times of hundreds thousand years (^{99}Tc - 211 thousand years, ^{125}Sn - 100 thousand years, ^{79}Se - 650 thousand years) They are a strong emitters of the nuclear radiation. And since in the power plant industry they are produced in significant amount their total radio-toxicity impose a need for their storage in the way assuring the medical safety for the world not only in presence but over an incredible periods ranging to hundreds of thousands years ! The control of the hazard crated when these fission fragments are disposed in the geological repositories in such long periods is naturally questionable.

The idea of nuclear waste transmutation with the so-called Accelerator Driven Systems (ADS) arose in 90-th of XX century (for subject overview see e.g. [33, 34, 35, 36]). It consists in utilizing of proton induced spallation to produce the intense neutron fluxes. The nuclear waste would be exposed for these neutrons. In effect the transuranic elements to the great extent will undergo the fission and create the stable elements. The lighter radioactive elements of the longest life

time could be driven into rapid disintegration and transmutation by a neutron capture with the so-called Adiabatic Resonance Crossing (ARC).

The key issues in such ADC are the powerful (order of MW) proton beam accelerator and such control of the spallation process which allows the creation of the neutron fluxes of the most appropriate energies and intensities.

2.3 Experiment driven development of spallation physics

As mentioned above the unified mathematical description of the unstable nuclear matter is still not feasible. Instead, the attempts to describe the mechanisms of reactions where the decay of the excited nuclear systems are observed are done with the use of the reaction models where various assumptions and simplifications have to be done. The models have to be benchmarked on the experimental data. The higher merit of the theoretical model the broader set of observables it is able to describe properly.

The proper definition of the set of experimental observables required in order to draw the justified conclusion about the nature of the relevant mechanisms is very important. Conclusions are based on the interpretation of the experimental results within the applied theoretical model. The validation of the predictive power of the models and concluding about the nature of the implemented mechanisms will be of significant confidence only with the use of the exclusive and precise data.

In this respect the ideal experiment providing the data for interpretation with the spallation models would be of 4π solid angle acceptance, with detection system of high granularity, where all nuclear products are registered event-by-event in a broad energy range allowing for full reconstruction of event and tagging of all possible coincidences and correlations. Unfortunately such an experiment was not performed up to now. Instead more simple setups were used.

The experimental studies on proton-nucleus interaction at energies relevant to the spallation processes ($T_p > 100$ MeV) are performed over decades. They were originally motivated by the intensive research in the field of neutron physics. It was realized that although the spallation is a source of less neutrons than e.g. the nuclear reactors but the neutrons from spallation can be more easy handled than those from reactors. The new increase of interest on spallation processes has been triggered by development of ideas about powerful spallation sources or accelerator driven nuclear waste transmutation.

The available data base concerning the spallation is broad. However, only the results obtained during last 20 years where application of event-by-event detection techniques, the usage of precise solid state detectors and high granulation of detector distributed over broad solid angle permitted to collect the sets of exclusive observables like double differential cross section giving the deeper insight into the complexity of the spallation processes.

Experiments like NESSI [37, 38], PISA [1], the neutron measurements at SATURNE [39] and few others supplied the vast collection of the valuable data. The double differential cross sections $d\sigma/d\Omega dE$ have been measured at many emission angles for diverse reaction products including nucleons, Light Charged Particles (LCP) (particles with Z $\leq$ 2) Intermediate Mass Fragments (IMF) (A $\leq$ 0.3 * target mass), heavy fragments, fission products, reaction residua and pions. These experiments were performed in broad range of incident energies (few hundreds of MeV - few GeV) and for varied target materials (^{12}C - ^{238}U).

The most valuable data, which are suggested as a benchmark for contemporary theoretical models of spallation reactions were collected and presented in consistent form under the auspices of International Atomic Energy Agency (IAEA) (see [40, 41] and references therein).

In the following subsections the two of experiments which are among those of the greatest impact on the spallation model development in the recent years will be presented in shortened way. In the next chapter the PISA experiment performed at the COSY accelerator in Jülich (Germany), which supplied the broader and the most precise set of experimental spallation data up to now will be described with details. The results of PISA form an experimental material predominantly used in this dissertation.

2.3.1 The NESSI experiment

The NESSI experiment [37, 38] was performed in Research Center Jülich (Germany) with the use of the external proton beam of the COSY accelerator [42] (about the COSY storage ring see section 3.1). The experimental apparatus of NESSI has been constructed as a silicon detector ball (Berlin Silicon Ball - BSiB) [43] embedded within the spherical tank called the Berlin Neutron Ball (BNB) [44, 45]. The outer diameter of the setup was equal to 1.4 m.

The volume of 1500 liters of the BNB was filled with the liquid scintillator doped with gadolinium. This detector was used to measure the neutron fluxes. The thermalized neutrons from the spallation were captured by gadolinium. The γs from gadolinium deexcitation have been detected with the use of 24 photomulipliers installed at the outer shell of BNB. Detection efficiency of BNB was a function of a kinetic energy of detected neutrons and varied from 80 % for slowest neutrons to about 10 % for the ones of 90 MeV. As the majority of detected neutrons had energies $E_{kin} < 10$ MeV, the actual detection efficiency of BNB was rather high.

The internal detection ball of diameter equal to 20 cm was constructed out of 158 silicon detectors of the 500 μm thickness. This detector served as a charged ejectiles counter. Charged particles have been identified with the time of flight (TOF) versus kinetic energy (E_{kin}) technique. As a "START" detector for the TOF measurement the thin scintillation counter located in the beam line before the NESSI apparatus was used. Other scintillators installed also in the beam line were used for beam monitoring and for determination of the absolute beam luminosity. The TOF-E_{kin} technique permitted for the mass A resolution of ± 3 for particles of mass number of A = 20. The mass resolution gets worse with increasing the registered mass.

Silicon Ball has been equipped additionally with the six telescopes consisting of 80μm and 1000 μm thick silicon ΔE detectors followed by a 7 cm thick CsI scintillator working as E detector. The telescopes intended for isotopes identification of light reaction products by means of ΔE-E method were installed at laboratory emission angles of 30°, 75°, 105° and 150°.

The targets were installed in the center of the detection sphere with a movable target holder The angular acceptance of NESSI detector was equal to 90 % of full solid angle. The NESSI experiment as a first one permitted the registration of the correlations between the charged spallation products and the neutrons.

The experimental program of NESSI was conducted over many years and was very successful. It comprised both the measurement with the thin targets for *intra*-nuclear (within the same target nucleus) interaction as well with the thick target permitting the *inter*-nuclear (ejectiles of one nuclei induced the reaction in other ones within the thick solid state target) reactions studies. Measurements were performed for the targets from broad range of materials - between ^{12}C and ^{238}U and in the almost whole range of COSY energy (from 0.4 to 2.5 GeV). The NESSI collaborations published the data for the neutron multiplicities, the correlation between the

neutrons and charged particles multiplicity, the total reaction cross sections, total cross sections for individual ejectiles, distributions for excitation energies and the double differential cross sections for spallation products.

Before installation in Jülich the NESSI apparatus was used for studies of antiproton induced excitation of nuclear matter at LEAR and PS (CERN). The details about the NESSI experimental setup, applied detection techniques and the scientific achievements of the NESSI collaboration can be found in the following references: [37, 38, 46, 47, 48] and in the references therein.

2.3.2 Neutron production at SATURNE

Very useful and precise data for double differential cross section for neutron production in proton induced spallation were obtained in experiment performed in CEA Research Center in Saclay, France [39]. The proton beams of SATURNE accelerator have been exposed to metallic targets of Al, Fe, Zr, W, Pb and Th. The thicknesses of the targets varied between 8.1 g/cm^2 and 39.8 g/cm^2. The neutrons from spallation had to be selected from the charged particles and various sort of background induced mainly in secondary reactions.

In order to select, count and determine the energy of the neutrons from initial spallation the two detection techniques were used. For the low energy neutrons of the energy from 3 MeV to 400 MeV the time of flight (TOF) technique was sufficient. The separations and registration of neutrons of energy higher than 200 MeV required more complicated apparatus and data processing. As a "START" counter the 1 mm thick plastic scintillator was used. It registered the impinging protons, which afterwards impacted onto the target. The ejected neutrons were registered by a liquid scintillator located at the distance of 8 m from the "START" detector. Behind the target the magnet was installed that deflected the charged particles outside the acceptance of the neutron detector. A neutron collimator made of concrete, shadow bars and set of anticoincidence detectors were required in order to suppress the spurious events. With this technique the energy resolutions was of the order of few percent but with increase in energy of registered neutrons above 200 MeV it worsened significantly.

For this reason in order to measure precisely the distributions of higher energy neutrons the indirect method of their registration was needed. An additional liquid hydrogen target was used in which the high energy spallation neutrons were converted into protons by the elastic scattering. In order to measure the momenta of resulting protons the dipole magnet of the field of 0.5 T was applied. The proton trajectories were determined with the use of positive sensitive wire chambers. Momentum of initial neutrons were calculated with assumption of neutron-proton conversion with the elastic (n,p) process. Other processes contributing to the proton production in hydrogen converter target were suppressed by identification of charged particles of different masses with the TOF versus momentum dependence. This method permitted for precise registration of neutrons of energies up to 1600 MeV.

The double differential cross sections were measured in reaction plane in almost whole neutron emission range. The angular range spanned from 10° to 160° with the step of 15°. The experimental arrangement permitted also to collect data at 0°. Since the rotation range of the apparatus used for indirect registration of higher energy neutrons covered the detection angles from 0° to 85 ° only for these forward emission directions the neutrons of the energies up to 1600 MeV could be detected.

The experiments were performed for all mentioned above target materials at three incident proton beam energies of 0.8, 1.2 and 1.6 GeV. The absolute normalization uncertainty for the measured cross sections was estimated to be lower than 16 %.

For details of setup, experimental procedures and obtained results see [39, 49, 50, 51] and references therein.

The vast spectrum of subjects related to the explorations of spallation physics which include also the exhaustive presentation of the motivations related both to the fundamental research as well as to the multiple current and future applications of spallation physics is given in handbook of Filges and Goldenbaum [52].

3 The PISA experiment

Below the description of the PISA experiment as an example of modern spallation experiment will be given.

The main objective of the PISA experiment was to provide a new precise set of spallation data which cast a new light on the reaction mechanisms and will serve as a restrictive criterion for the development and validation of spallation models. Since the PISA experiment was associated with the big international project of construction of the European Spallation Source (ESS) it was especially important to put attention on the measurements with the typical construction materials. The aim was to study the energy- and mass dependence of the spallation cross sections with the measurement of the distributions of double differential cross sections, $\mathrm{d}^2\sigma/d\Omega dE$, of an isotopically identified products of target bombardment with protons. The energy range of projectiles in the PISA experiment was defined by the kinetic energies of accelerated protons from the COSY storage ring and spanned from 100- to 2500 MeV. As a targets the selected solid state materials of the masses between C and Au have been used.

3.1 COSY accelerator

A very suitable machine to perform such spallation experiment occurred to be a COller SYnchrotron (COSY) in Research Center Jülich, Germany [42]. The PISA apparatus was installed at the internal station of COSY ring taking advantage of the multiple beam-target interaction due to circulating accumulated proton packages. (cf. fig. 3.1). The main features of the COSY accelerator are as follows: energy range 0.045 – 2.6 GeV (protons), 0.023 – 2.3 GeV (deuterons), transverse and longitudinal cooling (electron and stochastic), beam and targets polarization, internal and extracted beams. The internal beam intensity range reaches 10^{11} protons/cycle. The best (lowest) achievable proton beam momentum spread is $\frac{\Delta p}{p} \leq 5{\cdot}10^{-5}$.

3.2 Experimental setup

Earlier experimental studies of proton induced spallations showed that the production yield of particles is dependent on the emission angle but the shapes of experimental distributions vary smoothly over the θ angle. Thus, when the PISA detection system was designed it was decided that the reaction products will be detected at a few emission angles only. The location of the detectors was selected in order to allow a reliable extrapolation of the measured cross sections over the whole angular range of the detection plane. Fig. 3.2 presents the location of the detection arms installed at the scattering chamber of the PISA experiment. In order to study the angular dependence of the cross section and to permit the angular interpolation of measured quantities it was decided that particles will be registered at nine angles: 15°, 16°, 20°, 35°, 50°, 65°, 80°, 100° and 120°. The relatively low detection angles of 15° and 16° were achieved by locating the target position outside of the center of scattering chamber. The target position was shifted from the chamber axis upwards of the beam trajectory.

In order to conclude on both the general as well as the detailed features of recorded spallation spectra the energy detection threshold of the detectors should be about 1 MeV/nucleon and the

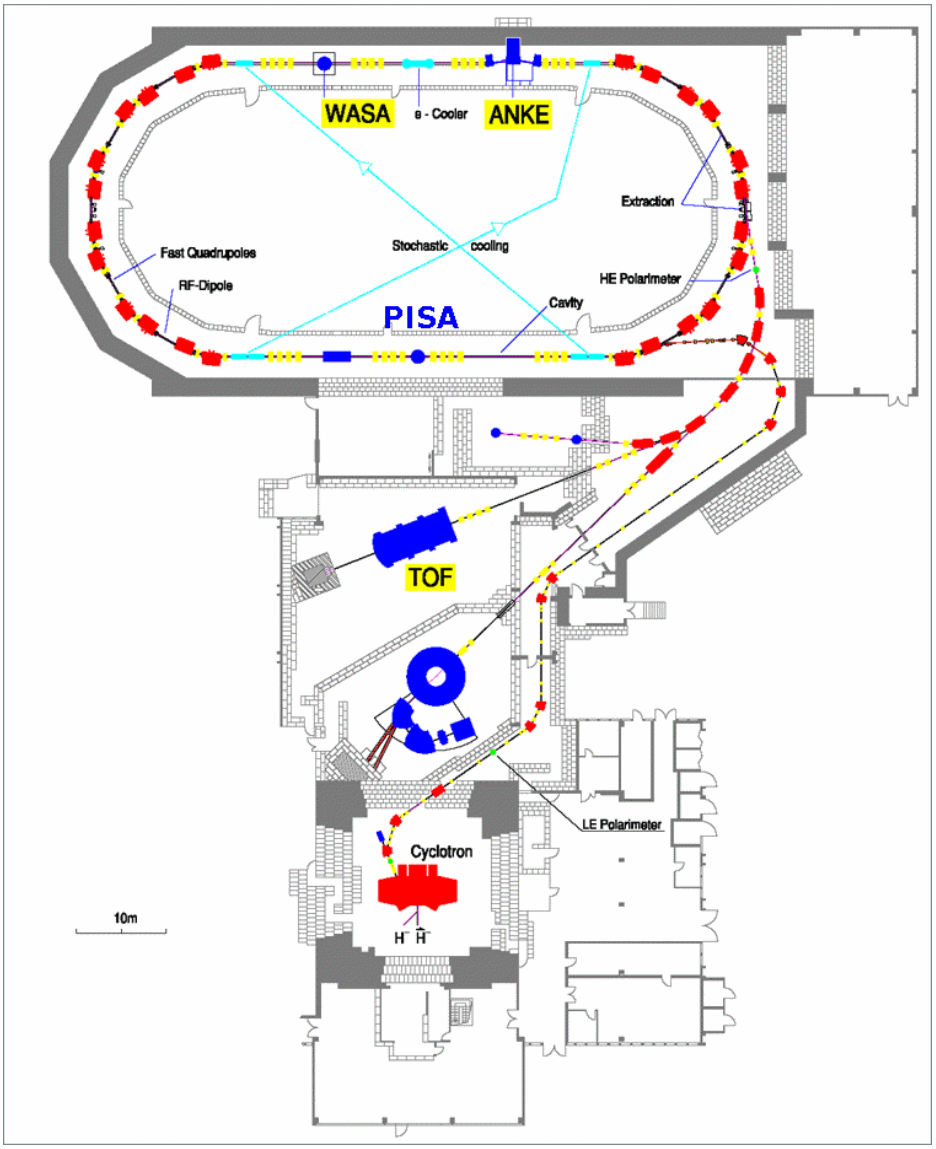

Figure 3.1: The experimental infrastructure of the COller SYnchrotron (COSY) in Juleich, Germany. The accumulating ring (on the top of the figure) is supplied with 45 MeV protons or deuterons from Cyclotron JULIC (bottom side of the figure). The beams are cooled and accelerated up to 2.6 GeV energy and utilized in the internal beam experiments installed in the ring or are extracted and guided to the external experimental areas. The position of the installation of the PISA experiment in the internal beam station is indicated.

detection range shall extend up to few hundreds of MeV. This aim was achieved by application of a combinations of various kinds of detectors:

- silicon detectors operated in the vacuum of the scattering chamber. They formed the telescopes installed in a suitable cooling station and operated at temperature of -10° C. The first detector in the telescope of the thickness about 50 μm assured the low detection threshold whereas the following detectors (of the typical thicknesses about 400 μm and 6000 μm) served as degraders/stoppers for higher energy particles. The thermal noise suppression of the cooled silicon detectors increased their energy resolution permitting the

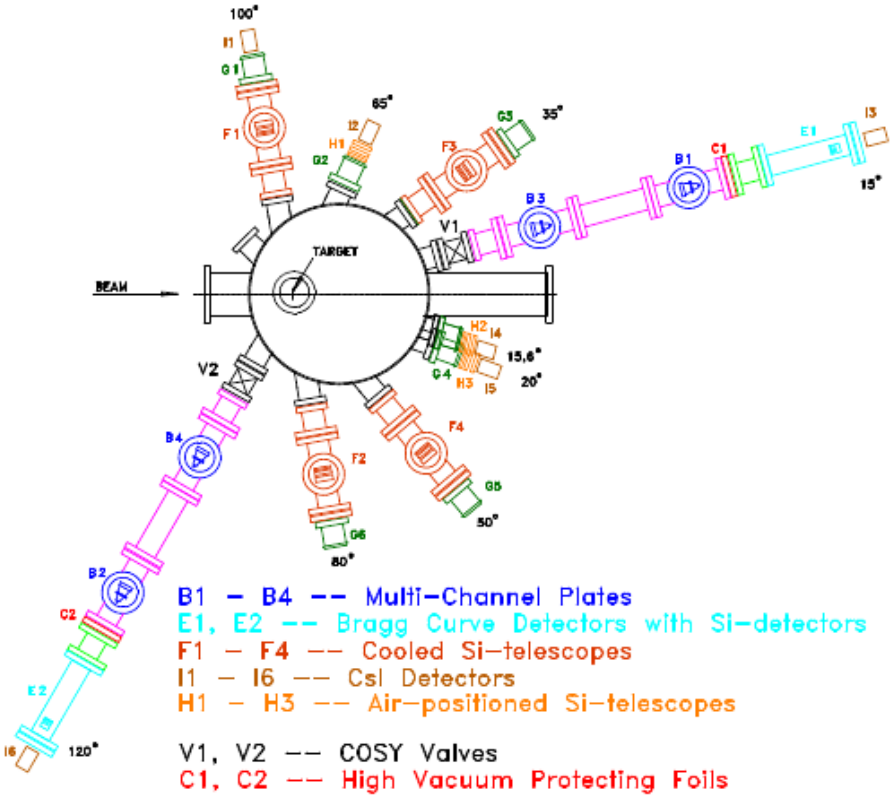

Figure 3.2: Scattering chamber and detection arms of the PISA experiment. The detection arm situated at 16° detection angle is not shown.

isotopic identification of detected particles. With such telescopes the detection arms at 35°, 50° and 80° were equipped;

- similar Si-detector telescope as those described above, cooled and operated as well in vacuum, but followed by an CsI scintillation detector (thickness 7 cm). The scintillators were placed outside the vacuum chamber but separated from the vacuum only by a thin 50 μm thick stainless steel window. Such an arrangement of detectors was used for registration of particles emitted at 100°;

- the detection arms situated at 16°, 20° and 65° were formed by the four silicon detectors of the thicknesses between 90 and 1000 μm in the telescope followed by a 7 cm thick CsI scintillator. All these detectors were placed in the air just after the 50 μm thick window made of stainless steel;

- most complicated were the detection arms at 15° and 120°. The reaction products could be registered or stopped in the system consisting of:

  – assembly for the time of flight (TOF) measurement formed of two Micro Channel Plate (MCP) detectors at distance of 27.4 cm and installed in the properly designed frames assuring the transition of the detected particles;

  – axial ionization chamber called Bragg Curve Detector (BCD) permitting the measurement of a charge and energy of the particles. Together with the preceding TOF

system they were intended for full identification of the particles stopped within the detector volume;

- two large area silicon detectors of the thicknesses of 150 and 500 μm;
- CsI scintillating detector of the thickness of 7 cm.

First three components of these detection arm were operated within the vacuum system of the experiment whereas the scintillators have been separated from a vacuum by a 50 μm stainless steel window.

The Bragg Curve Detectors shown in fig. 3.4 was implemented into the PISA experimental system also due to their low energy detection threshold. As gaseous detectors with thin entrance window they were able to register and identify the reaction products of the kinetic energies down to 0.5 MeV/nucleon [1]. It has to be however stressed, that the operation of ionization chambers of the typical work pressure of the isobutane at the level of 300 mbar within the vacuum system of the COSY accelerator where the demanded vacuum should be better than 10^{-8} mbar was a challenging task. Fig. 3.3 shows the arrangements of the 15° and 120° detection arms which was equipped with axial ionization chambers. Proper sequence of pumping of individual part of the detection arm, condition to start the gas flow and procedures of venting the system had to be developed. The automatic vacuum safety system of the detection arms was built and incorporated into the COSY vacuum operation system. Continues monitoring of the vacuum conditions in the PISA scattering chamber and in the detection arms was performed. I case of any worsening of the vacuum in the intermediate part of the detection arm or in the PISA chamber the whole section of the COSY ring where the PISA apparatus was installed would be cut-off and the beam would stop. The construction of BCD (cf. fig. 3.4) was optimized in order to assure an endurance of the thin entrance window of the detector (working as a cathode of the chamber) to withstand the pressure difference of few hundreds mbar. The BCD windows, before qualified to the usage had to undergo a tests of their tightness as well as the mechanical and electrical stability. In fig. 3.5 the detail description of the MCP ensemble is given.

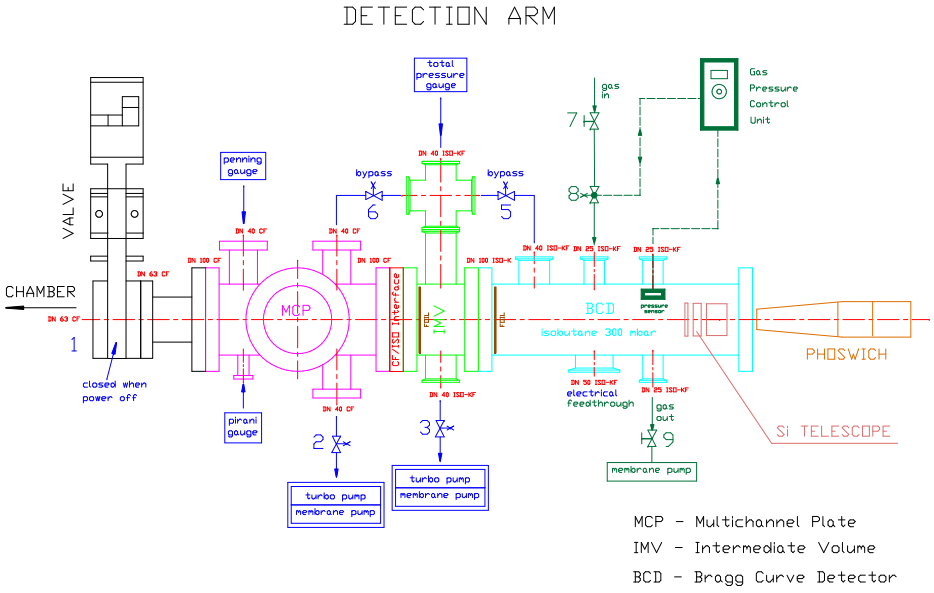

Figure 3.3: A scheme of a detection arm installed at 15° and 120°. Beside the detectors also the elements of the vacuum and gas flow system are shown. For details see the main text.

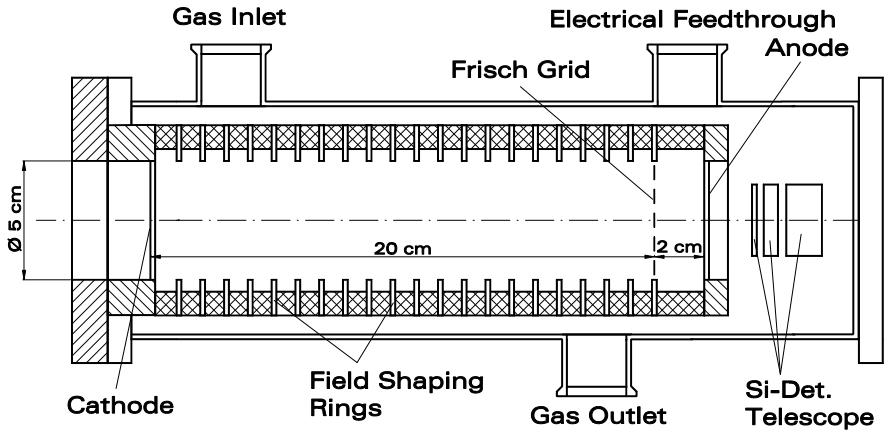

Figure 3.4: The cross section of the axial ionization chamber (so-called Bragg Curve Detector (BCD)) used in the PISA experiment at internal beam of the COSY accelerator. The internal location of additional Si-telescope is indicated as well.

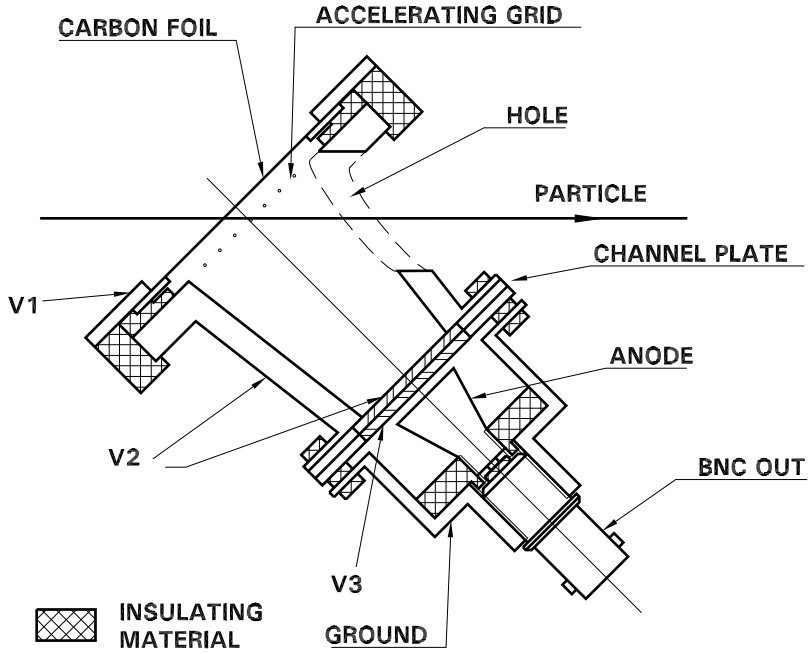

Figure 3.5: Assembly and idea of working of transition micro channel plate detectors used in the detection arms at 15° and 120°.

The great advantage of the experiment conducted at the internal beam of the COSY accumulator ring was a high luminosity resulting from the multiple beam circulations and irradiation of the

target during each beam revolution. During each of the operation periods of COSY (beam injection, acceleration, on-target interaction and dump) the number of beam revolutions per second was $\sim 10^6$. With this feature of the internal beam experiment an opportunity was gained to apply a very thin targets, minimize the reaction product rescattering in the target and avoid the high energy losses in the solid state target.

The target (fig. 3.6) had form of a thin, typically ~ 150 μg/cm^2, narrow strip (with the width of 2 mm) stretched horizontally on a stainless steel frame of a fork shape as it is shown in fig. 3.6. During the filling of the ring with protons and their acceleration the beam was steered to pass underneath the PISA target. When the beam achieved the required kinetic energy it had an elliptical cross section with a horizontal diameter of less than 3 cm. It could be then gradually bumped onto the target strip avoiding the interaction with target frame. The beam was steered towards the target in the feedback mode assuring the almost constant beam-target interaction rate and optimal detection load on the detectors. When the whole accumulated beam was used the new proton injection took place and acceleration process has been initialized again. In order

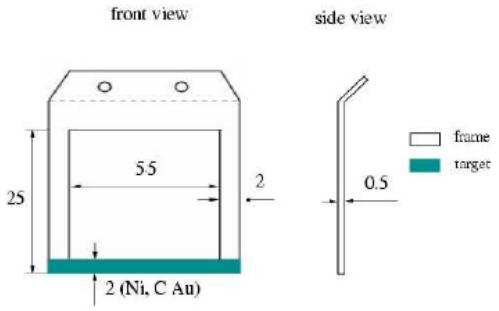

Figure 3.6: The PISA target as a thin ~ 150 μg/cm^2) narrow strip of 2 mm width, stretched horizontally on a stainless steel frame of a fork shape. The accelerated proton beam of an elliptical cross section and horizontal diameter of less than 3 cm interacted only with target material avoiding hitting the frame.

to assure the possibility to exchange a target during the experimental run without disturbing the ultra-high vacuum (UHV) conditions in the chamber and in the COSY ring the reaction chamber of PISA was equipped with a target magazine, of the capacity of up to eight targets. They could be exchanged with the use of pincer grip and a movable target holder.

Another very fortunate effect of usage of the internal COSY beam for the PISA experiment consisted in an application of so-called "supercycle" mode of COSY operation. In the subsequent COSY cycles the beam could be accelerated to various final energies. This feature permitted the data collection for various selected proton bombarding energies but at exactly the same experimental conditions. In this way the systematic uncertainties resulting from variations of experimental conditions were significantly diminished.

Utilization of the internal beam of the COSY storage ring and its unique advantages permitted the PISA collaboration to collect valuable data of high statistic and unbiased with uncertainties resulting from energy or angular straggling. However, it should be mentioned that this kind of internal beam experiment like PISA is also charged with inconveniences resulting from the specific place of a setup installation. They are:

- restricted access to the apparatus. Since the chamber and detection setup was located inside the COSY ring any kind of work concerning the installation, tests, improvements, and maintenance of the equipment had been possible only in few periods in the year free of

routine operation of an accelerator. Otherwise, the demanded access to the apparatus was possible during the experiment but then obviously at the expense of the user's beamtime;

- observing of stringent vacuum conditions. The PISA scattering chamber with almost whole detection system was an integral part of the COSY vacuum system. As mentioned already in the description of the gaseous detectors used in PISA experiment the special precautions had to be taken during PISA experimental runs. Any worsening of the vacuum conditions inside the COSY sector comprising the PISA chamber resulted in immediate cut-off of this sector from the ring vacuum system and break in the accelerator operation. The chamber had to be designed and built in the Ultra High Vacuum (UHV) standard. This concerned also all components of equipment which had a contact with UHV vacuum of the COSY ring. They had to be constructed out of vacuum-friendly materials (e.g. stainless-steel, aluminium, Teflon) with polished surfaces, and exposed to mechanical and chemical cleaning procedures. Special care had to be put on the assuring of ideal tightness of the silicon detector cooling system;

- necessity of the late installation of the radiation sensitive components. The silicon detectors could be installed shorty prior to the beam time when beam tuning was already done. They had to be dismounted right after the beamtime in order to protect them from radiation damage;

- necessity to obey the radiation safety rules. It concerned especially the access to the experimental area and transportation out of the irradiated elements of vacuum and detection system when there was a need of their testing or reparation outside the restricted area;

- significant drawback of internal beam experiment is a lack of a total beam current integration and thus an impossibility of direct absolute normalization of measured cross section. Instead an indirect method need to be applied. The problem of absolute normalization in the PISA experiment is explained in section 3.4.

3.3 The data treatment

The presentation of the electronic setup and data acquisition system as well as a detailed description of a careful data calibration, selection and analysis is presented in [7]. Here only some examples of collected data will be given in order to present they features and quality.

In fig. 3.7 and 3.8 an example of particle identification with the use of BCD is given. The data were collected for reaction of p-Ni at 1.9 GeV beam energy. Fig. 3.7 shows a scatter plot of events registered in BCD. The amplitude of a Bragg peak is plotted vs. the kinetic energy of the stopped particles. A clean separation of elements from He up to Si is visible. This allows to fit the center of gravity lines along the individual distributions and project them onto the Z axis (cf. fig. 3.8). A blow-up of the rectangle area marked on panel (a) visible in panel (b) presents the onsets of separated individual distributions for a few elements. The separation of the distribution from the low energy continuum defines the detection energy threshold.

Details about the construction, performance and achievements of BCDs used in the PISA experiment are given in [1].

The housing of the telescopes of silicon detectors operated in vacuum has been designed in the way permitting the cooling of the detectors with the use of liquid flow. The working temperature of these detectors was set to -10° C causing a reduction of thermal noise of detectors of a factor

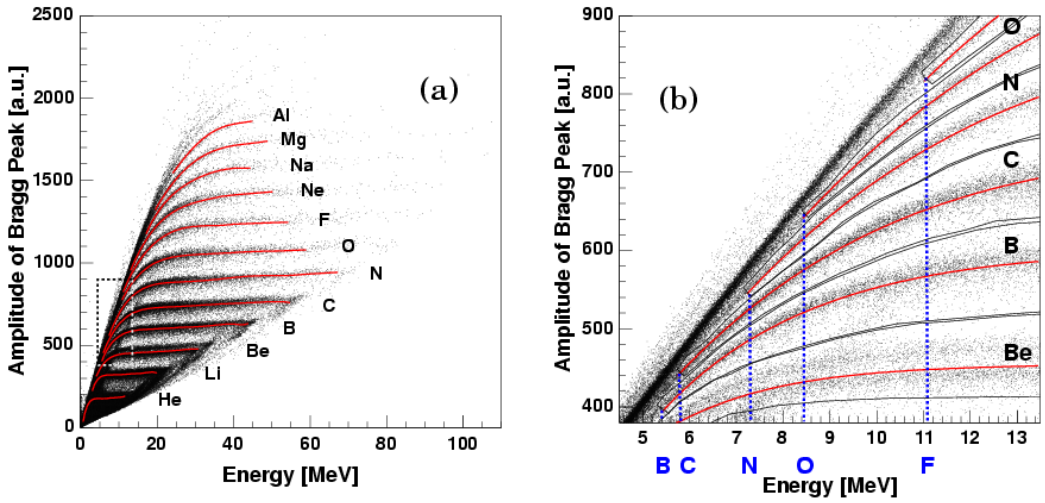

Figure 3.7: (a) the scatter plot of the Bragg peak amplitude vs. the kinetic energy of the stopped particles measured in BCD is shown. Along the centers of gravity of the individual distributions the lines are fitted. Along these lines the Z distributions were linearized individually. The histogram resulting from the projection of the linearized Z distributions onto the Bragg peak axis is depicted in fig. 3.8. For heavier elements, due to poor statistics at higher energies, the fitted lines do not cover the full stopping energy range of the detector. Both the lower- as well as the upper energy limits used for histogramming corresponds to the left and right ends of the fitted curve, respectively. (b) A detail of the upper panel (marked there with a dashed rectangle) is depicted. It presents the lower energy limits, above which the individual elements can be resolved. The common value is about 0.5 MeV/nucleon. The Z gates used for linearization (see above) are indicated as well.

two in comparison to room temperature operation. Together with high quality of detectors it resulted in excellent resolution of detectors and high quality of registered energy distributions. The spectra recorded with the use of silicon detector telescope extended by 7 cm thick CsI(Tl) scintillators allowed for isotopic identification of reaction product with the use of ΔE-E technique in broad range of energies and masses. Fig. 3.9 presents the scatter plot of energy losses of spallation products of p-Ni reaction at 1.9 GeV energy registered in silicon detector 1 and silicon detector 2 in the telescope at detection angle of 35°.

The clearly separated components originating from different isotopes of detected spallation products are well visible. Starting from the lower left corner the individual groups of distributions are formed by isotopes of H, He, Li, Be, B, C, N. Splitting of the signals from Si-detectors and feeding them into two signal processing branches of different amplification factors permitted to register and sufficiently separate also the low energy-loss contributions of H and He isotopes. This is shown in the insert on histogram in the right-upper corner of fig. 3.9.

Similar example but for third Si detector in detection arm at 65° followed by CsI scintillator is given in fig. 3.10. A black lines superimposed onto the distributions present the energy losses calculated with taking into account the nonlinear response of scintillator due to the light quenching. It can be concluded that obtained energy calibration for PISA scintillation detectors was of high quality.

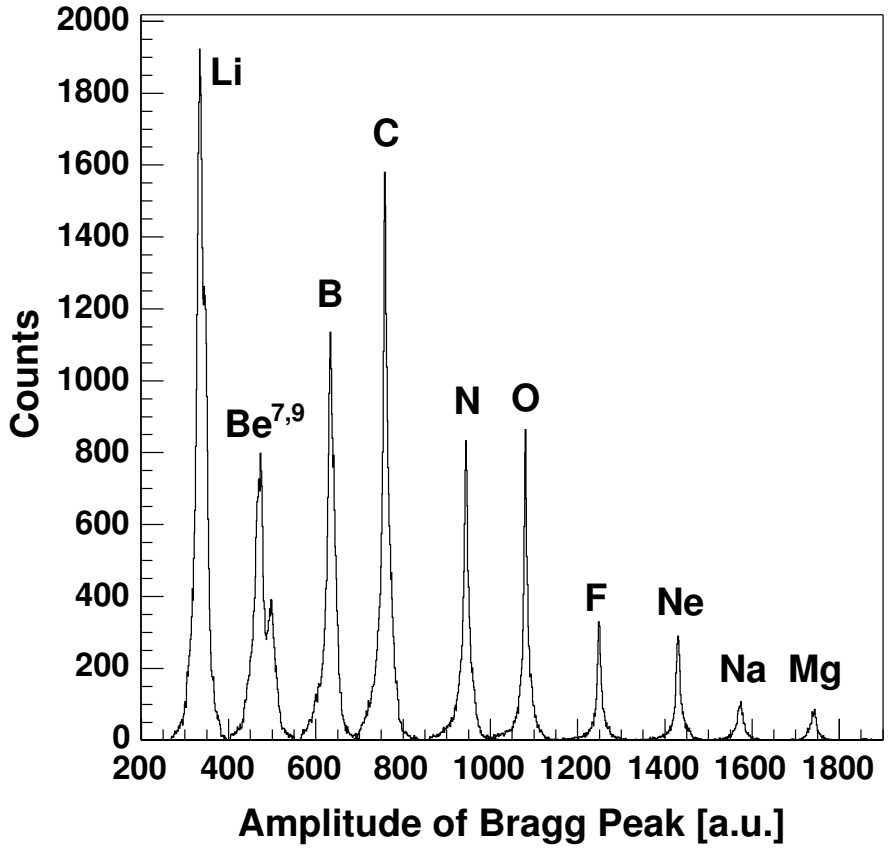

Figure 3.8: The histogram resulting from the projection of the linearized Z distributions onto the BP axis as depicted in caption of fig. 3.7. Identification spectrum of the charges of the p + Ni reaction products measured at 15° at 1.9 GeV proton incident energy. The achieved resolution is $\Delta Z \leq 14\%$ of one charge unit.

3.4 Absolute normalization

In order to achieve the absolute normalization of the double differential cross sections measured in the internal beam experiment at COSY the two different procedures were applied:

- cross sections measured for p-Ni reaction at 175 MeV energy were compared and normalized to the data from [53];
- the PISA experimental results obtained for all other beam energies and target materials were absolutely normalized by means of comparing the total production cross section for ^{7}Be isotope obtained by PISA with the values known from the literature. This procedure is described in [54].

The $\frac{d^2\sigma}{d\Omega dE}$ for Ni(p,p$'$) at 175 MeV proton energy has been measured at external beam [53] for several emission angles in the angular range from 15° to 120°. It has been determined with the uncertainty of 10%. The comparison with the PISA experimental results obtained for the exactly the same emission angles were possible for 15°, 20°, 65° and 100°. The effect of this comparison and normalization is shown in fig. 3.11 for 20°, 65° and 100°. The shapes of the relevant

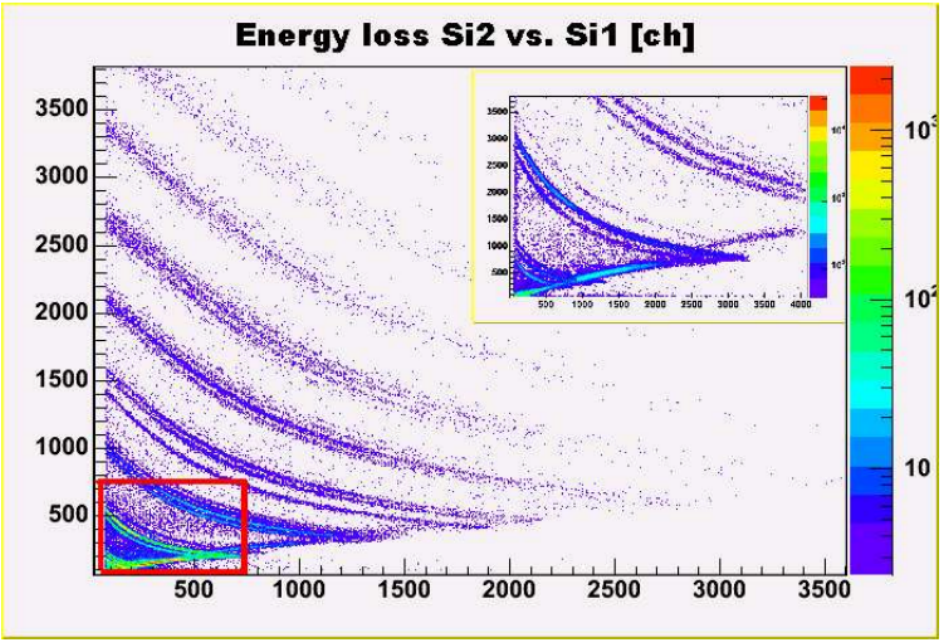

Figure 3.9: A scatter plot of energy losses in silicon detector no. 1 (48 μm) and no. 2 (426 μm) of cooled Si-telescope at 35°. Individual groups of distributions are formed by isotopes of H (most lower-left), He, Li, Be, B, C, N and O (unresolved component). The insert on the histogram in the right-upper corner shows resolved contributions of H and He isotopes recorded due to higher amplification factor used for one branch of split signals. The units are arbitrary. This figure is adapted from [7]

distributions obtained in both experiments agree very well. Distributions usually overlap. The discrepancies in the magnitudes visible in some parts of the energy spectra are never bigger than 15%. With the usage of the minimization procedures described in [7] it was concluded that the overall error of the absolute normalization of PISA experiment results for 175 MeV energy is lower than 18%.

The compilation of literature information about the total production cross section for ^{7}Be are comprised in [54]. Since in the PISA experiment only the double differential cross section at a few emission angles has been measured thus, in order to compare the PISA data to those from the literature an energy- and angle integration was needed. The integration over the emission angle was based on the interpolation between the known values with the use of phenomenological formula of single moving source. Description of the hypothesis of the moving sources responsible for the observed distributions of spallation products will be given in chapter 7. Since the angular dependence of cross section vary smoothly the interpolation error is negligible.

Integration over the energy was more complicated due to a cut-off of the experimental spectra at the detection threshold. Usually the position of the low energy maxima attributed to the height of the Coulomb barrier between the residual nucleus and emitted ^{7}Be particle have been missing. This fact introduced the interpolation uncertainty in the region where the cross section is the biggest. On the basis of the results of reverse kinematics experiment [55] it was assumed that dominating component of energy spectra has a Maxwellian shape. The measured in [55] position of the peaks where slightly lower than the values of the Coulomb barrier calculated from classical formula assuming the spherical charge of Z comprised within the sphere of a radius proportional to $A^{1/3}$ (Z, A - atomic and mass numbers of relevant nuclei).

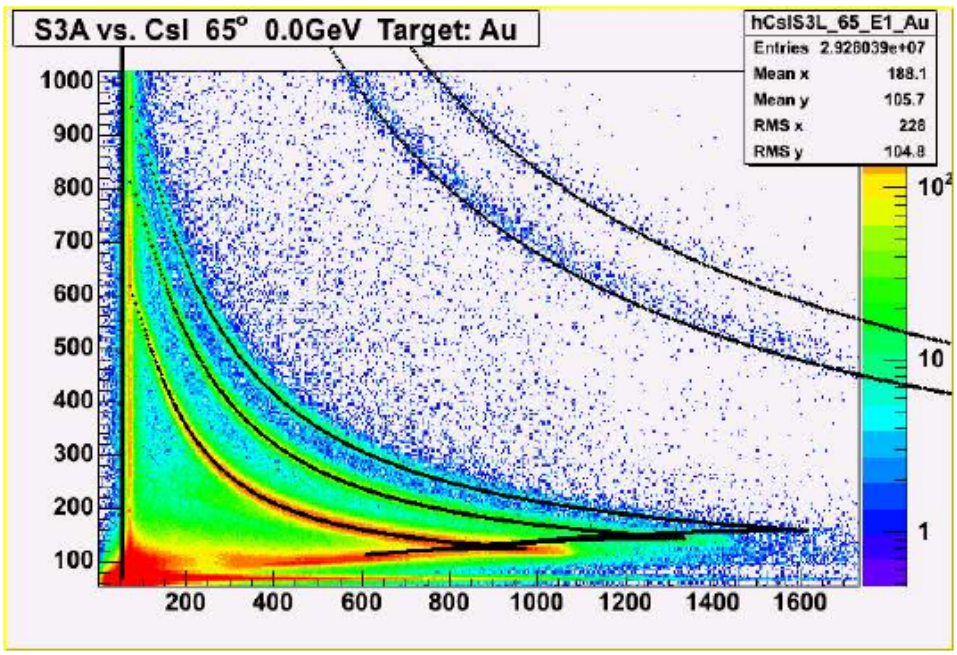

Figure 3.10: A scatter plot of energy losses in silicon detector no. 3 vs. energy losses in subsequent scintillation counter CsI(Tl) in the detection arm situated at 65°. The thicknesses of the detector were 1 mm and 7 cm, respectively. Superimposed curves depict the calculated energy losses. The appropriate energy calibration for nonlinear light output of scintillators has been used. The units are arbitrary. This figure is adapted from [7]

Under the above assumption and corrections the phenomenological formula of one emitting source was fitted simultaneously to all ^{7}Be spectra measured in the PISA experiment at seven scattering angles. Obtained in this way the total cross sections for ^{7}Be production have been compared to the literature values as described in [54]. The agreement was very good. The total uncertainty of this method of the cross section normalization was estimated to be 20%.

A direct comparison of results of both methods of cross section normalization applied to the data for 175 MeV incident energy collected by the PISA collaboration showed their agreement within a 20% error as well. Thus, taking into account high statistics of the collected data and the good control of systematic components of measurements uncertainty the maximal total error for the cross sections measured in the PISA experiment was estimated to be 20%.

3.5 Verification of PISA results with other experimental measurements

First of all the shapes and magnitudes of cross sections measured in the PISA experiment had to be confronted with results of other experiments performed at the same or similar conditions. It is possible in few cases. As already mentioned in section 3 the data of [53] have been used as a reference for absolute normalization of distributions resulting from 175 MeV proton bombardment of ^{nat}Ni target. Fig. 3.11 in section 3 proves the very good agreement of shapes of ^{1}H distributions registered in both experiments at the same laboratory emission angles of 20°, 65° and 100°.

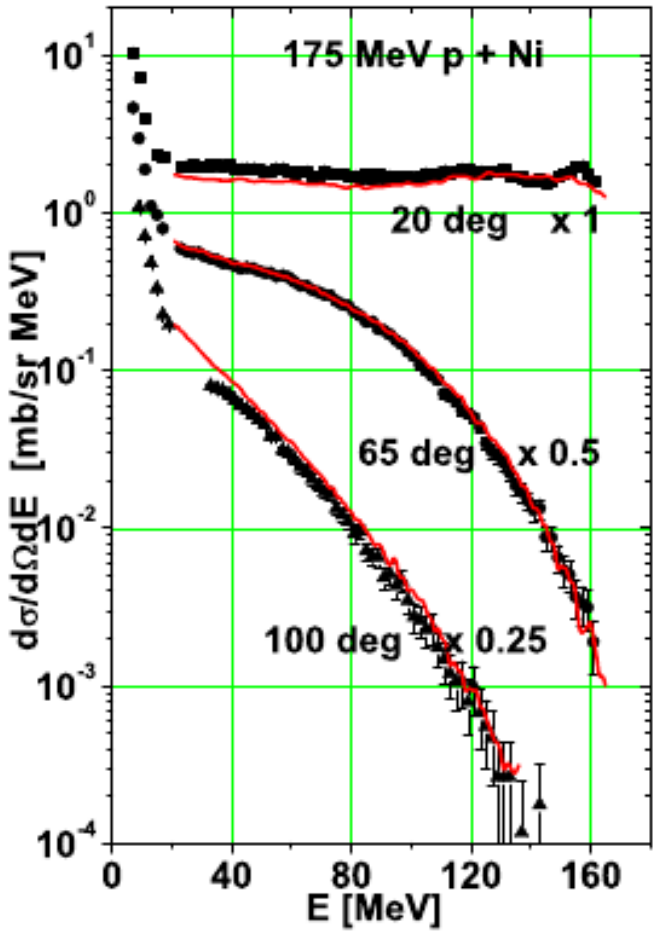

Figure 3.11: Comparison of the $\frac{d^2\Sigma}{d\Omega dE}$ for Ni(p,p$'$) at 175 MeV published in [53] (symbols) with those obtained in the PISA experiment (lines) for 20°, 65° and 100° laboratory emission angles. Good agreement of the shapes of the distributions prove a validity of the normalization of results from the internal beam experiment PISA with the values obtained in [53] where the number of beam protons was measured directly.

Taking into account the obtained normalization factor, an overall agreement of experimental data lays within 20% error.

For higher reaction energies the overlapping or similar experimental conditions as in PISA experiment were used in few cases in the NESSI experiment. The examples of good agreement of distributions collected in both experiments at proximate conditions are given in figs. 3.12 - 3.17 for protons, deuterons, tritons, ^{3}He, ^{4}He and ^{6}Li collected when ^{197}Au target has been bombarded with 2.5 GeV energy protons.

It has to emphasized that in these cases when the experimental conditions like bombarding energy, detection angle, range of detection energy of the PISA experiment were the same or similar to those of other experiments the shape and magnitudes of obtained cross sections agree very well with the results of other groups. Yet the results of the PISA experiment are biased with lower uncertainty due to higher statistic collected at the internal beam experiment and lower systematic error.

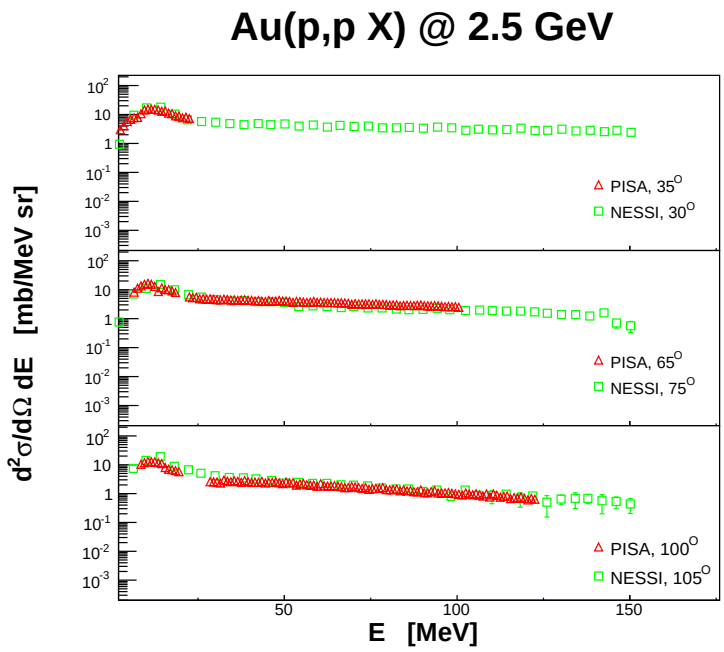

Figure 3.12: Comparison of double differential cross sections derived from data collected in the NESSI (squeres, green) and PISA (triangles, red) experiments. In both cases the 2.5 GeV proton beam has been impinged onto the ^{197}Au nuclei. The selected detection angles in both experiments were in close proximity as indicated.

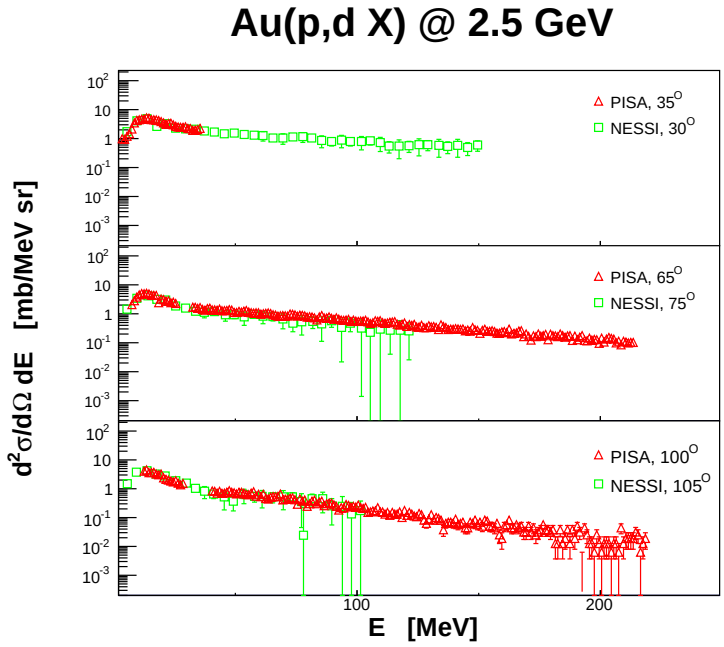

Figure 3.13: The same as in fig. 3.12 but for deuterons.

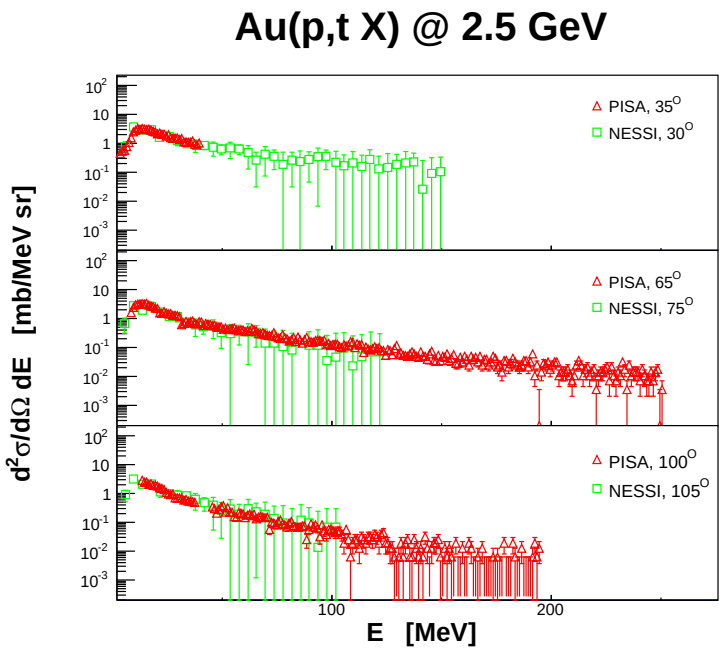

Figure 3.14: The same as in fig. 3.12 but for tritons.

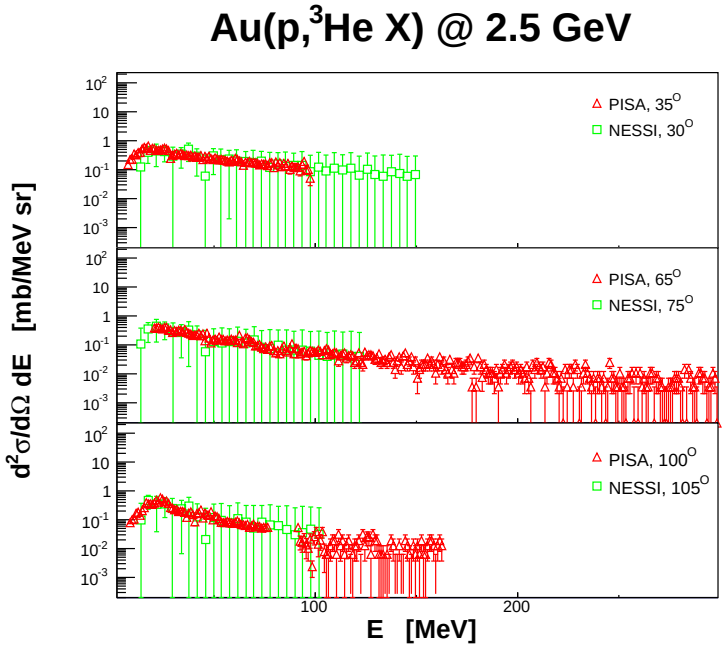

Figure 3.15: The same as in fig. 3.12 but for ^{3}He.

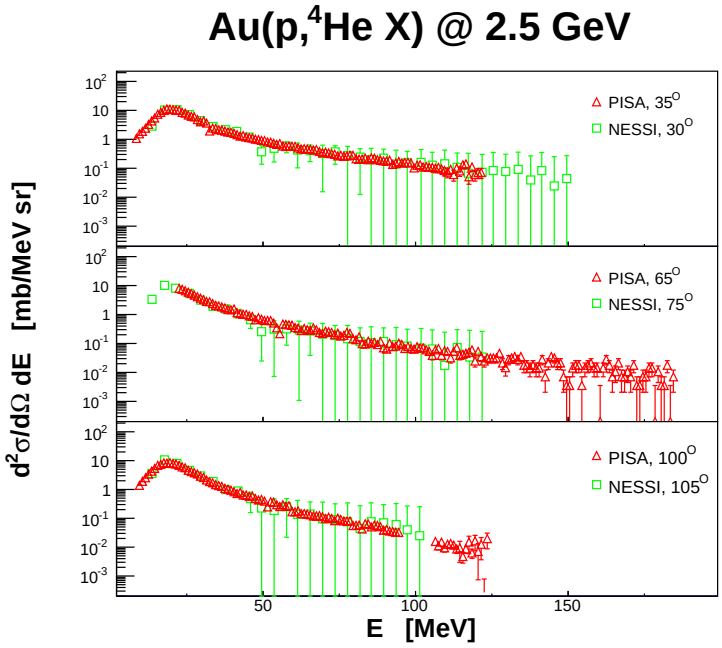

Figure 3.16: The same as in fig. 3.12 but for ^{4}He.

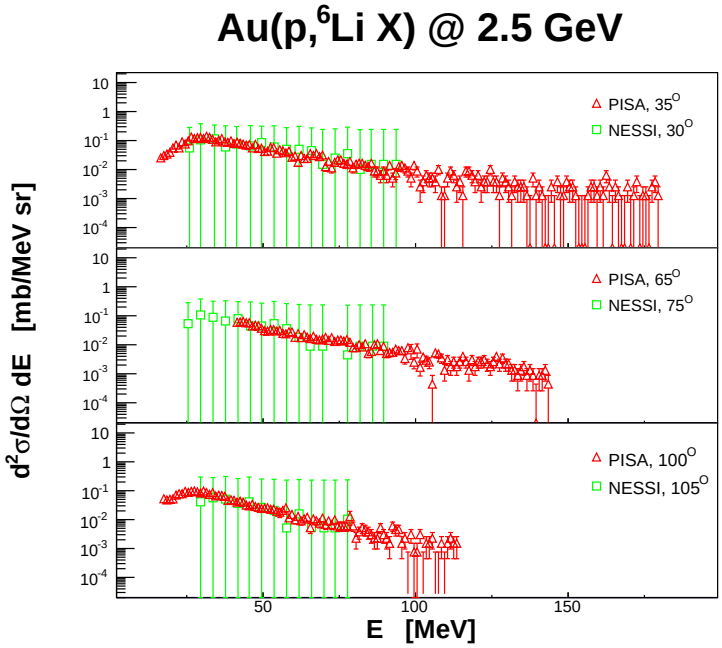

Figure 3.17: The same as in fig. 3.12 but for ^{6}Li.

4 Results of PISA experiment

4.1 Double differential cross section measured in PISA experiment

The data collected in the PISA experiment show the variety of incident energies and target materials combinations. The nuclear targets used in experiment consisted of ^{197}Au, ^{nat}Ag, ^{nat}Ni, ^{27}Al, ^{12}C. All these target nuclei were bombarded by protons of energies 2.5 -, 1.9-, and 1.2 GeV. For the Ni target additionally a low beam energy of 175 MeV was used. Detectors installed at nine fixed laboratory angles, registered the reaction products in various energy ranges depending on their detection thresholds, granularity and total thickness. The relevant spectra for reaction ejectiles of ^{1}H, ^{2}H, ^{3}H, ^{3}He, ^{4}He, ^{6}He, ^{6}Li, ^{7}Li, ^{8}Li, ^{7}Be, ^{9}Be, ^{10}Be, ^{10}B, ^{11}B and isotopic unresolved of C, N and O were derived from the data. In this way the largest ever obtained set of double differential cross sections, $\mathrm{d}^2\sigma/d\Omega dE$, for proton induced spallation has been collected. Out of this huge data base a representative selection of double differential cross section will be shown in order to indicate all the noticeable features of distributions in their dependence on the incident energy, the target nucleus, an emission angle and a kind of ejectile.

The experimental results are presented in the way allowing the direct comparison of distribution's shapes dependence both on projectile energy and emission angle as well as on the mass of bombarded target. Figures from 4.1 to 4.16 comprise the double differential cross sections for three laboratory detection angles for proton incident energy of 2.5 GeV (red triangles), 1.9 GeV (blue squares) and 1.2 GeV (green circles). For Ni target also the data for low bombarding energy of 175 MeV were collected and they are depicted with purple stars. The distributions of LCPs are presented for emission angles of 16°, 65° and 100°, whereas these of IMFs were registered at 35°, 50° and 100°. For individual ejectiles the ranges of all histograms in the figures are the same.

An inspection of presented distributions permits to conclude about the following general features of energy- and angle dependence of cross section for proton induced spallation products:

- The shapes of the spectra for individual ejectiles are almost the same for three highest bombarding energies of 2.5 GeV, 1.9 GeV and 1.2 GeV. The noticeable differences are observed only when the distributions registered at lowest incident energy of 175 MeV are included;
- The angular dependence of distributions' shapes is monotonical;
- The magnitude of cross sections varies very little among bombarding energies of 2.5, 1.9 and 1.2 GeV. The differences are higher for heavier targets and are comprised within a factor 2 for ^{197}Au target whereas for ^{27}Al and ^{12}C the distributions for three highest beam energies overlap. For these cases where cross section depends on bombarding energy it is bigger for higher kinetic energy of projectile;
- Even when the bombarding proton has only 175 MeV kinetic energy the yield of forward emitted protons and deuterons is similar as these for higher incident energies. It drops however with increase of the emission angle and the mass of emitted ejectiles;

- If the detection range is sufficient at the low energies (< 50 MeV) the component with peak and steeply falling edge is visible. The peak position is stable. This component is independent of emission angle;
- A few times less abundant but extending over longer energy range component is observed at higher emission energies. It is less steep but anisotropic - the slope is rising with detection angle;
- The yield of particles of the second component decrease with the mass of ejectile and its emission angle;

Interesting are differences between the cross sections for isobars like ^{3}H and ^{3}He, ^{6}He and ^{6}Li ^{7}Li and ^{7}Be, ^{10}Be and ^{10}B. For heavy targets (^{197}Au,^{nat}Ag) the emission yield of isotopes containing more neutrons is higher. For ^{3}He the low energy component, namely the dominating peak at energies lower than 40 MeV is missing. However, this component is present for neighboring isotopes of ^{3}H and ^{4}He.

The interpretation of the shapes of the measured cross sections on the basis of the existing theoretical models and beyond them will be presented in chapters 6, 7 and 9.

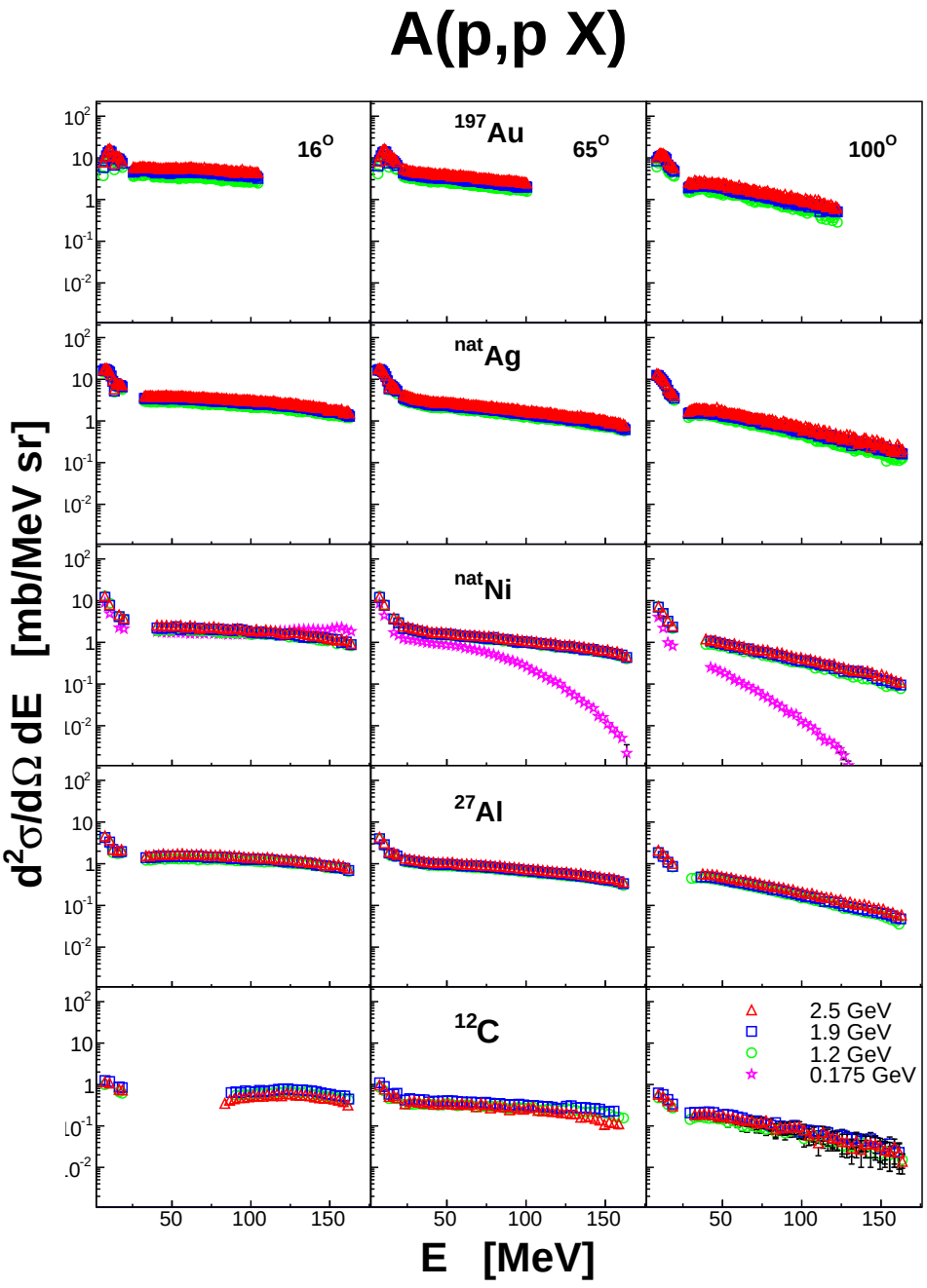

Figure 4.1: Results of the PISA experiment: double differential cross section for proton emission after bombardment of various target nuclei by protons of kinetic energies of 2.5 GeV (triangles, red), 1.9 GeV (squares, blue), 1.2 GeV (circles, green) and 0.175 GeV (stars, purple). Left column: forward emission angle of 16° in the laboratory system; middle column: laboratory emission angle of 65°; right column: backward emission angle of 100°. The most upper row comprises data related to disintegration of heaviest target nuclei used in the PISA experiment, namely the ^{197}Au. Following rows presents data for ^{nat}Ag (second one), ^{nat}Ni (third one), ^{27}Al (forth row) and ^{12}C (fifth row). The lowest incident proton energy data of 175 MeV are available only for Ni target nuclei. Both vertical as well as horizontal ranges of all histograms are the same.

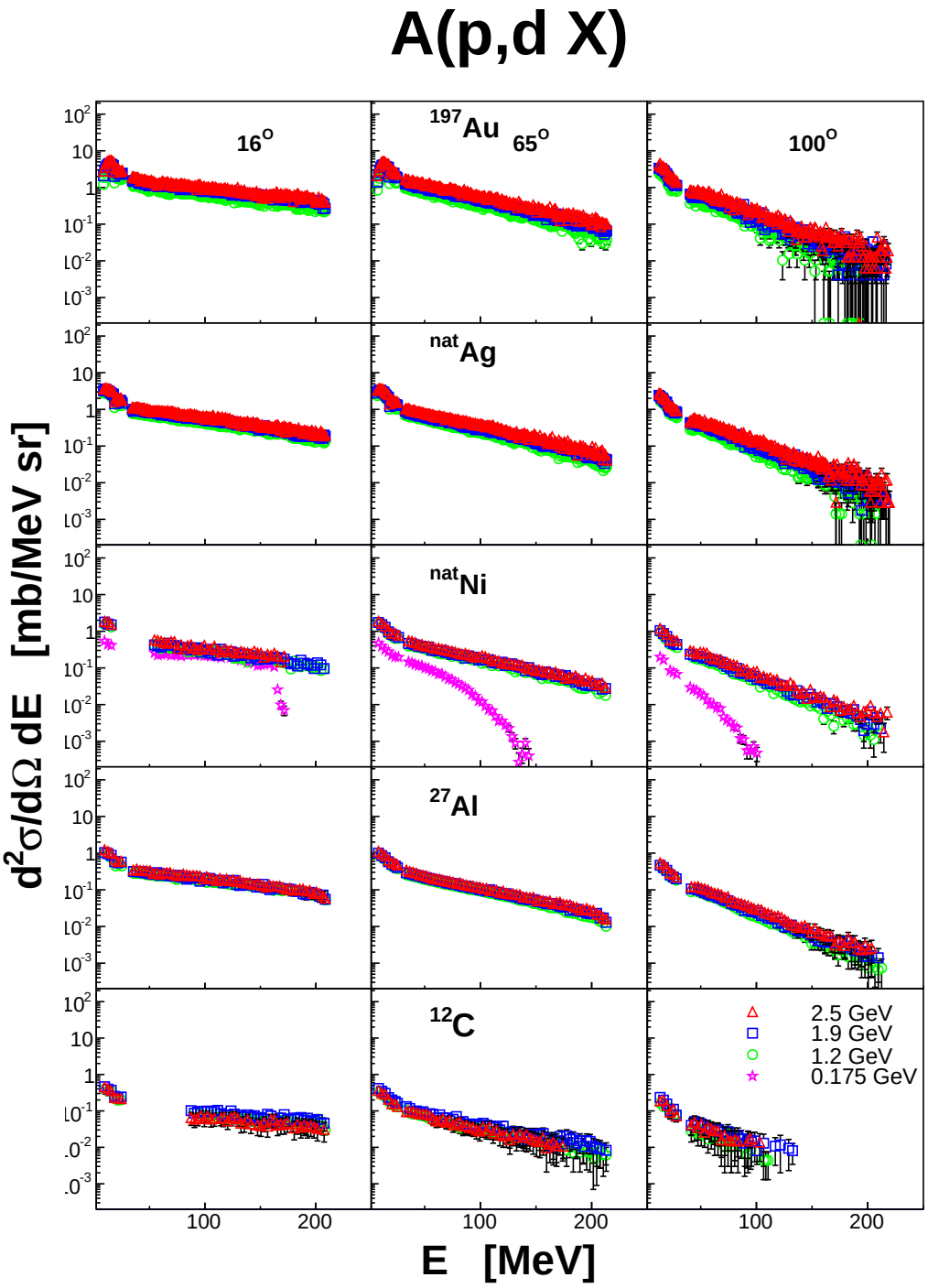

Figure 4.2: The same as in fig. 4.1 but for emission of deuterons.

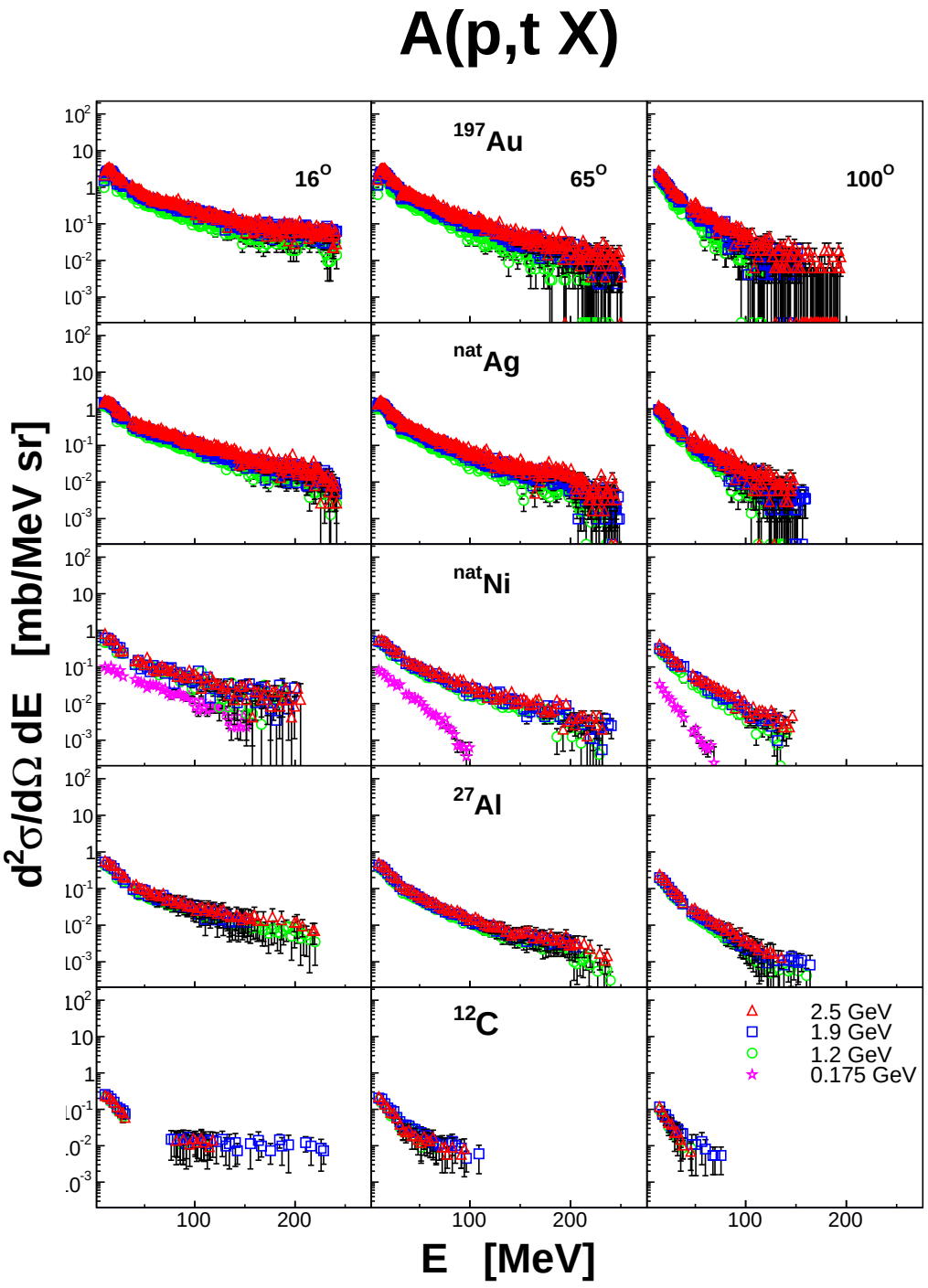

Figure 4.3: The same as in fig. 4.1 but for emission of tritons.

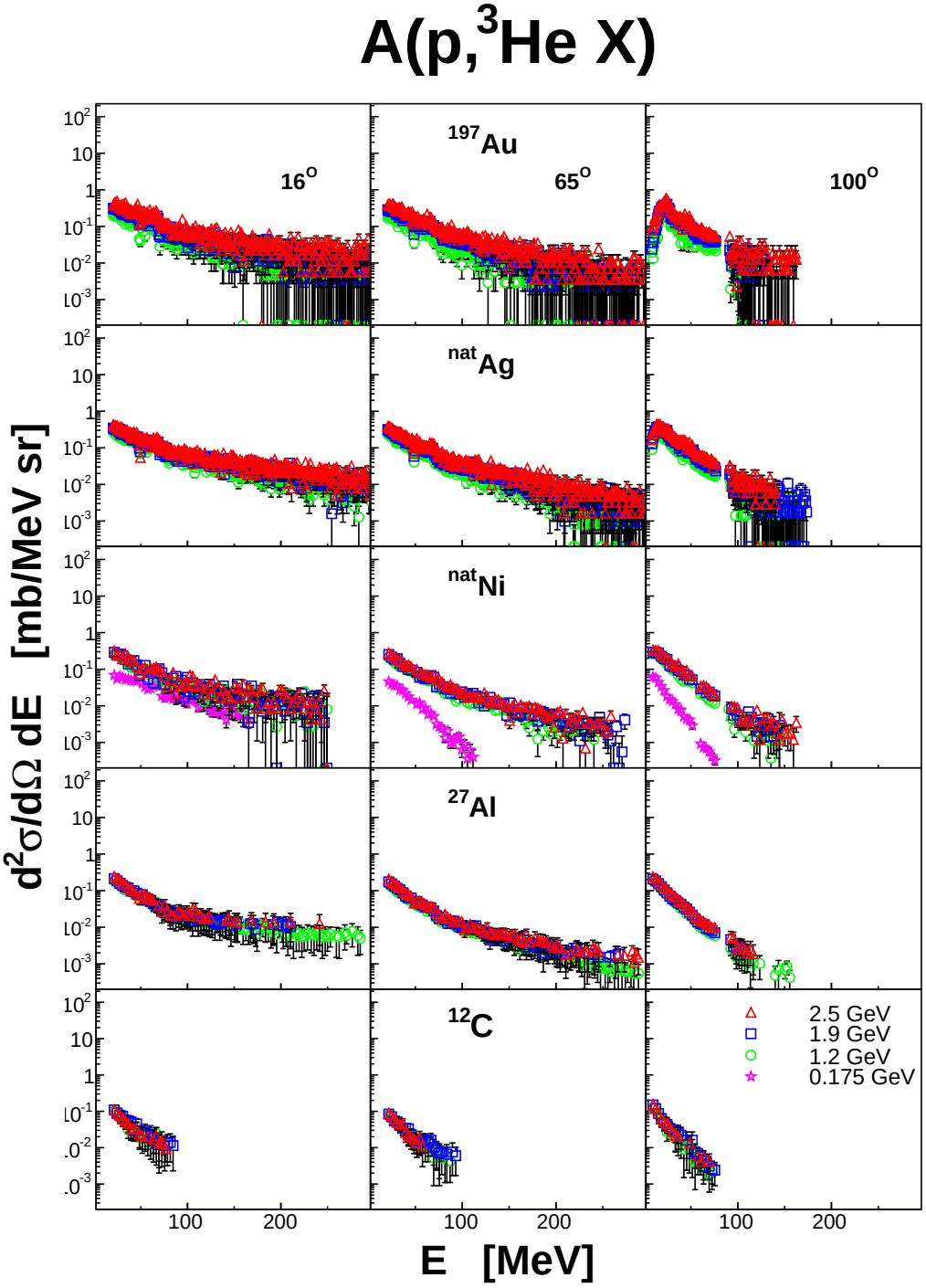

Figure 4.4: The same as in fig. 4.1 but for emission of ^{3}He.

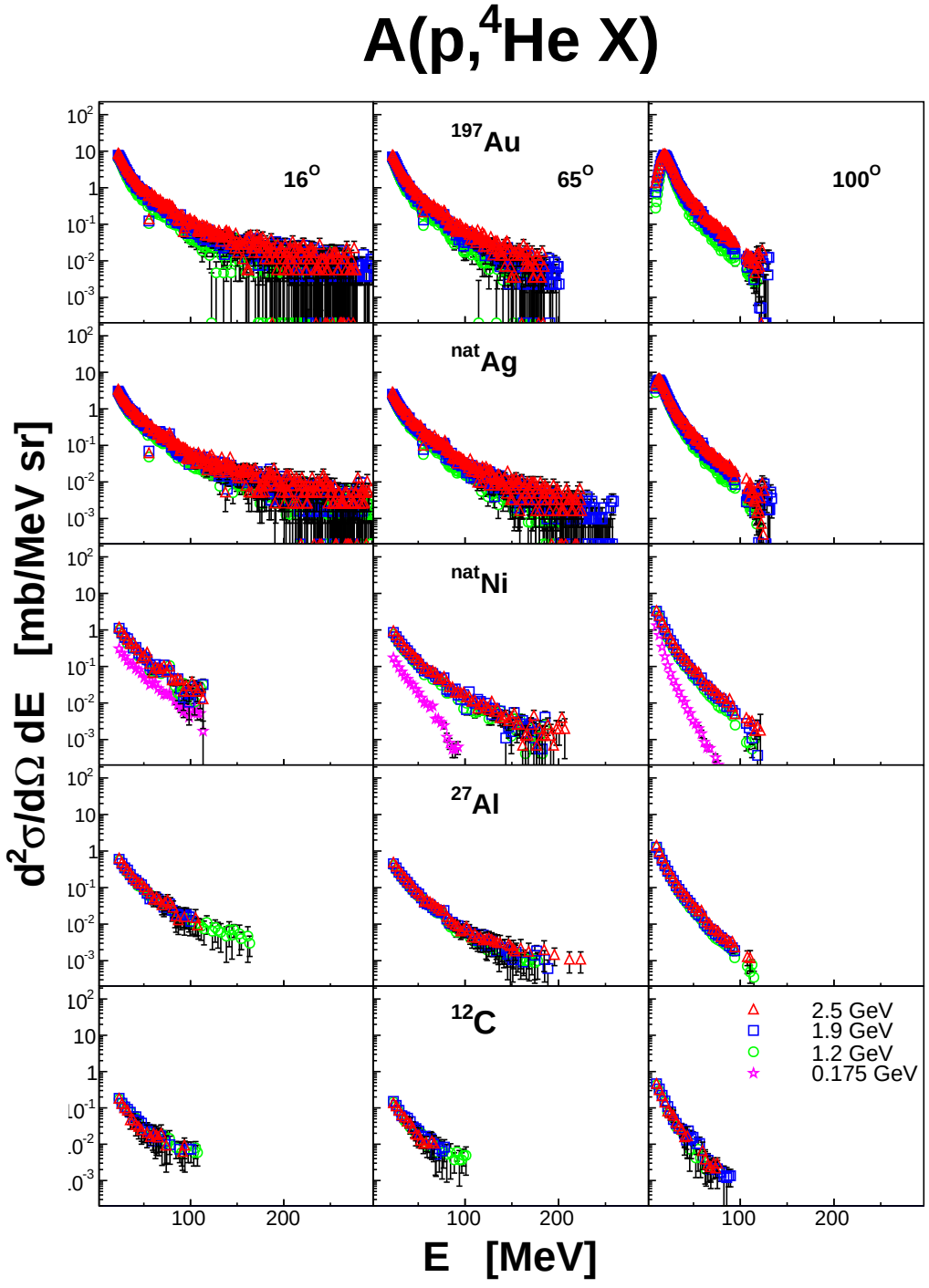

Figure 4.5: The same as in fig. 4.1 but for emission of ^{4}He.

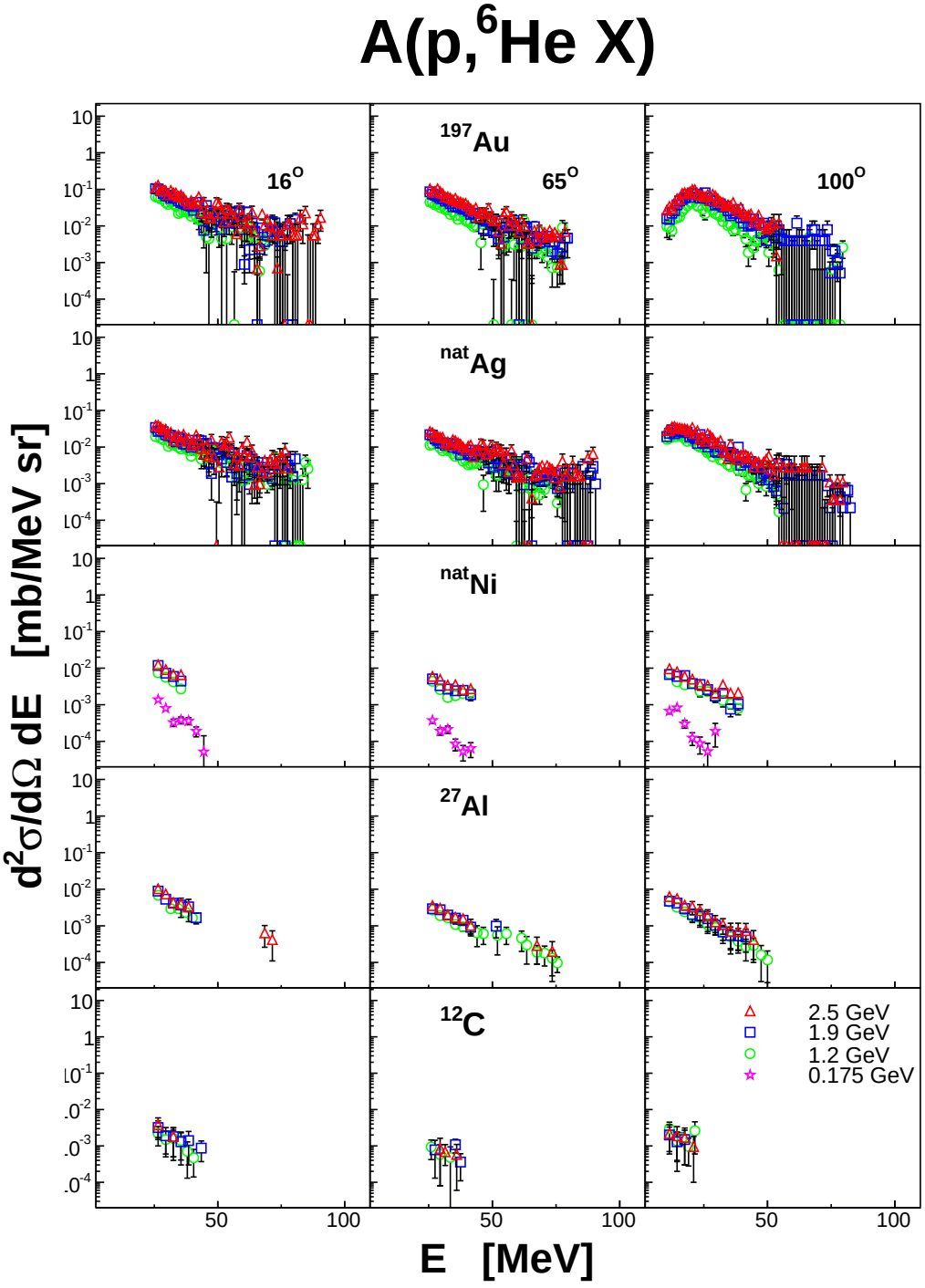

Figure 4.6: The same as in fig. 4.1 but for emission of ^{6}He.

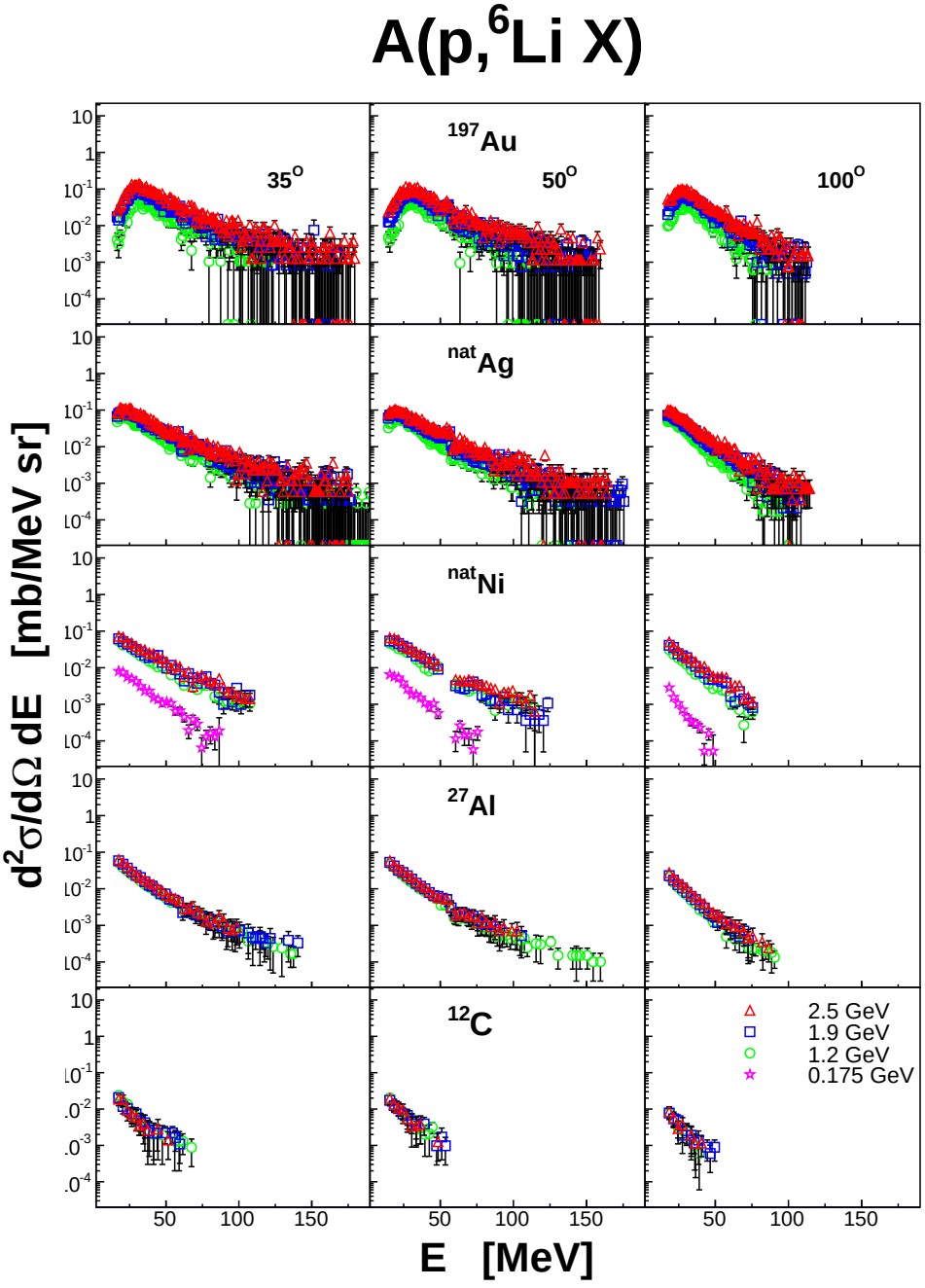

Figure 4.7: Results of the PISA experiment: double differential cross section for ^{6}Li emission after bombardment of various target nuclei by protons of kinetic energies of 2.5 GeV (triangles, red), 1.9 GeV (squares, blue), 1.2 GeV (circles, green) and 0.175 GeV (stars, purple). Left column: emission angle of 35° in the laboratory system; middle column: laboratory emission angle of 50°; right column: backward emission angle of 100°. The most upper row comprises data related to disintegration of heaviest target nuclei used in the PISA experiment, namely the ^{197}Au. Following rows presents data for ^{nat}Ag (second one), ^{nat}Ni (third one), ^{27}Al (forth row) and ^{12}C (fifth row). The lowest incident proton energy data of 175 MeV are available only for Ni target nuclei. Both vertical as well as horizontal ranges of all histograms are the same.

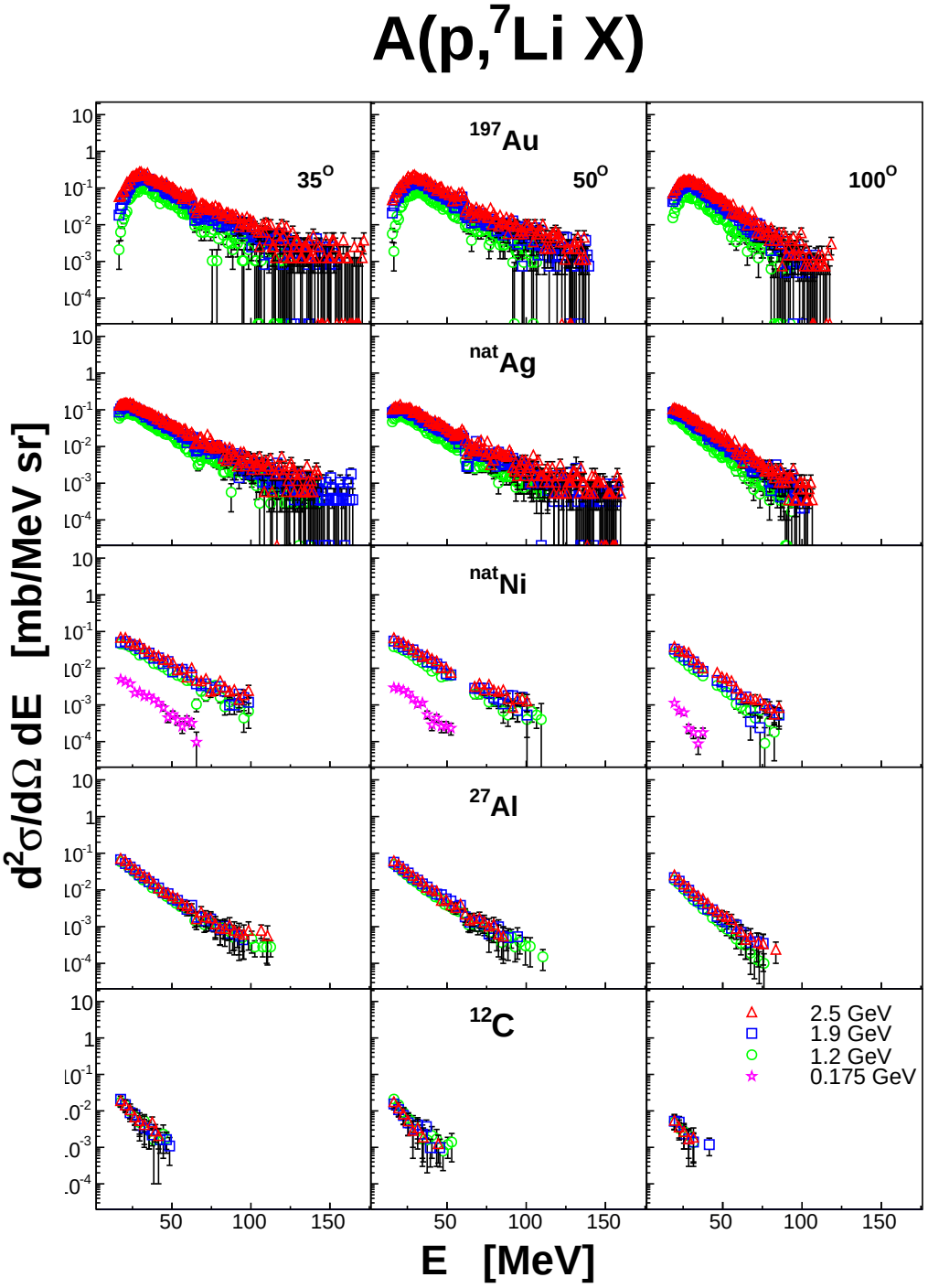

Figure 4.8: The same as in fig. 4.7 but for emission of ^{7}Li.

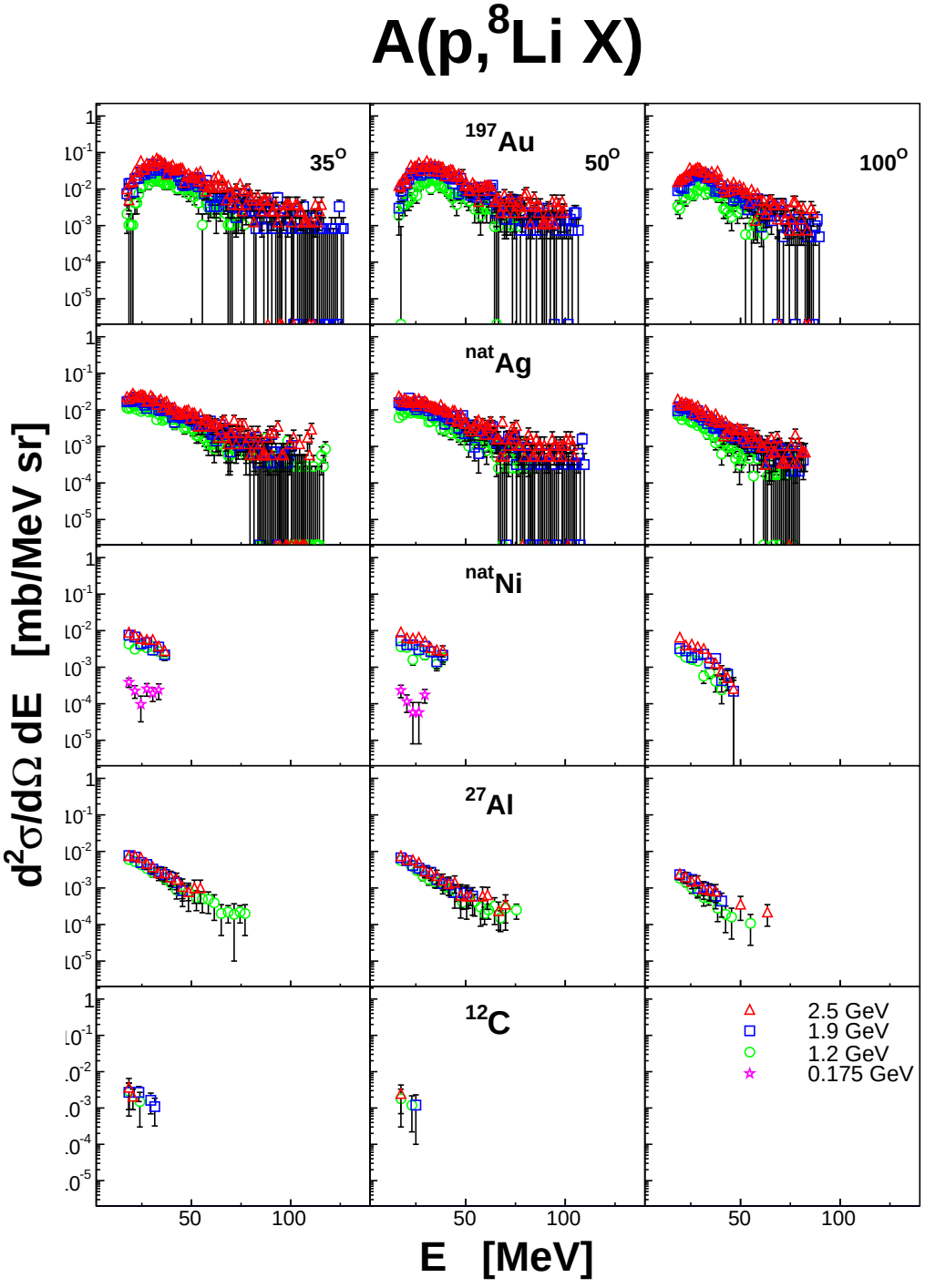

Figure 4.9: The same as in fig. 4.7 but for emission of ^{8}Li.

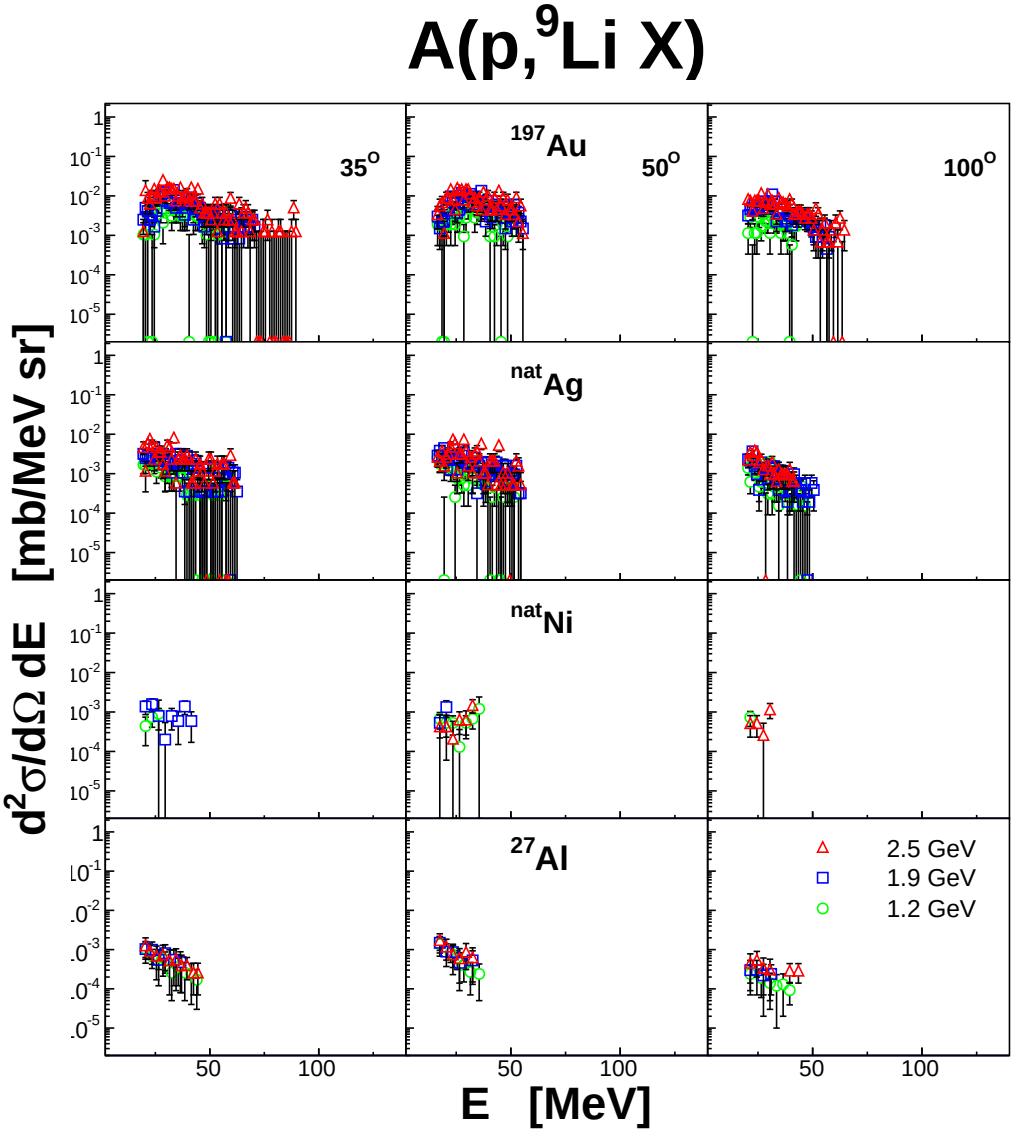

Figure 4.10: The same as in fig. 4.7 but for emission of ^{9}Li. No sufficient statistics has been registered for ^{9}Li emission from ^{12}C target.

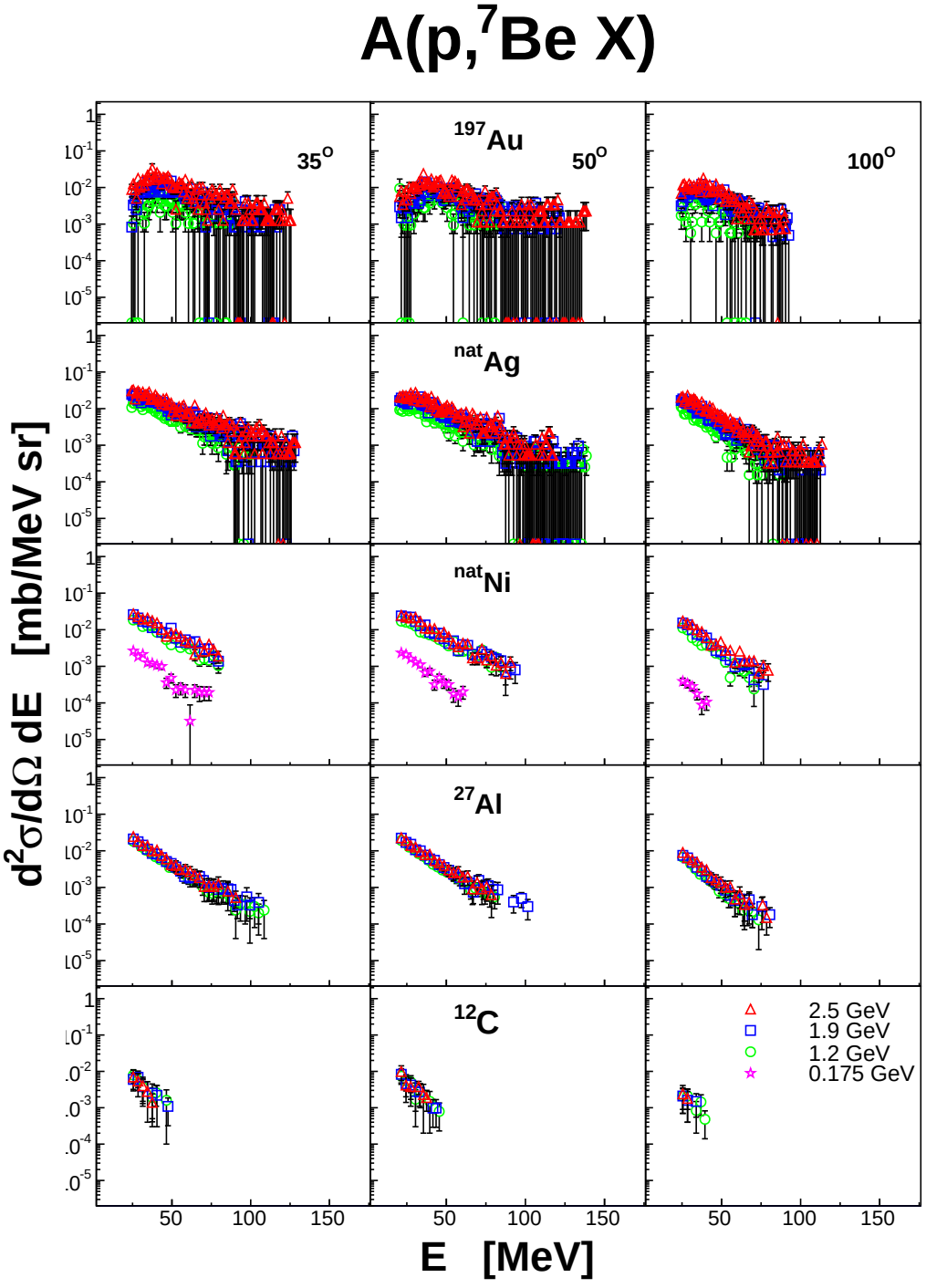

Figure 4.11: The same as in fig. 4.7 but for emission of ^{7}Be.

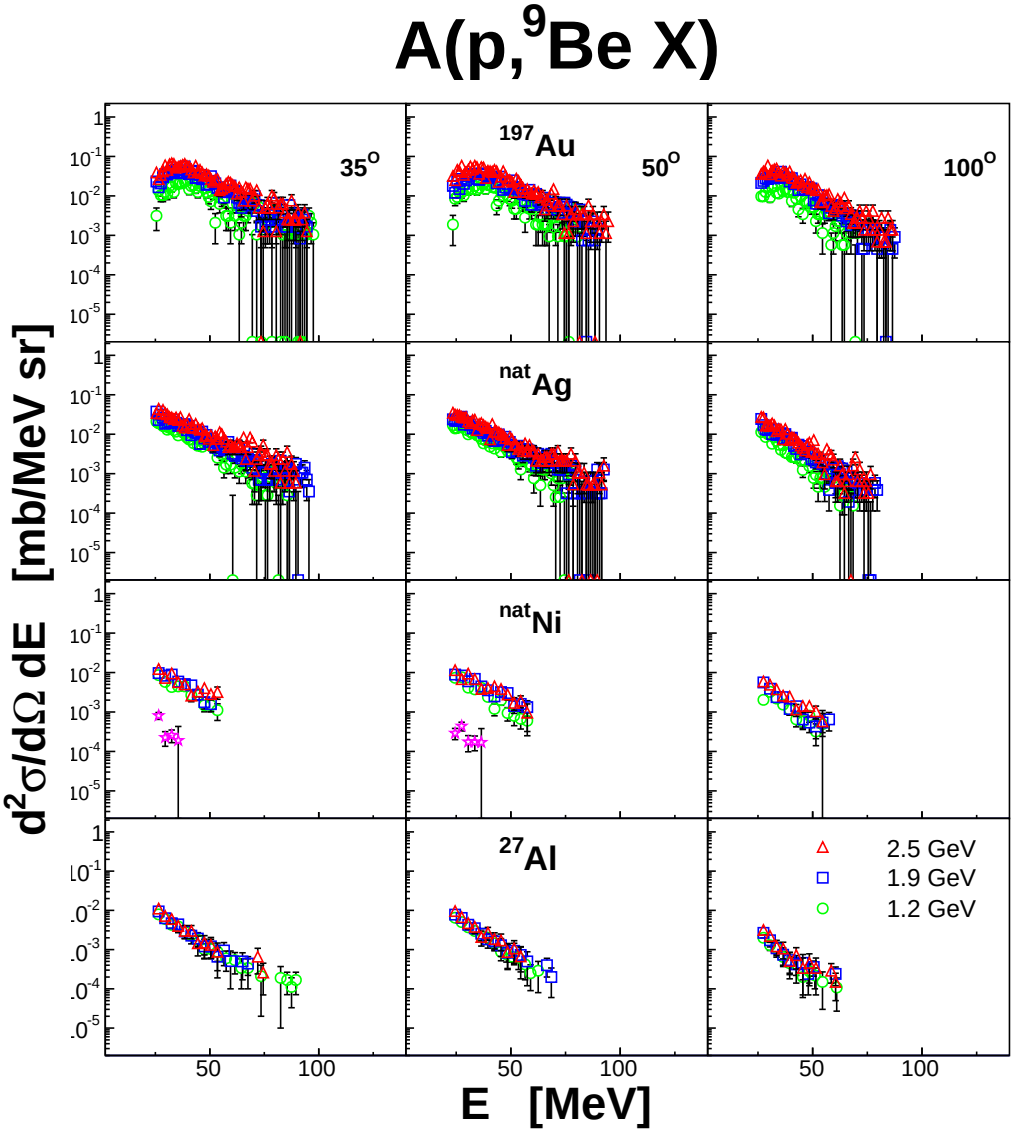

Figure 4.12: The same as in fig. 4.7 but for emission of ^{9}Be. No sufficient statistics has been registered for ^{9}Be emission from ^{12}C target.

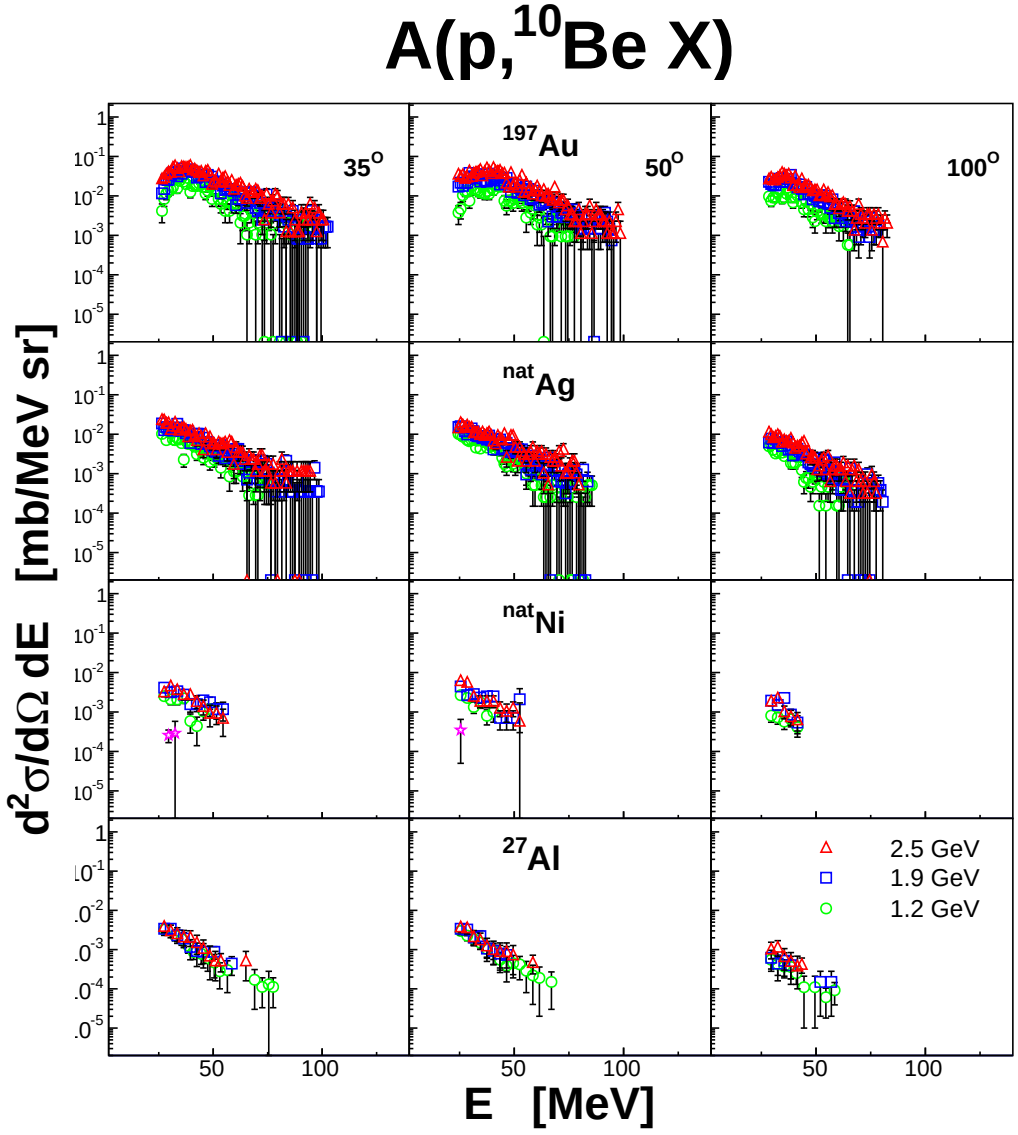

Figure 4.13: The same as in fig. 4.7 but for emission of ^{10}Be. No sufficient statistics has been registered for ^{10}Be emission from ^{12}C target.

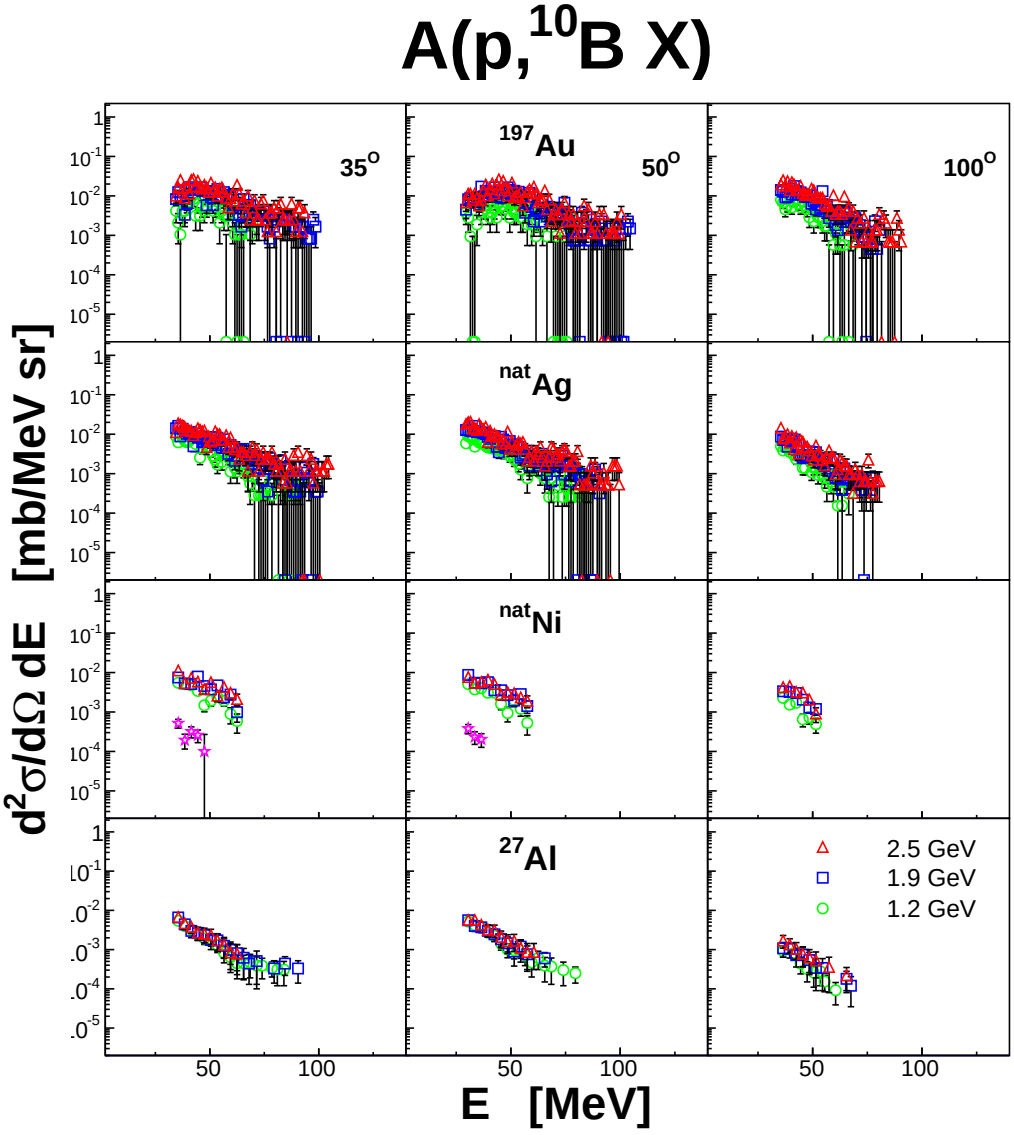

Figure 4.14: The same as in fig. 4.7 but for emission of ^{10}B. No sufficient statistics has been registered for ^{10}B from ^{12}C target.

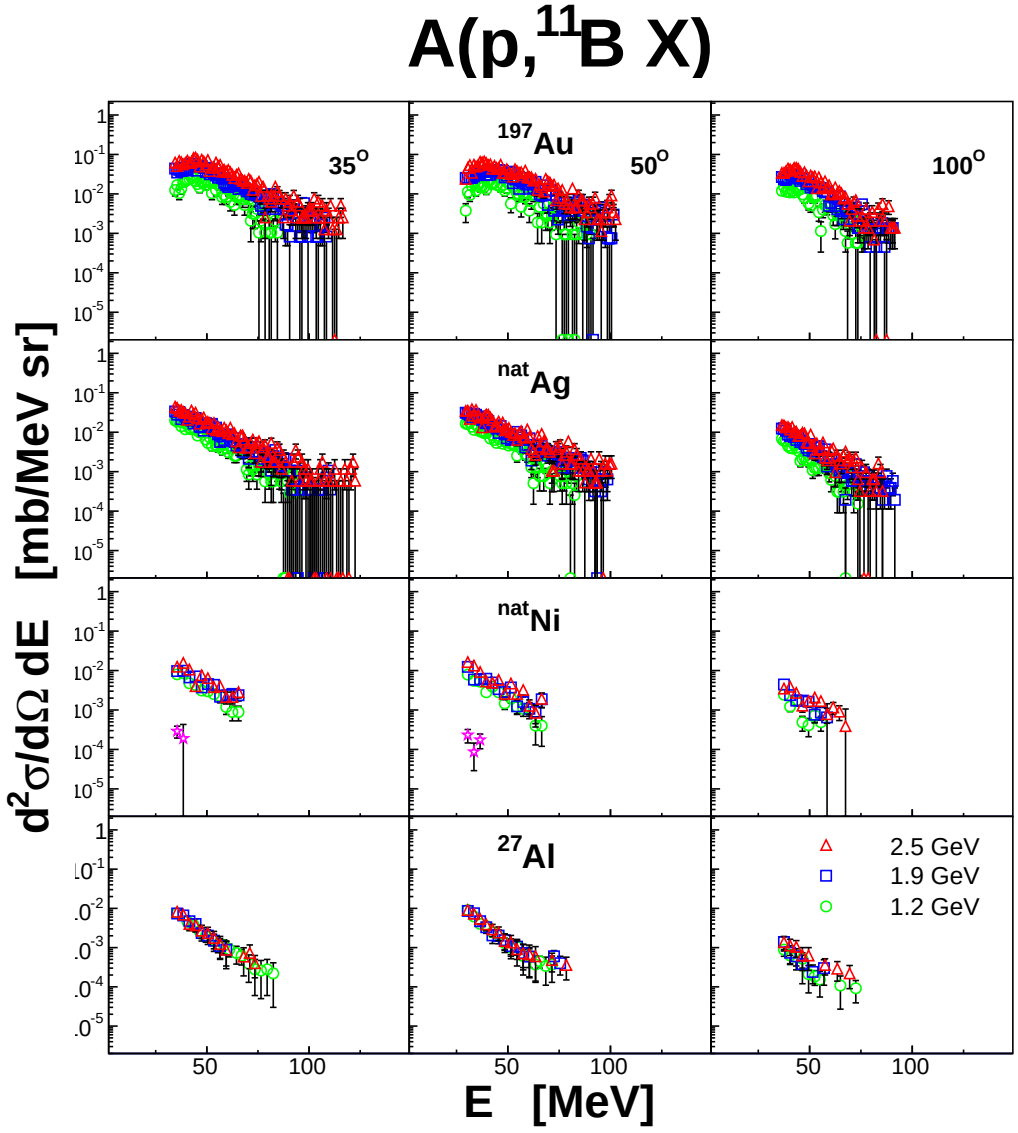

Figure 4.15: The same as in fig. 4.7 but for emission of ^{11}B. No sufficient statistics has been registered for ^{11}B emission from ^{12}C target.

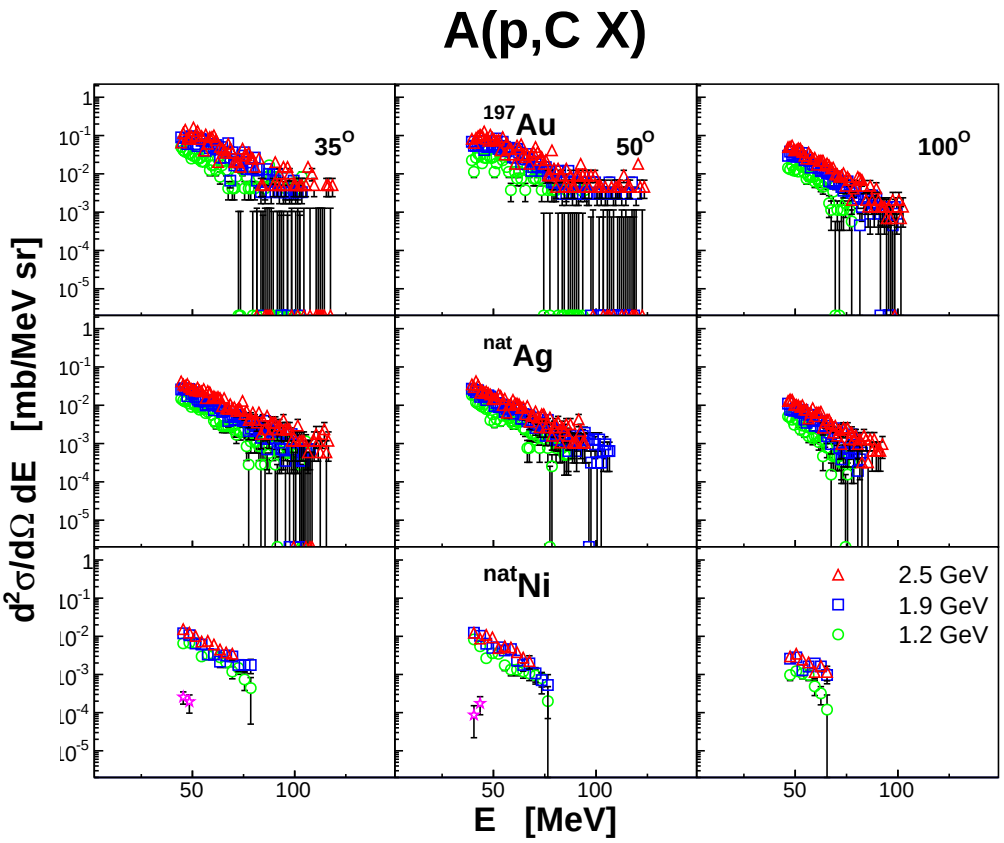

Figure 4.16: The same as in fig. 4.7 but for emission of isotopic unresolved C nuclei. No sufficient statistics has been registered for C nuclei emission from ^{12}C as well as from ^{27}Al target.

5 Theoretical approaches to the spallation processes

Since spallation involves an energetic many body interaction of nuclear objects in nuclear medium - the processes still insufficiently explored by basic theories - predictions of the individual reactions have to be carried on by simplified nuclear physics models implemented into a computer code and simulated with the Monte Carlo technique.

Moreover, a high complexity of physical processes interplaying during and after the hadron-nucleus collision implicate a need of combination of various models expected to describe different stages of the reaction. In effect the kind of hybrid models are created where the result of earlier calculations is an input for modeling of the subsequent phenomenons with the use of different computer code. Also the various scenarios of the reaction can be considered and then the individual mechanisms are treated as alternative ones. Their activation depends on the current conditions of the excited nuclear system and predefined probability functions.

5.1 Two step model

At the incident energy up to a few GeV it is generally assumed that a two step process is able to describe the observed spallation phenomenons. Such approach was originally proposed by Serber [56]. There is a common agreement that the low energy part of spallation distribution of nuclear ejectiles is a product of process which can be successfully approximated by the statistical processes of sequential evaporation or simultaneous fragmentation, either, where it is applicable, by fission of exited nuclei. Depending on the mass and charge of an unstable nucleus, its excitation energy and angular momentum, deformation and fissility the competence of the mentioned decay modes is taking part. The theoretical bases for description of these statistical processes were established already in [57] and [58]. The computer codes utilizing the ideas of evaporation, fragmentation and fission like Gemini [59], Abla [60, 61, 62], GEM2 [63, 64], SMM [65] are used for predictions of the yield and distributions of the dominating low energy component of spallation products. The statistical processes can be considered to play a role after the remnant of target-like nucleus attained the global thermal equilibrium or the thermalization has been achieved in the dominant part of its volume. The relevant time scale of the onset of statistical phenomena is of the order of 10^{-20} s.

In the current work the main interest is focused on the earlier stage of the spallation reaction. It is of high importance to understand and describe the processes, which lead the knocked out of balance target nucleus to the equilibrated state. It is convenient to refer to the period of spallation reaction before the thermalization is achieved as a "preequilibrium" phase. It covers the relatively short time after impinging particle had touched the target nucleus and before the latter has achieved the statistical balance.

The models of the processes acting in the preequilibrium stage should take into account the mechanisms of proton-nucleus interaction, the momentum and energy transfer to the target, the phenomenons responsible for internal energy dissipation, the possibilities of the formation and emission of abundantly observed diversity of reaction products. The preequilibrium models have to reproduce total yields and the broad spectra of ejectiles' energies and emission angles.

5.1.1 First step - a cascade of binary collisions

Nowadays the approaches to the microscopic modeling of a nuclear collisions in the prequlibrium stage of spallations can be grouped into three branches which differ in the assumed general philosophy of the hadron-nucleus interaction, the introduced assumptions and the accepted simplifications. They are:

- application of the model of intranuclear casade which proceeds inside target nucleus after the collision;
- application of the transport equation (like BUU or VUU) in order to generate the time development of nuclear system;
- application of the so-called Quantum Molecular Dynamics (QMD) - the approach which can be thought as a most advanced from point of view of implemented knowledge about the quantum phenomena in the nuclear ensembles;

The three classes of the models differ in approximating the realistic shapes and dynamics of nuclear potential. They could also take into account or disregard the particle correlations. In all of these classes of models it is assumed that in the preequilibrium phase the cascade of intranuclear binary interactions take part.

These three most popular in the recent decades approaches can be supplemented by the submodels responsible for phenomena not considered in the main model. This is often a case for mechanism responsible for creation and emission of complex particles. A surface coalescence of nucleons as proposed by Gutbrod et al. [66] or in the form of phenomenological mechanism called a "snowball" [67] are used in INCL or BUU calculations [47], [68] or even are implemented into the QMD model [69].

5.1.1.1 Models of Intranuclear Cascade

The idea of intranuclear cascade will be presented with an example of the Intra-Nuclear Cascade Liege (INCL) model - the one which was strongly developed over last three decades with significant manpower engagement and close collaboration with experimental groups. INCL will be presented here with more details than other models dealing with the first step of spallation reactions since results of calculation with INCL are frequently utilized and recalled in this dissertation.

The INCL model was originally intended both for heavy ion collisions as well as for light particles induced reactions in energy range from few hundreds MeV to few GeV. In the latest version of INCL (INCL4.6) [70] it is emphasized that the applicability of the model is extended to energies as low as a few tens of MeV. With this model a significant improvement of description of experimental data in the domain of energy spectra of single nucleons as well as for composite spallation products and pions was achived. The development of the model in time can be traced with the following references: [71, 72, 73, 74, 75, 76, 77, 78, 79, 80, 81, 82, 83, 84, 85, 86, 87, 68, 88, 89, 90, 91, 70, 92]. The theoretical basis of the model and its applicability constrains are summarized in [93].

The basic assumption of intranuclear cascade model consist in the treatment of the nucleus as a Fermi gas consisting of independent nucleons freely propagating in the phase space. The phase space is limited by the radius of nucleus R_{max} and the maximal Fermi momentum P_F. A constant, time and position independent nuclear potential V_0 is assumed which influence only the

particle's emission probability and kinetic energy of ejectiles. (In INCL4.6 the isospin distinction of potential depths for protons, neutrons and pions has been introduced). The movement of the particles inside the nucleus is not correlated and their interaction is purely accidental. The interaction rely on energy and momentum exchange between two counterparts which are at the close distance each to the other. The collision can be elastic or lead to an excitation of an new state. Probability and kind of interaction depends on the Monte Carlo sampling of the parametrized experimental cross sections for the free nucleon-nucleon and nucleon-pion reactions.

5.1.1.1.1 Target nucleus For the initial spatial distribution of nucleons in the target nucleus the Saxon-Woods formula of density distribution $\rho(r)$ is used:

$$\rho(r) = \begin{cases} \frac{\rho_0}{1 + exp(\frac{r-R_0}{a})} & \text{for } r \leq R_{max} \\ 0 & \text{for } r > R_{max} \end{cases} \tag{5.1}$$

In the foregoing equation the r is a vector of a nucleon position in the Cartesian frame. The origin of the reference system is located in the center of the nucleus. $R_{max} = R_0 + 8a$, where R_0 and a are the parameters of the Saxon-Woods distribution depending on the mass number A_T of the nucleus: R_0 is the radius of the half-density and a is a diffuseness of the density distribution. The experimental values of parameters of the Saxon-Woods distribution are derived from electron scattering. They are available e.g. in [94]. ρ_0 is a parameter related to nuclear ground state density. Its actual value is selected in order to assure that the number of nucleons in the assumed volume target nucleus is equal to the mass number A_T.

In INCL values of R_0 and a were parametrized in the following way:

$$R_0 = (2.745 \cdot 10^{-4} A_T + 1.063)\ A_T^{1/3} \text{ fm},$$
$$a = 0.51 + 1.63 \cdot 10^{-4} A_T \text{ fm}.$$

The positions of nucleons are generated randomly inside the boundary volume.

The momentum distribution is generated randomly as well. Vectors of momenta p are homogeneously distributed inside the sphere extending to maximal Fermi momentum p_F:

In the versions of INCL later than 4.2 the correlation between the momentum p of the nucleon and the achievable position r in the nucleon volume was introduced. It was done in order to reflect the fact that nucleons of higher momenta have a larger probability to propagate closer to the nucleus surface than those of the low momenta.

5.1.1.1.2 Projectile The incident particles considered in INCL4.x versions are nucleons and light clusters up to ^{4}He. In case of composite projectiles the intrinsic energies, space- and momentum distributions of their nucleons are generated in similar way as for the target nucleus. The impact parameters are taken as random from the distributions covering the area of maximal nuclear radius of R_{max}. In order to take into account the rise of NN cross section, σ_{NN}^{tot}, with decrease of collision energy, at low incident energies the R_{max} is extended by the so-called "range of interaction", r_{int}:

$$r_{int} = \sqrt{(\sigma_{NN}^{tot}/\pi)}\ . \tag{5.2}$$

At the beginning of the simulations the projectile is positioned at the surface of a sphere of the target nucleus. The Coulomb interaction is taken into account.

5.1.1.1.3 Collision Inside the target the particles move along straight lines according to their current momentum vector. Collision are considered if for a pair of them the distance of a mutual approach d is:

$$d \ \leq \ \sqrt{(\sigma^{tot}/\pi)} \ , \tag{5.3}$$

where σ^{tot} is a total cross section relevant for energies of interacting particles.

The following elementary interactions are included to INCL:

$NN \rightarrow NN$	$(elastic)$
$NN \rightarrow N\Delta(1232)$	
$N\Delta(1232) \rightarrow NN$	$(delta\ absorption)$
$\pi N \rightarrow \pi N$	$(elastic)$
$\pi N \rightarrow \pi\Delta(1232)$	

The origin of pions is a decay process of the $\Delta(1232)$ resonance:

$$\Delta(1232) \rightarrow \pi N \ .$$

The isospin conservation is fulfilled by construction.

The cross sections used in INCL are derived from experimental distributions obtained for free particles. The possible in-medium effect are disregarded. In the computer code of INCL the probability of individual reaction is sampled with the use of cross sections parametrizations proposed in [83, 85]. The angular dependence of cross sections $\frac{d\sigma}{d\Omega}$ is introduced via a Mandelstam variable t and the following formula is used:

$$\frac{d\sigma}{d\Omega} \ \sim \ exp(B \cdot t) \ . \tag{5.4}$$

B is a parameter dependent on momentum and isospin of colliding particles and is parametrized. $t = (p_1 - p_3)^2 = (p_2 - p_4)^2$, where p_i are the four-momenta of initial colliding particles (i = 1,2) and outgoing ones (i = 3,4).

The relation of t to the scattering angle θ reads:

$$t = -2p_{CM}^2(1 \ - \ cos\theta) \ . \tag{5.5}$$

The above dependences permit to take into account angular cross section and to calculate the momentum transfer in the collision as well as to derive the appropriate scattering angle.

Collisions are allowed only for the so-called participants. These are the beam particles and primary or secondary target constituents which interacted and gained an energy. Their energies must be above the Fermi energy level. Otherwise, they are qualified as spectators similar like the target nucleons which avoided interaction.

Another restriction for colliding particles introduced to INCL is the energy limit for collisions. Neglected are so-called soft collisions of the CM energy $\sqrt{s} < \sqrt{s_0} = 1925$ MeV (here s is a Mandelstam variable). Such collisions of the low energy-momentum transfer do not influence significantly the particle flow in the nuclear medium. Moreover they are usually blocked since they lead to the phase-space states which are occupied (see below 5.1.1.1.5). In the INCL4.6 version the CM energy threshold for colliding particles was decreased since authors realized that for the low incident energies of several tens of MeV the $\sqrt{s_0}$ limit as above is too strict and it was reduced to $\sqrt{s_0} = 1910$ MeV.

Throughout the simulation of the whole cascade of interaction the relativistic kinematics is used.

5.1.1.1.4 Emission Nucleons, pions and possible clusters which in their propagation through the target nucleus attain the R_{max} are checked if they can leave the potential well. Their kinetic energy, E has to be higher than the potential well. The asymptotic kinetic energy, E_∞ of emitted particle is equal to:

$$E_\infty = E - E_F - S \ , \tag{5.6}$$

where E_F and S are the Fermi energy and separation energy for the ejectile, respectively. The values of S can be taken as a differences between the assumed potential depth and the individual Fermi energies of particles. The precise physical values from the tables of nuclear masses could be used as well. The charged ejectile have to additionally overcome the Coulomb barrier. For this aim the Gamow factors for electrostatic barrier penetration are calculated and probability of emission is sampled.

Particles of insufficient energy at the border of target nucleus are reflected back into the nuclear medium. It is also the case for Δ resonances which are not allowed to leave the potential well.

5.1.1.1.5 Quantum effects - the Pauli blocking The collision of particles or the decay of Δ resonance will be blocked if the states of the resulting particles are already occupied in the available phase space. The Pauli blocking probability can be calculated in the strict way or the so-called stochastic Pauli blocking is applied. In the strict Pauli blocking the interaction is always blocked if the states of reaction products do not lie outside the "Fermi sea". The stochastic Pauli blocking is less restrictive. The strength of the blocking is related to the number of nucleons occupying the vicinity of the final state and comprised within the spheres of r_{PB} and p_{PB}. The probability P of interaction is given by:

$$P \ = \ (1 \ - \ f_i)(1 \ - \ f_j) \ , \tag{5.7}$$

where f_i, f_j are phase-space occupation factors for particles i and j. They are calculated as follows:

$$f_i \ = \ \frac{1}{2} \ \frac{(2\pi\hbar)^3}{\frac{4\pi}{3} r_{PB}^3 \ \frac{4\pi}{3} p_{PB}^3} \sum_{k \neq i} \Theta(r_{PB} - |r_k - r_i|) \times \Theta(p_{PB} - |p_k - p_i|) \ , \tag{5.8}$$

where r_i, p_i are the vectors of position and momenta, respectively of the final state particles, r_k, p_k are the vectors of position and momenta, respectively of the "Fermi see" particles of the same isospin as i-particle and localized in the spacial and momentum sphere of $r_{PB} = 3.18$ fm and $p_{PB} = 200$ MeV/c, respectively.

In the latest versions of INCL the first collision of the projectile with the in-medium particle has to obey the strict Pauli blocking whereas a feasibility of the subsequent collisions is checked with the stochastic Pauli blocking.

5.1.1.1.6 Composite particle production in INC - hypothesis of surface coalescence The mechanism of surface coalescence in INCL was implemented first in the 4.3 version and adapted from work of Letourneau and the NESSI collaboration [47]. The need of mechanism responsible for composite ejectiles production in INCL stem from the limitation of binary cascade processes only to the nucleons and pions in the output channel. The hypothesis of surface coalescence states that outgoing nucleon which has sufficient kinetic energy in order to leave the target nucleus is able to carry along the another nucleons. If the states of candidates for coalescence fulfill the predefined conditions concerning the relative distances, momenta and isospins then out of those nucleons a cluster is formed.

In INCL the cluster is constructed as follows. Each outgoing nucleus being on the nuclear surface is traced back to the nuclear medium to the depth D:

$$D = R_0 + h \ , \tag{5.9}$$

where h is a parameter. Along this path, in vicinity, other nucleons are searched for. They are candidates for cluster formation together with the leading one. They can be adjoined successively from the closest nucleon to the most distant one increasing the size of the cluster. The criterion of proximity in the phase-space has to be fulfilled:

$$r_{i,[i-1]} \ p_{i,[i-1]} \ \leq \ h_0(A_{cl}) \ , \tag{5.10}$$

where:
$r_{i,[i-1]}$, $p_{i,[i-1]}$ - the position and momentum coordinates of the checked i-th nucleon with respect to the coordinates of the current cluster formed out of $[i-1]$ nucleons (the leading nucleon has index $i = 1$);
$h_0(A_{cl})$ - combined radius of the phase-space sphere delimitation.

In INCL4.3 the h_0 parameter was independent of A_{cl} and was equal to 387 MeV fm/c. But then only creation of the the lightest clusters i.e. ^{2}H, ^{3}H, ^{3}He and ^{4}He were considered. In the current version of INCL (INCL4.6) the stable cluster of the mass number up to $A_{cl} = 8$ are constructed. h_0 vary with the mass of created cluster an take the following values:

$$h_0(A_{cl}) = \begin{cases} 424 \ \text{fm MeV/c} & \text{for } A_{cl} = 2 \\ 300 \ \text{fm MeV/c} & \text{for } A_{cl} = 3 \\ 300 \ \text{fm MeV/c} & \text{for } A_{cl} = 4 \\ 359 \ \text{fm MeV/c} & \text{for } A_{cl} > 4 \end{cases} \tag{5.11}$$

The value of h is taken as 1 fm in the current version of INCL.

The cluster which was constructed according to the described above rule is checked if it can overcome the potential and Coulomb barrier. If its net kinetic energy is greater than zero it is ejected at the emission angle resulting from the sum of momenta of the contributing nucleons. Its kinetic energy is calculated in a similar way as for the single ejectile. If cluster can not be emitted it is deconstructed and involved nucleons are considered as single in-medium particles with the states as before the cluster construction.

The implementation of the hypothesis of the surface coalescence improved the INCL outcome in the domain of composite particle production. It caused, however, a deterioration of the prediction power of the model for single nucleon emission and increased number of free parameters in the model.

5.1.1.1.7 Duration of cascade calculation The time t_{stop} in which the energy needed to drive the cascade process is exhausted and the remaining target-like nucleus attain the thermal equilibrium in the INCL model is related to the mass number A of the initial target nucleus:

$$t_{stop} \ = \ 70 \cdot \left(\frac{A}{208} \right)^{0.16} \quad \text{(fm/c)}. \tag{5.12}$$

After this time the simulation of the cascade for a given event is stopped and model selected for the second reaction step is activated (see below the discussion in subsection 5.1.2).

5.1.1.2 BUU transport equations

A suitable tool for simulating the fate of the particles embedded in the nuclear medium of bombarded target nucleus is the so-called transport equation developed originally by Boltzmann for classical gasses and adapted for quantum gasses by Uehling and Uhlenbeck [95]. From these names the acronym BUU was created which is commonly used in order to refer to the model used to describe various nuclear phenomena [96], [97], [98], and among them also the preequilibrium part of spallation reaction [99].

Nucleons (counted with the index i) are described by their phase-space distributions $f_i(\vec{r},\vec{p},t)$. They can move in the nuclear mean field U and collide with other particles according to the differential cross section $\frac{d\sigma}{d\Omega}$ and the relative velocity of colliding particles i,j: v_{ij}.

The BUU transport equation has a form:

$$\frac{\partial f}{\partial t} \; + \; \vec{v_i} \; \cdot \; \bigtriangledown_r f_i \; - \; \bigtriangledown_r U \; \cdot \; \bigtriangledown_p f_i \; = \; -\frac{4}{(2\pi)^6} \int d^3p_j d^3p_{j'} \; d\Omega \frac{d\sigma}{d\Omega} \; v_{ij}$$

$$\times \left\{ \Big[f_i f_j (1 \; - \; f_{i'})(1 \; - \; f_{j'}) \; - \; f_{i'} f_{j'} (1 \; - f_i)(1 - \; f_j) \Big] \times (2\pi)^3 \delta^3(\vec{p_i} + \vec{p_j} - \vec{p_{i'}} - \vec{p_{j'}}) \right\} \; , \tag{5.13}$$

where the left hand side describes the propagation of particle i of the velocity $\vec{v_i}$ in the mean nuclear field U. The collision term on the right hand side of the equation takes into account an interaction among the nucleus constituents. The Dirac's delta assures the momentum conservation whereas the term in square parentheses impose the fulfilling of the Ferimi-Dirac statistics for nucleons and allows to block the interaction when resulting conditions do not obey the Pauli exclusion principle.

The evolution of the mean field in the course of reaction has to be assumed. Usually it is postulated that the dependence between the mean field and the density distribution of the nuclear ensemble has a form of the Skyrme parametrization:

$$U(\rho) \; = \; A \left(\frac{\rho}{\rho_0} \right) \; + \; B \left(\frac{\rho}{\rho_0} \right)^{\sigma} \; . \tag{5.14}$$

In the above equation ρ_0 and ρ are ground state and current nuclear densities, respectively. Coefficients A and B represent the attractive and repulsive part of the potential. Parameter σ is constant and has to be greater than unity. Its value is related to the incompressibility of the nuclear matter.

Another form of nuclear mean field is used in the BUU model developed in Giessen [100]. There the Skyrme potential is supplemented by a Yukawa term and the Coulomb potential (V_{Coul}) for protons:

$$U(\vec{r}) \; = \; A \left(\frac{\rho(\vec{r})}{\rho_0} \right) \; + \; B \left(\frac{\rho(\vec{r})}{\rho_0} \right)^{\frac{4}{3}} \; + \; V_0 \int d^3\vec{r} \; \frac{exp(-\mu|\vec{r} - \vec{r'}|}{\mu|\vec{r} - \vec{r'}|} \; \rho(\vec{r}) \; + \; V_{Coul} \; . \tag{5.15}$$

The selected parameters are as follows: A = -141.62 MeV, B = 165.23 MeV, V_0 = -378 MeV, μ = 2.175 fm^{-1}, ρ_0 = 0.168 fm^{-3}.

Spatial distribution of nucleons at the beginning of the process in the Gissen BUU has a form of Woods-Saxon function:

$$\rho(r) \; = \; \frac{\rho_0}{1 \; + \; exp(\frac{r - R_0}{a})} \; , \tag{5.16}$$

with $\rho_0 = 0.168$ fm^{-3}, R = 1.124 A$^{1/3}$ fm and a = 0.025 A$^{1/3}$ + 0.29 fm. The momentum distribution of nucleons depends on the spatial density and is homogenous in the sphere of the radius equal to maximal Fermi momentum $p_F(r)$:

$$p_F(r) = \left(\frac{3\pi^2\rho(r)}{2}\right)^{1/3} . \tag{5.17}$$

The spatial density $\rho(\vec{r})$ important for the variation of the mean field during the reaction is calculated for the grid of points in the volume of the target nucleus with the selected time step.

Between collisions the particles are displaced according to their current momentum and field strength with the use of a classical equation of motion. Their trajectories are straight lines. The collision can occur if the shortest distance of two particles is smaller than the geometrical cross section $\sqrt{\sigma_{tot}/\pi}$. Production and decay of nuclear resonances are included.

Solution of BUU equation is performed by Monte Carlo simulations of motion of involved particles [96]. Interesting technical feature of the BUU calculations is the way of simulations of the fate of the nuclear system. It is done with the set of test particles. n of test particles replace each of a reaction constituent. For creation of phase space distribution or the momentary density distribution the contributions from all test particles are summed up with appropriate weights.

The BUU model calculations of spallation are able to produce the distributions of single nucleons and mesons. The remnant nucleus of the cascade can be defined with its mass, charge, energy, angular momentum and excitation energy. However, due to a lack of a mechanism allowing for particle correlations the simulation of production of complex particles cannot be performed.

An obvious advantage of the BUU method over the INC approach is the application of the dynamically changing, space density dependent nuclear potential. It is done at the expense of much more complicated mathematical model and time consuming calculations. The BUU model has broad application in various fields, from heavy ion collisions to simulations of elementary hadronic processes in nuclear medium. However, for proton induced spallation currently there are not obvious advantages in the predictive power of this model over the much simpler INC approach.

5.1.1.3 Quantum Molecular Dynamics

The goal of Quantum Molecular Dynamics (QMD) model is to reproduce the microscopic conditions of interaction in n-body quantum systems as realistic as possible. Thus, they can be specially useful to simulate the evolution of the atomic nuclei during the reaction induced by single or composite projectile. Significant care is put on the creation of an initial target nucleus in its ground state. The Hamiltonian of the system comprises more possible components than these assumed in simple cascade or BUU models. In the simulation of an evolution of the struck nucleus the fluctuation of nuclear density are allowed. Overlapping of wave function of nucleons may lead to creation of stable composite particles and their emission.

In the literature various formulations of models are available, which follow the philosophy of QMD approach in description of the interaction in nuclear n-body systems. They are created for different applications and may vary as to individual components, assumption, parameters. A review article about QMD models can be found in [101]. Here, in order to give an example of one of the QMD model realization the model described in [102] called JQMD (Jaeri Quantum Molecular Dynamics) will be discussed.

In the QMD model nucleons are described with the wave functions of $\phi_i(\vec{r},\vec{p},t)$. i is the nucleon index, t is time and $\vec{r}$ and $\vec{p}$, are Cartesian coordinates of position and momentum in selected reference frame, respectively. The wave functions have a Gaussian shape of the width L. The whole interacting system is described by a product of the wave functions of participating particles:

$$\phi(\vec{r},\vec{p},t) \;=\; \prod_i \phi_i(\vec{r},\vec{p},t) \;=\; \prod_i \frac{1}{(2\pi L)^{3/4}}\; exp\left[-\frac{(\vec{r}-\vec{R}_i(t))^2}{4L} + \frac{i}{\hbar}\vec{P}_i(t)\cdot\vec{r}\right] . \qquad (5.18)$$

$\vec{R}_i(t)$ and $\vec{P}_i(t)$ describe the position and momentum evolution of the center of wave packet in time. The initial target nucleon (for $t = 0$) is constructed in the following way:

- the spatial positions of centers of nucleons' wave packets are sampled randomly within the assumed Woods-Saxon distributions (cf. equation 5.1). In order to limit the initial density fluctuations the constraints on the mutual distances of nucleons are put on: minimal distance between proton and neutron is 1.0 fm and for nucleons of the same isospin - 1.5 fm;
- the momenta of nucleons are distributed randomly in a sphere of the radius equal to the Fermi momentum;
- with the known density distribution the nuclear potential distribution is constructed.
- the unbound particles of the positive energy (sum of kinetic and potential energy) are disregarded;
- the particles which violate the Pauli exclusion principle are disregarded as well;
- the binding energy per nucleon must agree with the value calculated from the drop model formula within the error of 0.5 MeV.

The Hamiltonian H given below comprises the components from total relativistic energy (first term), nuclear potential parametrized with the effective Skyrme interaction (second and third terms), Coulomb interaction (fourth term) and symmetry energy (fifth term):

$$H \;=\; \sum_i \sqrt{m_i^2 + P_i^2} \;+\; \frac{1}{2}\frac{A}{\rho_0}\sum_i \langle\rho_i\rangle \;+\; \frac{1}{1+\sigma}\frac{B}{\rho_0^\sigma}\sum_i \langle\rho_i\rangle^\sigma \;+$$
$$\frac{1}{2}\sum_{i,j\neq i} c_i c_j \frac{e^2}{|\vec{R}_i - \vec{R}_j|}\Delta\left(\frac{|\vec{R}_i - \vec{R}_j|}{\sqrt{4L}}\right) \;+\; \frac{C_S}{2\rho_0}\sum_{i,j\neq i}(1 - 2|c_i - c_j|)\rho_{ij} \;, \qquad (5.19)$$

where:

$$c_i = \begin{cases} 1 & \text{for protons} \\ 0 & \text{for neutrons} \end{cases}$$

C_S = 25 MeV - parameter of the symmetry energy,
function Δ - error function,
$\langle\rho_i\rangle$ - overlap of nucleon density of i-th nucleon with the nucleon density of the rest of the nuclear ensemble.

The meaning of other parameters is the same as in case of the BUU model (cf. subsection 5.1.1.2). The selected values of parameters are: L = 2 fm, A = -219.4 MeV, B = 165.3 MeV, σ = 4/3.

In order to simulate the reaction process the wave functions representing the moving nucleons are propagated in the target nucleus according to the classical Newtonian equation of motion in the mean field. Particles can collide if the minimal distance of their approach is lower than the appropriate geometrical cross sections. Interactions are allowed only among projectile and medium particles or among those medium particles which already experienced the collision. Elastic and inelastic scattering are taken into account. In inelastic collisions the production of $\Delta(1232)$ and $N^*(1440)$ are included. Decay of these resonances is an origin of pions. Collisions with the final state violating the allowed phase space occupation are blocked.

The advantage of the QMD model over the described above INC and BUU ones consist in explicitly included mechanism of composite particle creation. Approximation of nucleons with their wave function permits observation of the density fluctuation and application of further criteria on space, momentum, isospin, binding and excitation energy in order to judge about the probability of composite cluster formation.

A significant disadvantage of the QMD approach is the complexity of the model and number of mathematical calculations needed for such realistic simulation of the reaction process. A time consuming calculations and relatively low predictive power of the QMD model which is not higher than these of much simpler microscopical models (as e.g. INC) makes the QMD nowadays still not really competitive to INC or BUU. The obvious advantage of QMD in providing the intrinsic mechanism for composite particle production can be compensated by adapting of the coalescence mechanism for cluster emission as it is done in INCL or BUU calculations.

Other examples of realization of the QMD modeling of the problems related to the spallation physics can be found in [103], [69], [104].

All three described above models can be used as the tools for simulation of the initial phase of projectile-target interaction. In this period the energy and momentum are transferred to and dissipated in the target via the cascade of subsequent collisions among the nucleons and created particles. This first step is fast and its duration is of the order of few hundreds of fmc. After this dynamical stage, when the remnant nucleus could be already thermalized, it is reasonable to apply the statistical models in order to simulate the further fate of a struck target nucleus.

5.1.2 Second step - statistical processes

In the two step model of spallation the statistical processes apply when the energy and momentum transfer from the impinging particle was finished and the energy dissipation inside the remnant nucleus was completed. Under such conditions the target-like remnant can be considered as an exited but energetically equilibrated compound nucleus. Below the presentation of a few models describing the statistical processes relevant to the spallation physics is given.

5.1.2.1 Generalized Evaporation Model GEM

According to the Weisskopf-Ewing formalism [57] the nucleus i excited to the energy E^* can emit a particle j of the CM kinetic energy ϵ with the probability $P_j(\epsilon)$ dependent on the cross section of the inverse reaction $\sigma_{inv}(\epsilon)$ and the densities of states of the parent and the daughter nucleus ρ_i, ρ_d, respectively. This probability is given by the formula:

$$P_j(\epsilon) \;=\; g_j \sigma_{inv}(\epsilon)\; \frac{\rho_d(E_i^* - Q - \epsilon)}{\rho_i(E_i^*} \; \epsilon d\epsilon \;, \tag{5.20}$$

where:
Q - the reaction heat;
$g_j = (2S_j + 1)\ \frac{m_j}{\pi^2\hbar^2}$;
S_j = spin of j particle;
m_j = mass of j particle.

For the purpose of the General Evaporation Model [63], [64], where the emission of particles from the exited nucleus in energy equilibrium is simulated with the Monte Carlo technique the density of states given by formula of Gilbert-Cameron [105] with modification as in LAHET code [106] was adapted. The inverse reaction cross section $\sigma_{inv}(\epsilon)$ was parametrized in the appropriate way.

The kind of emitted particle j is determined by sampling the probability distribution p_j:

$$p_j = \frac{\Gamma_j}{\sum_j \Gamma_j}\ . \tag{5.21}$$

Above Γ_j is a probability of emission of particle j and is given by:

$$\Gamma_j\ =\ \frac{g_j}{\rho_i(E_i^*)}\ \int_V^{E_i^*-Q} \sigma_{inv}(\epsilon)\rho_d(E_i^* - Q - \epsilon)\ \epsilon d\epsilon\ . \tag{5.22}$$

In the above formula the integration over the energy takes place in the range from the relevant value of Coulomb barrier, V, to maximal available energy, $E_i^* - Q$.

In the GEM model the emission of both the stable as well as the exited ejectiles is considered. They must have a half-life time longer than 1 ms. In total 66 isotopes of Z < 13 are probed for emission.

For the angular dependence of simulated double differential cross section in the GEM model isotropic emission in CM system of parent nucleus is assumed.

Since the Weisskopf-Ewing formalism disregards the orbital degrees of freedom also in the GEM model the angular momenta of involved particles are not taken into account.

5.1.2.2 Model GEMINI of sequential emission

In the model GEMINI [107, 59] describing the sequential evaporation from exited compound nucleus differently than in the Weisskopf-Ewing approach the angular momenta of nucleons, the energies of rotation and deformation are taken into account.

For the description of emission of light products with Z ≤ 2 the Hauser-Feshbach formalism is utilized [58] whereas for calculation of the emission probability of heavier ejectiles of Z > 2 the formalism of Moretto [108] is used. In both cases the decay widths Γ are calculated. For Z ≤ 2:

$$\Gamma_{J_2}(Z_1, A_1, Z_2, A_2)\ =\ \frac{2J_1 + 1}{2\pi\rho_0} \sum_{l=|J_0-J_2|}^{J_0+J_2} \int_0^{E^*-B-E_{rot}(J_2)} T_l(\epsilon)\rho_2(U_2, J_2)\ d\epsilon\ , \tag{5.23}$$

where Z_i, A_i, J_i are atomic number, mass number and spin of ejectile ($i = 1$) and daughter nucleus ($i = 2$), respectively. l, ϵ are angular momentum and kinetic energy of the ejectile and $\rho_2(U_2, J_2)$ is a level density of the daughter nucleus dependent on its spin and thermal excitation energy U_2. Moreover, Γ depends on the transition coefficient $T_l(\epsilon)$ taking a value of 0 or 1 depending on the value of ϵ compared to the Coulomb barrier. In the integration the upper limit of the total excitation energy is diminished by an appropriate binding energy of the ejectile in

the parent nucleus and the rotation and deformation energy $E_{rot}(J_2)$ of the daughter nucleus. The latter is calculated according to formula given by Sierk [109].

The decay width for emission isotopes with Z > 2 is dependent on ρ_{sad} and U_{sad}, which are the level density and the thermal excitation energy of the parent nucleus at the saddle point. The formula for calculation of Γ is as follows:

$$\Gamma(Z_1, A_1, Z_2, A_2) \;=\; \frac{1}{2\pi\rho_0} \int_0^{E^*-E_{sad}(J_0)} \rho_{sad}(U_{sad}, J_0)\; d\epsilon \;. \tag{5.24}$$

U_{sad} is obtained from:

$$U_{sad} \;=\; E^* \;-\; E_{sad}(J_0) \;-\; \epsilon \;, \tag{5.25}$$

whereas the $E_{sad}(J_0)$ - the rotation and deformation energy at the saddle point is calculated again according to [109]. The index "0" applies here to the parent nucleus and remaining quantities have the same meaning as described above.

Level densities needed for calculation of decay probabilities are calculated in the framework of the Fermi gas model:

$$\rho(U, J) \;=\; (2J+1) \left[\frac{\hbar^2}{2\xi}\right]^{3/2} \frac{\sqrt{a}\; exp(2\sqrt{aU})}{12\; U^2} \;, \tag{5.26}$$

where ξ is the inertia moment of daughter nucleus and a is equal to $A/8.5\; MeV^{-1}$ and is a level density parameter.

In order to make a sampling of the probabilities feasible with the Monte Carlo technique simplifications of the above formulae are introduced consisting in replacing of the integrals with summations over proper ranges.

The products of binary decay can be an excited particle, which undergoes a subsequent decay. Thus, apart from its mass and charge also the excitation energy and spin have to be calculated.

In the GEMINI model the compound nucleus is sampled for subsequent binary decays as long as γ-decay probability takes over or until the remaining excitation energy will be insufficient for another particle emission.

5.1.2.3 Simultaneous fragmentation - Fermi Breakup Model

The Fermi Breakup [110] adapted to spallation reaction in [111] is the oldest among described here models of decay of exited compound nucleus. In this model it is assumed that the disintegration of exited nucleus occurs in one act of violent fragmentation. The breakup takes place when due to internal excitation the density of the nucleus drops below the normal nuclear density of $\rho = 0.16$ nucleon/fm^{-1} and the volume, V, of a nucleus attains the so-called freeze-out value:

$$V = \frac{4\pi}{3}\; r_0^3 A_0 \tag{5.27}$$

depending on the r_0 parameter, which is usually fixed to 1.3 - 1.4 fm. A_0 is a mass number of a decaying nucleus.

Considered are probabilities of various fragmentation channels with n particles in the final state. In the nonrelativistic approximation the probability of fracture of a nucleus of mass M into n particles of masses m_i can be calculated as:

$$P(E_{kin}, n) \;\propto\; S_n \cdot G_n \left(\frac{V}{\hbar^3}\right)^{n-1} \cdot \left(\frac{\prod_{i=1}^{n} m_i}{M}\right)^{3/2} \cdot \frac{(E_{kin} - U_C)^{\frac{3n-5}{2}}}{(2\pi)^{\frac{3}{2}(n-1)}\; \Gamma(\frac{3}{2}(n-1))} \;. \tag{5.28}$$

In the above equation $\hbar$ is a reduced Planck constant and $\Gamma(\frac{3}{2}(n-1))$ is a mathematical Γ function. The spin, s, degeneracy factor, S_n, is given by:

$$S_n = \prod_{i=1}^{n} (2s_i + 1) \tag{5.29}$$

and the possible identity among the emitted particles is taken into account by introducing the permutation factor G_n:

$$G_n = \prod_{j=1}^{k} \frac{1}{n_j!} \, . \tag{5.30}$$

. A sum of all kinetic energies of emitted particles have to be equal to:

$$E_{kin} = E^* + M_0 c^2 - \sum_{i=1}^{n} m_i c^2 \, , \tag{5.31}$$

where E^* is the excitation energy and M_0 is the rest mass of a parent nucleus. The Coulomb energy of the initial nucleus at the freeze-out moment is given by a Wigner-Seitz approximation:

$$U_C = \frac{3e^2}{5r_0} \left[\frac{Z_0^2}{A_0^{1/3}} - \sum_{i=1}^{n} \frac{Z_i^2}{A_i^{1/3}} \right] \, . \tag{5.32}$$

A_0 and Z_0 are the mass- and atomic number of initial nucleus whereas the A_i and Z_i apply to the mass- and atomic numbers of fragments.

With the increase of the mass of the initial nucleus the number of possible final configurations increases rapidly. This is a factor which limits the application of the Fermi breakup model to the sampling of decay probabilities of only relatively light nuclei composed of up to several nucleons.

5.1.2.4 Statistical Multifragmentation Model (SMM)

The authors of the Statistical Multifragmentation Model - Bondorf at al. ([65]) assume that if a large amount of energy is accumulated in the compound nucleus its disassembly will proceed by a simultaneous breakup into fragments. But different than in a simpler Fermi Breakup Model, where the resulting particles are stable isotopes in their ground state, in SMM the fragments can be objects in the states far from stability. They may undergo subsequent decay via evaporation or breakup. The interaction of fragments when they are already released from the initial nucleus is taken into account as well.

A detailed consideration of the dynamics of individual decay channels as it is done in the models described above are replaced by a statistical approach. It is postulated that the decaying system is thermalized, all microscopic states of a system are of the same probability and the thermodynamical parameter like temperature T can characterize the examined nuclear ensemble.

The SMM is a very advanced model which includes the formalism of thermodynamic with consideration of various statistical ensembles (microcanonical, canonical, macrocanonical), their entropy and free energy.

The model is able to predict the main features of nuclear disintegration in a broad range of temperatures or excitation energies. For the lowest excitation energies ($E^* < 5$ MeV/nucleon) the mass distribution is similar like in the case of a decay of weakly excited compound nucleus - one large remnant-like fragment and a few light clusters. In this energy range the SMM

model is equivalent to a Fermi breakup mechanism. At $E^* \approx 5$ MeV/nucleon the onset of mulifragmentation is observed which is accompanied with a decrease of the masses of ejectiles. With further increase of the E^* the system has a tendency to breakup into more fragments of the lower masses. At still higher excitation energies exceeding 10 - 15 MeV/nucleon only the lightest cluster and nucleons are predicted which is attributed to the vaporization of the nucleus.

A detailed description of the Statistical Multifragmentation Model is given in [65].

5.2 Alternative hypotheses of nuclear disintegration

An alternative approach to describe the spallation process is based on an assumption that when a bombarded nucleus accumulates a sufficiently high amount of excitation energy it undergoes an expansion with decreasing density and increasing temperature. In this way it may reach the thermodynamical condition when a transition from a liquid phase into a gaseous one takes place. There are theoretical papers, e.g. [112], [113], predicting the possibility of this scenario of nuclear disintegration. The liquid-gas phase transition was also applied to interpretations of experimental results of various experiments. In [114] and [115] an evidence is claimed to be found of a continuous phase transition for p-Au and ^{3}He-Ag reaction already at 5 GeV incident energy. In [116] and [117] the authors report a phase transition for p-Au collision at 8.5 GeV. There is, however, a disagreement in the extracted value of critical temperature for onset of the transition. It seems that the mechanism of liquid - gas phase transition concerns the reactions with high beam energies which are beyond the scope of the present work. A review of the achievements in the field of nuclear phase transition mechanism is given in [118].

A hypothesis which may have an application in the interpretation of the data collected in the PISA experiment and other experimental efforts performed in a similar energy range is formulated in [119]. According to this hypothesis an energetic proton impinging onto the target nucleus induces its fast fragmentation into a few exited prefragments. These prefragments would deexcite with emission of single and composed particles observed in experiments. The initial breakup of the target nucleus can be induced by a creation of so-called fireball - an instantaneous knock-out from the bombarded nucleus of a group of a few nucleons being subjected to the direct interaction with a projectile. There are several papers dealing with interpretation of various experimental results in the framework of the initial fragmentation mechanisms. Among them are [120], [121], [122], [123], [124], [125]. The incident energy range of the recalled experiments lays in the range from 0.45- to 400 GeV and concerns the heavy target of uranium.

The hypothesis of the fireball formation and its more advanced version of firestreak was also proposed and developed in the context of heavy ions reactions in [126, 127, 128, 129, 130].

6 The two step model confronted with experimental results of PISA

In this chapter the most general successes as well as the deficiencies of the theoretical two step model in the description of the real experimental distributions will be presented. For this purpose the INCL4.3 simulations of the first step of reaction coupled with the GEM2 used for modeling of the evaporation part of the spectra will be confronted with the experimental distributions obtained by the PISA collaboration. Since, as concluded in chapter 4, the shapes of the experimental distributions obtained for proton beam energies of 1.2, 1.9 and 2.5 GeV are the same and the distributions varies only a little in their magnitudes for comparison with the model calculation only the data collected at 1.9 GeV bombarding energy will be used. Selecting the INCL model among other available "first step" models is well justified since its results are representative for the binary cascade approach and are better than these of available QMD models (see e.g. [131]).

Applicability of the INCL4.3 model is restricted only to predictions of the LCPs up to ^{4}He. This limitation is an effect of the complicated software realization of the coalescence mechanism assumed in the INCL model. In the INCL4.6 version the creation of the LCP has been extended up to mass A=8, however, the number of arbitrary parameters in the model had to be increased [70].

In order to keep the consistency of the theoretical results of different models which are used in this dissertation for their reliable comparison it was decided that distributions obtained from the model calculations are always normalized to the value of the total reaction cross section calculated with the use of the same parametrization. Of course, the values of projectile energy and the type of the target nucleus are taken into account. For an absolute normalization of the theoretical results shown in this chapter as well as throughout this dissertation the semiempirical parametrization of the total reaction cross sections as proposed by Letaw, Silberberg and Tsao [132] is used. The advantage of the Letaw et al. parametrization over other available parametrizations of the total reaction cross section (see e.g. [133, 134, 135, 136, 137, 138]) consist in the simple mathematical formulation and the precision which is sufficient for the considered here range of energies, target materials and the accuracy of applied theoretical calculations. For incident proton energies higher than 1.0 GeV the estimated error of the Letaw semiempirical formula is about 2%.

The PISA spectra (open circles) supplemented with the theoretical distributions for p, d, t, ^{3}He and ^{4}He (dashed green line) are shown in figures 6.1, 6.2, 6.3, 6.4 and 6.5, respectively.

The conclusions drawn from the inspection of the above figures and a comparison of experimental data with the model calculations are as follows:

- the description of the low energy part of the spectra attributed to the evaporation process is rather satisfactory. Both the slopes, as well as the magnitudes and the positions of the maxima (in these cases where they are visible in the data) are well reproduced with the GEM2 model. It shows that both the GEM2 model is appropriate to simulate statistical evaporation processes in the relevant physical conditions as well as the INCL4.3 simulations create the cascade remnants of the realistic parameters as concern their mass, charge, recoil momenta and excitation energy;

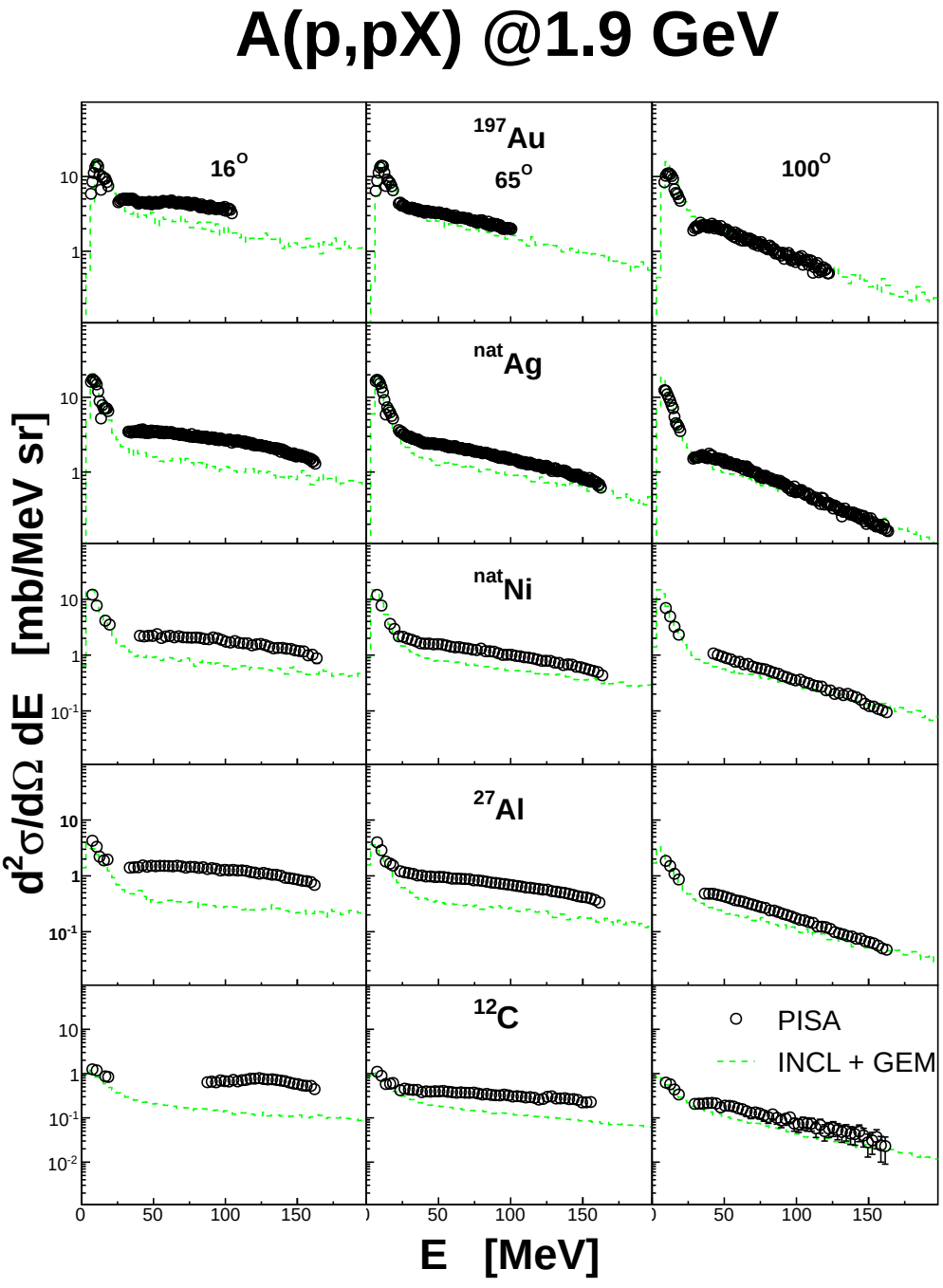

Figure 6.1: INCL model calculations of double differential cross section for proton emission from various target nuclei bombarded by 1.9 MeV protons (dashed line, green). Simulations are compared to experimental distributions of the PISA experiment (open circles).

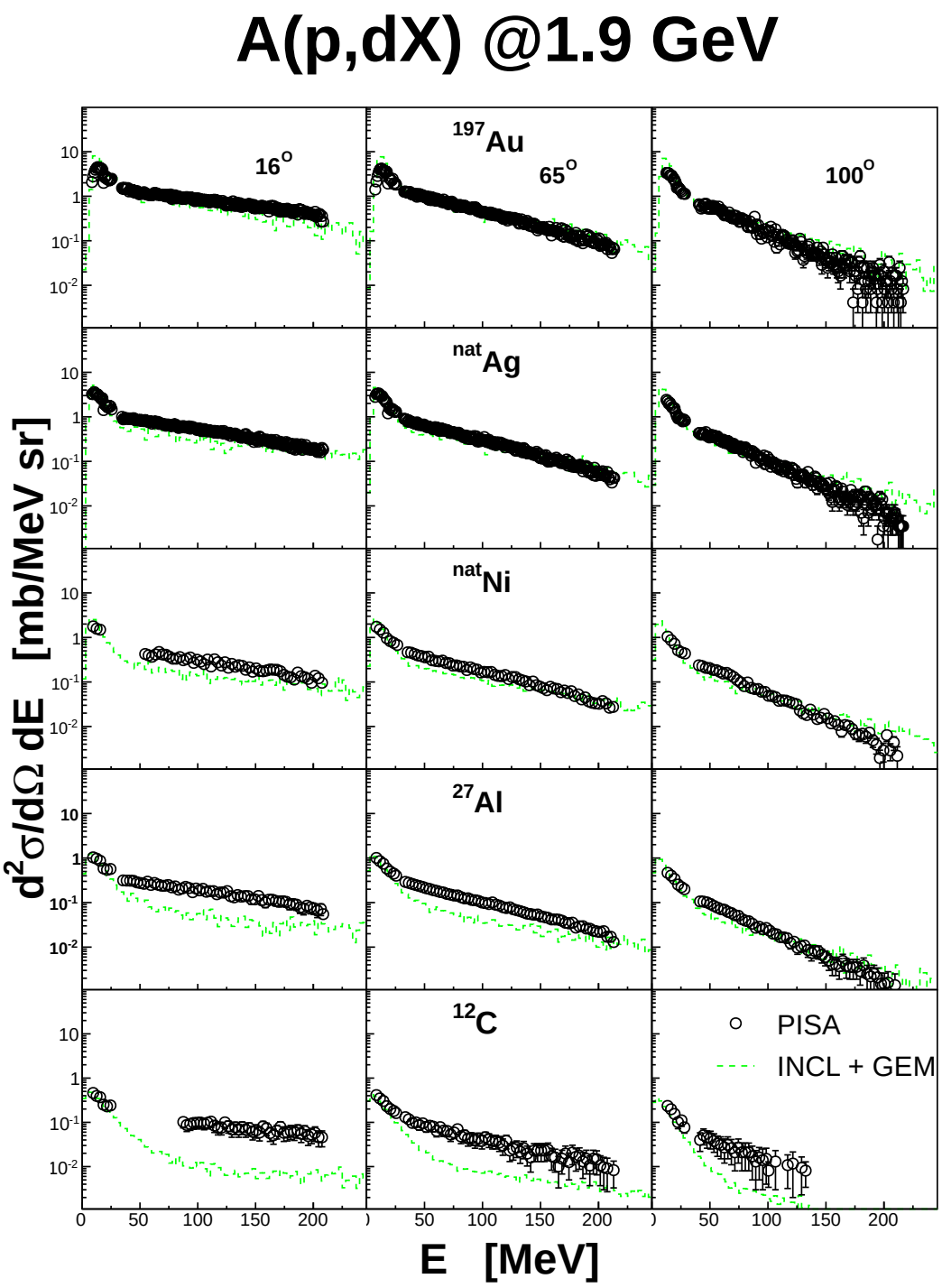

Figure 6.2: The same as in fig. 6.1 but for deuterons.

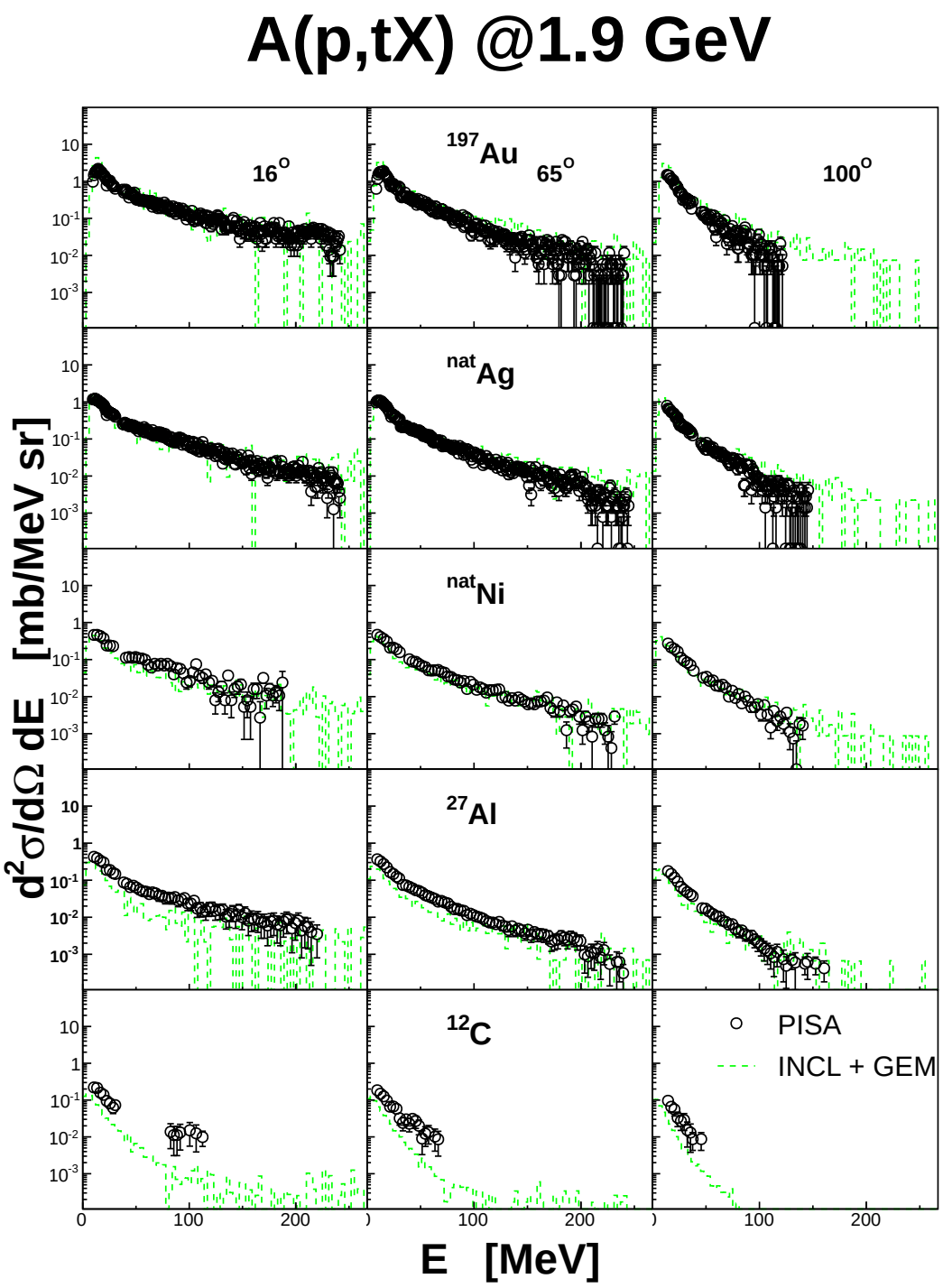

Figure 6.3: The same as in fig. 6.1 but for tritons.

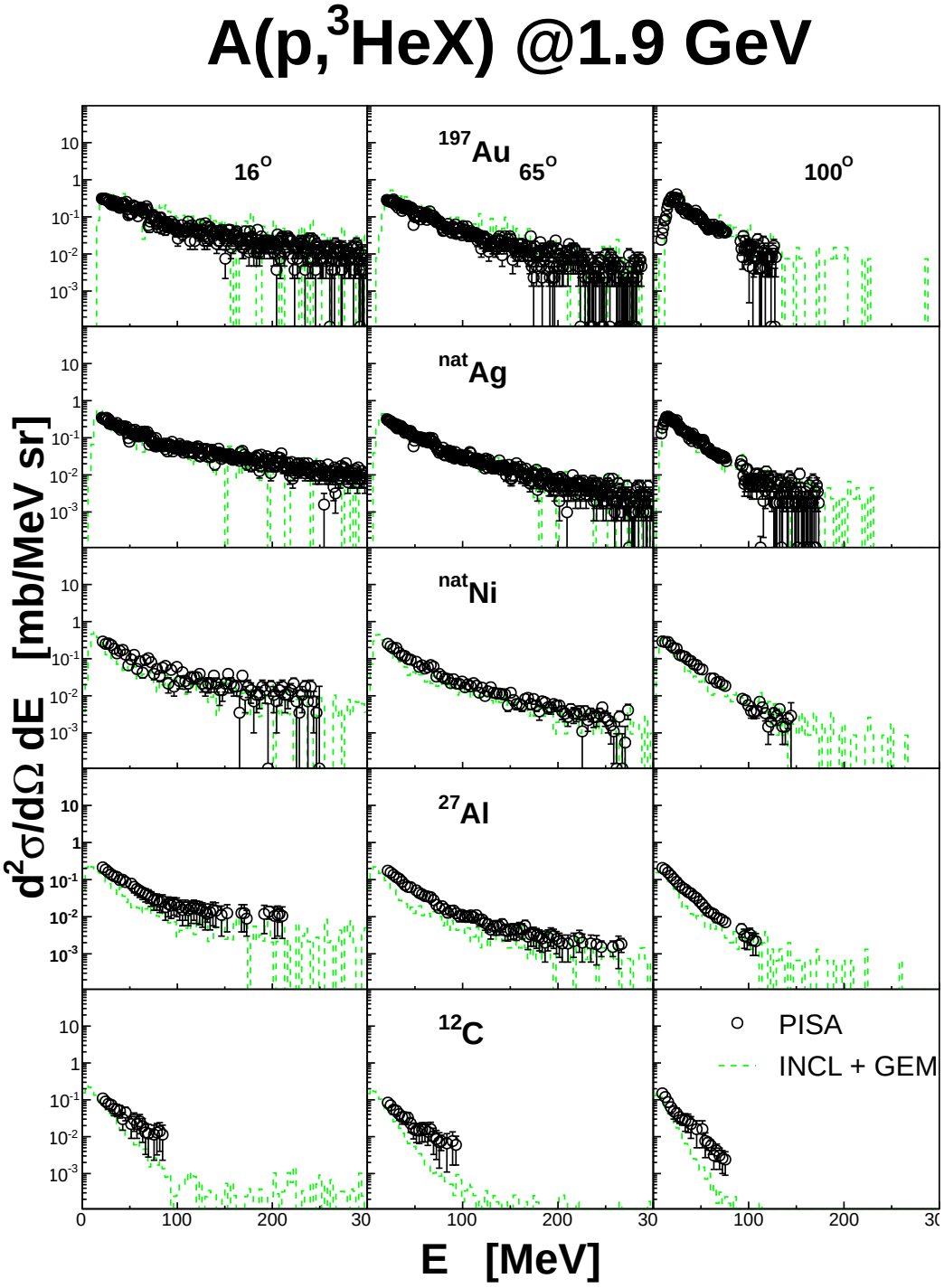

Figure 6.4: The same as in fig. 6.1 but for ^{3}He.

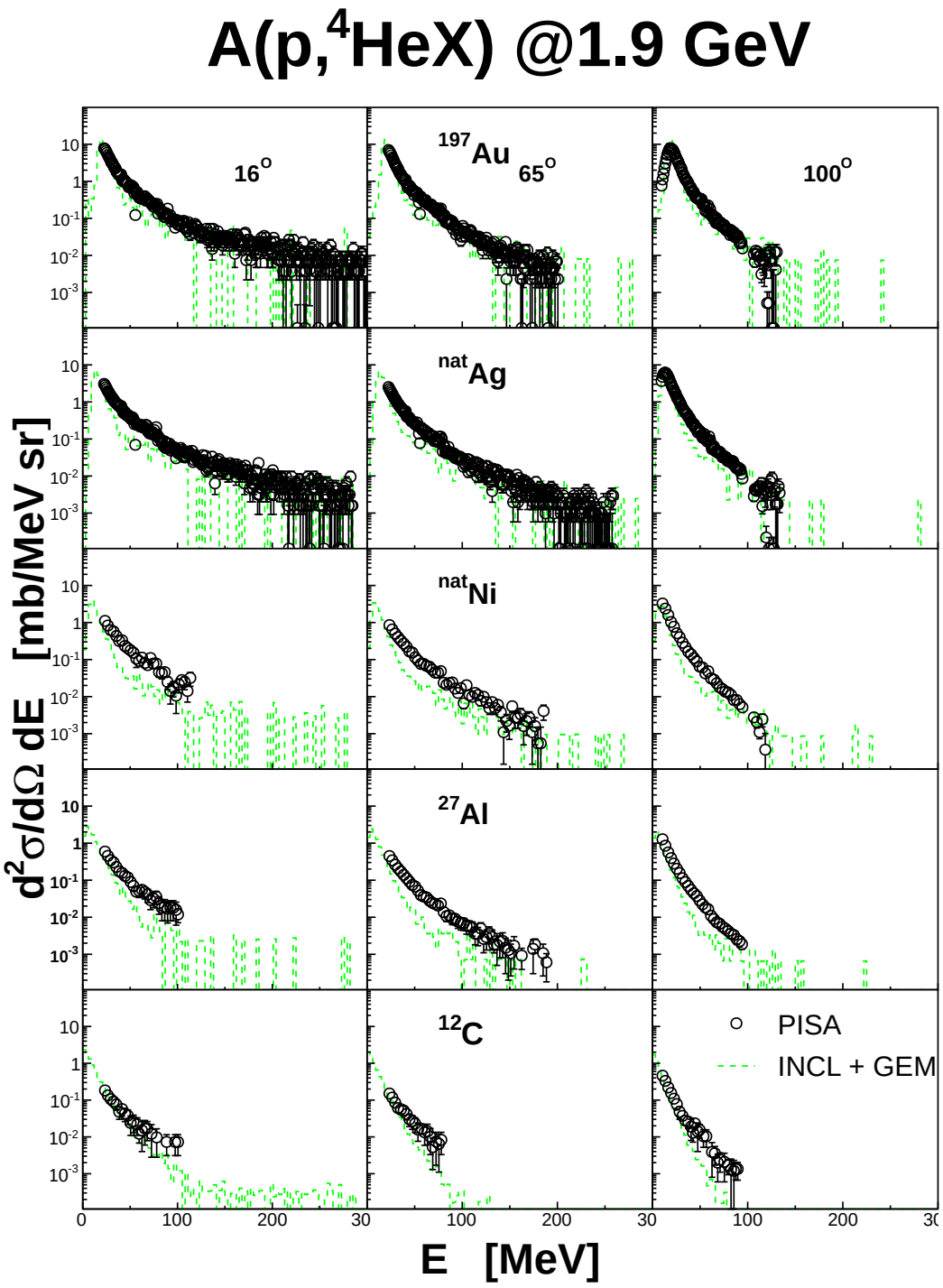

Figure 6.5: The same as in fig. 6.1 but for ^{4}He.

- the part of spectra attributed to the intranuclear cascade are underestimated for protons emitted at low angles. This deficiency is less pronounced for heavy targets like Au or Ag (about factor two) but for Al or C the discrepancy between experiment and the model is very strong and reaches a factor 5 or more;
- with the increase of the emission angle the agreement of the model and experiment improves and for backward angles is quite good. However, still the yields of protons emitted from the heavier targets are better reproduced than those for light ones;
- for composite particles the mechanism responsible for creation and emission of these ejectiles used in INCL4.3 is the surface coalescence. Despite of different nature of mechanisms responsible for single particle emission and composite ones the behavior of the simulated spectra for deuterons, tritons, ^{3}He and ^{4}He is similar to that for protons. The agreement with the experimental distributions is better for heavy target than for the light ones. Also similarly as for protons the differences are stronger for low detection angles and gradually vanish with the increase of the emission angle. It has to be noted that overall agreement of the experimental distributions with the model is better for light composite particles than for protons;
- in general the most significant discrepancies in the description of experimental data are observed for the particle's energies in the range 50-150 MeV and low emission angles.

For the low beam energies the experimental distributions at low emission angles are underestimated for protons and deuterons whereas for the heavier reaction products the model reproduces the data much better.

As it was noticed by the authors of the INCL model the introduction of the coalescence mechanism for extension of the model applicability also to light composite particles deteriorated the predictive power for single ones. Moreover, a significant increase of the number of free parameters of the model was demanded [70].

The simulated distributions of those composite spallation products, which are not considered in the coalescence mechanism (heavier than alpha-particle for the case of INCL4.3) can originate only from statistical processes (evaporation, multifragmentation). As it was shown in [7] and [8] for those IMFs experimental distributions, where the component from the preequilibrium stage might be present their reproduction by the model simulation is wrong for the whole emission energy range, even for the lowest energy where evaporation plays dominant role (cf. fig 6.6). The experimental distributions are underestimated even by one order of magnitude. It shows forcibly that when production of IMFs is disregarded in the preequilibrium reaction stage the parameters of the remnant expected to evaporate these particles are predicted incorrectly. The remnant is insufficiently excited in order to emit the heavier composite particles. However, for the target-ejectile combinations favoring only the evaporation emission the agreement is again better especially for higher emission angles.

The deficiencies of the two step model in reproducing the experimental spallation spectra can not be avoided by a better tuning of the parameters of the involved reaction models. Optimization of parameters like depth of the potential well, radius of nucleus, transparency of the barrier, effectiveness of Pauli blocking, shape of density distribution or even the modification of the values of assumed reaction cross sections may lead to an improvement in a specific region of target-ejectile-energy combinations but will cause the deterioration in the other domains.

For the matter of completeness is has to be mentioned that the two step model with the INCL code as an cascade simulator is very successful in reproduction of the neutron and pion data. The

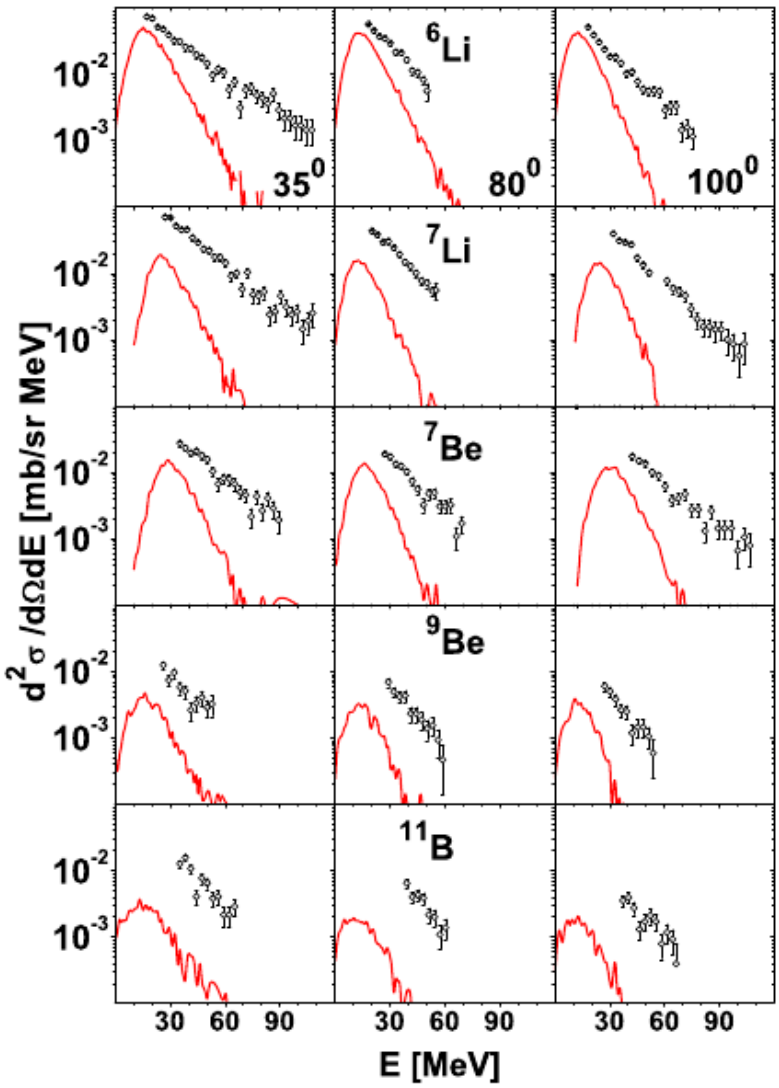

Figure 6.6: Examples of spectra for Li, Be and B isotopes measured in p+Ni reaction at 2.5 GeV in the PISA experiment (open circles). Results of simulations with the two step model (INCL4.3 + GEM2) are presented by the solid line.

quality of the model calculations for these spallation products can be checked in [70] where the experimental data of [39] and [139] are used for validation of theoretical simulations of neutron and pion distributions, respectively.

The partial inadequacy of the two step model in some aspects of the spallation physics, especially in the domain of preequilibrium emission of both the LCP as well the IMF, was a subject of some publications of the PISA collaboration. Similar findings were realized already earlier and quoted both by the experimentalist who tried to interpret their data with the two step model [47], [46] but also by the authors of the codes. The critical summary of the achievements in the field of modeling of nuclear spallation is given in [140]. A broad collection of the appropriate data and their graphical representations are available in [41].

7 Phenomenological analysis of PISA results

As presented in chapter 6 the efforts aiming at interpretation of the spallation product distributions registered in the PISA experiment in the frame of the two step model have confirmed the partial inadequacy of mechanisms implemented in the applied models. This inadequacy concerns in general the yields of preequilibrium particles emitted at forward angles which in the model calculations are usually underestimated. In some cases the disagreement with to the experimental data reaches an order of magnitude.

In order to determine the features of the alternative or the additional mechanisms which could contribute to experimental spallation spectra the model calculations have been supplemented with phenomena not considered in the classical two step model.

The simulations of the fate of the cascade remnants were extended by introducing the multifragmentation mechanism for highly excited remnant nuclei. Alternative scenarios of the spallation reaction was considered with the phenomenological model of moving sources.

7.1 Multifragmentation of the light target nuclei

In the thermalized remnants created after the intranuclear cascade in the light target nuclei such as ^{27}Al and ^{12}C the possible excitation energies per nucleon are higher than in the case of heavier targets bombarded with the protons of the same impinging energy. Thus, it was checked whether the inclusion into the two step model of the mechanism consisting in the fast multifragmentation - the Fermi breakup (cf. chapter 5) of the remnants would improve the simulated spectra. It was executed by simulating the decomposition of remnant, alternatively, either with the evaporation (code GEM2) or with the Fermi break mechanism (code ROZPAD [141]). The selection of the applied mechanism was made on the basis of the actual excitation energy per nucleon of the remnant. For small excitation per nucleon the sequential evaporation of particles was assumed whereas in case of high excitation per nucleon the remnant was subjected to the Fermi breakup. For a simplification of the model calculation it was assumed that occurrence of the both alternative processes is governed with the one sharply defined parameter of the critical excitation energy per nucleon. The value of this parameter was determined by a fit to the data.

Introduction of the multifragmentation as a possible mechanism of the remnant decay helped in better description of the IMF spectra. Some examples are shown in fig. 7.1 for lithium isotopes detected after reaction p+Al at 1.2 GeV and in fig. 7.2 for beryllium isotopes. The sum of contributions from evaporation and multifragmentation reproduces much better the experimental data than the evaporation process alone.

The contribution of the Fermi breakup mechanism to the production of the LCPs turned out to be insignificant.

The critical excitation energy per nucleon obtained from the fit to the experimental data can be related to the studies of a possible liquid - gas phase transition expected for highly excited nuclear matter and examined mainly with the heavy ion collisions. A compilation of experimental values of $(E^*/A)_{cr}$ for different nuclear system was published by Natowitz et al. [142]. In fig. 7.3 the critical energies obtained in the PISA p+^{27}Al data analysis together with those derived from

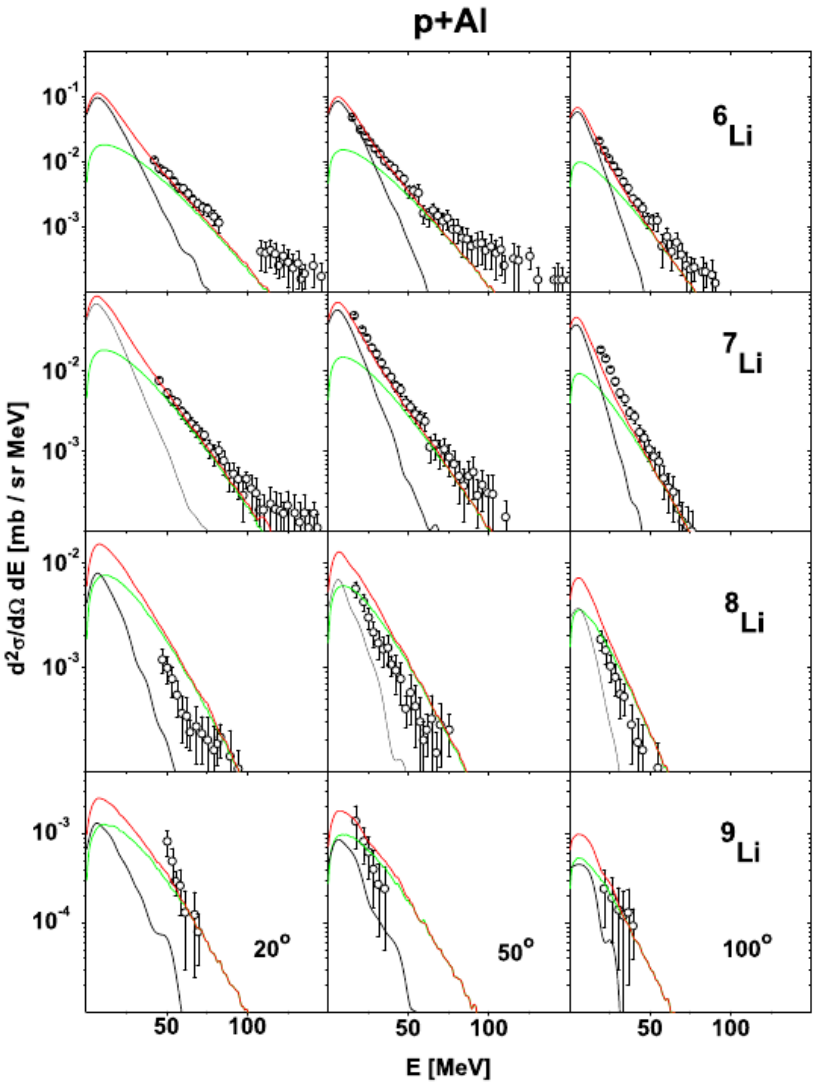

Figure 7.1: The results of the evaporation (black line)/multifragmentation (green line) simulations of the p+^{27}Al reaction at 1.2 GeV proton energy for A = 6, 7, 8 and 9 lithium isotopes detected at 20^0, 50^0, and 100^0 emission angle. The red line represents the sum of both alternative processes. They are compared to the experimental distributions of the PISA experiment (circles). This figure is adapted from [8].

[142] are given. Values of 7.7, 7.0 and 6.1 MeV were obtained for 1.2-, 1.9- and 2.5 GeV beam energy, respectively. They agree with the expected value of $(E^*/A)_{cr}$ for ^{27}Al nuclei within the one standard deviation error of the linear regression to the data of [142].

$(E^*/A)_{cr}$ obtained for p+^{12}C data set have values of 9.0, 7.6 and 8.6 MeV for 1.2, 1.9 and 2.5 GeV proton energy, respectively. Thus, they fit to the values of the compilation of [142] also very well.

An exhaustive discussion of the application of Fermi breakup mechanism to the analysis of the PISA experiment data, the description of fitting procedure and interpretations of the results is given in [8].

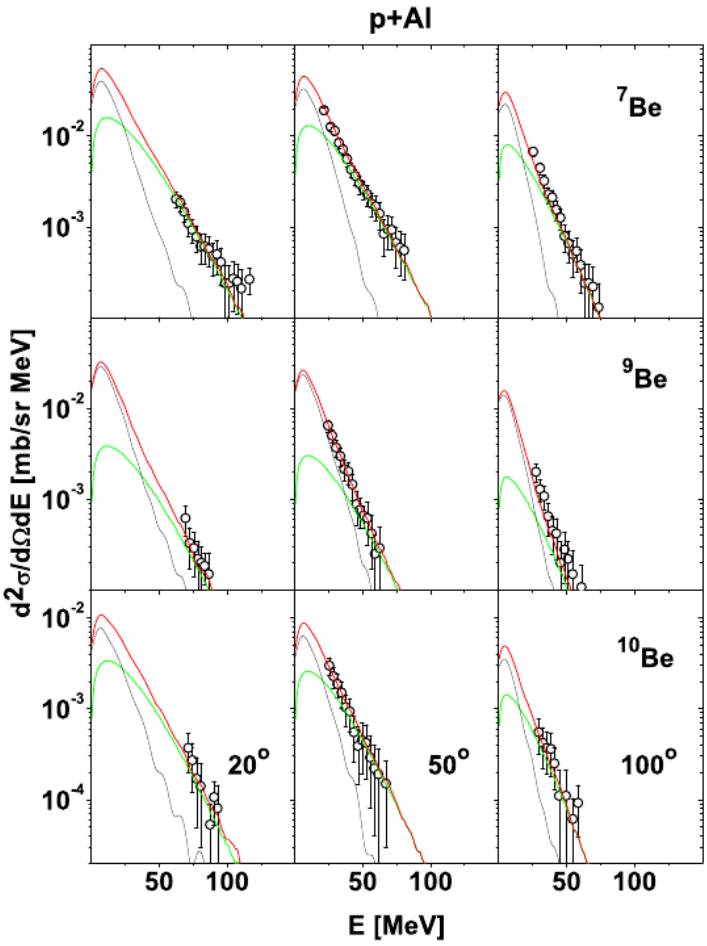

Figure 7.2: The same is in fig. 7.1 but for A = 7, 9, and 10 beryllium isotopes. This figure is adapted from [8].

7.2 The moving source model

The clearly distinguishable at least two components in the energy distributions of the spallation products induced the idea of the Moving Source Model [130]. This model helped to notice and determine the general features of the spallation processes which turned out to be common for broad range of projectile energies and target masses.

In the model it is assumed that observed particles are emitted from the sources which posses some excitation energy and are moving with various velocities along the beam direction. These sources would be an intermediate stage of the target nucleus disintegration after the bombardment and the initial energy dissipation. Target nucleus is then already fractured into separable pieces which are carrying different masses and energies. These fragments, when cooling down, emit particles being the sources of observed ejectiles.

Excited sources are assumed to be thermally equilibrated thermodynamical objects. For emission from such a system a Maxwellian formalism can be applied, which provides analytical probability distribution function. The fitting of the distribution function to the experimental data with some free parameters permits to get information about important features of the emitting source.

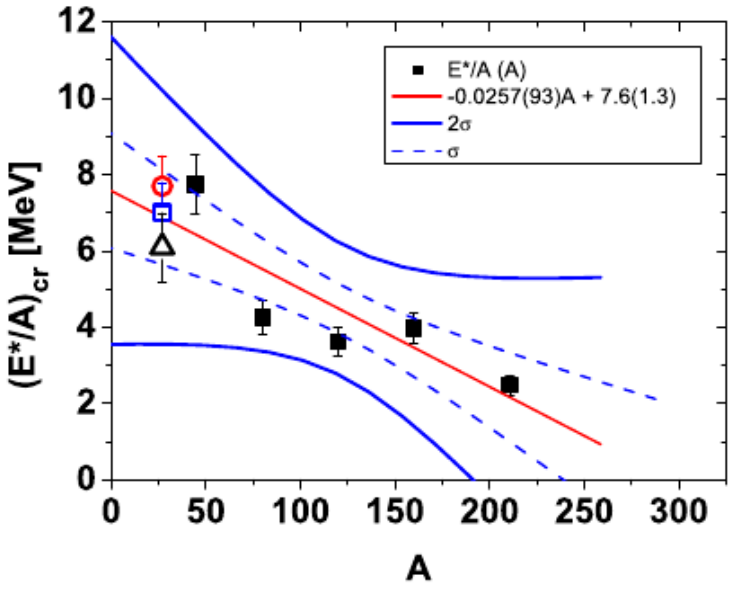

Figure 7.3: A comparison of literature data [142] on the critical excitation energy for the multifragmentation of various nuclei (full squares) with the critical energy parameters derived from the analysis of the experimental results of the PISA experiment. The open triangle, square and circle depict the values obtained for the data of p+^{27}Al collisions collected at 2.5-, 1.9- and 1.2 GeV beam energy, respectively. The red line is an effect of a linear regression to the data from [142]. The blue dashed and blue solid hyperbolas outline the confidence region of the regression for one and two standard deviations, respectively. The values obtained in the PISA data analysis agree well with the literature data. This figure is adapted from [8].

Each of the emitting sources is characterized by an apparent temperature T. The actual temperature τ of the system could be calculated when its exact kinetic energy is accounted for as well. Then:

$$\tau = \nu T \ , \tag{7.1}$$

where,

$$\nu = \frac{A_S}{A_S - A_F} \ . \tag{7.2}$$

A_S, A_F are the masses of the source end emitted fragments, respectively and the factor ν is a measure of the recoil energy of the source.

For each of the emitting sources the energies of emitted particles should be distributed according to a Maxwellian function. The probability distribution of the excitation energy E* of the system characterized by a temperature τ is given by the formula:

$$f(E^*) = \frac{1}{2(\pi\tau)^{3/2}}\sqrt{E^*}exp\left[-\frac{E^*}{\tau}\right] \ . \tag{7.3}$$

The sources emit the particles isotropically in their own reference frame. In the frame of the moving source of mass A_S the ejectile of mass A_F has a kinetic energy $E^{'}$ given by:

$$E^{'} = \frac{E^*}{\nu} \ . \tag{7.4}$$

When normalized to the total production cross section σ the probability distribution can be associated with the double differential cross section and rewritten as:

$$\frac{d^2\sigma}{dE'd\Omega'} = \frac{\nu\sigma}{2(\pi\tau)^{3/2}}\sqrt{\nu E'}exp\left[-\frac{\nu E'}{\tau}\right] . \tag{7.5}$$

The necessary transformation of the cross section calculated for the rest frame of the moving source to the laboratory system is given by the equation:

$$\frac{d^2\sigma}{dEd\Omega} = \frac{p}{p'}\frac{d^2\sigma}{dE'd\Omega'} \approx \sqrt{\frac{E}{E'}}\frac{d^2\sigma}{dE'd\Omega'} . \tag{7.6}$$

Above p and $p^{'}$ are momenta of the ejectile in the laboratory- and source rest frame system, respectively. E is the energy of ejectile registered in laboratory reference system at angle θ_{LAB}. The second approximation in the above formula is valid in nonrelativistic limit. For emitting source which is moving with a velocity β the energy E of the ejectile of mass m is given by the transformation relation:

$$E^{'} = E + \frac{m\beta^2}{2} - \sqrt{2mE}\beta cos(\theta_{LAB}) . \tag{7.7}$$

In the above consideration the suppression of the emission of low energy charged particles due to existence of Coulomb barrier is omitted. Thus, in order to retain the interpretation of the parameter σ as a total production cross section and preserve a direct comparison of fitted function to the experimental spectra, the energy dependent probability function $P(E)$ of barrier penetration was introduced in the form:

$$P(E) = \frac{1}{1 + exp[-\frac{(E-kB)}{d}]} . \tag{7.8}$$

Here B is the height of Coulomb barrier for the two touching spherical nuclei of charges Z_F and $Z_S - Z_F$ and radii $A_F^{1/3}$ and $(A_S - A_F)^{1/3}$ and is given by the equation:

$$B = \frac{Z_F(Z_S - Z_F)e^2}{1.44[A_F^{1/3} + (A_S - A_F)^{1/3}]} . \tag{7.9}$$

In this sense the parameter k should be smaller than 1 and describe the height of the Coulomb barrier of actual source-ejectile system. The d has interpretation of the diffuseness of the barrier. The use of the k and d as free parameters of the fit let to introduce a realistic spread of the barrier heights for various combinations of sources and ejectiles. It let to take into account the tunneling effects smoothing the low energy edge of the energy spectra, as well. The probability function $P(E)$ has to be used as an additional factor in the formula for the cross section (equation 7.5).

A detailed description of the model of the emission from moving sources used for phenomenological interpretation of double differential cross section measured in the PISA experiment is given in [10, 7, 8].

It was shown in [130] that a sum of at least two Maxwell-Boltzmann distributions is needed for a simple reproduction of the two observed components in the spallation energy spectra. It was however noticed [143] that exact description of complicated phenomenons hidden behind the word "spallation" may imply the needs of a "continuum" of various emitting sources.

7.3 Idea of competition of various mechanisms

In order to aid for the missing yields of particles in the two step model calculation it was tried to combine the mechanisms of evaporation and intranuclear cascade supplemented with coalescence with the emission from the moving sources. The idea of competition of the two step model and the moving sources is presented schematically in fig. 7.4. The contribution of individual scenarios of the reaction is governed by a probability given by the parameter F.

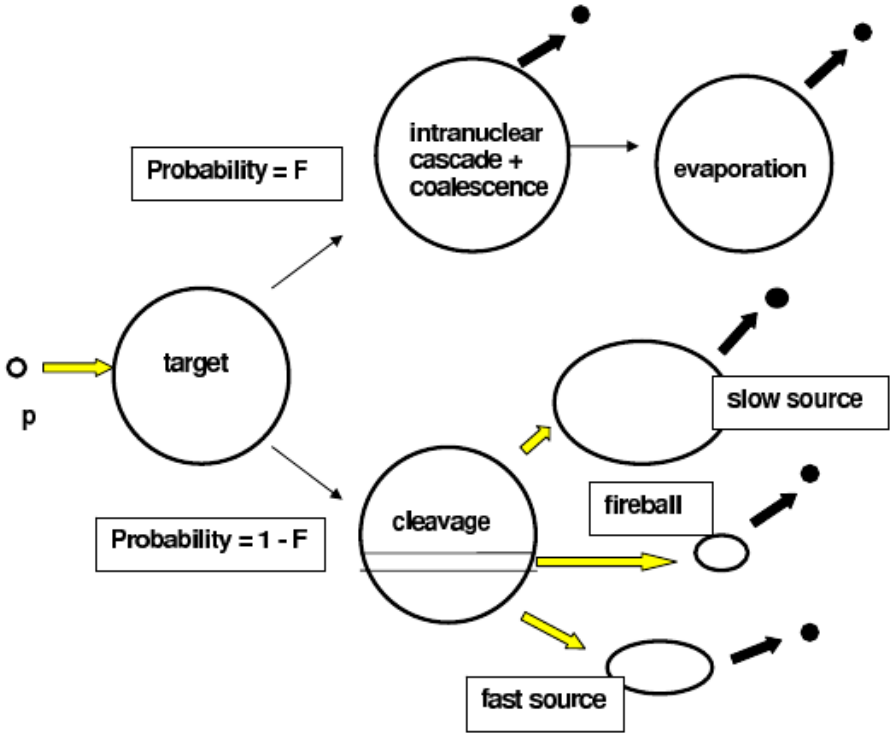

Figure 7.4: The idea of competition of the two alternative scenarios of the spallation reaction as applied in the interpretation of the experimental data of the PISA experiment. The probability F depicts the occurrence of a scenario realized with the two step model. More involved mechanisms are then a cascade of binary interaction, a coalescence and evaporation. An alternative scenario i.e. a fragmentation of the target nucleus into three intermediate objects being the sources of the observed particles appears with probability 1 - F. This figure is adapted from [7].

Besides of the "two step" scenario occurring with the probability F and consisting of intranuclear cascade associated with the surface coalescence and followed by evaporation it is assumed that the spallation reaction can proceeds with the probability 1-F via the target breakup into two or three pieces of different masses, momenta and excitation energies. As the reason of the fracture of the initial target nucleus a significant distortion of the nucleus stability due to sudden expel of a few nucleons is assumed. These target nucleons which are in head-on collision with the projectile are emitted in the initial phase of the reaction as a so-called "fireball" - a fast and highly excited piece of nuclear matter.

For the analysis of the PISA data the assumption of at least one moving source has been needed. A description of the reactions with the heavier targets needed more sources - up to three ones. They were called as follows: fireball - the smaller but the fastest fragment of the target breakup, fast source - composed of several nucleons and of significant kinetic energy, and slow source -

a massive fragment with low velocity. Each of these fragments is responsible for emission of different classes of observed spallation products.

The features of the sources and the branching probability F of the type of the spallation scenario were determined by a fitting procedure of the above described model with the free parameters characterizing each source: the temperature, T, the velocity, β, and the energy and angle integrated cross section for production of an individual particles, σ. The best values of the parameters was derived from a simultaneous fit to the experimental data collected at seven emission angles: 16^0, 20^0, 35^0, 50^0, 65^0, 80^0 and 100^0.

In order to overcome the problems resulting from the missing in the data position of the Coulomb barrier peaks the necessary assumptions have to be done. The heavy source was attributed to the cascade remnant of the two step model and thus reasonable cross sections, source velocities, and Coulomb barrier heights could be fixed as the average values of those obtained from the intranuclear cascade and evaporation. The problems related to the fitting procedures, introduced simplifications and their influence on the obtained results are exhaustively presented in [7].

The procedure of parameter fitting of the moving sources supplemented with the two step model has been applied to interpret the experimental results of both the heavy target like ^{197}Au [11], the intermediate mass target (^{nat}Ni [12], [13], [7]) as well as the light ones (^{27}Al and ^{12}C [14], [8]). In the case of light target i.e. the ^{27}Al and ^{12}C contribution of the Fermi breakup mechanism of the target-like remnant was considered in addition. For the two latter targets of the lowest masses and the lowest probability of splitting them into a few massive fragments instead of fitting three moving sources the fit of only the fireball component was applied.

Some examples of simulation results of competition between assumed scenarios for the proton induced spallation are given in the following subsections. It has to be pointed out that in all examined cases the particle emission from intermediate reaction states - the postulated moving sources - has compensated very well the deficiency of the two step model. In the course of analysis it was realized that each of the assumed moving sources contribute mainly to production of one class of particles. It was found that the fireball is a source of protons and other light charged particles. The IMFs particles originate predominantly from the decay of fast source whereas the slow source can be attributed to the after-cascade remnant and might be responsible for distributions of the lowest energy particles.

7.4 Results for Light Charged Particles

It was found for all targets that the dominant source of LCPs (besides of those which are produced in the cascade, coalescence and evaporation) is the fastest and lightest fragment of target splitting, namely the fireball. The obtained results of simulations of the competing scenarios compared with the PISA experimental data for p, d, t production at 2.5-, 1.9-, and 1.2 GeV in p-^{197}Au reaction are shown in figs. 7.5, 7.6 and 7.7, respectively. The data were registered at 16^0, 65^0 and 100^0 of the laboratory detection angle. As an example for lighter target nucleus the p, d, t spectra detected at three emission angles after the p+^{nat}Ni at 175 MeV impinging energy is given in fig. 7.8. The contribution of the fireball decay to the LCP emitted from the very light target of ^{12}C is presented in figs. 7.9 and 7.10 for p, d, t, ^{3}He and ^{4}He emitted as the effect of target bombardment with 1.2 GeV protons.

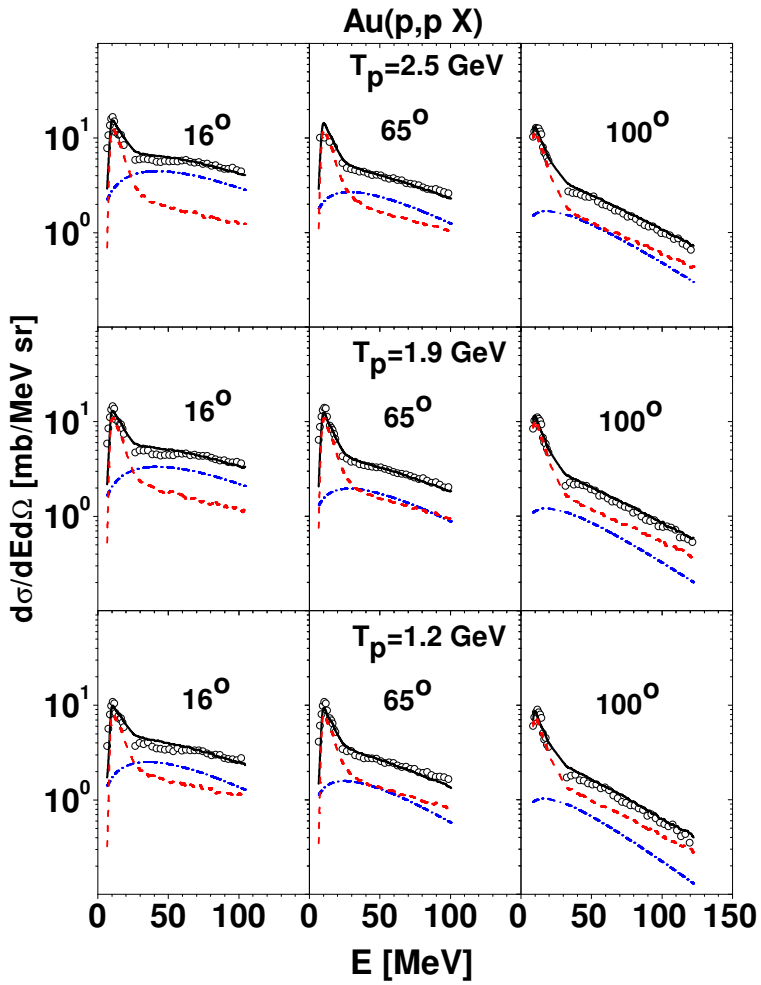

Figure 7.5: The simulations of competing processes in the spallation reaction of proton with ^{197}Au nucleus at 2.5-, 1.9- and 1.2 GeV bombarding energy. The distributions obtained for three detection angles of 16^0, 65^0 and 100^0 for protons, deuterons and tritons are compared with relevant experimental spectra measured in the PISA experiment (circles). The simulated contribution from the two step model (INCL4.3 + GEM2 codes) is presented with the dashed, red line. The postulated contributions from alternative process (emission from fireball) is given with the dot-dashed, blue line. The sum of both processes is drawn with the solid, black line.

7.5 Results for Intermediate Mass Fragments

In the angular and energy regions where the IMFs production is underestimated by the two step model it is well compensated by the emission from the so-called fast source of the moving source model. This source is composed of up to several nucleons. Masses of the emitted IMFs are too big to be the products of the decay of the fireball which is of the few nucleon mass only. On the other hand the excitation of the so-called "slow source" is not sufficient to expel the IMFs of the energies typical for the preequilibrum production. The appropriate examples of simulations compared to the experimental data are given in fig. 7.11 for beryllium and boron isotopes emitted from ^{197}Au target. Here, instead of the INCL model for the first step of the

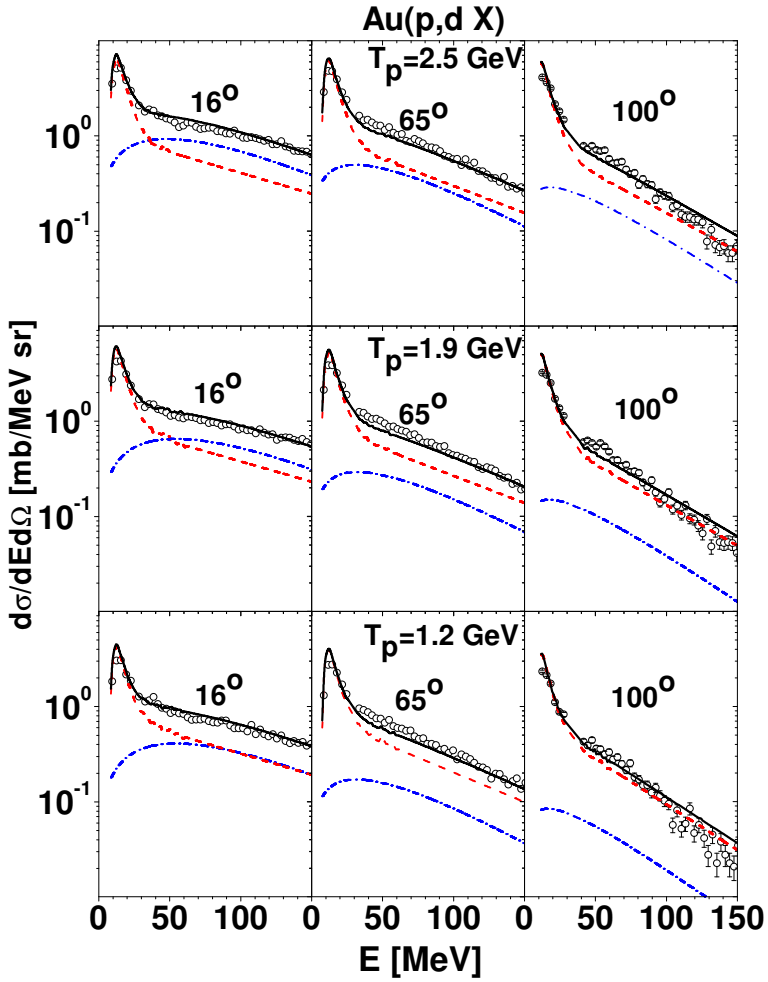

Figure 7.6: The same as in fig. 7.5 but for deuterons.

reaction the simulations with the BUU model were performed. Also very good agreement with the experimental data was achieved for lighter target nuclei. As an example the Li, Be and B isotopes spectra for p+^{nat}Ni reaction at 175 MeV and 2.5 GeV are presented in figs. 7.12 and 7.13, respectively.

7.6 Features of the mechanisms contributing to the spallation

In the applied analysis of competing spallation mechanisms the spectra of IMFs were well reproduced with assumption of their origin only from the second step of reaction, namely from evaporation or from multifragmentation of the cascade remnant (for light targets) or from emission from a so-called fast source (for heavy targets).

The LPCa are produced predominantly during the initial phase of the reaction where the cascade of intranuclear collision is assumed as well as during the formation and decay of the fireball. However, this class of particles is created as well in the later evaporation or - to some extend -

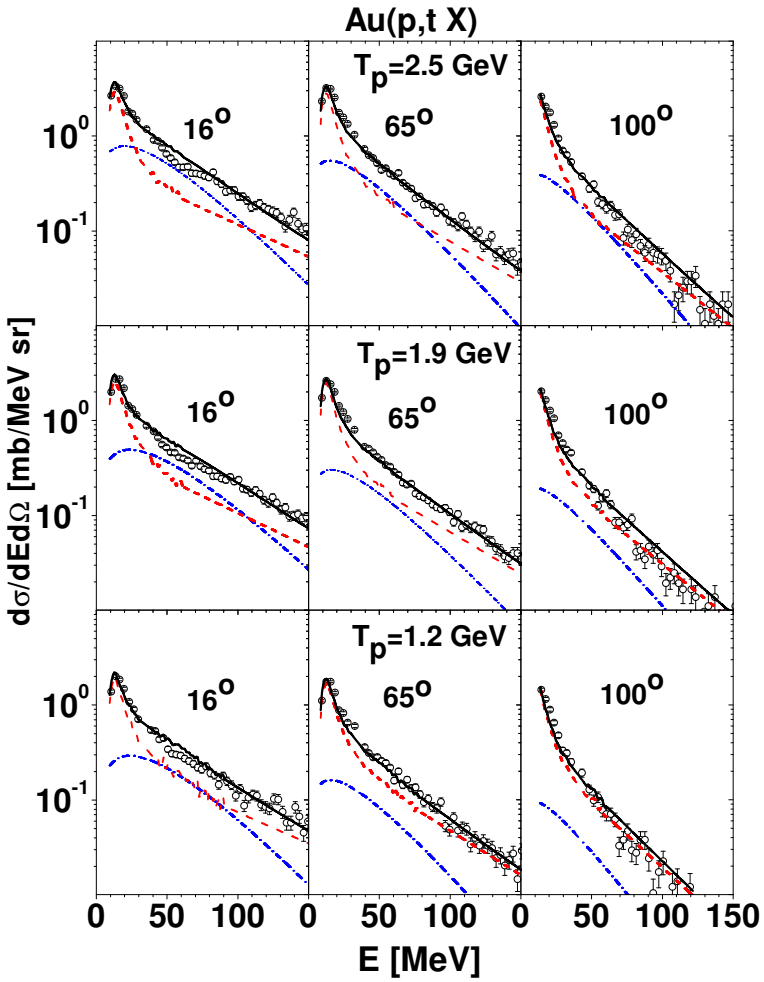

Figure 7.7: The same as in fig. 7.5 but for tritons.

in the multifragmentation of light targets. But this concerns only the LCPs of the lower kinetic energies ($E_{kin} < 50$ MeV).

The scaling factors F obtained from the analysis vary in the range from about 50% to about 90% depending on the target mass and beam energy. An example of the relative contribution of INCL, GEM and fireball emission to the total reaction cross section for LCPs in ^{197}Au and ^{nat}Ni targets bombardment with protons at 1.2, 1.9 and 2.5 GeV energy is given in fig. 7.14. The dependence on the initial kinetic energy is rather week. An exception is observed for Au target where the dependence on the beam energy is well visible especially for production of ^{3}He. Contribution of mechanism embedded in the INCL model (binary collisions + coalescence) decreases with the impinging proton energy giving a room for fireball production and decay.

For light targets (^{12}C and ^{27}Al) where the fireball is composed of smaller number of nucleons than for heavier ones its decay contributes most effectively to proton production whereas the yield of heavier LCPs drops monotonically (with some small superiority for ^{3}He cross section over this for triton). For ^{nat}Ni nucleus it is no more a case since the production of composite isotopes

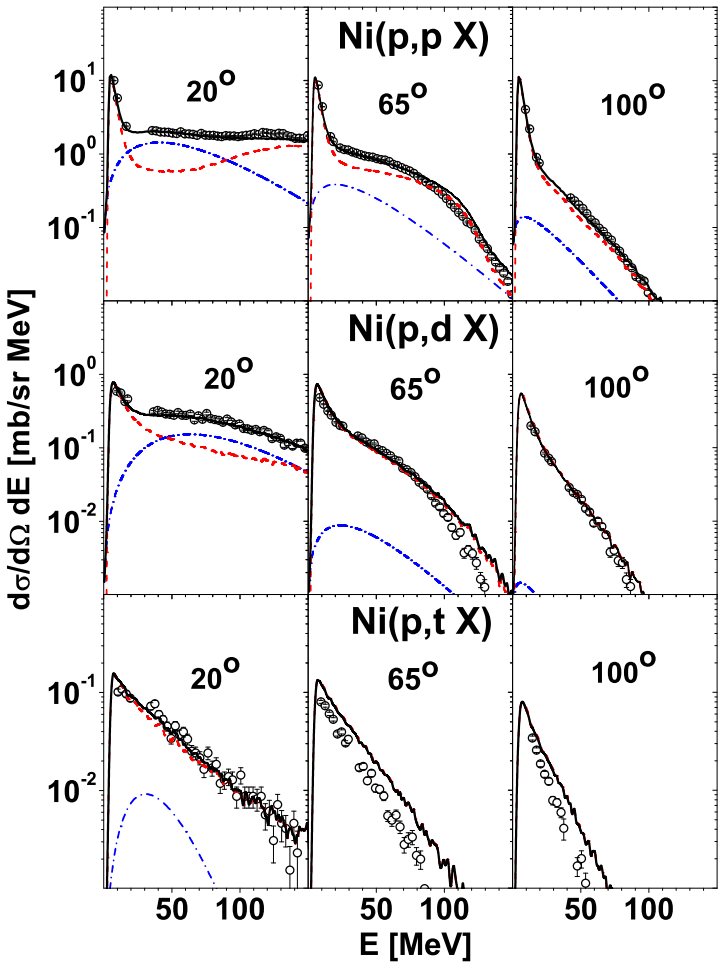

Figure 7.8: The same as in fig. 7.5 but for p+^{nat}Ni reaction at 175 MeV impinging energy. Here the lowest presented detection angle is 20^0 instead of 16^0.

is dominant. For ^{197}Au the dominant fireball decay isotope is ^{3}H. The ^{4}He production for all targets is very small. These dependences are presented in fig. 7.15 - upper panel. The middle and lower panel of fig. 7.15 shows examples of temperature and velocity of fireball, respectively as obtained from the fit of the moving source model. Individual quantities shown in the figure were obtained by averaging results for beam energy of 1.2, 1.9 and 2.5 GeV.

It can be concluded that on average the lighter emitted LCP the higher excitation and velocity of the fireball. This rule is not valid for helium isotopes where alpha-particles are emitted from the source of slightly higher temperature and moving faster than those being the origin for ^{3}He.

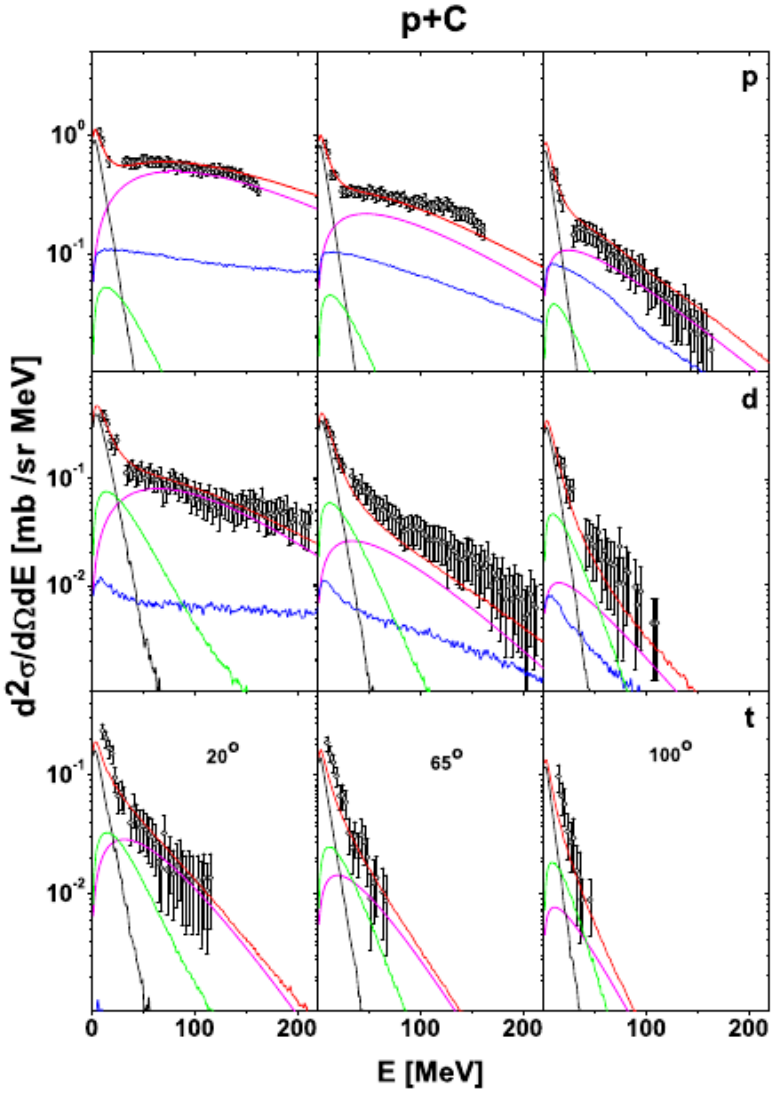

Figure 7.9: The simulations of competing processes in the spallation reaction induced by proton in ^{12}C nucleus at 1.2 GeV bombarding energy. The distributions obtained for three detection angles of 20^0, 65^0 and 100^0 for protons, deuterons and tritons are compared with the relevant experimental spectra measured in the PISA experiment (circles). The contribution of individual processes is marked as follows: black line - evaporation (GEM2), blue line - intranuclear cascade and coalescence (INCL4.3), green line - Fermi breakup (ROZPAD), magenta line - emission from fireball, red line - the sum of all processes. The figure is adapted from [8].

Despite of unquestionable successes of the above described hypothesis of a competition between various mechanisms contributing to the nuclear spallation it must be stressed that the actual understanding and successful modeling of spallation processes remains a still not accomplished goal. The success of the phenomenology used in the emitting source model as well as increase of the predictive power of models utilizing the concept of coalescence induced the work oriented for supplementing the current description of pA reaction as a cascade of binary collision with more complex interaction where collective behavior of target nucleons is allowed. The details and results of the undertaken efforts will be presented in the following chapters.

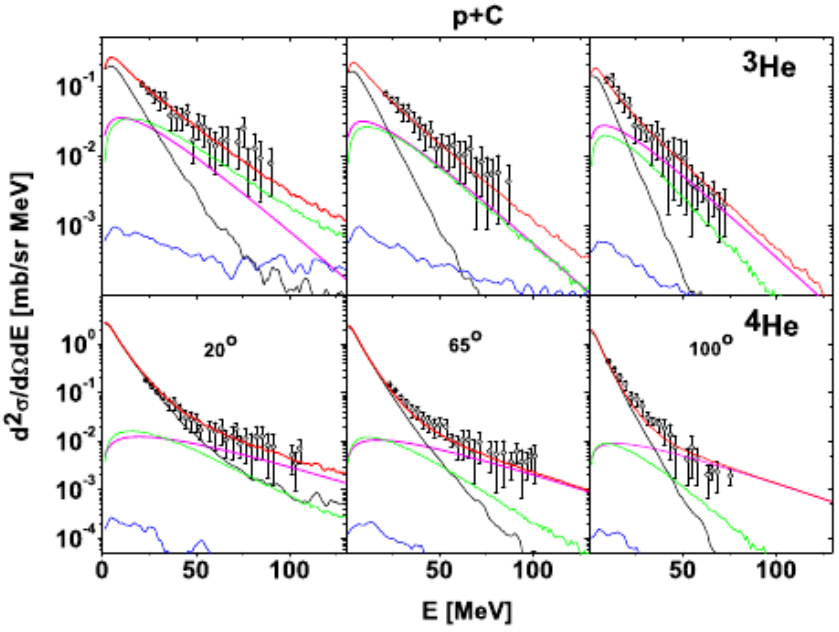

Figure 7.10: The same as in fig. 7.9 but for ^{3}He and ^{4}He. The figure is adapted from [8].

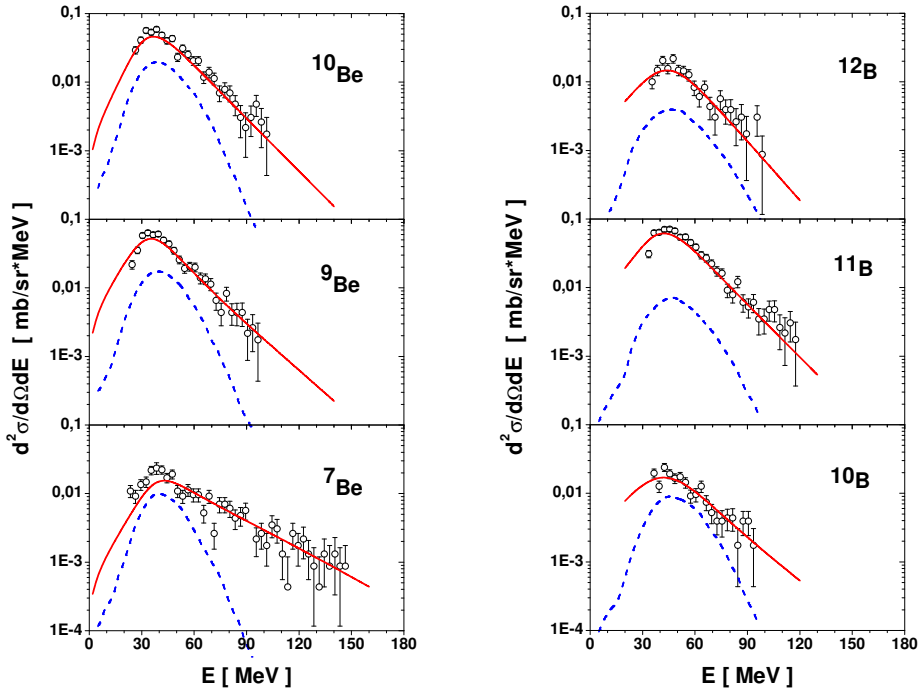

Figure 7.11: Moving source model applied to interpret the IMFs emitted in the reaction of p+^{197}Au at 2.5 GeV energy for beryllium isotopes (left panel) and for boron isotopes (right panel). The solid, red line presents the total contribution from fast and slow source whereas the dashed, blue line depicts the results of simulations done with BUU + GEM2 models. The experimental data (circles) were measured at 35^0 of laboratory detection angle.

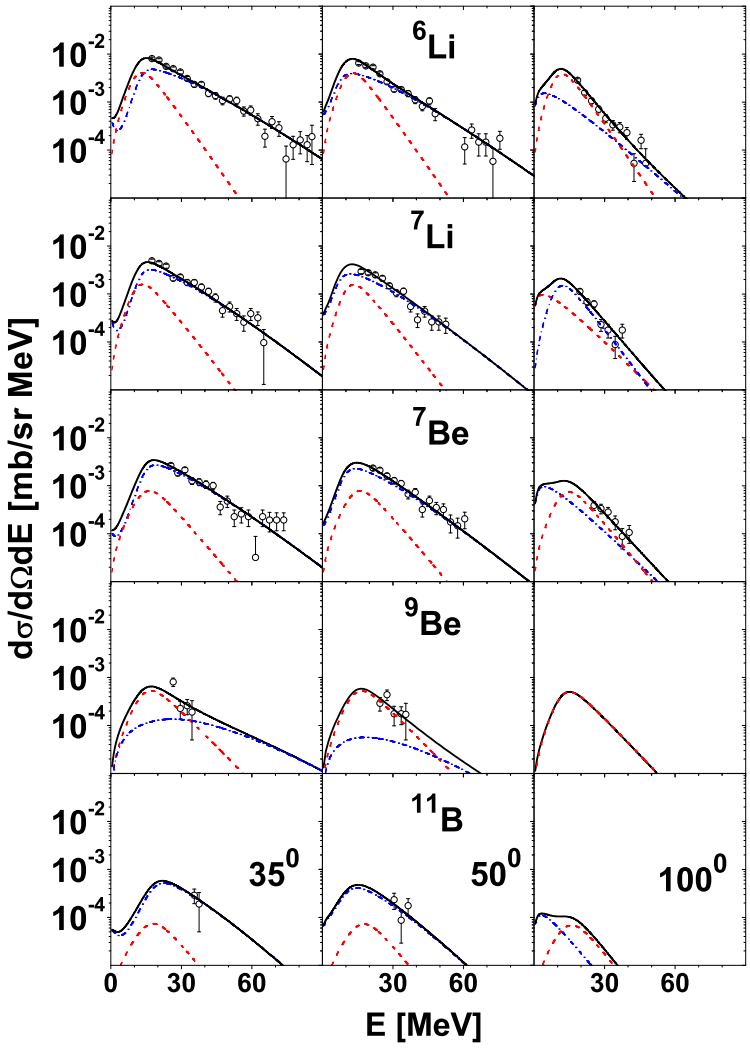

Figure 7.12: The simulations of competing processes in the spallation reaction of proton with ^{nat}Ni nucleus at 175 MeV bombarding energy. The distributions obtained for three detection angles of 35^0, 50^0 and 100^0 for the so-called LiBeB isotopes are compared to the relevant experimental spectra measured in the PISA experiment (circles). The simulated contribution from the two step model (INCL4.3 + GEM2 codes) is presented with the dashed, red line. The postulated contributions from an alternative process (emission from fast source) is given with the dot-dashed, blue line. The sum of both processes is drawn with the solid, black line.

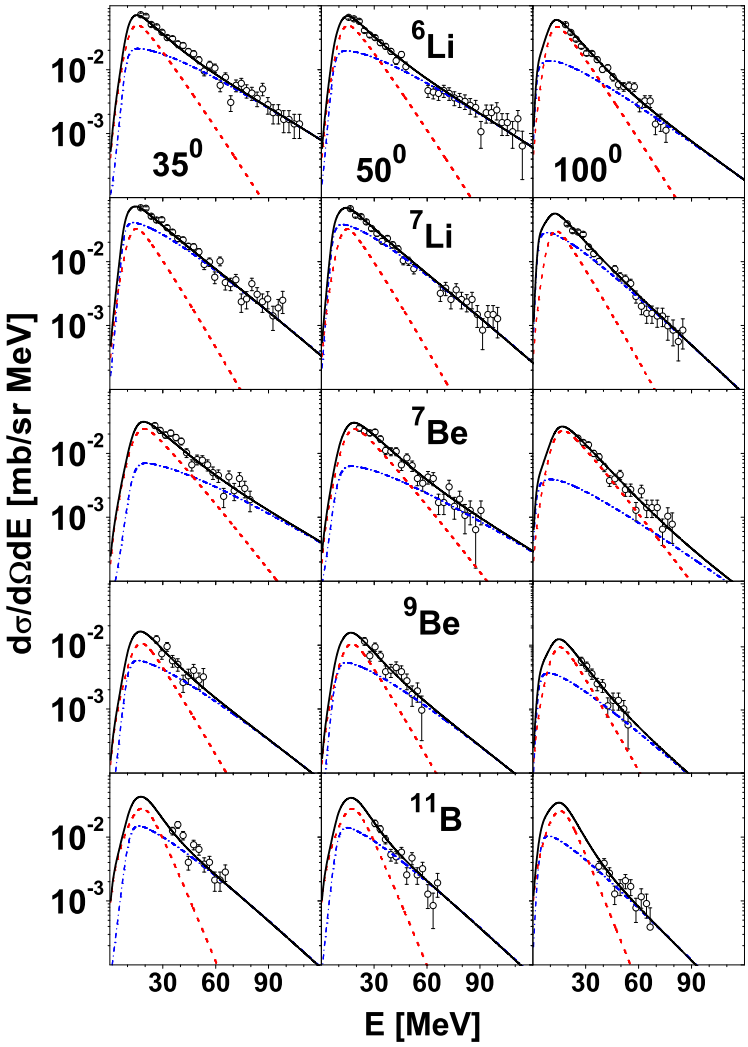

Figure 7.13: The same as in fig. 7.12 but for 2.5 GeV proton beam energy.

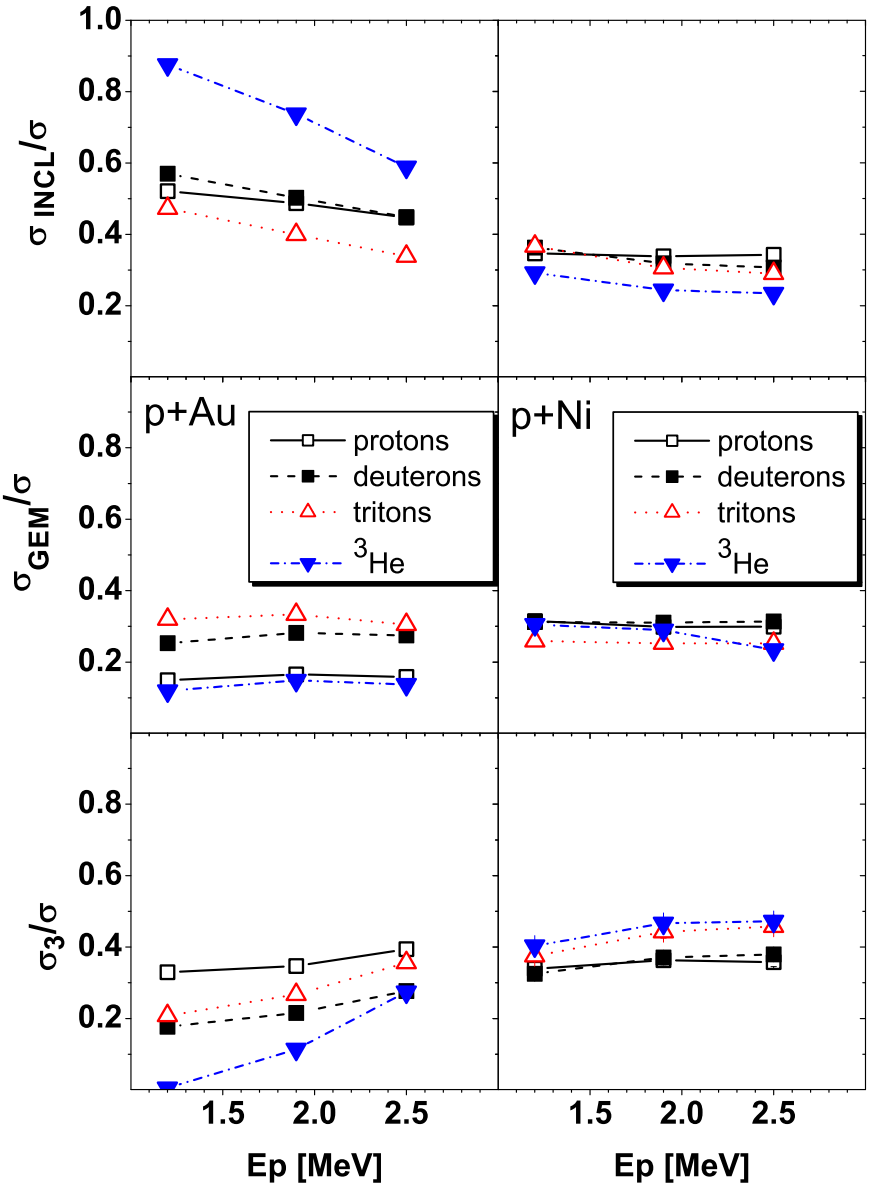

Figure 7.14: A comparison of the contribution of various processes considered in the simulations of alternative scenarios of the spallation reaction to the total cross section of protons (open squares), deuterons (full squares), tritons (open triangles) and ^{3}He (full triangles) production in p+^{197}Au and p+^{nat}Ni at 1.2-, 1.9- and 2.5 GeV energy. Shown are contributions of intranuclear cascade + coalescence (σ_{INCL}) - upper panel, evaporation (σ_{GEM}) - middle panel, and emission from fireball (σ_3) - lower panel.

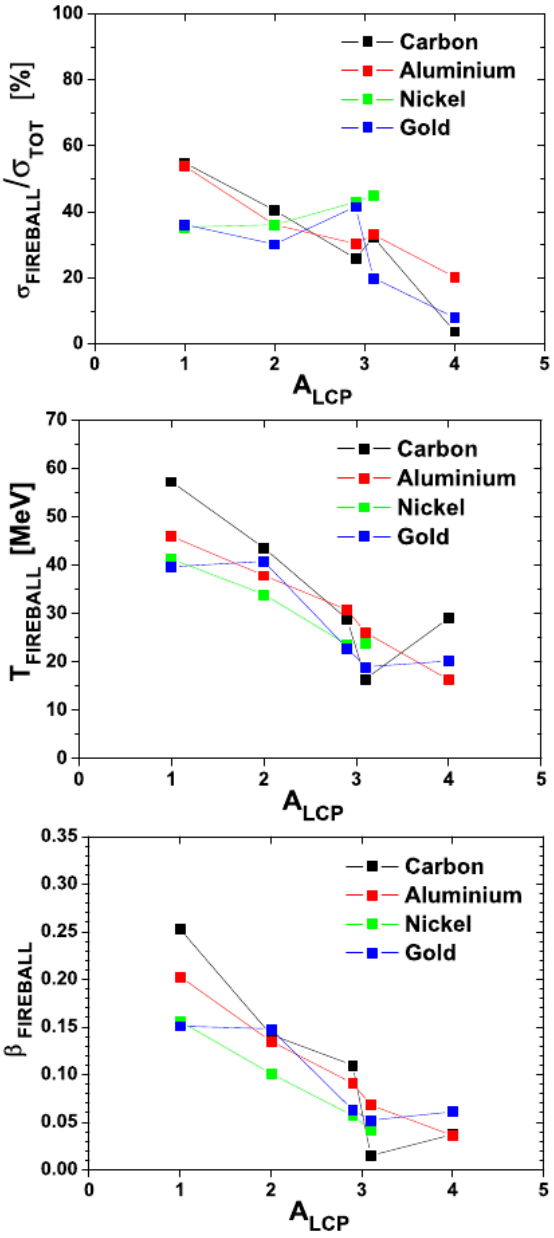

Figure 7.15: Upper panel: the relative yield of various LCPs emitted from the fireball in p + ^{12}C, ^{27}Al, ^{nat}Ni and ^{197}Au reactions as obtained in the phenomenological interpretation of results of the PISA experiment. Middle panel: dependence of the fireball temperature on the mass of emitted particles. Lower panel: dependence of the fireball velocity on the mass of emitted particles. The values for ^{3}H and ^{3}He are shown for A around 3. The ^{3}H data are more to the left. Individual quantities shown are obtained by averaging results for beam energy of 1.2-, 1.9- and 2.5 GeV. This figure is adapted from [8].

8 Spallation Model with Cascade++

The significant improvement of the description of experimental spallation data with the application of the idea of moving sources and the concept of fireball as described in the preceding chapter motivated the work aiming at implementation of correlated propagation of few nucleons into the microscopic model. The appropriate mechanism should permit a creation of the composite excited object as an intermediate states in the production of spallation ejectile. As the result of these efforts a new model of internuclear interaction called a Spallation Model with Cascade++ (SMC++) was constructed.

The described here model concerns only a part of the processes responsible for observed distribution of spallation products. Similarly like for instance in INCL or other models of the first step of spallation reaction it is assumed that the statistical effect appearing when nuclei get unstable due to the proton bombardment in a few GeV region are described correctly with the present models of evaporation, fragmentation or fission. The main attention in SMC++ is put onto the dynamics of the initial phase of the reaction before the equilibrium is attained. The existing models which try to describe this part of the struck nucleus evolution suffer from insufficient understanding of the nature of hadronic processes in nuclear medium and are unable to describe the distributions of experimental reaction products.

As it was emphasized already a few times a pure theoretical description of spallation processes does not exist nowadays. Instead, a well established set of nuclear physics knowledge and commonly used reasonable approximation like e.g. the Fermi Gas Model, mean nuclear field, Coulomb force, nuclear density are used. SMC++ remains still a model of partially phenomenological nature.

The SMC++ is an effort to go beyond the limitations of the contemporary cascade models utilizing only the binary hadronic interaction. They results in strong underestimation of the experimental spectra especially at low emission angles and for lighter targets. The realized deficiency of the interpretation of the initial phase of nucleon-nucleus reaction as a purely binary interaction impose a conclusion that in the description of examined reactions another mechanism permitting for a greater participation of the target nucleons in the reaction and for faster four-momentum transfer and dissipation in the target nucleus is needed.

This hypothesis is motivated even more after analyzing the PISA results with the use of moving source model and significant improvement of the quality of model simulation after introducing the intermediate excited states contributing to particle production.

Thus, important novelty of the SMC++ consists in introduction of the idea of the Dynamic Clustering in Nuclear Medium (DCNM) - a hypothetical mechanism which takes into account fluctuations of the nuclear density during the cascade process and resulting modifications of the local nuclear field. The proposed mechanism significantly influences the production of single particles. Introduction of DCNM increases both the energy and momentum transfer from the projectile to the target as well as the number of target nucleons involved in the interaction. The transferred energy is effectively dissipated among the reaction participants. This causes an increase of the number of particles of the kinetic energies sufficient to leave the potential well. The higher momentum transfer from the projectile to the system enforces as well particle emission at small angles.

In the SMC++ the DCNM mechanism is also entirely responsible for creation of LCPs. The dynamically formed clusters are the intermediate states in the target nucleus evolution towards

emission and thermalization. In this way a significant deficiency of the binary collision models where intrinsic mechanism of composite particle production do not exist has been overcome. As a consequence there is no need to apply any additional mechanism for LCP creation (e.g. the surface coalescence).

A justification of the existence of the proposed mechanism of DCNM currently comes predominantly from an improvement of the description of the experimental data when compared to spallation models where collective phenomena are disregarded. To some extent the idea of DCNM could be related to the recent approaches where nuclei are described as a set of well established clusters of nucleons, especially alpha-particle clusters [144].

It has to be emphasized that SMC++ despite of a introduction of the new mechanism, which involves the interaction of a few nucleons remains still a relatively simple and easy to use model. The simulation with SMC++ of statistically useful samples of data needs only a moderate CPU time usage even for heaviest target nuclei.

Below the description of the model component is given with emphasis on similarities and differences to the standard nuclear cascade model. As a reference and an example of the standard cascade model the INCL model described already in 5.1.1.1 can be used.

8.1 Target Nucleus

In SMC++ similarly as in INCL the target nucleus is considered as a set of non interacting Fermi gas particles embedded within the sphere of the radius R_{max}. The positions of nucleons are sampled randomly. But as it is shown in figs. 8.1 - 8.5 the experimentally established distributions [94, 145] of nuclear densities are better approximated with the Fourier-Bessel series expansion than the Woods-Saxon distributions (equation 5.1) used in INCL. It concerns especially light targets. For targets about mass of Nickel the Woods-Saxon distribution and the Fourier-Bessel expansion agree well. Thus, in the SMC++ model the initial distribution of densities of the target nuclei are constructed according to a sum of Fourier-Bessel series expansion for A $\leq$ 58 whereas for heavier ones the Saxon-Woods distributions are selected. In both cases the parameters of the distributions (R_{max}, R_0, a) are taken from [94]. The cutoff radius of the Fourier-Bessel expansion is assigned to R_{max} of the density distribution. It means that beyond R_{max} the density is equal to zero. The Saxon-Woods distribution and its parameters are equivalent to those of the two-parameter Fermi model as it is called in [94].

The momenta of the nucleons are sampled randomly and have to be lower than the Fermi momentum. During the sampling procedure of the initial positions and momenta of nucleons the Pauli Blocking is checked in order to avoid the multiple occupation of the local phase-space volumes.

It is assumed that the nucleons are trapped in the common potential well of the depth V_0.

8.2 Impinging particle

At present the SMC++ allows reaction of the target nucleus only with single nucleon - proton or neutron. A bombarding particle propagates along z-axis of the Cartesian reference frame with the selected laboratory momentum until it experiences the first interaction inside the target nucleus. The impact parameter is selected at random in order to cover the initial geometrical

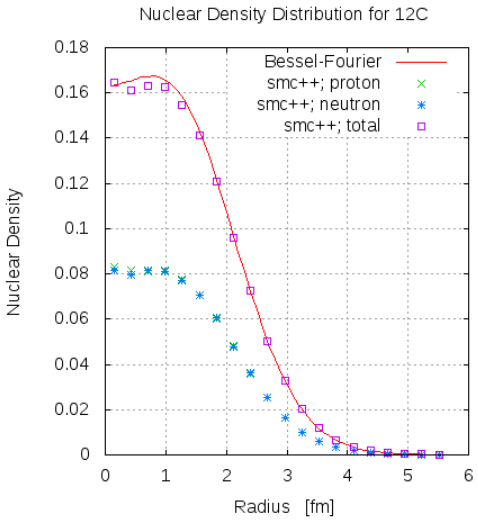

Figure 8.1: Initial nuclear density distribution of ^{12}C used in SMC++. The experimental distribution parametrized with the Fourier-Bessel series expansion (red solid line) according to [94]. Proton (green crosses), neutron (blue stars) and total (magenta open squares) nuclear density distribution as sampled for initial target nuclei in SMC++.

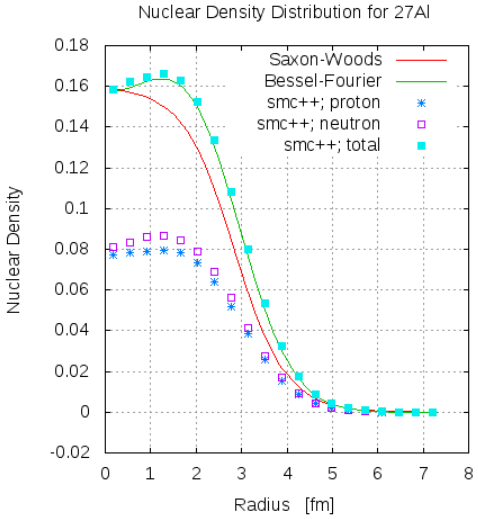

Figure 8.2: Initial nuclear density distribution of ^{27}Al used in SMC++. The experimental distribution parametrized with the Fourier-Bessel series expansion (green solid line) according to [94]. Proton (blue stars), neutron (magenta open squares) and total (blue full squares) nuclear density distribution as sampled for initial target nuclei in SMC++. For comparison the Saxon-Woods distribution (red solid line) as used in INCL model is given.

target nucleus cross section in x-y plain (*i.e.* a circle of the radius R_{max}). The entrance position of the projectile into the target is calculated accordingly.

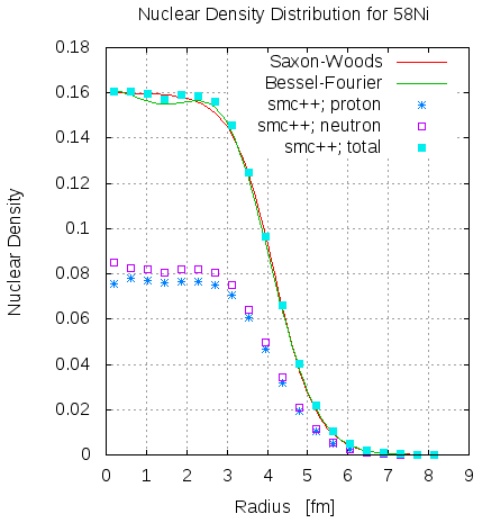

Figure 8.3: The same as in 8.2 but for ^{nat}Ni target nucleus.

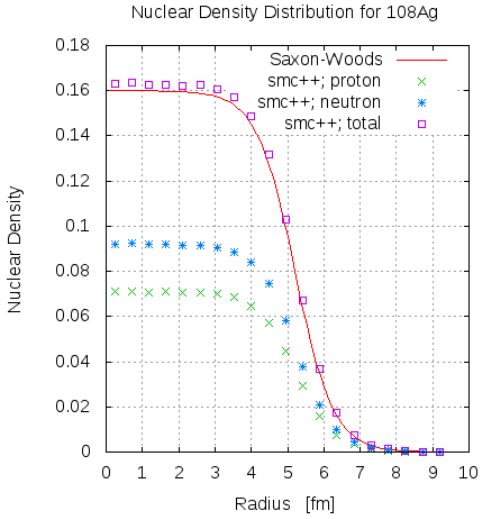

Figure 8.4: Initial nuclear density distribution of ^{nat}Ag used in SMC++. The experimental distribution parametrized with the Saxon-Woods function (red solid line) according to [94]. Proton (green crosses), neutron (blue stars) and total (magenta open squares) nuclear density distribution as sampled for initial target nuclei in SMC++.

8.3 Cascade

The main prerequisite of the SMC++ is the whole control of the state of each component of the cascade process during the course of the reaction. In order to achieve this aim it was decided to perform a modeling of the reaction process in the time steps. Cascade starts with time $t_0 = 0$ when the projectile touches the border of the target nucleus. The duration of the time step was selected to be $\Delta t = 0.3$ fm/c. For the considered in the model range of the kinetic energies (up to a few GeV) even for the highest particles momenta their displacement during one time step

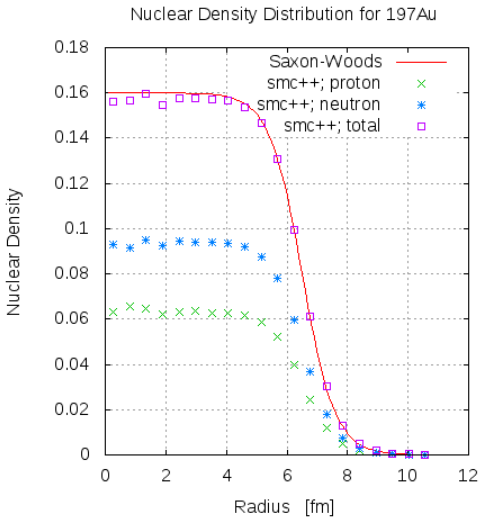

Figure 8.5: The same as in 8.4 but for ^{197}Au target nucleus.

is lower than the half of the nuclear radius (1 fm). For the highest kinetic energy of impinging particles considered in the SMC++ up to now which is equal to 3.0 GeV its propagation during the 0.3 fm/c time step is equal only to 0.292 fm. Thus, the sampling of the probability of possible processes (collision, clustering, emission, decays) is always sufficiently frequent.

The duration of the cascade i.e. the time needed for thermalization of the remnant of the target nucleus depends on the initial mass of the target. The formula to calculate the time needed to complete the cascade is adapted from the INCL - see equation 5.12.

Each step of the cascade process in SMC++ comprises the following components:

- movement of the particles according to their momenta,
- check for emission or reflection of the particles which are at the nucleus border,
- check for interaction of particles. Possible interaction are:
  - two particle collision: depending on a type of the particles and their four-momenta the most probable type of interaction is calculated and simulated. It includes the elastic and inelastic scattering with Δ resonance creation or its reabsorption,
  - formation of a momentary cluster,
- check for the decay of existing Δ resonances,
- check for the decay of existing clusters.

The emitted composite clusters are immediately checked for decay. A Fermi breakup mechanism is used for this purpose.

8.4 Propagation of particles

During the cascade evolution at each step of the simulation only these particles are shifted that already took part in any interaction (collision, recombination, clusterization, decay), i.e.

their states are different from the initial ones. As the result the overall shape of the density distributions of bombarded nucleus varies slowly but local fluctuations could be formed.

It is assumed that the nuclear potential of the target nucleus is constant over its whole volume. Thus, every object inside the potential well propagates along straight line trajectory according to its current momentum. During a given step of the cascade (between time t and $t + \Delta t$) the particle changes its position by $\Delta\vec{r}$:

$$\Delta\vec{r} = \overrightarrow{r}(t + \Delta t) - \overrightarrow{r}(t) = \overrightarrow{\beta} \cdot \Delta t \cdot c \ , \tag{8.1}$$

where:
$\overrightarrow{\beta} = \frac{\overrightarrow{p}}{E}$;
$\overrightarrow{p} = (p_x, p_y, p_z)$ - momentum of particle;
$E = m^2c^4 + p^2c^2$ - total relativistic energy of particle;
c - speed of light.

8.5 Criterion for particle emission

Particles which interact and move toward the nucleon surface are checked for emission only when they attain the R_{max}. In this way the particles localized in the outer region of nucleus, where density is low, can still be considered as constituents of the target nucleus and take part in the interactions. Particles of the positions of $r \geq R_{max}$ are checked if their net kinetic energy permits to overcome the potential barrier. For the charged particles the Coulomb barrier is taken into account and the barrier penetration probability with the use of the Gamow factors is calculated. If the kinetic energy is sufficient the particle of $r \geq R_{max}$ is considered as emitted from the target nucleus. Otherwise it is reflected from the nuclear surface back into the volume of the target nucleus. The emission angle of the ejectile is determined according to its current vector of momentum. The same procedure is applied both to the single particles as nucleons or pions as well as to composite objects like clusters. Resonances Δ when reaching the nucleus border are always reflected back.

8.6 Collisions of particles

8.6.1 Collision criteria

For binary collision only these pairs of current target nucleus constituents are designated, for which at least one counterpart took already part in any interaction or is a projectile. Moreover, collision is allowed only if the total CM energy is higher than 50 MeV over the mass of the colliding pair. Following the INCL the so-called soft collisions of very little momentum transfer are avoided. They are insignificant for reactions at a GeV energy range. In each step of the cascade the relative distances of each pair of particles which fulfill the collision criteria are checked for collision probability. Since the colliding particles may have high energies the relativistic effects have to be taken into account. Relativistic particles have their own times, t'_1, t'_2, different than the current time, t, of cascade when the judgment about the collision has to be done. Thus, when calculating the relative distance of particles the concept of Cugnon [72] is utilized. It is assumed that the most meaningful in this case is the spatial distance of the colliding particles calculated in their own CM system. If the spatial distance of the pair of particles is smaller than $\sqrt{\frac{\sigma_{tot}}{\pi}}$ then such particles undergo collision.

The meaning of σ_{tot} and the criterion of selection of the type of collision will be described below.

8.6.2 Cross sections and reaction type

The σ_{tot} is a total cross section for interaction of a pair of involved particles. It is a sum of the cross sections for different types of processes dependent on their isospin, energy, and hadronic state. The following processes are included:

- elastic nucleon-nucleon cross section, $\sigma_{NN}^{elastic}$;
- inelastic nucleon-nucleon cross section, $\sigma_{NN}^{inelastic}$;
- nucleon-delta interaction cross section, $\sigma_{N\Delta}$;
- nucleon-pion interaction cross section, $\sigma_{N\pi}$;

The $\sigma_{NN}^{inelastic}$ comprises only the contribution of the most dominant process in this respect, namely the excitation of the resonance $\Delta(1232)$.

The cross sections were parametrized by J. Cugnon et al. [83, 85] for the application in INCL. The same formulae are used in SMC++.

The momentum transfer in the collision is sampled with the use of the differential cross section for NN collisions parametrized as well in [83].

Collision of particles is allowed only if the resultant states of both colliding particles are not occupied. The so-called stochastic Pauli blocking is applied with the parameters like: $r_{PB} = 3.18$ fm and $p_{PB} = 200$ MeV/c (cf. chapter 5.1.1.1).

8.7 Treatment of the resonances

The $\Delta(1232)$ particle created during the collision can also collide with the nucleon. In this case the resonance can be reabsorbed ($N\Delta \rightarrow NN$) or elastically scattered ($N\Delta \rightarrow N\Delta$). Δ can collide with another Δ as well. To calculate the collision probability and the four-momentum transfer in this case the $\sigma_{NN}^{elastic}$ is used.

Existing resonances $\Delta(1232)$ can undergo a spontaneous decay in the reaction $\Delta(1232) \rightarrow N\pi$. The decay probability is sampled with the use of exponential dependence with the value of the life time equal to this of a $\Delta(1232)$ in free space multiplied by a factor 10:

$$\tau_{\Delta(1232)^{SMC++}} = 10 \cdot \tau_{\Delta(1232)^{free}} \tag{8.2}$$

where $\tau_{\Delta(1232)^{free}} = (5.63 \pm 0.14) \times 10^{24}$ s is an average life time of free $\Delta(1232)$ resonance [146].

The constant factor 10 was introduced on order to reflect the extension of the lifetime of $\Delta(1232)$ resonance in the nuclear medium due to limited phase space. Effective blocking of $\Delta(1232)$ decay in the nuclear environment depends on the actual energy of the resonance and is not constant. But in order to suppress the CPU time during the calculations with SMC++ only one value of in-medium $\Delta(1232)$ lifetime was selected. Selection was based on the best fit of SMC++ simulations to the experimental distributions of double differential cross section of pions obtained in [139] and LCPs measured in the PISA experiment. Similar order of in-medium $\Delta(1232)$ lifetime extension was proposed in [6] for a simulation of the spallation pion spectra with the use of Hadron String Dynamics (HSD) model.

Since the lifetimes of all isospin states of $\Delta(1232)$ are of similar value in SMC++ only the mean value of all of them is taken as a common to calculate the decay probability for all of the $\Delta(1232)$ charge states.

The decay of $\Delta(1232)$ can be performed only if the states of both the resulting nucleon as well as a pion are available. The stochastic Pauli blocking probability is calculated with the same parameters as for colliding particles.

The Δ-particles which survive to the end of the assumed thermalization time are forced to decay in the last step of the cascade.

8.8 Dynamic Clustering in Nuclear Medium (DCNM)

The underestimation of light spallation products which is most significant for low emission angles and ejectile's energies in the range 50 - 150 MeV in the cascade models which consider only pure binary collisions suggests that the process which is possibly missing in these models should induce the following effects:

- the increase of energy/momentum transfer from a projectile to the target,
- more nucleons of the nuclear medium have to be involved into interaction,
- the latter should enhance the energy dissipation.

Moreover, if possible, the proposed mechanism should contribute to the production of composite particles since their yields are in many cases not sufficiently reproduced in cascade+coalescence models as well.

In the course of the model development with the benchmarking on the whole set of the PISA experiment data collected at beam energies higher than 1.0 GeV and supplemented with neutron cross section data collected at SATURNE [39], LCP cross section measured in the NESSI experiment [47, 46] and available pion production cross section [139] the idea and details of the mechanism of Dynamic Clustering in Nuclear Medium (DCNM) has been worked out [15].

In the current version of the SMC++ the postulated mechanism of DCNM [15] is implemented in the following way:

- it is assumed that due to a nuclear density fluctuation the nucleon groups can form a momentary cluster;
- the spatial interaction range allowing for the considered group of nucleons as a temporary cluster is momentum dependent and is equal to the de Broglie wave length of the nucleon propagating in the nuclear medium. The particles, which current positions in a given step of cascade are within the sphere of the $R_c = h/p_i$ (p_i - total momentum of nucleon i, h - Planck's constant) are candidates to form the cluster together with this $i-th$ nucleon. The cluster formation is suppressed for high momentum nucleons of short de Broglie wave. In order to avoid situation that the low momentum nucleons of long de Broglie wave interact with the target nucleus as a whole the limit for the range of cluster formation was set to be $R_c < 3$ fm;
- momentary clusters can be formed if the energy of the system is sufficient. It was estimated that the total kinetic energy of the cluster components must be higher than 60 MeV/nucleon;

- it is also assumed that among nucleons which form the cluster the interaction takes place causing internal energy and momentum exchange;
- clusters move across the nuclear medium along the straight lines according to their current momenta. When attain the nucleus border they can be emitted or reflected depending on their net kinetic energy;
- existing clusters can grow-up by joining surrounding nucleons which are met at close distance (lower than R_c) on their path of propagation if the available kinetic energy of the new cluster is sufficient;
- existing clusters undergo decay in-medium according to exponential probability with appropriate life time; The mechanism of Fermi Breakup is assumed for this process. The life time of clusters will be discussed below.
- mechanism of temporary cluster formation compete with binary NN collisions.

Very important assumption of the DCNM mechanism is that nucleons embedded in clusters interact mutually. This leads to equalizing the energy and momentum of cluster constituents. The mechanism of this interaction is not specified in the present version of SMC++. As a first approximation it is assumed that soon after the formation the cluster attains energy equilibrium and bound nucleons loss the memory about their state before they joined a cluster.

The free parameters of the model related to the DCNM mechanism are the low momentum limit of the range of cluster formation ($R_c < 3$ fm), the total kinetic energy of the involved nucleons demanded for cluster formation (higher than 60 MeV/nucleon) and the life time of the cluster in-medium. The values of all of them were selected with the use of the best fit of simulated spectra to the experimental data in the whole considered here range of mass and energy.

The life time of the in-medium cluster is a parameter of the fit. It turned out that in order to obtain the demanded energy dissipation in the target nucleus the decay rate needs to be high. The width Γ for two nucleon cluster was roughly estimated to be $\Gamma(\mathrm{n}{=}2) = 2000{\cdot}\Gamma(\Delta(1232))$, where $\Gamma(\Delta(1232))$ is a width of free $\Delta(1232)$. Since decay of clusters composed of more nucleons shall be more effectively blocked by nuclear medium the widths of heavier cluster (n>2) are assumed to obey the relation: $\Gamma(\mathrm{n}) = 0.01{\cdot}\Gamma(\mathrm{n\text{-}1})$.

Selected life times have only approximate physical meaning. In the current model they are biased by a process used to perform the cluster decay. When a cluster decays either in-medium or outside, in order to disperse its components in physical way with energy and momentum conservation in SMC++ the mechanism of Fermi Breakup is used [141]. Usage of this mechanism is well justified for excited nuclei in the free space. In the nuclear medium however limitations of available phase-space should extend the decay time as well as modify the mass distribution of the products.

The proposed mechanism of decay of dynamic cluster is an attempt to realize the concept of fast interacting but weakly bounded groups of nucleons forming the molecular resonances or fireball-like clusters. Majority of them are only a short living fluctuations of nuclear matter but among them are the objects bounded more firmly or more effectively blocked against the decay. This kind of momentary clusters can propagate inside the target nucleus and if having sufficient kinetic energy can leave the target nucleus. They can give the contribution to the yield of composite particle production.

In the SMC++ the d, t, and ^{3}He light nuclei are produced predominantly in the decay of heavier clusters emitted from the target nucleus. The mean mass of the source of these particles is

between 5 and 6 which is in good agreement with estimated mass of fireball responsible for d, t, and ^{3}He production in the moving source model by the PISA collaboration [13].

8.9 Interplay of the collision and clusterization

The momentary cluster formation is related to the momentum of the particles and is governed by a lengths of de Broglie wave of the relevant nucleons. For the lower momenta of nucleons their de Broglie waves are usually longer than the radii of the geometrical cross section calculated from the total hadronic cross section for binary collisions. Thus, for lower momenta the cluster formation is more preferable than binary collisions. But with increase of the nucleon momentum the cluster formation gets suppressed due to a drop of its de Broglie wave length. This opens a room for the binary collisions which play dominant role in the interactions of higher momenta nucleons. Particles released from the clusters due to their decay gain the momentum what causes a decrease of their de Broglie waves and enlarges the following binary collision probability.

8.10 Sampling of interaction probabilities

The evolution of interacting nuclear system during initial reaction phase in SMC++ is simulated in equally distant time intervals. It creates a technical problem of reliable probability sampling of individual processes relevant to the current conditions of the system. Thus, when any nuclear component attain predefined interaction conditions (mutual distance to counterpart, sufficient energy) it is examined for interaction probability only once. In the following steps of the cascade this particle can be considered for a subsequent interaction only when at least one of the interaction counterparts has taken part in the other interaction in between (with other particle or in other process).

9 Discussion of results of Spallation Model with Cascade++

In this section the theoretical distributions obtained with the SMC++ model will be discussed and confronted with the broad set of experimental data. For p, d, t, and ^{3}He ejectiles the whole range of target masses and impinging proton energies as those explored in the PISA experiment is represented. The distributions of neutrons will be compared to the experimental ones obtained at SATURNE [39]. The simulated pion spectra are compared to the data of Cochran et al. [139]. Moreover, for LCP's the equivalent theoretical distributions obtained with the use of INCL4.3 will be shown in order to facilitate the comparison of both theoretical models and to indicate the effects of the dynamic clustering mechanism proposed in SMC++.

The SMC++ model was coupled with GEM2 code permitting simulations of evaporation from the thermalized remnant of the first phase of the pA reaction (performed by SMC++).

Throughout this chapter, if not stated otherwise, in the attached figures the components from the binary collisions of nucleons as well as the low energy components resulting from the evaporation are summed together and represented by dashed line. In this way the main processes of the traditional two step model of the spallation are given as one contribution.

The contribution of the DCNM is marked with the dotted line. It is formed out of these emitted particles which at least once have been a part of a momentary cluster. Beside of participation in clusters, prior to it or when already released from the cluster, these nucleons can undergo the binary collisions as well.

Only these nucleons that never took part in cluster formation but during the cascade interacted only via NN collisions contribute to the distribution marked with the dashed line.

It has to be stressed that due to the interplay of the binary collisions and the clusterization in the SMC++ model in the presented below figures, the components from binary collision cannot be directly compared to the results of simulation done with models where the binary collision is the only considered mechanisms.

9.1 Neutrons

The valuable information of the double differential cross section of neutron emission after the pA collision at the GeV energy was collected in experimental campaign performed at SATURNE. The Fe and Pb targets were bombarded with proton energies of 0.8, 1.2 and 1.6 GeV energy [39].

In figure 9.1 examples of simulated with the use of SMC++ the neutron double differential cross section for Pb target and proton energy of 1.6 GeV are shown.

Thanks to the whole kinematic range of the neutron double differential cross sections measured at SATURNE some important features of the assumed clustering mechanism can be noted. The assumed momentum dependence of cluster formation probability results in dominant role of DCNM for low momenta nucleons of the large de Broglie waves. The products of the decay of momentary clusters contribute predominantly to the lower energy part of the emission spectra. The influence of DCNM decreases with increasing momentum. Above about 1000 MeV of particle emission energy the responsible mechanism is predominantly of binary character. The position

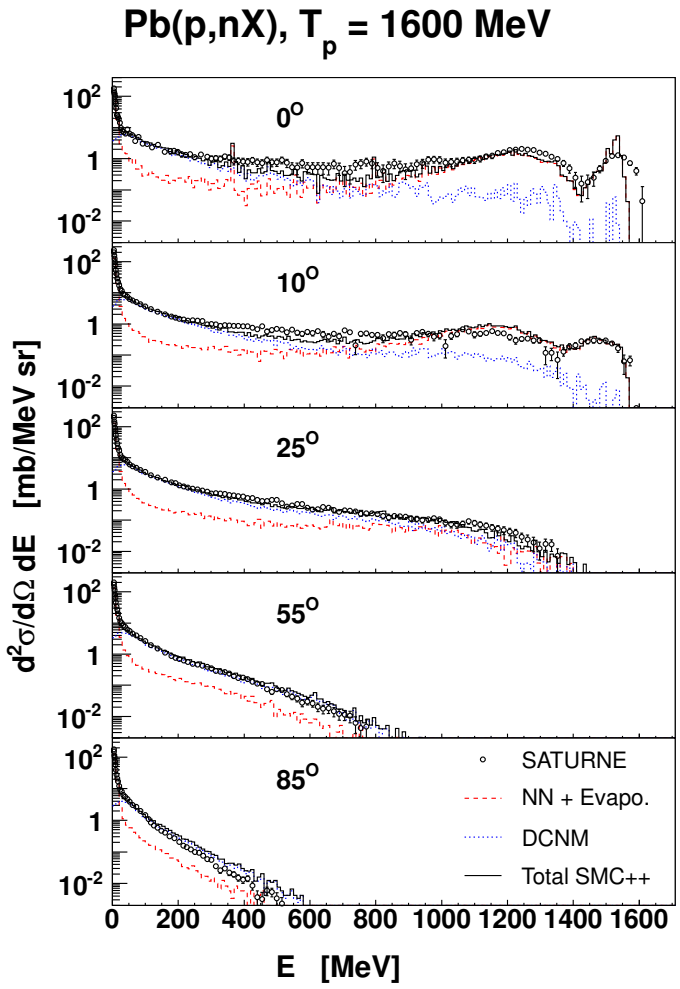

Figure 9.1: Distribution of neutrons emitted in p+Pb reaction at proton impinging energy of 1600 MeV simulated with SMC++ and compared to experimental spectra (circles) by Leray et al. [39]. A comparison is done for a few emission angles between 0° and 85°. The dashed line represents the sum of evaporation component (peak at low energies) simulated by GEM2 [63, 64] and contribution from a cascade of pure binary collisions (marked as NN) of SMC++. The dotted line outlines the contribution from a process where in-medium nucleon at least once interacted within a momentary cluster (DCNM).

and shapes of quasi-elastic peaks visible at low emission angles in the SMC++ (as well as in INCL simulations - cf. [70]) are well reproduced with binary interaction component alone.

Definitely, in the domain of low emission energies, where the observed discrepancy between the experiment and theory were up to now the strongest, the DCNM mechanism contributes very effectively to the observed yields of spallation products and compensates their underestimation in the pure binary collision approach.

More examples of the SMC++ simulation of the neutron spectra and their comparison to the experimental ones is given in appendix 11.1.

9.2 Light Charged Particles (LCPs)

9.2.1 Protons

In the intermediate energy region where the discrepancies between the experiment and theoretical models were so far most significant the merit of the proposed DCNM mechanism is illustrated in figs. 9.2, 9.3, 9.4 and 9.5 (last two only upper row) where measured in PISA and NESSI experiments proton double differential cross sections registered for p-Ta, p-Au, p-Ni and p-Al collision at 2.5- 1.9- and 1.2 GeV are compared with the SMC++ simulations. The simulated distributions reproduce the experimental ones with a precision always better than that achieved earlier in microscopic simulations.

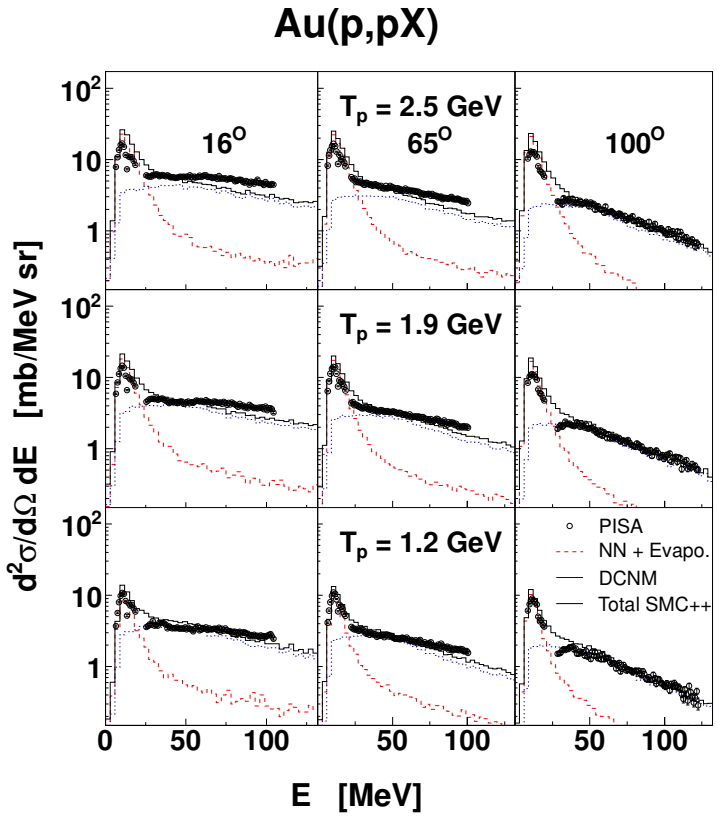

Figure 9.2: SMC++ simulation (solid line) compared to double differential cross section for proton produced in ^{197}Au target bombarded with protons. Experimental data were measured in the PISA experiment (open circles) [11]. The upper row shows results for 2.5 GeV beam energy, where three detection angle are selected: 16° (left panel) 65° (middle panel) and 100° (right panel). The middle and lower rows show the data for 1.9- and 1.2 GeV proton beam energy, respectively. The sequence of the detection angles is the same as in the upper row. The meaning of particular components of theoretical calculations is the same as in fig. 9.1.

Creation and decay of the momentary clusters induces much faster energy dissipation among the nucleons of the target and increase of number of medium nucleons involved in the dissipation process. As a result, for these regions of energy and emission angles where classical two step

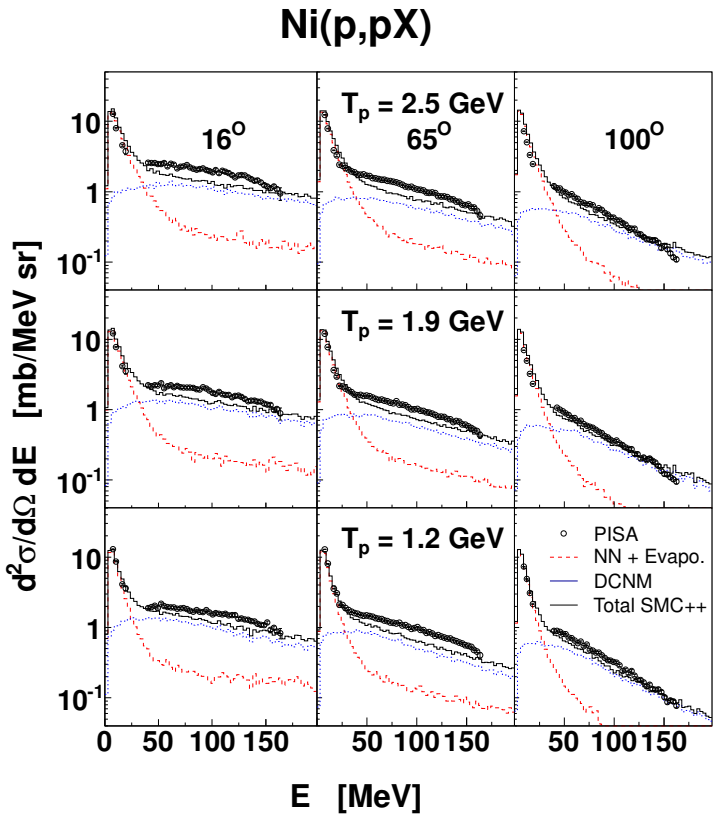

Figure 9.3: The same as in 9.2 but for ^{nat}Ni target. Experimental data (open circles) were measured in the PISA experiment [13].

models failed in reproducing the double differential cross sections with SMC++ a significant improvement is observed. The angular and energy dependence of the yields of ejectiles of reactions with heavy targets are reproduced rather well. For the light targets the discrepancy with respect to the experiment is still visible but is much smaller than for the INCL calculations (cf. figs. 11.7, 11.11, 11.15 of appendix 11.2).

In the emission of protons in the energy range where transition between the evaporation and preequilibrium components exist the experimental data measured at large detection angles (here 100°) show a structure which can be interpreted as an onset of preequlibrium spectrum. Especially for heavier targets such as Au and Ag (for Ag data see appendix 11.2) and for all three presented here collision energies there is a broad but distinct peak around emission proton energy of 40 MeV. Neither the SMC++ nor the INCL model is able to reproduce this structure. The data would be better reproduced by the simulation in which preequilibrium emission of protons both these originating from binary collisions as well as those from DCNM were more suppressed in the lowest emission energy range. Since this onset of preequilibrium is more distinct for heavy targets than for the light ones it may suggest that the calculation of the emission probability is oversimplified in both models.

9.2.2 Composite LCPs

The composite isotopes emission in the proposed SMC++ model is related only to creation and decay of dynamical clusters. In the model calculations the clusters have finite lifetime. Most of them decays instantly but those which live longer propagate in the target nucleus and can be expelled after reaching the nucleus surface. In majority they are a kind of fireballs - pieces of excited nuclear matter. Outside the target they may undergo an instantaneous disintegration into ground state particles.

The SMC++ simulation of LCPs production are compared in fig. 9.4 to double differential cross sections obtained in the NESSI experiment for proton-^{181}Ta reaction at 1.2 GeV. The distributions of composite ejectiles are shown in the second row (deuterons), in the third row (tritons) and in the fourth row (^{3}He). Some examples of SMC++ simulation of LCPs production

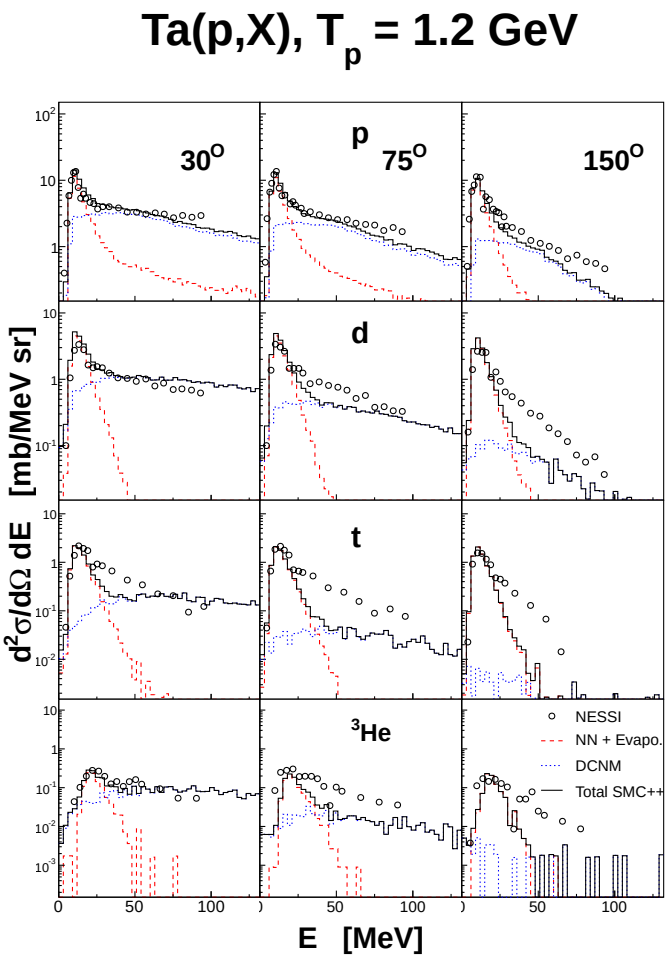

Figure 9.4: SMC++ simulation (solid black line) compared to double differential cross section for protons, deuterons, tritons and ^{3}He produced in ^{181}Ta target bombarded with protons at 1.2 GeV energy. Experimental data (open circles) were measured in the NESSI experiment [46] at three detection angles of 30°, 75° and 150° with respect to the beam direction. The meaning of particular components of theoretical calculations is the same as in fig. 9.1.

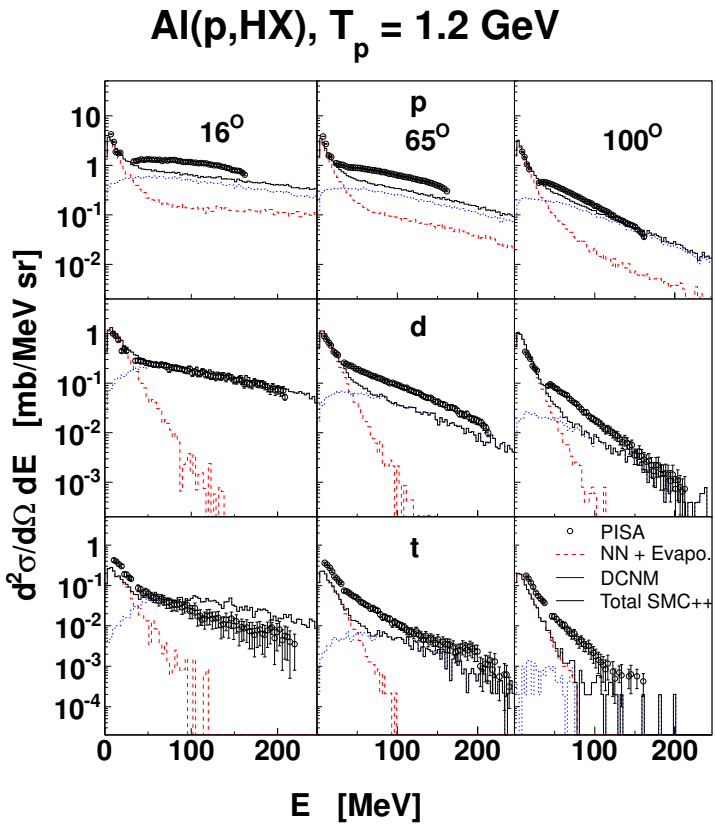

Figure 9.5: SMC++ simulation (solid line) compared to double differential cross section for protons, deuterons and tritons produced in ^{27}Al target bombarded with protons at 1.2 GeV energy. Experimental data (open circles) were measured in the PISA experiment [14] at three detection angles of 16°, 65° and 100° with respect to the beam direction. The meaning of particular components of theoretical calculations is the same as in fig. 9.1.

in the light target nucleus are compared in fig. 9.5 to to double differential cross sections for p, d, t production in ^{27}Al target bombarded with 1200 MeV protons. Figs. 9.6, 9.7, 9.8 show double differential cross sections for d, t, ^{3}He obtained for proton-^{nat}Ni reaction at 2.5- 1.9- and 1.2 GeV beam energy.

It is clear that the simplification used in SCM++ consisting in assumption about instantaneous thermalization of the matter embedded in the momentary clusters is too strong. It is visible especially in the simulated spectra of composite particles. There is a tendency that results of the simulations overestimate the measured yield of particles at low emission angles whereas at higher emission angles simulated cross sections are lower than experimental ones. It comes from the fact that cluster formation is predominantly initialized by energetic nucleons of the resultant momenta pointed forward with respect to the beam axis. Under assumption of fully compound and equilibrated clusters their decay give stronger contribution to the forward directions than it is required. It would be better for the data description to assume not fully equilibrated clusters. During their decay the spread of dispersing particles could then to some extent reflect the initial momenta of particles before they joined together. And the decay product would give less contribution to the particle flow at small angles with respect to the beam axis. A proper

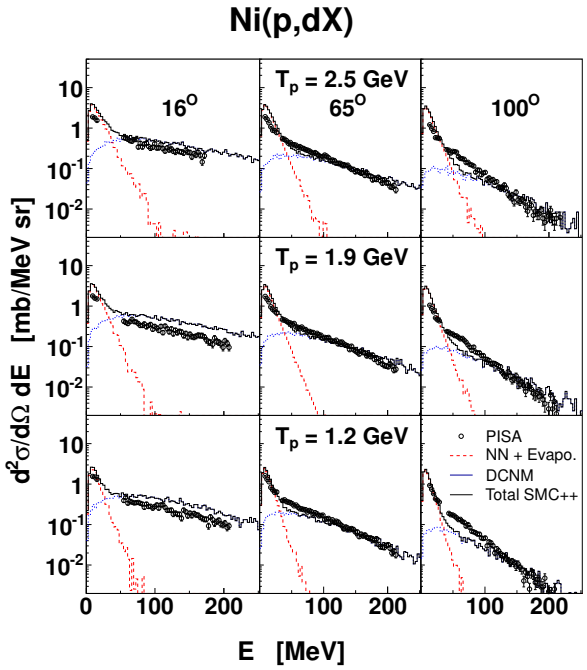

Figure 9.6: The same as in fig. 9.3 but the presented cross sections are for deuterons.

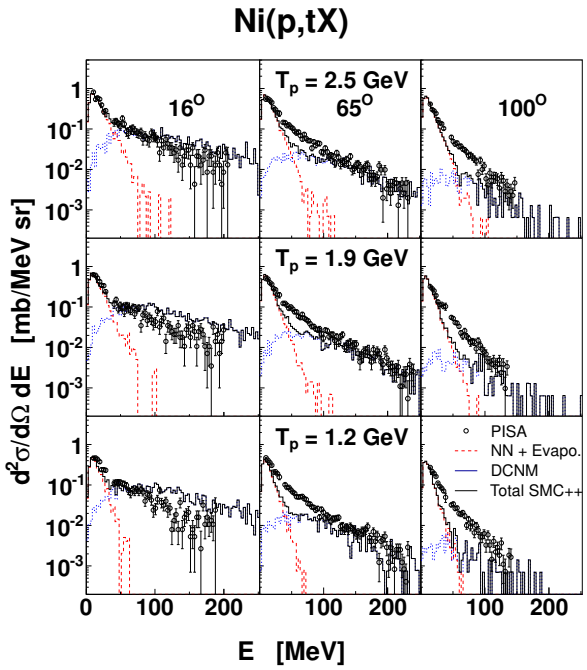

Figure 9.7: The same as in fig. 9.3 but the presented cross sections are for tritons.

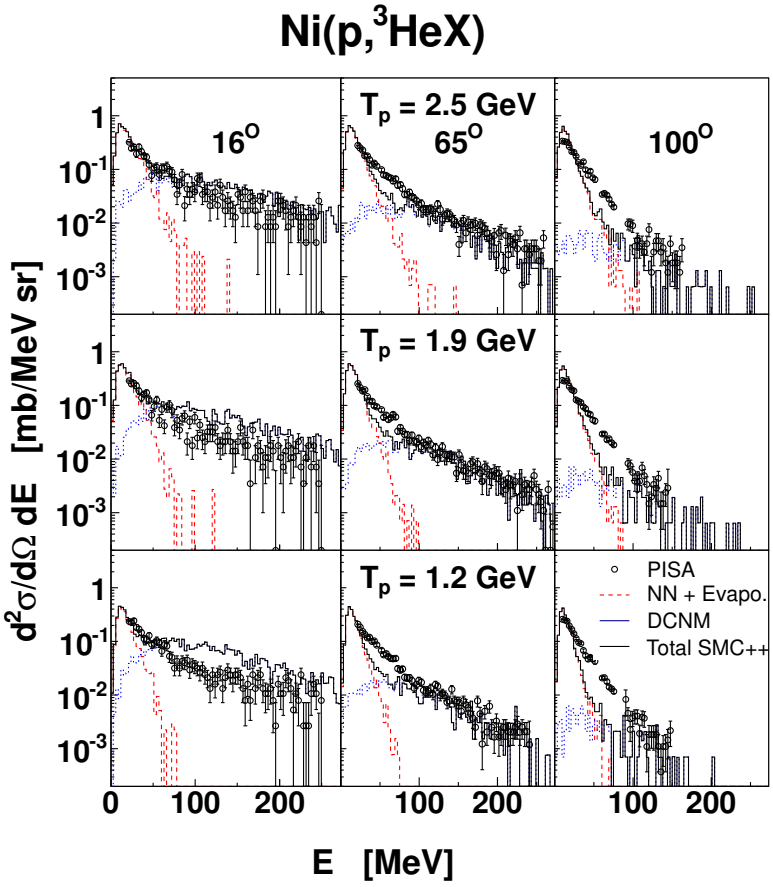

Figure 9.8: The same as in fig. 9.3 but the presented cross sections are for ^{3}He.

modeling of interaction of nuclear constituents within the momentary cluster is an appealing aspect of the proposed DCNM mechanism.

In the SMC++ the d, t, and ^{3}He particles are produced predominantly in the decay of heavier clusters emitted from the target nucleus. The mean mass of the source of these particles is between 5 and 6 which is in good agreement with estimated mass of fireball assigned to be responsible for d, t, and ^{3}He production in moving source model of the PISA collaboration [13].

An extensive comparison of the results of SMC++ simulation of the LCP's double differential cross section to the experimental data of the PISA experiment is shown in appendix 11.2. The presented there figures contain also the results of simulations obtained with INCL4.3+GEM2.

9.3 Pions

The emission of pions in the initial phase of the spallation process is an important factor influencing the speed of the remnant thermalization. The rate of pion production to great extent determines the excitation energy of the remnant. Thus, the prediction power of the spallation model concerning the pion yields is an important benchmark for the model construction and its tuning.

The pion spectra in the proposed model result entirely from NN→NΔ(1232) excitation and Δ(1232) decay. They are important indication of an inelastic process rate in NN collisions. In current versions of SMC++ the nucleons captured in the dynamic clusters cannot take part in the Δ resonance excitation and thus in the pion production. But the pion spectra of SMC++ remains almost unaffected when compared to the results obtained in the INCL simulations [70, 89]. It means that the parameters of SMC++ responsible for the probability of momentary clusters formation and decay are selected properly in the sense that cluster formation does not suppress the pion production in the NN→NΔ(1232) process. The pion rate results as well from the decay rate of the existing Δ's. In this respect the simplified recipe for in-medium Δ lifetime determination applied in SMC++ (cf. 8.7) seems to be sufficient.

Unfortunately, the experimental data for the pion production in the demanded here energy range are scarce. Figures 9.9, 9.10, 9.11 and 9.12 show the SMC++ simulations of π^+ and π^- double differential cross sections for 730 MeV proton induced spallation in C, Al, Cu and Pb target, respectively. The theoretical predictions are compared to the only available experimental data of [139].

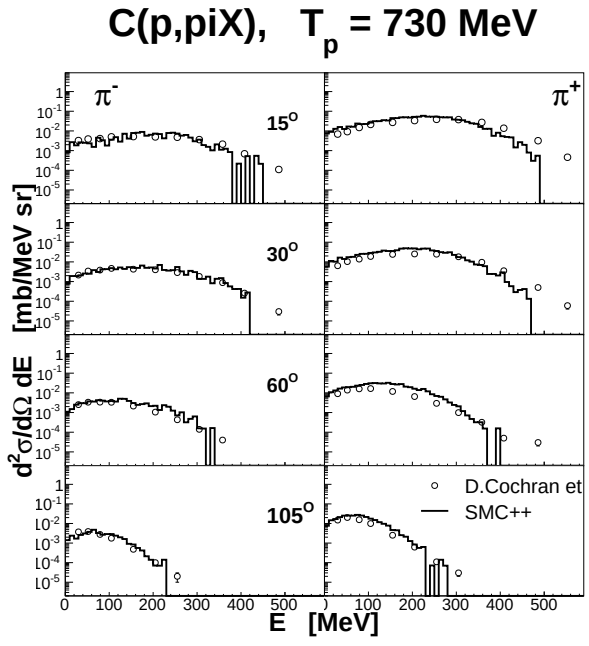

Figure 9.9: Distribution of pions emitted in reaction of p+C at 730 MeV simulated with SMC++ compared to experimental spectra by Cochran et al. [139]

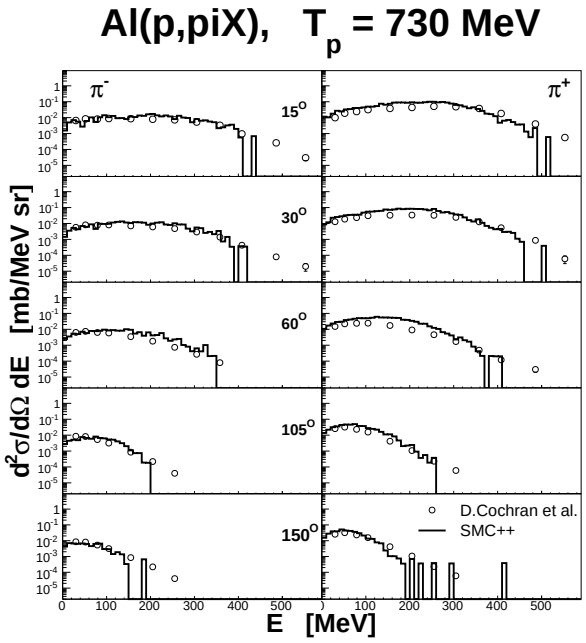

Figure 9.10: The same as in fig. 9.9 but for Al target

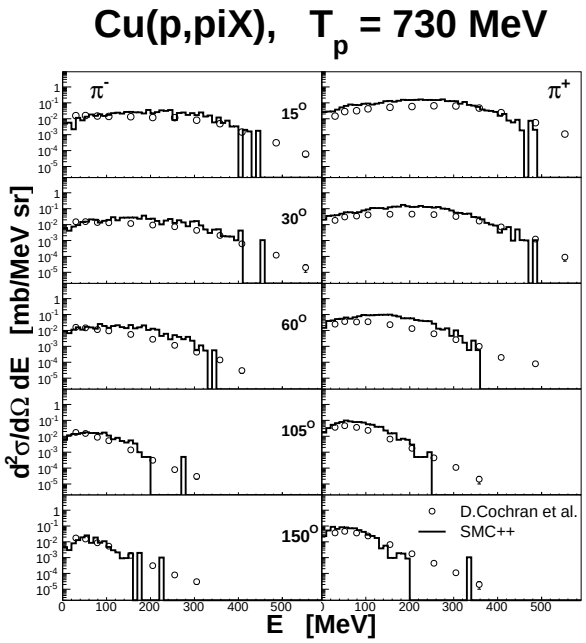

Figure 9.11: The same as in fig. 9.9 but for Cu target

The shapes of distributions and their magnitudes of both the positive as well as the negative pions are well reproduced by SMC++. It concerns all examined targets and the whole range of emission angles. The model underestimates only the higher energy part of the pion spectra.

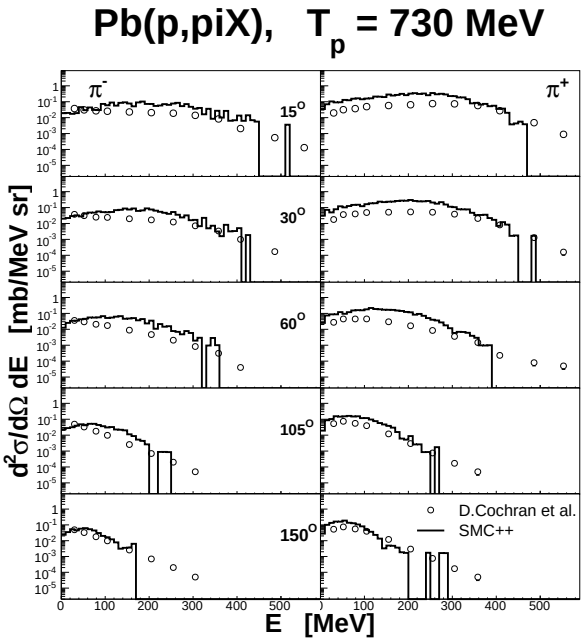

Figure 9.12: The same as in fig. 9.9 but for Pb target

The correct reproduction of the low energy components of the neutron and LCPs distributions assigned to the evaporation process indicates that the assumed processes of SMC++ are properly balanced permitting the creation of the hot residual nuclei with realistic physical parameters.

It has to be emphasized that the dynamical clustering in nuclear medium proposed here is a process different from the purely kinematical fireball creation governed by geometry of overlapping ions like in [126, 128]. It is also different than fireball used in interpretation of results of the PISA experiment by means of moving source method (see chapter 7 and [10, 11, 13]) where again only geometry plays a role. A mechanism named snowball [67] is based on the idea similar to coalescence and has different nature as well.

10 Summary

The experimental investigations of the spallation mechanism performed by the PISA collaboration followed by the extensive efforts for theoretical interpretation of obtained double differential cross sections bring the significant progress for the understanding of the very complicated domain of proton-nucleus interactions at GeV energy region.

The obtained experimental data base for $\frac{d^2\sigma}{dEd\Omega}$ ranges from production of protons to carbon nuclei emitted from target nuclei of ^{197}Au, ^{nat}Ag, ^{nat}Ni, ^{27}Al and ^{12}C is the broadest set of spallation data obtained up to now by one experiment. The bombarding kinetic energies of protons are from 175 MeV to 2.6 GeV. The reaction products were registered at 9 detection angles by an advanced detection system composed of detectors of diverse types.

Applied experimental technique utilizing the internal beam of the COSY accelerator in the Research Center Jülich (Germany) and the operation mode permitting for interruption-free collection of data at few beam momenta as well as very careful data selection and calibration benefited in creation of a broad, reliable and precise experimental data base of double differential spallation cross sections.

The obtained experimental distributions were interpreted in the framework of the hypothesis of the two step spallation process with the use of the best contemporary models of spallation reaction - Intranuclear Cascade Liege (INCL), transport equations of Boltzmann-Uehling-Uhlenbec (BUU), Generalized Evaporation Model (GEM), multifragmentation process as a Fermi Breakup mechanism (computer code ROZPAD). The analysis has shown that the low energy components of the experimental spectra can be reproduced with good precision under the assumption of the statistical decay (evaporation or mulifragmentation) of a target remnant. It was also realized that the mechanism assumed for the initial step of the proton-target interaction, namely cascade of binary hadronic collisions supplemented with surface coalescence mechanism, is insufficient for reproducing the double differential cross section for all types of spallation products. Contemporary models underestimate the experimental spectra for all target masses and for all beam energies. The most significant discrepancies are observed for small emission angles and in the emission energy range of 50 - 150 MeV. The disagreement is stronger for light target of ^{12}C (up to factor 5) and decrease with the target mass. For ^{197}Au the discrepancy is about a factor 2.

For this reason a further interpretation of the data has been performed with a classical two step model extended by the phenomenological modeling of moving sources. Assumption about alternative mechanisms contributing to the emission of spallation products resulted in the success in reproducing the experimental distributions within this hybrid model. It was achieved at the expense of introduction of a few but reasonable and well justified model parameters which are universal for the whole considered range of energy and mass.

The analysis of the experimental distributions obtained in the PISA experiment have shown that currently there is no one consistent model permitting to interpret the proton-nucleus interaction at energies higher than a few hundreds of MeV. In order to account for observed shapes of $\frac{d^2\sigma}{d\Omega dE}$ there is a need of application of a conglomerate of mechanisms which contribute to the particle yield. The conditions of occurrence of individual mechanisms are not fully defined. The simulation of the reaction where various mechanisms are introduced permits to establish their significance for different target masses, ejectiles and energy regions.

Besides of statistical emission in the form of evaporation from thermalized target-like remnant, which is responsible for a low energy component of all types of ejectiles it seems that accumulated energy in the bombarded nucleus in the case of light targets can induce a more rapid disintegration of the target which can take a form of multifragmentation. This phenomenon can be described by a Fermi breakup mechanism. Performed simulations with the multifragmentation mechanism of light targets (^{12}C, ^{27}Al) resulted in an improvement in calculated yields for IMFs, whereas there is almost no effect for LCPs.

In order to reproduce the high energy component of the double differential cross sections which extends from about 30 MeV and is more pronounced for low emission angles, the microscopic models which take into account the general nuclear properties and experimental cross section of relevant hadronic interaction (in this respect the intranuclear cascade model - INCL and BUU calculation have been checked) have to be supplemented with the hypothesis of nuclear coalescence or the phenomenological models utilizing the general features of the excited thermodynamical ensembles. In this context the moving source model has been applied indicating the possible existence of three sources of observed particles. Among them the most significant is the possible formation of a light and fast propagated object emitting LCPs. This object is referred to as a "fireball".

The results of the phenomenological analysis of the data using the moving sources model was an inspiration for the search of the lacking reaction mechanism in the more microscopic manner. The intermediate stage of the reaction could efficiently contribute to production yields underestimated by the classical two step model. For this purpose a new spallation model has been constructed with partial utilization of the achievements of the decade long development of the INCL model family, but structurized in the way permitting an easy implementation of the hypothetical mechanisms of the reaction. The model called Spallation Model with Cascade++ (SMC++) is implemented into the computer code written in C++ programing language.

The requirements of the additional mechanism contributing to the spallation yields, but missing in the classical two step approach, have been defined as follows: the increase of energy/momentum transfer from a projectile to the target, involvement into interaction of more nucleons of the nuclear medium, enhancement of the the energy dissipation within the target nucleus during the initial reaction phase. The postulated mechanism should also contribute to the production of composite spallation ejectiles.

It was found that the process fulfilling the above mentioned requirements, and called a Dynamical Clustering in Nuclear Medium (DCNM), may consists in the creation of the momentary aggregates of the mutually interacting nucleons in the whole volume of a nuclear medium. The appearance of such clusters can be an effect of the fluctuations of the nuclear density in the nucleus thrown off balance by impact of a projectile and created in this way local nuclear field modifications. The postulated objects have to be of the nature of fireballs or molecular resonances rather than the well established nuclear composite objects. In order to obtain the demanded energy dissipation rate the fast interaction among the cluster constituents has to be assumed and be followed by the cluster decay. The estimated life times for majority of dynamic clusters have to be very short - significantly shorter than the lifetime of a free Δ resonance. Permitting, however, a broad spread of the life times for these of the clusters which are more firmly bounded allows to realize a self consistent concept of the composite particle production in spallation reaction.

It was noted already in the past that some form of the internal substructures in the nuclear systems are needed in order to account for the observed problems in the theoretical descriptions of observed phenomena. In the low energy domain, where the shell model is applicable, the cluster formation in the light nuclei was introduced in the formal mathematical manner by Wildermuth

[147]. From that time the so-called nuclear cluster physics is a lively developing branch within the nuclear spectroscopy research (see e.g. [148]). In the field of heavy ion collisions the ideas of fireball and firestreak have been explored [126, 128]. Recently the ideas about the excitation of the nuclei to the state of the alpha-particles gas are explored both experimentally [149] and on the ground of theoretical models [144]. In the spallation physics the concept of snowball were introduced by Boal [67]. The idea of surface coalescence [47] is broadly used in order to aid in the production of composite particles both in intranuclear cascade models [68, 70] as well in the Quantum Molecular Dynamics [69]. In the latter case the cluster formation can be also permitted due to the overlap and interference of the nucleon wave functions [144]. The enhancement of the nucleon emission rate in spallation processes was studied within QMD with an assumption about a noninstantaneous and nonlocal character of NN collisions [150, 151].

The postulated new process of DCNM is an attempt to go beyond the limitations of the contemporary concepts of the in-medium nuclear interactions. It is tried to account for the actual density fluctuations over the whole volume of the target nucleus and during the whole time before the spallation remnants attain the thermal equilibrium. The DCNM mechanism is also an attempt to include into still simple model of cascade an effect of non zero probability of interaction among a few closely remaining nucleons. The proposed process depends not only on geometry but also on the suitable energy and momentum conditions have to be fulfilled. The achieved good agreement of SMC++ calculations with experimental data obtained for various proton beam energies and broad range of target masses indicates that nuclear density fluctuations have to be taken into account when nucleon-nucleus processes are studied and that in-medium interaction involving a few nucleons on very short time scale is a mechanism actually realized in nature.

The experimental program of the PISA collaboration have to be evaluated as very successful. Huge set of precise experimental data have been collected. Careful interpretation of the obtained results was performed within the existing theoretical models. The areas of the models inadequacy to the observed physics phenomena have been defined. The creative approach to the analysis of experimental data resulted in development of fresh ideas on the mechanisms of spallation reactions. It gained in both qualitative as well quantitative definitions of mechanisms and conditions required in order to obtain a better description of observed in experiment phenomena. All these efforts have resulted in unquestionable progress in the understanding of the mechanism of the nucleon-nucleus interaction in a few GeV region of bombarding energies. As open question remains whether the new identified features of spallation reactions can be derived from first principles.

11 Appendix - results of Spallation Model with Cascade++

In this appendix a broad set of distributions obtained with the SMC++ model will be confronted with the experimental data of the PISA experiment. As mentioned already in chapter 8 the SMC++ model was used to simulate the initial phase of pA reaction whereas the evaporation from the thermalized remnant was performed with the use of GEM2 model. Both model were coupled together in one computer code and simulation have been performed event-by-event.

11.1 Neutrons

The convention of the labeling of the individual components of spallatiom mechanism is here the same as in chapter 9: the components from the binary collisions of nucleons and the low energy components resulting from the evaporation are given as a one distribution marked with the dashed line. The contribution of the DCNM is marked with the dotted line.

In all figures the experimental data (open circles) used as a reference originate from the measurements performed at SATURNE [39] where the Fe and Pb targets were bombarded with proton energies of 0.8, 1.2 and 1.6 GeV energy.

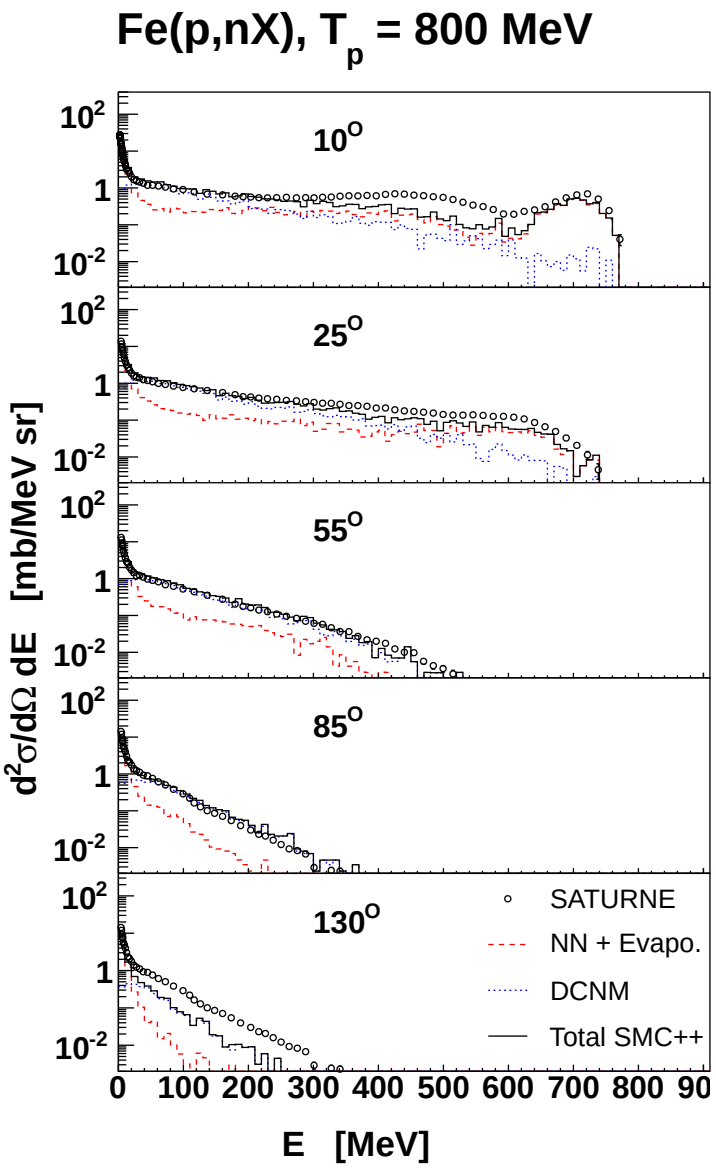

Figure 11.1: Distribution of neutrons emitted in reaction of p+Fe at proton impinging energy of 800 MeV simulated with SMC++ and compared to experimental spectra of Leray et al. [39]

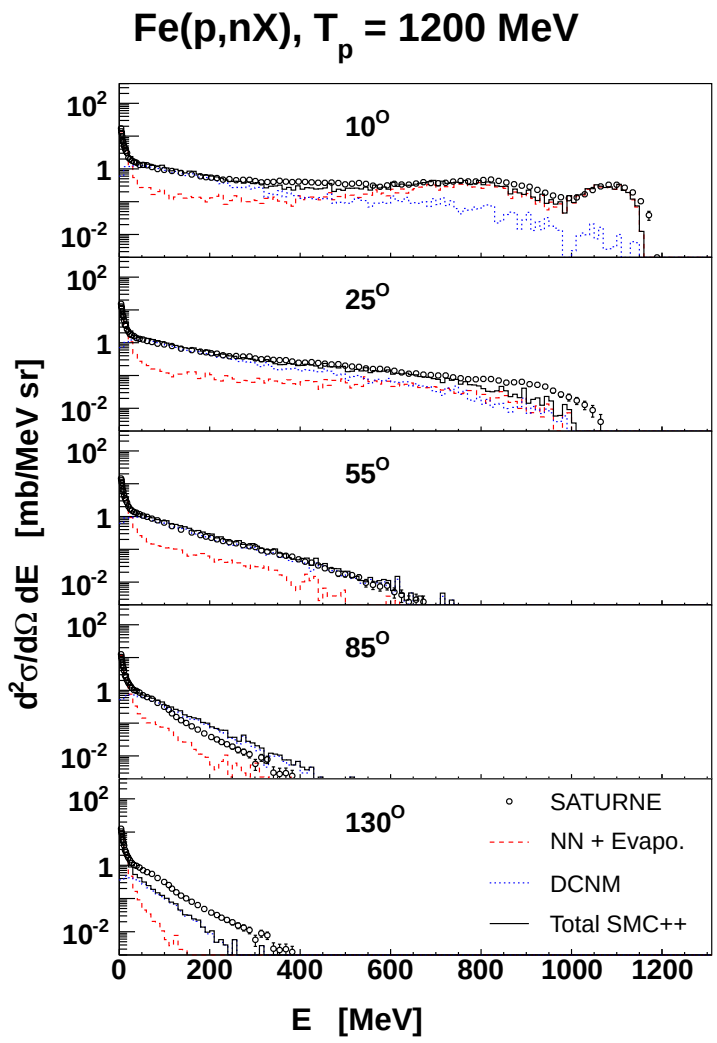

Figure 11.2: The same as in fig. 11.1 but for proton impinging energy of 1200 MeV.

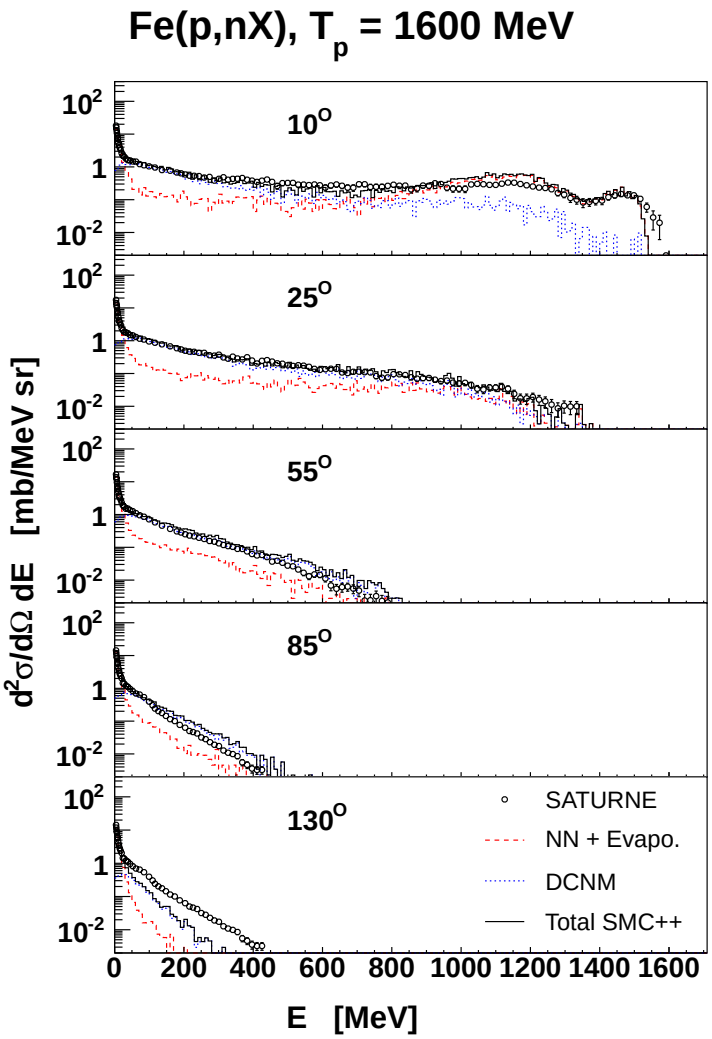

Figure 11.3: The same as in fig. 11.1 but for proton impinging energy of 1600 MeV.

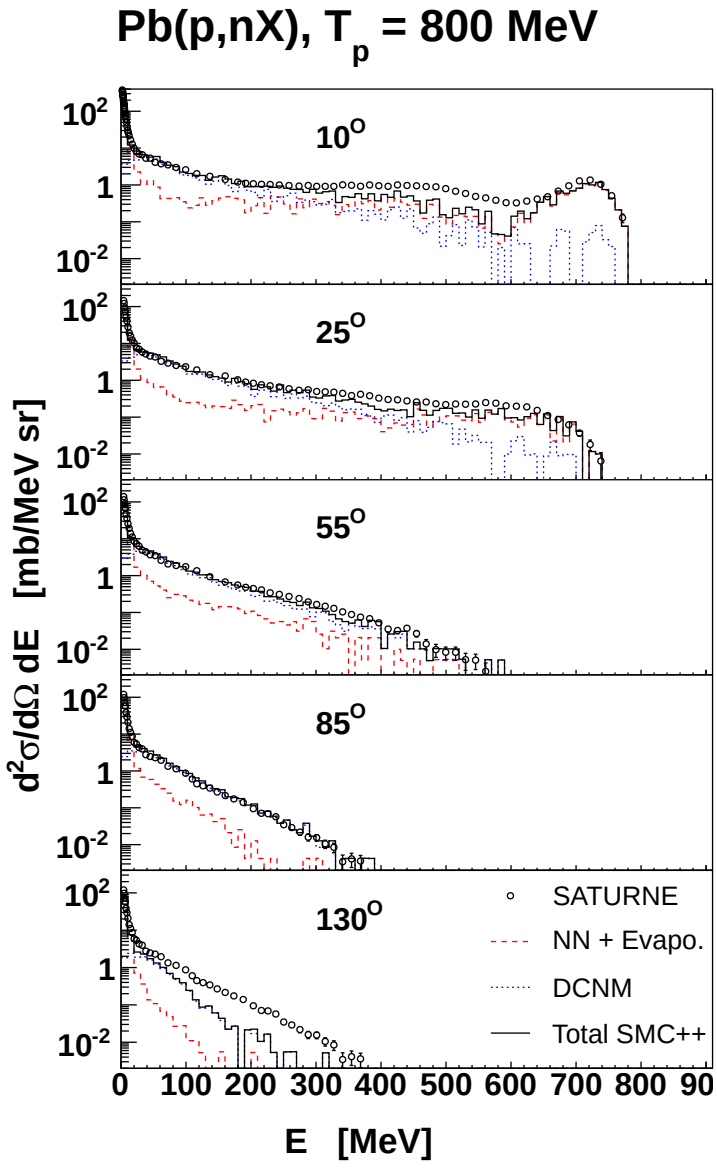

Figure 11.4: Distribution of neutrons emitted in reaction of p+Pb at proton impinging energy of 800 MeV simulated with SMC++ and compared to experimental spectra of Leray et al. [39]

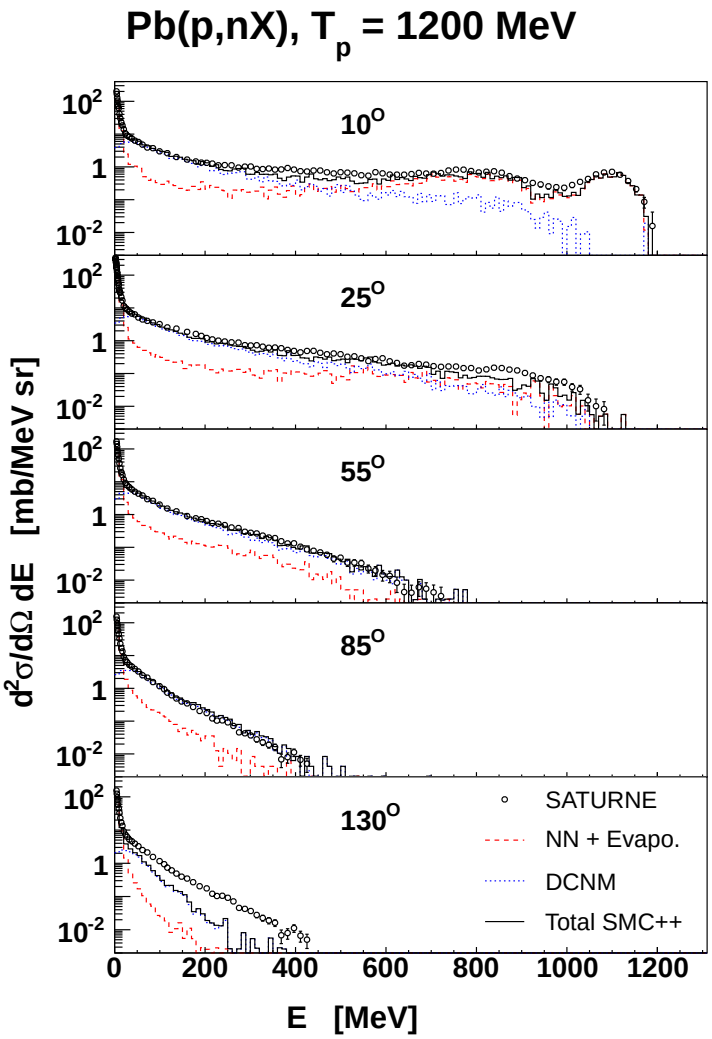

Figure 11.5: The same as in fig. 11.4 but for proton impinging energy of 1200 MeV.

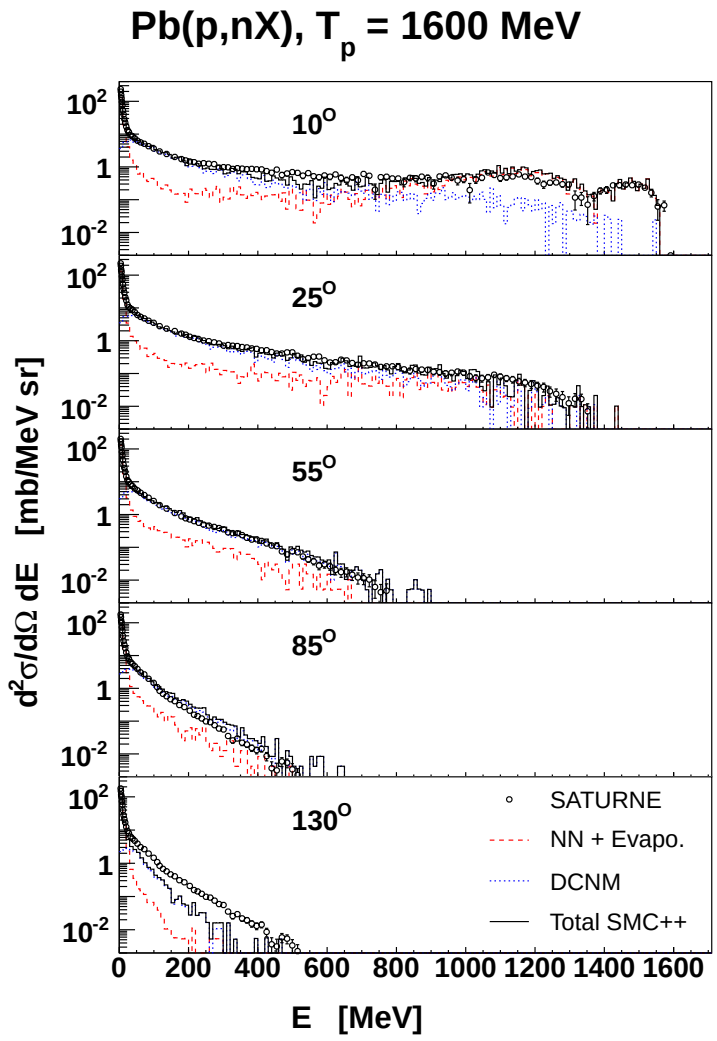

Figure 11.6: The same as in fig. 11.4 but for proton impinging energy of 1600 MeV.

11.2 Light Charged Particles (LCPs)

The LCPs simulations of SMC++ (solid red line) are compared to the analogous results of INCL4.3 (green dashed line). The evaporation process in both cases has been performed with the GEM2 model. The reference experimental data were obtained in the PISA experiment (open circles).

11.2.0.1 Proton bombarding energy of 2.5 GeV

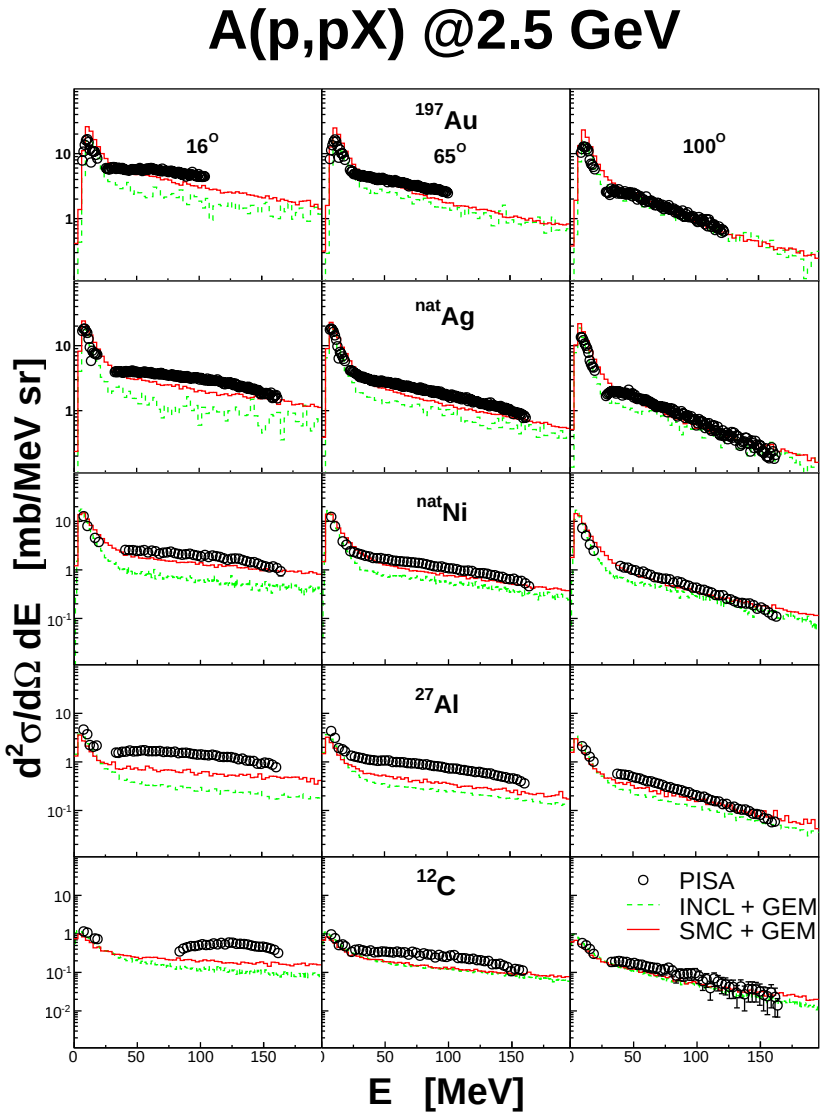

Figure 11.7: A comparison of results of simulations with SMC++ and INCL4.3 [68] with the experimental distributions of protons measured in collisions of protons with various target nuclei at energy of 2.5 GeV. Experimental data originate from the PISA experiment.

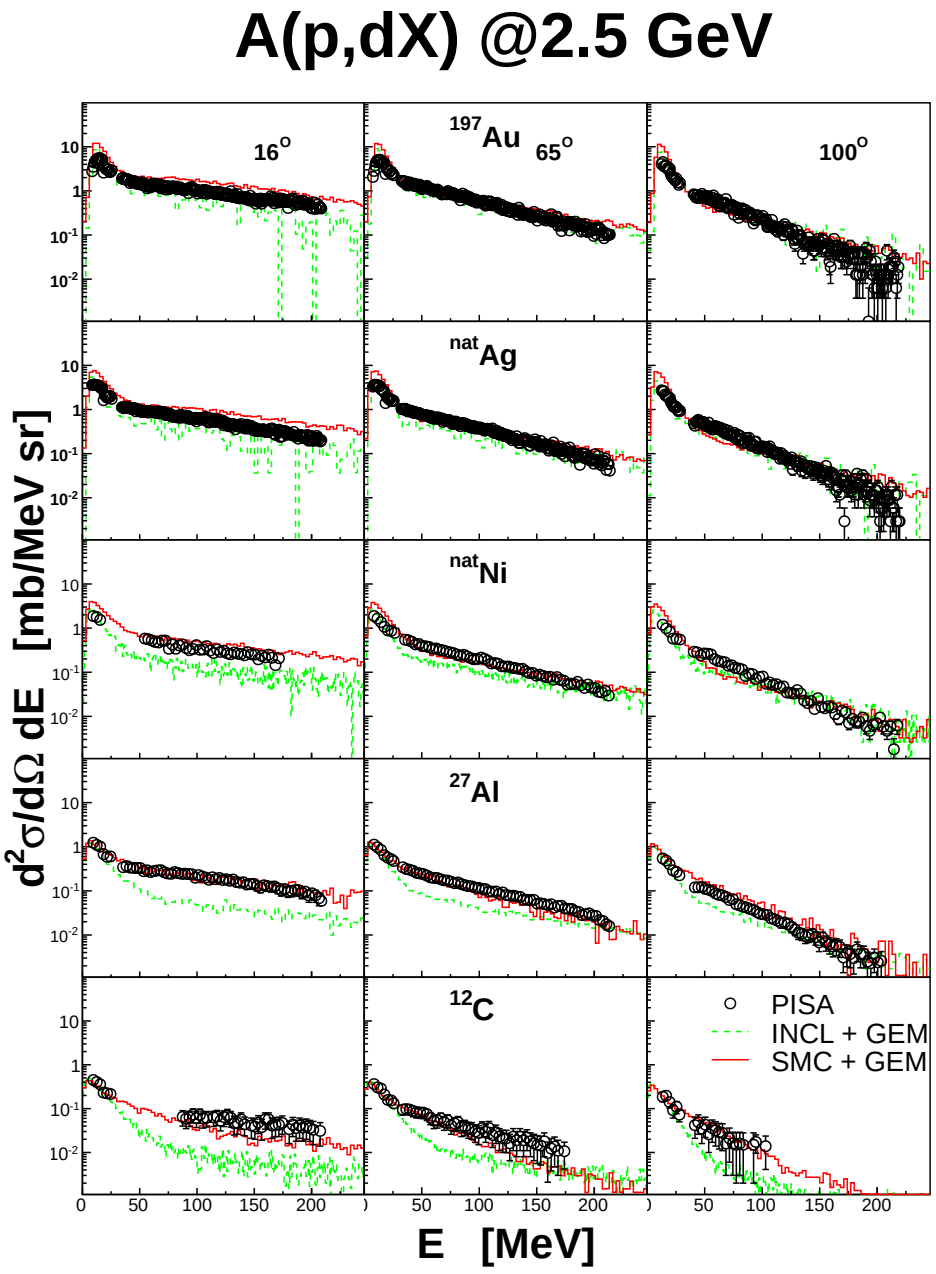

Figure 11.8: The same as in fig. 11.7 but for deuterons.

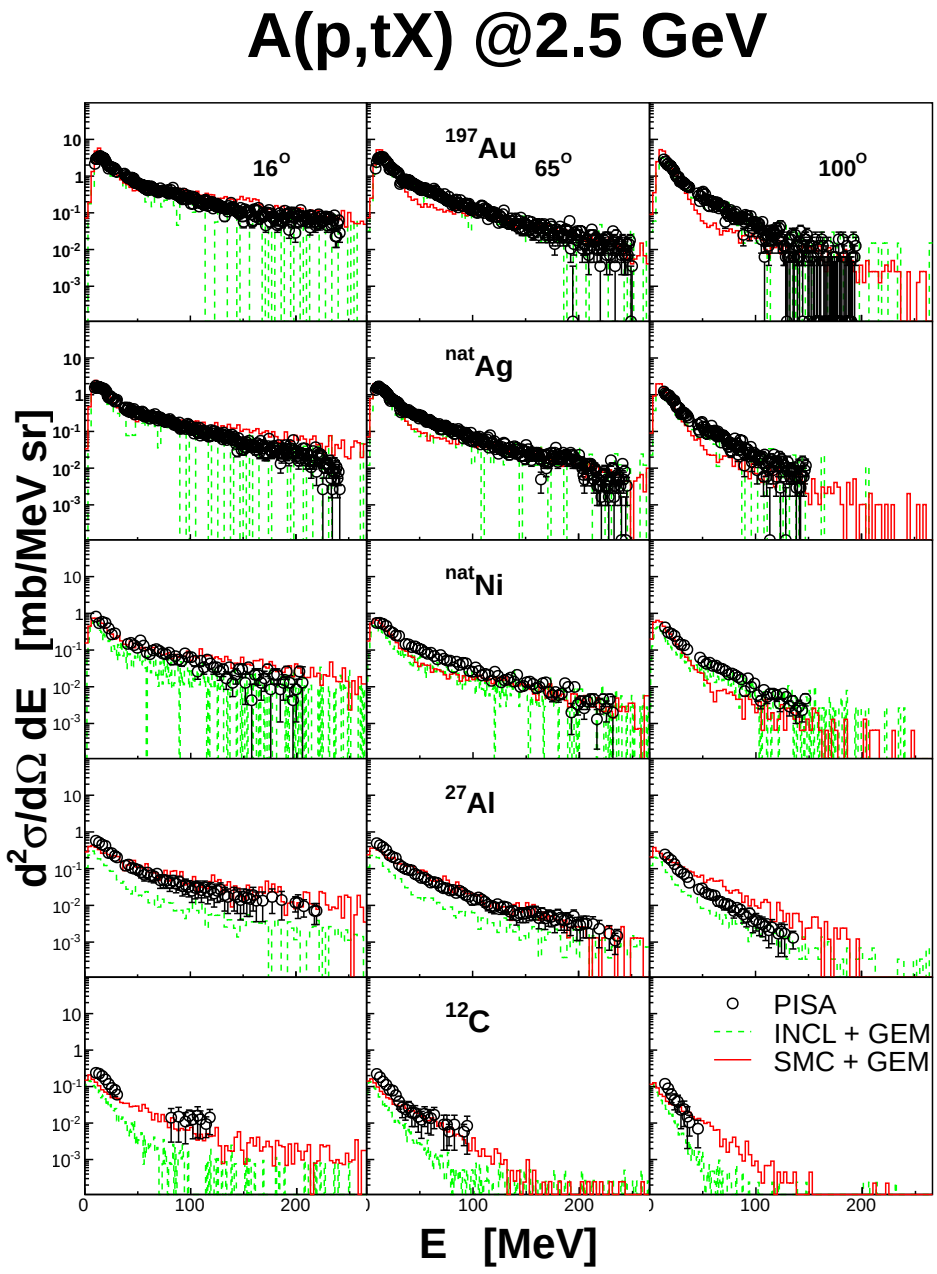

Figure 11.9: The same as in fig. 11.7 but for tritons.

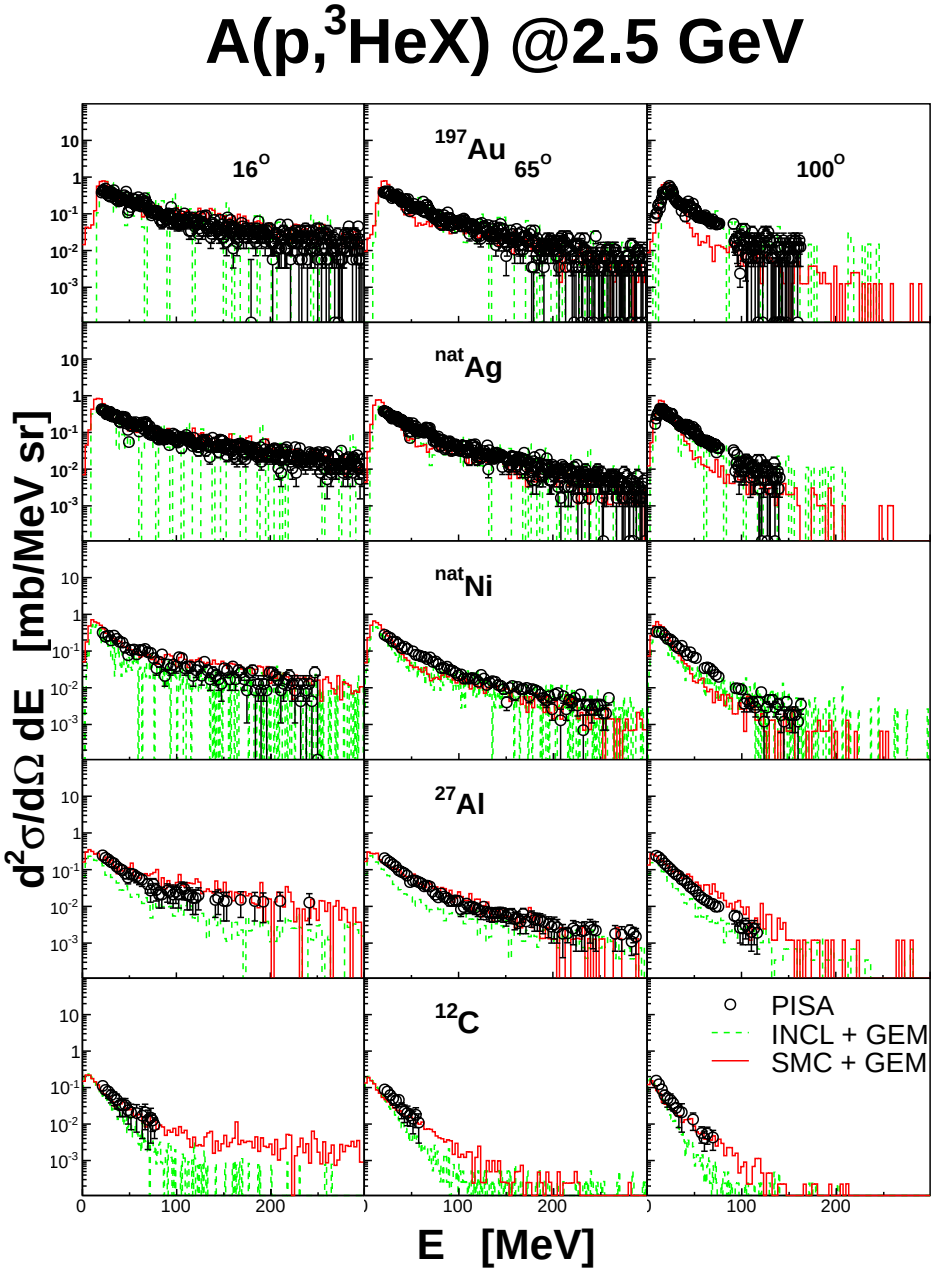

Figure 11.10: The same as in fig. 11.7 but for ^{3}He.

11.2.0.2 Proton bombarding energy of 1.9 GeV

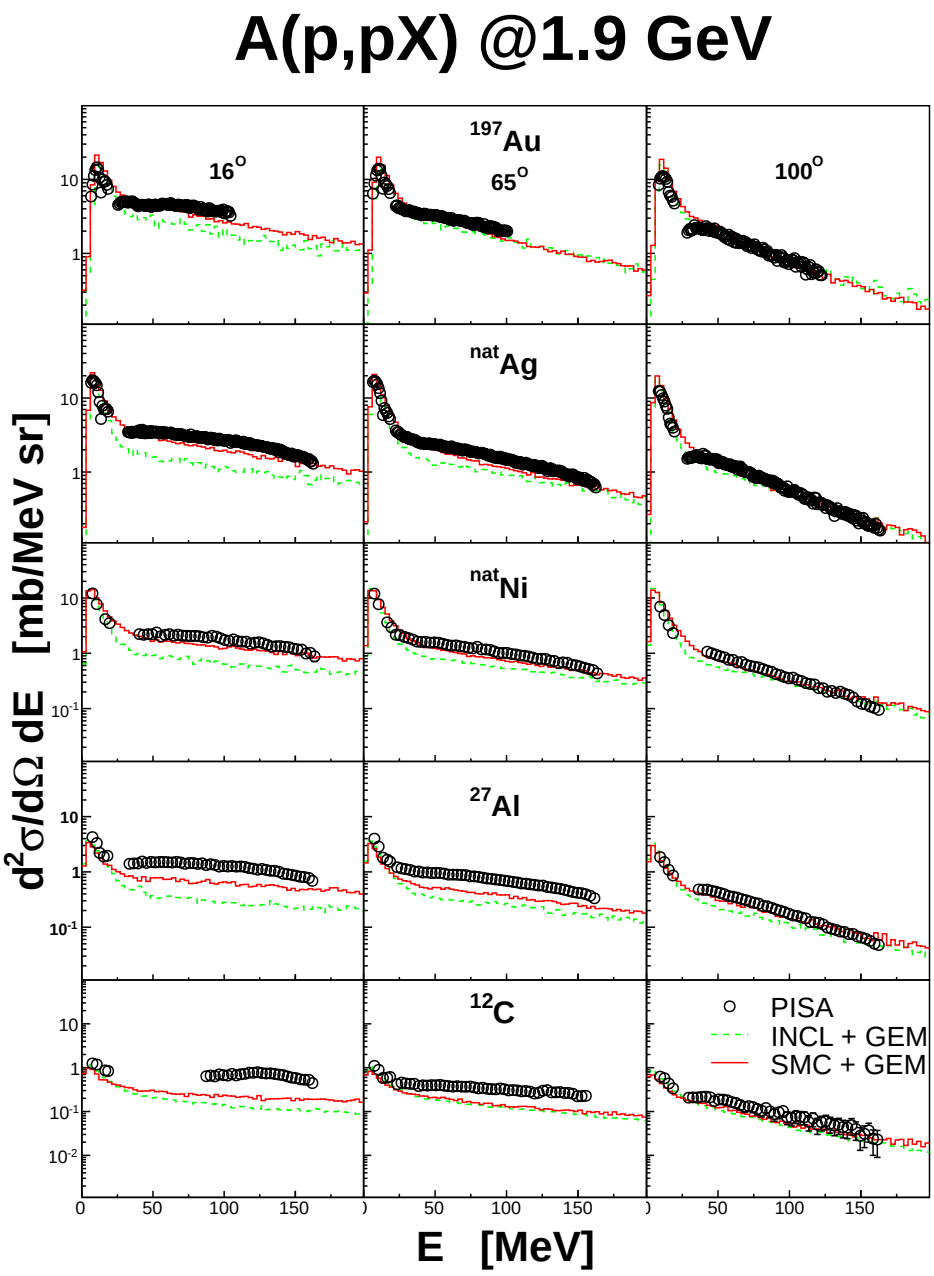

Figure 11.11: A comparison of results of simulations with SMC++ and INCL4.3 [68] with the experimental distributions of protons measured in collisions of protons with various target nuclei at energy of 1.9 GeV. Experimental data originate from the PISA experiment.

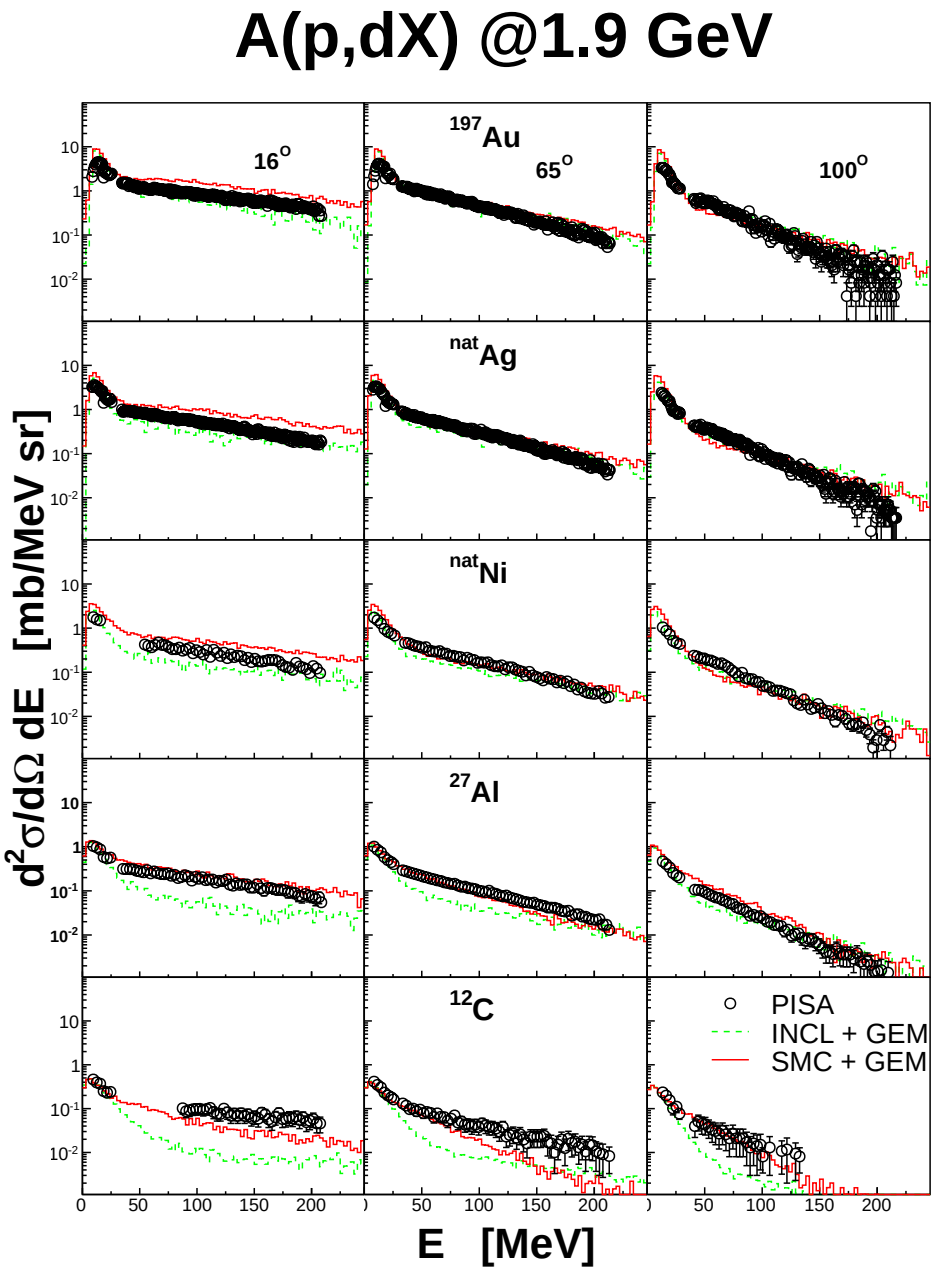

Figure 11.12: The same as in fig. 11.11 but for deuterons.

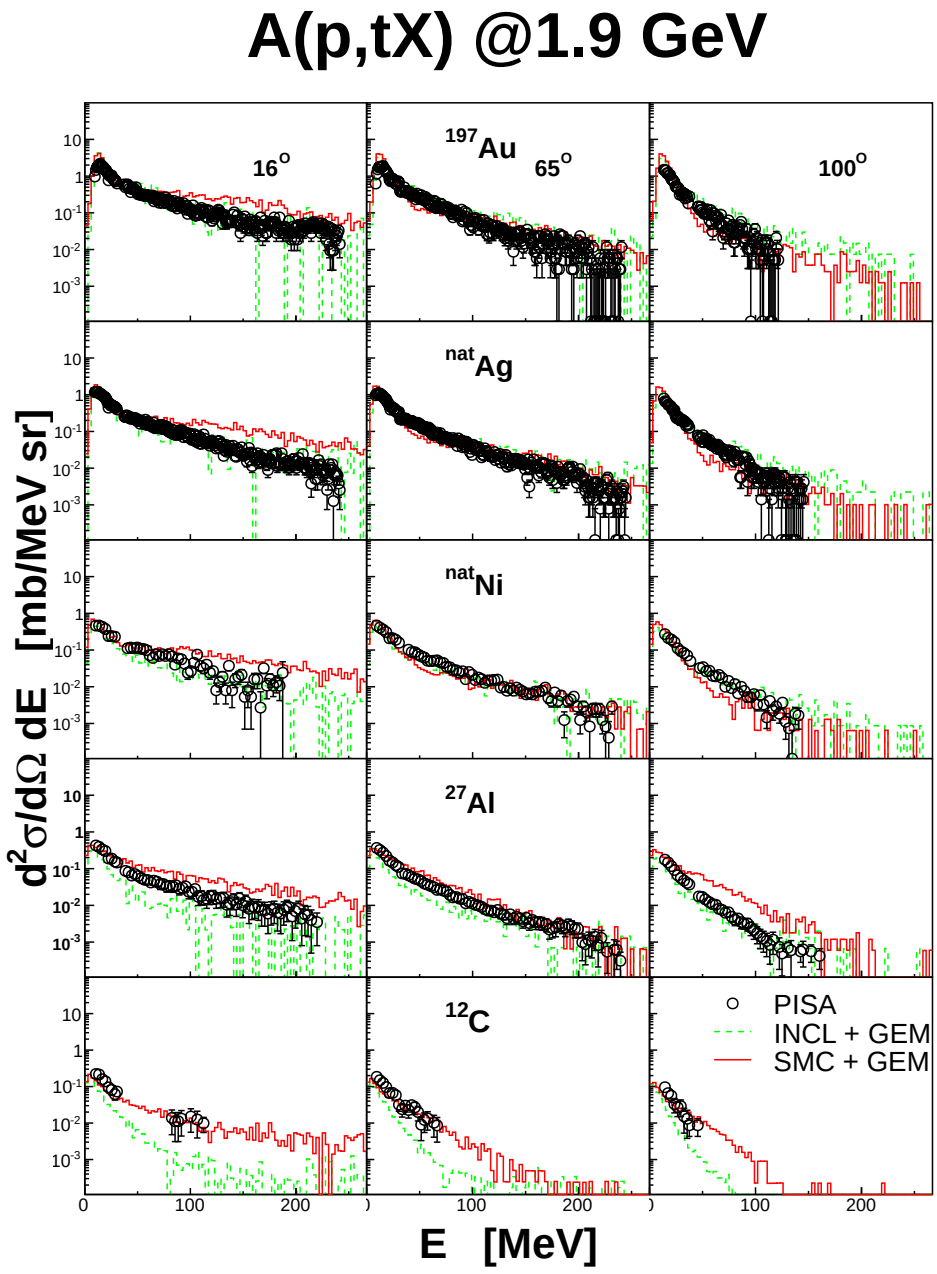

Figure 11.13: The same as in fig. 11.11 but for tritons.

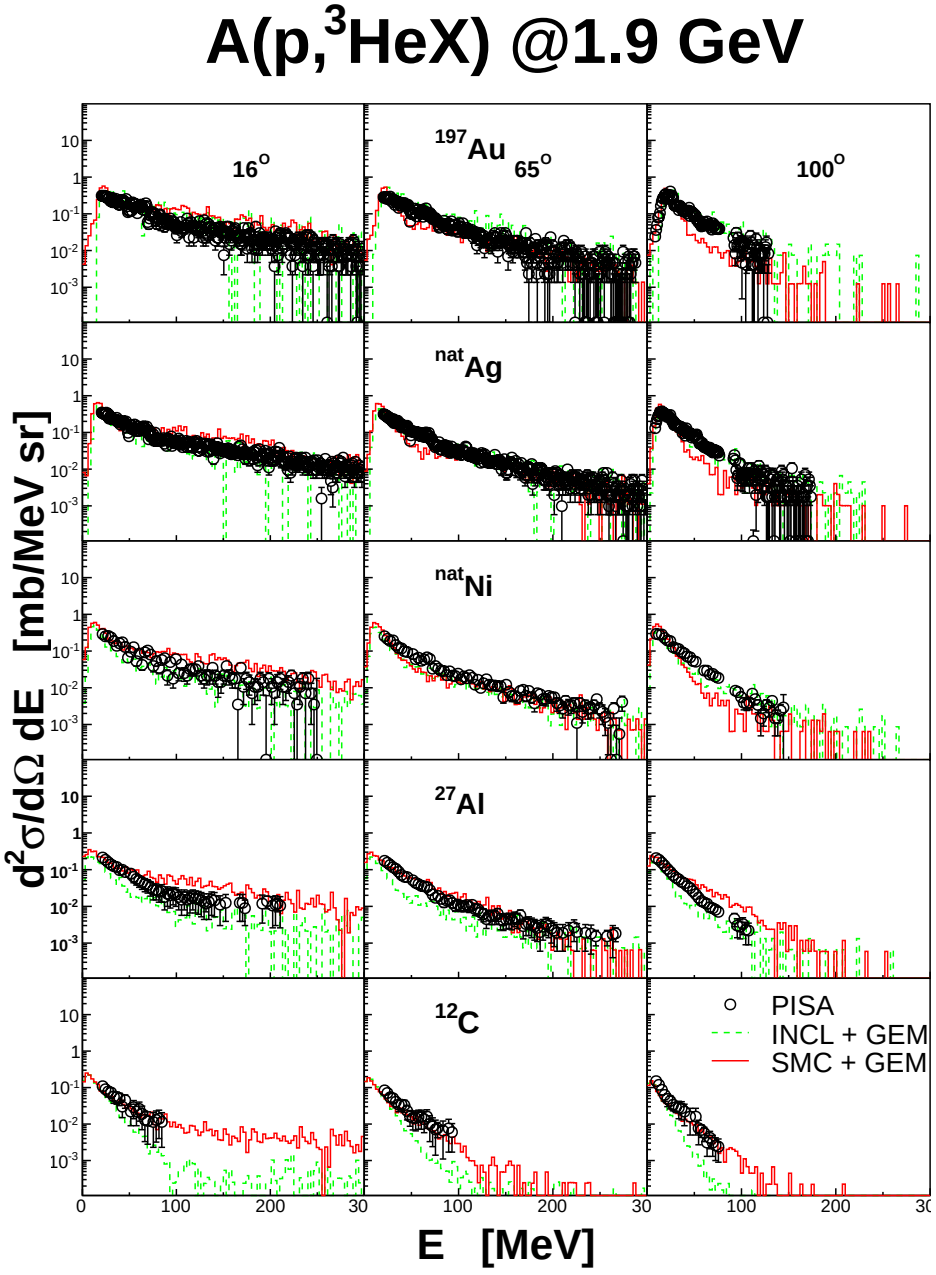

Figure 11.14: The same as in fig. 11.11 but for ^{3}He.

11.2.0.3 Proton bombarding energy of 1.2 GeV

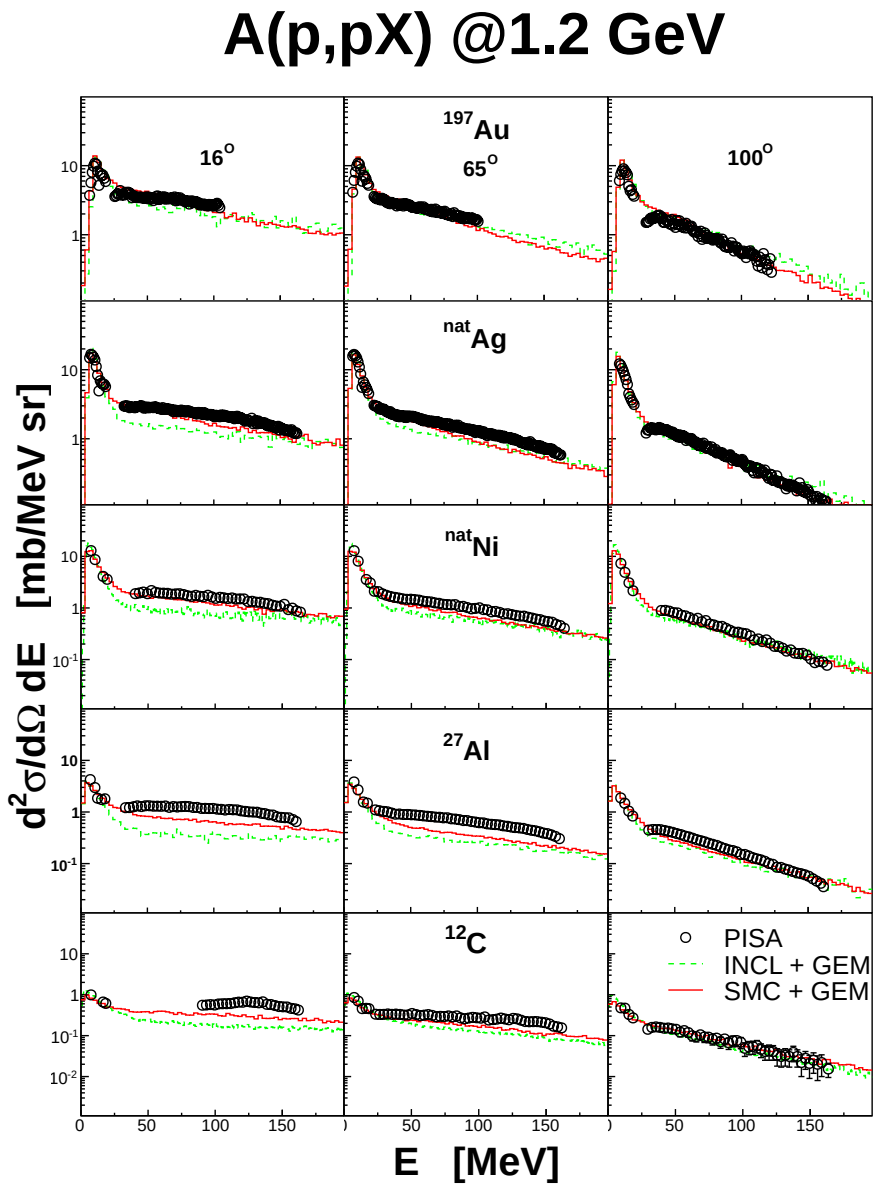

Figure 11.15: A comparison of results of simulations with SMC++ and INCL4.3 [68] with the experimental distributions of protons measured in collisions of protons with various target nuclei at energy of 1.2 GeV. Experimental data originate from the PISA experiment.

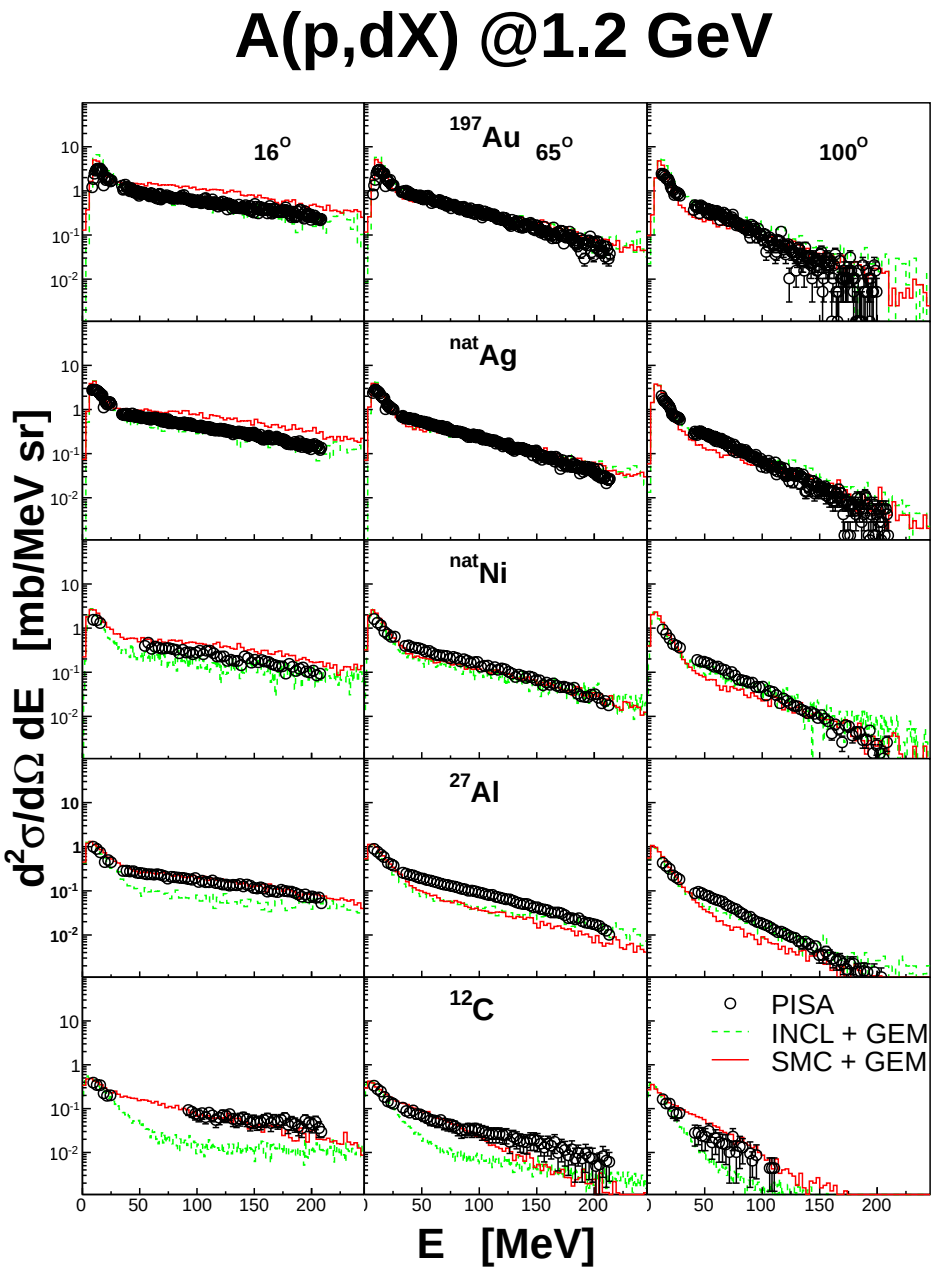

Figure 11.16: The same as in fig. 11.15 but for deuterons.

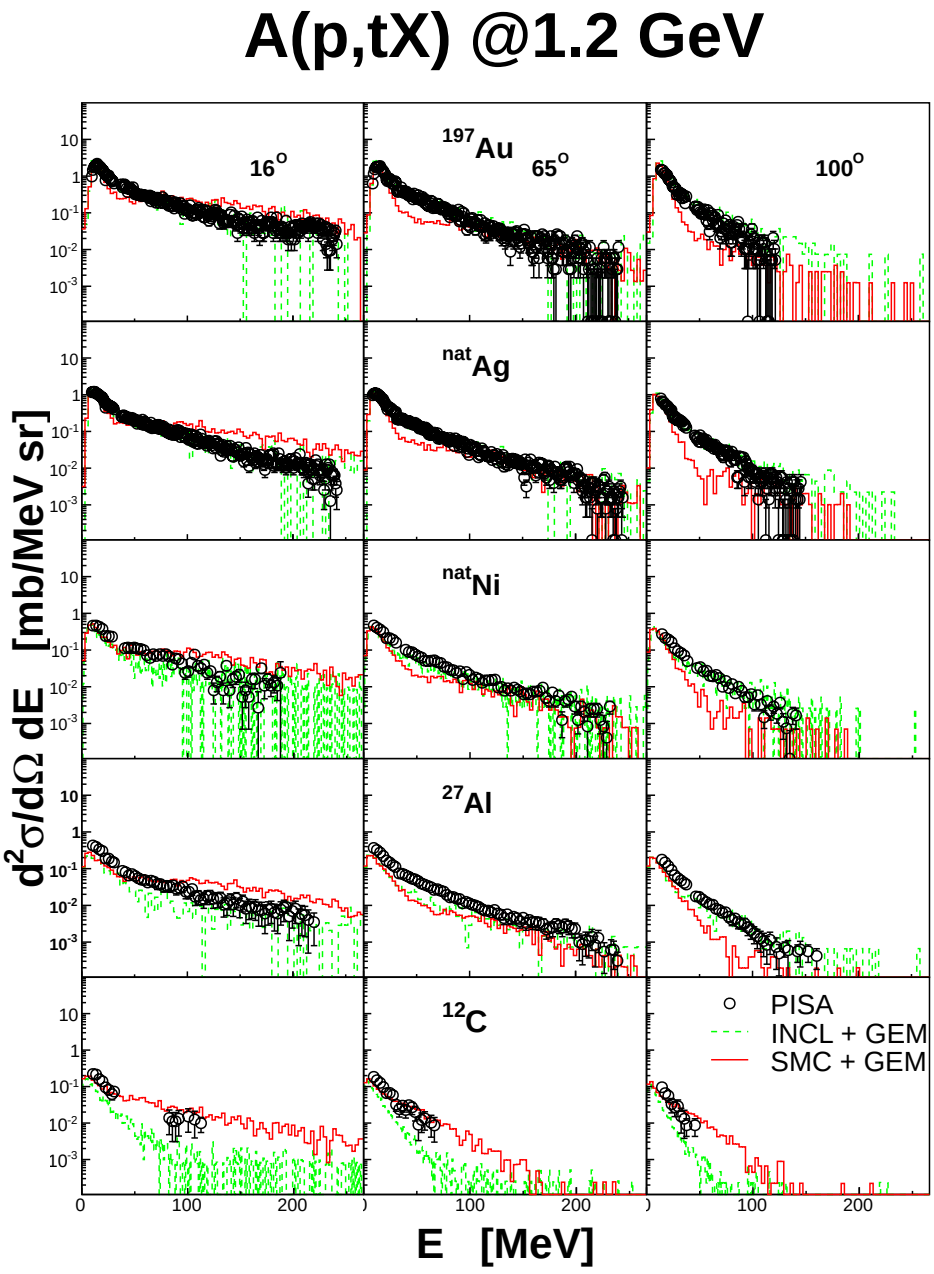

Figure 11.17: The same as in fig. 11.15 but for tritons.

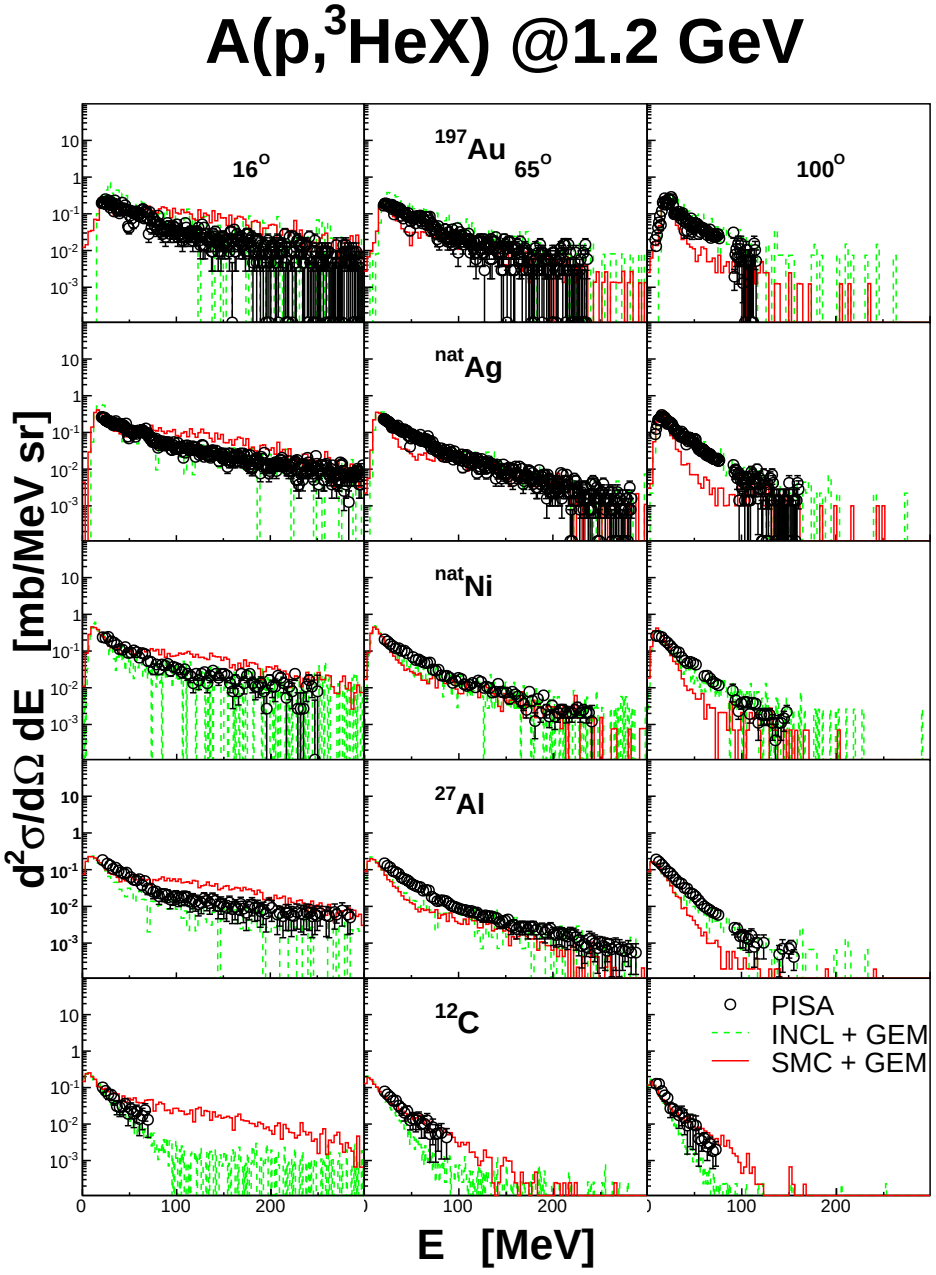

Figure 11.18: The same as in fig. 11.15 but for ^{3}He.

12 Acknowledgement

The PISA experiment, the data analysis and their interpretation were conducted over several years. The results are a consequence of harmonious collaboration of the group of skilful, diligent and assiduous persons.

The PISA Collaboration consists of many members. The list of members was subjected to several changes. There is no way here to indicate every member of PISA collaboration and express a gratitude for commitments and a specific contributions to the achievements of the collaborations. I am deeply indebted to **ALL** members of the PISA collaboration for their commitment to the project and for creation of a friendly atmosphere during the years of common work. I would like to emphasize my privilege to be a member of the PISA collaboration.

I hope that nobody of the PISA members will feel to be overlooked if instead of appreciate everybody separately the names of involved institutions will be given. They are: Research Center Jülich, Germany, Jagiellonian University, Kraków, Poland, Institute of Nuclear Physics PAN, Kraków, Poland, University of Silesia, Katowice, Poland, iThemba Labs, Kapstadt, South Africa, Messina University, Italy and Bonn University, Germany.

But the names of the leading persons cannot be avoided. They are those who made the PISA experiment possible and who, despite of numerous difficulties and adversities, kept to conduct the experiment until the whole scientific goals had been achieved. Among them are: Prof B. Kamys from Jagiellonian University, Prof. D. Filges from Research Center Jülich, Prof. L. Jarczyk from Jagiellonian University and the one who is already not among us - Prof. A. Budzanowski from Institute of Nuclear Physics PAN. They were also the leaders of the groups and institutions which gave the strongest conceptional, organizational, financial and personal contributions to the PISA collaboration.

Over the whole time of its existence the PISA collaboration was led and chaired by Prof. B. Kamys. I would like to express a special gratitude to him for his friendliness, helpfulness, understanding and an unusual patience. He always is ready to share his broad knowledge and deep understanding of nuclear physics with his collaborators which was always very beneficial for me.

I would like also warmly mention a continuous support and encouragement from my boss Prof. A. Szczurek in the past years when the works related to this dissertations were performed.

Among those who influenced the most my scientific life is Dr. H. Ohm from Research Center Jülich. I appreciate a lot his great friendliness, support and continues willingness to help.

A special acknowledgements are given to Prof Z. Rudy from Jagiellonian University and to Prof. A. Szczurek from Institute of Nuclear Physics PAN, who sacrificed their time for critical reading of this dissertation and have expressed their very valuable comments and suggestions.

Finally, a deep gratitude is expressed to my Family - wife Beata and children - Ludwika, Antonina and Jan. They have shown a great patience and understanding when during recent years I could not be available for them as much as it would be required. My children had to encounter also an additional inconvenience: when the work on this dissertation was being conducted our home computer, such suitable for gaming was frequently busy with the simulations of spallation processes.

References

[1] R. Barna, V. Bollini, A. Bubak, A. Budzanowski, D. D. Pasquale, D. Filges, S. Förtsch, F. Goldenbaum, A. Heczko, H. Hodde, A. Italiano, L. Jarczyk, B. Kamys, J. Kisiel, M. Kistryn, S. Kistryn, S. Kliczewski, A. Kowalczyk, P. Kulessa, H. Machner, A. Magiera, J. Majewski, W. Migdał, H. Ohm, N. Paul, B. Piskor-Ignatowicz, K. Pysz, Z. Rudy, H. Schaal, R. Siudak, E. Stephan, G. Steyn, R. Sworst, T. Thovhogi, M. Wojciechowski, and W. Zipper, "PISA - an experiment for fragment spectroscopy at the internal beam of COSY: application of an Axial Ionization Chamber," *Nuclear Instruments and Methods in Physics Research Section A: Accelerators, Spectrometers, Detectors and Associated Equipment*, vol. 519, no. 3, pp. 610–622, 2004.

[2] "ROOT - An object oriented data analysis framework."
https://root.cern.ch/.

[3] R. Brun and F. Rademakers, "ROOT - An object oriented data analysis framework," *Nuclear Instruments and Methods in Physics Research Section A: Accelerators, Spectrometers, Detectors and Associated Equipment*, vol. 389, no. 1–2, pp. 81–86, 1997. New Computing Techniques in Physics Research V.

[4] A. Bubak, *Emission of intermediate mass fragments in the p(1.9-GeV) + Ni-nat reaction.* PhD thesis. Silesia University, Katowice, 2004.

[5] V. Bollini, *Proton Induced Fragmentation of Gold Nuclei at Incident Energy of 2.5 GeV.* PhD thesis. Wuppertal University, 2004.

[6] A. Kowalczyk, *Proton induced spallation reactions in the energy range 0.1 - 10 GeV.* PhD thesis. Jagellonian University, Cracow, 2007.

[7] B. Piskor-Ignatowicz, *Energy Dependence of Proton Induced Fragmentation of Atomic Nuclei.* PhD thesis. Jagellonian University, Cracow, 2009.

[8] M. Fidelus, *Model Description of Proton Induced Fragmentation of Atomic Nuclei.* PhD thesis. Jagellonian University, Cracow, 2010.

[9] V. Bollini, A. Bubak, A. Budzanowski, J. Cugnon, D. Filges, F. Goldenbaum, A. Heczko, H. Hodde, L. Jarczyk, B. Kamys, M. Kistryn, S. Kistryn, S. Kliczewski, A. Kowalczyk, P. Kulessa, H. Machner, A. Magiera, W. Migdal, K. Nünighoff, N. Paul, B. Piskor-Ignatowicz, K. Pysz, Z. Rudy, R. Siudak, M. Wojciechowski, and E. Kozik, "Light charged particle and intermediate mass fragment cross-sections in GeV proton-induced reactions," *Nuclear Instruments and Methods in Physics Research Section A: Accelerators, Spectrometers, Detectors and Associated Equipment*, vol. 562, no. 2, pp. 733 – 736, 2006. Proceedings of the 7th International Conference on Accelerator Applications AccApp05 7th International Conference on Accelerator Applications.

[10] A. Bubak, A. Budzanowski, D. Filges, F. Goldenbaum, A. Heczko, H. Hodde, L. Jarczyk, B. Kamys, M. Kistryn, S. Kistryn, S. Kliczewski, A. Kowalczyk, E. Kozik, P. Kulessa, H. Machner, A. Magiera, W. Migdał, N. Paul, B. Piskor-Ignatowicz, M. Puchała, K. Pysz, Z. Rudy, R. Siudak, M. Wojciechowski, and P. Wüstner, "Non-equilibrium emission of

complex fragments from p+Au collisions at 2.5 GeV proton beam energy," *Phys. Rev. C*, vol. 76, p. 014618, Jul 2007.

[11] A. Budzanowski, M. Fidelus, D. Filges, F. Goldenbaum, H. Hodde, L. Jarczyk, B. Kamys, M. Kistryn, S. Kistryn, S. Kliczewski, A. Kowalczyk, E. Kozik, P. Kulessa, H. Machner, A. Magiera, B. Piskor-Ignatowicz, K. Pysz, Z. Rudy, R. Siudak, and M. Wojciechowski, "Competition of coalescence and "fireball" processes in nonequilibrium emission of light charged particles from p+Au collisions," *Phys. Rev. C*, vol. 78, p. 024603, Aug 2008.

[12] A. Budzanowski, M. Fidelus, D. Filges, F. Goldenbaum, H. Hodde, L. Jarczyk, B. Kamys, M. Kistryn, S. Kistryn, S. Kliczewski, A. Kowalczyk, E. Kozik, P. Kulessa, H. Machner, A. Magiera, B. Piskor-Ignatowicz, K. Pysz, Z. Rudy, R. Siudak, and M. Wojciechowski, "Variation of nonequilibrium processes in the p+Ni system with beam energy," *Phys. Rev. C*, vol. 80, p. 054604, Nov 2009.

[13] A. Budzanowski, M. Fidelus, D. Filges, F. Goldenbaum, H. Hodde, L. Jarczyk, B. Kamys, M. Kistryn, S. Kistryn, S. Kliczewski, A. Kowalczyk, E. Kozik, P. Kulessa, H. Machner, A. Magiera, B. Piskor-Ignatowicz, K. Pysz, Z. Rudy, R. Siudak, and M. Wojciechowski, "Comparison of nonequilibrium processes in p+Ni and p+Au collisions at GeV energies," *Phys. Rev. C*, vol. 82, p. 034605, Sep 2010.

[14] M. Fidelus, D. Filges, F. Goldenbaum, H. Hodde, A. Jany, L. Jarczyk, B. Kamys, M. Kistryn, S. Kistryn, S. Kliczewski, E. Kozik, P. Kulessa, H. Machner, A. Magiera, B. Piskor-Ignatowicz, K. Pysz, Z. Rudy, S. K. Sharma, R. Siudak, and M. Wojciechowski, "Sequential and simultaneous emission of particles from p + Al collisions at GeV energies," *Phys. Rev. C*, vol. 89, p. 054617, May 2014.

[15] K. Pysz, "Dynamic cluster contribution to the yield of light particles in the spallation process," *Phys. Rev. C*, vol. 91, p. 011602, Jan 2015.

[16] M. Naghdi, "Comparing some nucleon-nucleon potentials," *Phys.Part.Nucl.Lett.*, vol. 11, pp. 410–431, 2014.

[17] M. Naghdi, "Nucleon-nucleon interaction. A typical/concise review," *Phys.Part.Nucl.*, vol. 45, pp. 924–971, 2014.

[18] J. Haidenbauer, "The nucleon nucleon interaction," *Braz.J.Phys.*, vol. 34, pp. 845–849, 2004.

[19] H. Stöcker and W. Greiner, "High energy heavy ion collisions—probing the equation of state of highly excited hardronic matter," *Physics Reports*, vol. 137, no. 5–6, pp. 277–392, 1986.

[20] A. Dainese, "Review on heavy-ion physics." arXiv, hep-ph, 2010. CITATION = ARXIV:1012.4038.

[21] H. Reeves, W. A. Fowler, and F. Hoyle, "Galactic cosmic ray origin of Li, Be and B in stars," *Nature*, vol. 226, pp. 727–729, May 1970.

[22] M. Meneguzzi, J. Audouze, and H. Reeves, "The production of the elements Li, Be, B by galactic cosmic rays in space and its relation with stellar observations.," *Astronomy and Astrophysics*, vol. 15, pp. 337–359, 1971.

[23] T. P. Walker, V. E. Viola, and G. J. Mathews, "Astrophysical production rates for Li, Be, and B isotopes from energetic H(1) and He(4) reactions with HeCNO nuclei," *Astrophysical Journal*, vol. 299, pp. 745–751, Dec 1985.

[24] S. Read and V. V. Jr., "Excitation functions for A $\geq$ 6 fragments formed in 1H- and 4He-induced reactions on light nuclei," *Atomic Data and Nuclear Data Tables*, vol. 31, no. 3, pp. 359–397, 1984.

[25] E. Vangioni-Flam, M. Casse, and J. Audouze, "Lithium-beryllium-boron: origin and evolution," *Physics Reports*, vol. 333-334, no. 0, pp. 365–387, 2000.

[26] R. Ramaty, B. Kozlovsky, and R. Lingenfelter, "Cosmic rays, nuclear gamma rays and the origin of the light elements," *Physics Today*, vol. 51, no. 4, pp. 30–35, 1998.

[27] D. K. Duncan, D. L. Lambert, and M. Lemke, "The abundance of boron in three halo stars," *Astrophysical Journal*, vol. 401, pp. 584–595, dec 1992.

[28] R. Ramaty, B. Kozlovsky, R. E. Lingenfelter, and H. Reeves, "Light elements and cosmic rays in the early Galaxy," *Astrophysical Journal*, vol. 488, pp. 730–748, oct 1997.

[29] E. Vangioni-Flam and M. Casse, "Evolution of lithium-beryllium-boron and oxygen in the early Galaxy," *New Astronomy Reviews*, vol. 45, no. 8, pp. 583–586, 2001. Oxygen abundances in old stars.

[30] W. R. Webber, J. C. Kish, and D. A. Schrier, "Individual isotopic fragmentation cross sections of relativistic nuclei in hydrogen, helium, and carbon targets," *Phys. Rev. C*, vol. 41, pp. 547–565, Feb 1990.

[31] W. R. Webber, A. Soutoul, J. C. Kish, J. M. Rockstroh, Y. Cassagnou, R. Legrain, and O. Testard, "Measurement of charge changing and isotopic cross sections at $\sim$600 MeV/nucleon from the interactions of $\sim$30 separate beams of relativistic nuclei from ^{10}B to ^{55}Mn in a liquid hydrogen target," *Phys. Rev. C*, vol. 58, pp. 3539–3552, Dec 1998.

[32] S. G. Mashnik, "On Solar System and Cosmic Rays Nucleosynthesis and Spallation Processes," *ArXiv Astrophysics e-prints*, aug 2000.

[33] "A european roadmap for developing accelerator driven systems (ADS) for nuclear waste incineration," tech. rep., The European Technical Working Group on ADS, 2001. ISBN 88-8286-008-6.

[34] "Accelerator Driven Systems (ADS) and Fast Reactors (FR) in Advanced Nuclear Fuel Cycles." Nuclear Energy Agency - OECD, 2002.

[35] D. Vandeplassche and L. M. Romão, "Accelerator Driven Systems," in *Proceedings of IPAC2012 Conference, New Orleans, Louisiana, USA*, 2012.

[36] J. Meulders, A. Koning, and S. Leray, "HINDAS - High and Intermediate energy Nuclear Data for Accelerator-driven Systems. Detailed Final Report," tech. rep., 2005.

[37] U. Jahnke, C.-M. Herbach, D. Hilscher, V. Tishchenko, J. Galin, A. Letourneau, B. Lott, A. Péghaire, F. Goldenbaum, and L. Pienkowski, "A combination of two 4π detectors for neutrons and charged particles.: Part I. The Berlin neutron ball—a neutron multiplicity meter and a reaction detector," *Nuclear Instruments and Methods in Physics Research Section A: Accelerators, Spectrometers, Detectors and Associated Equipment*, vol. 508, no. 3, pp. 295–314, 2003.

[38] C.-M. Herbach, D. Hilscher, U. Jahnke, V. Tishchenko, W. Bohne, J. Galin, A. Letourneau, B. Lott, A. Péghaire, F. Goldenbaum, and L. Pienkowski, "A combination of two 4π-detectors for neutrons and charged particles.: Part II. The Berlin silicon ball {BSiB} for light- and heavy-ion detection," *Nuclear Instruments and Methods in Physics Research Section A: Accelerators, Spectrometers, Detectors and Associated Equipment*, vol. 508, no. 3, pp. 315–336, 2003.

[39] S. Leray, F. Borne, S. Crespin, J. Fréhaut, X. Ledoux, E. Martinez, Y. Patin, E. Petibon, P. Pras, A. Boudard, R. Legrain, Y. Terrien, F. Brochard, D. Drake, J. C. Duchazeaubeneix, J. M. Durand, S. I. Meigo, G. Milleret, D. M. Whittal, W. Wlazlo, D. Durand, C. Le Brun, F. R. Lecolley, J. F. Lecolley, F. Lefebvres, M. Louvel, C. Varignon, F. Hanappe, S. Ménard, L. Stuttge, and J. Thun, "Spallation neutron production by 0.8, 1.2, and 1.6 GeV protons on various targets," *Phys. Rev. C*, vol. 65, p. 044621, Apr 2002.

[40] D. Filges, S. Leray, Y. Yariv, A. Mengoni, A. Stanculescu, and G. Mank Joint ICTP-IAEA Advanced Workshop on Model Codes for Spallation Reactions, International Centre for Theoretical Physics, Trieste, Italy 4 - 8 February 2008
https://www-nds.iaea.org/publications/indc/indc-nds-0530/.

[41] IAEA Benchmark of Spallation Models - Experimental Data,
https://www-nds.iaea.org/spallations/spal_exp.html.

[42] R. Maier, "Cooler synchrotron COSY - Performance and perspectives," *Nuclear Instruments and Methods in Physics Research Section A: Accelerators, Spectrometers, Detectors and Associated Equipment*, vol. 390, no. 1-2, pp. 1–8, 1997.

[43] M. Enke, C.-M. Herbach, D. Hilscher, U. Jahnke, O. Schapiro, A. Letourneau, J. Galin, F. Goldenbaum, B. Lott, A. Péghaire, D. Filges, R.-D. Neef, K. Nünighoff, N. Paul, H. Schaal, G. Sterzenbach, A. Tietze, and L. Pienkowski, "Evolution of a spallation reaction: experiment and Monte Carlo simulation," *Nuclear Physics A*, vol. 657, no. 3, pp. 317–339, 1999.

[44] D. Hilscher, U. Jahnke, F. Goldenbaum, L. Pienkowski, J. Galin, and B. Lott, "Neutron production by hadron-induced spallation reactions in thin and thick Pb and U targets from 1 to 5 GeV," *Nuclear Instruments and Methods in Physics Research Section A: Accelerators, Spectrometers, Detectors and Associated Equipment*, vol. 414, no. 1, pp. 100–116, 1998.

[45] J. Galin and U. Jahnke, "Hot nuclei as viewed through 4π neutron multiplicity filters," *Journal of Physics G: Nuclear and Particle Physics*, vol. 20, no. 8, p. 1105, 1994.

[46] C.-M. Herbach, D. Hilscher, U. Jahnke, V. Tishchenko, J. Galin, A. Letourneau, A. Péghaire, D. Filges, F. Goldenbaum, L. Pienkowski, W. Schröder, and J. Tõke, "Charged-particle evaporation and pre-equilibrium emission in 1.2 GeV proton-induced spallation reactions," *Nuclear Physics A*, vol. 765, no. 3–4, pp. 426 – 463, 2006.

[47] A. Letourneau, A. Böhm, J. Galin, B. Lott, A. Péghaire, M. Enke, C.-M. Herbach, D. Hilscher, U. Jahnke, V. Tishchenko, D. Filges, F. Goldenbaum, R. Neef, K. Nünighoff, N. Paul, G. Sterzenbach, L. Pienkowski, J. Tõke, and U. Schröder, "Composite-particle emission in the reaction p+Au at 2.5 GeV," *Nuclear Physics A*, vol. 712, no. 1–2, pp. 133 – 166, 2002.

[48] L. Pienkowski, F. Goldenbaum, D. Hilscher, U. Jahnke, J. Galin, and B. Lott, "Neutron multiplicity distributions for 1.94 to 5 GeV/c proton-, antiproton-, pion-, kaon-, and

deuteron-induced spallation reactions on thin and thick targets," *Phys. Rev. C*, vol. 56, pp. 1909–1917, Oct 1997.

[49] B. E. Bonner, J. E. Simmons, C. R. Newsom, P. J. Riley, G. Glass, J. C. Hiebert, M. Jain, and L. C. Northcliffe, "Systematics of 0 degree neutron production by 800 MeV protons on targets with $27 \leq A \leq 238$," *Phys. Rev. C*, vol. 18, pp. 1418–1425, Sep 1978.

[50] F. Borne, S. Crespin, S. Leray, Y. Patin, M. Beau, A. Boudard, F. Boué, P. Bouyer, J. Boyard, F. Brochard, D. Drake, J. Duchazeaubeneix, J. Durand, J. Fréhaut, L. Kowalski, R. Legrain, J. Lochard, E. Martinez, S. Ménard, G. Milleret, E. Petibon, F. Plouin, Y. Terrien, J. Thun, M. Uematsu, S. Vuillier, and D. Whittal, "Spallation neutron spectra measurements Part I: Time-of-flight technique," *Nuclear Instruments and Methods in Physics Research Section A: Accelerators, Spectrometers, Detectors and Associated Equipment*, vol. 385, no. 2, pp. 339–344, 1997.

[51] E. Martinez, J. Thun, Y. Patin, S. Leray, M. Beau, A. Boudard, F. Boué, P. Bouyer, J. Boyard, F. Brochard, S. Crespin, D. Drake, J. Duchazeaubeneix, J. Durand, J. Fréhaut, L. Kowalski, R. Legrain, J. Lochard, S. Ménard, G. Milleret, E. Petibon, F. Plouin, Y. Terrien, M. Uematsu, S. Vuillier, and D. Whittal, "Spallation neutron spectra measurements Part II: Proton recoil spectrometer," *Nuclear Instruments and Methods in Physics Research Section A: Accelerators, Spectrometers, Detectors and Associated Equipment*, vol. 385, no. 2, pp. 345–353, 1997.

[52] D. Filges and F. Goldenbaum, *Handbook of Spallation Research, Theory, Experiments and Applications*. WILEY-VCH Verlag GmbH Co. KGaA.

[53] S. V. Förtsch, A. A. Cowley, J. J. Lawrie, D. M. Whittal, J. V. Pilcher, and F. D. Smit, "Continuum protons from ^{58}Ni(p , p ') at incident energies between 100 and 200 MeV," *Phys. Rev. C*, vol. 43, pp. 691–700, Feb 1991.

[54] A. Bubak, B. Kamys, M. Kistryn, and B. Piskor-Ignatowicz, "Parameterization of the total cross-section for (p,^{7}Be) reaction," *Nuclear Instruments and Methods in Physics Research Section B: Beam Interactions with Materials and Atoms*, vol. 226, no. 4, pp. 507–516, 2004.

[55] P. Napolitani, K.-H. Schmidt, A. S. Botvina, F. Rejmund, L. Tassan-Got, and C. Villagrasa, "High-resolution velocity measurements on fully identified light nuclides produced in ^{56}Fe+ hydrogen and ^{56}Fe + titanium systems," *Phys. Rev. C*, vol. 70, p. 054607, Nov 2004.

[56] R. Serber, "Nuclear reactions at high energies," *Phys. Rev.*, vol. 72, pp. 1114–1115, Dec 1947.

[57] V. F. Weisskopf and D. H. Ewing, "On the yield of nuclear reactions with heavy elements," *Phys. Rev.*, vol. 57, pp. 472–485, Mar 1940.

[58] W. Hauser and H. Feshbach, "The inelastic scattering of neutrons," *Phys. Rev.*, vol. 87, pp. 366–373, Jul 1952.

[59] R. Charity, K. Jing, D. Bowman, M. McMahan, G. Wozniak, L. Moretto, N. Colonna, G. Guarino, A. Pantaleo, L. Fiore, A. Gobbi, and K. Hildenbrand, "Sources of complex fragment emission in lanthanum-induced reactions at E/A = 14.7 and 18.0 MeV," *Nuclear Physics A*, vol. 511, no. 1, pp. 59 – 91, 1990.

[60] J.-J. Gaimard and K.-H. Schmidt, "A reexamination of the abrasion-ablation model for the description of the nuclear fragmentation reaction," *Nuclear Physics A*, vol. 531, no. 3–4, pp. 709 – 745, 1991.

[61] J. Benlliure, A. Grewe, M. de Jong, K.-H. Schmidt, and S. Zhdanov, "Calculated nuclide production yields in relativistic collisions of fissile nuclei," *Nuclear Physics A*, vol. 628, no. 3, pp. 458 – 478, 1998.

[62] A. Junghans, M. de Jong, H.-G. Clerc, A. Ignatyuk, G. Kudyaev, and K.-H. Schmidt, "Projectile-fragment yields as a probe for the collective enhancement in the nuclear level density," *Nuclear Physics A*, vol. 629, no. 3–4, pp. 635 – 655, 1998.

[63] S. Furihata, "Statistical analysis of light fragment production from medium energy proton-induced reactions," *Nuclear Instruments and Methods in Physics Research Section B: Beam Interactions with Materials and Atoms*, vol. 171, no. 3, pp. 251 – 258, 2000.

[64] S. Furihata and T. Nakamura , J. Nucl. Sci. Technol. Suppl. 2, 758 (2002).

[65] J. Bondorf, A. Botvina, A. Iljinov, I. Mishustin, and K. Sneppen, "Statistical multifragmentation of nuclei," *Physics Reports*, vol. 257, no. 3, pp. 133 – 221, 1995.

[66] H. H. Gutbrod, A. Sandoval, P. J. Johansen, A. M. Poskanzer, J. Gosset, W. G. Meyer, G. D. Westfall, and R. Stock, "Final-state interactions in the production of Hydrogen and Helium isotopes by relativistic heavy ions on Uranium," *Phys. Rev. Lett.*, vol. 37, pp. 667–670, Sep 1976.

[67] D. H. Boal, R. E. L. Green, R. G. Korteling, and M. Soroushian, "Tests of models for inclusive production of energetic light fragments at intermediate energies," *Phys. Rev. C*, vol. 23, pp. 2788–2790, Jun 1981.

[68] A. Boudard, J. Cugnon, S. Leray, and C. Volant, "A new model for production of fast light clusters inspallationreactions," *Nuclear Physics A*, vol. 740, no. 1–2, pp. 195 – 210, 2004.

[69] D. Wei, N. Wang, and L. Ou, "Mechanism of the production of light complex particles in nucleon-induced reactions," *Journal of Physics G: Nuclear and Particle Physics*, vol. 41, no. 3, p. 035104, 2014.

[70] A. Boudard, J. Cugnon, J.-C. David, S. Leray, and D. Mancusi, "New potentialities of the Liège intranuclear cascade model for reactions induced by nucleons and light charged particles," *Phys. Rev. C*, vol. 87, p. 014606, Jan 2013.

[71] J. Cugnon, T. Mizutani, and J. Vandermeulen, "Monte Carlo Calculation of Compression and Pion Multiplicity in Relativistic Central Heavy Ion Collisions," *Lett. Nuovo Cim.*, vol. 28, pp. 55–59, 1980.

[72] J. Cugnon, T. Mizutani, and J. Vandermeulen, "Equilibration in relativistic nuclear collisions. A Monte Carlo calculation," *Nuclear Physics A*, vol. 352, no. 3, pp. 505 – 534, 1981.

[73] J. Cugnon, J. Knoll, and J. Randrup, "Participant Intimacy - a Cluster Analysis of the Intranuclear Cascade," *Nucl.Phys.*, vol. A360, pp. 444–458, 1981.

[74] J. Cugnon, "Monte Carlo calculation of high-energy heavy-ion interactions," *Phys. Rev. C*, vol. 22, pp. 1885–1896, Nov 1980.

[75] J. Cugnon and S. Koonin, "Pion Spectra and the Geometry of Nuclear Collisions," *Nucl.Phys.*, vol. A355, pp. 477–504, 1981.

[76] J. Cugnon, "Nonequilibrium aspects in relativistic nuclear collisions," *Phys.Rev.*, vol. C23, pp. 2094–2099, 1981.

[77] J. Cugnon, J. Knoll, C. Riedel, and Y. Yariv, "Event by Event Emission Pattern Analysis of the Intranuclear Cascade," *Phys.Lett.*, vol. B109, pp. 167–170, 1982.

[78] J. Cugnon, "Intranuclear Cascade Model. A Review," *Nucl.Phys.*, vol. A387, pp. 191C–203C, 1982.

[79] J. Cugnon and J. Vandermeulen, "The $N\Delta \to NN$ Cross-Section From Detailed Balance," *Lett. Nuovo Cim.*, vol. 41, pp. 213–217, 1984.

[80] J. Molitoris, H. Stoecker, H. Gustafsson, J. Cugnon, and D. L'Hote, "Intranuclear Cascade Models Lack Dynamic Flow," *Phys.Rev.*, vol. C33, pp. 867–875, 1986.

[81] J. Cugnon, "Proton-nucleus interaction at high energy," *Nuclear Physics A*, vol. 462, no. 4, pp. 751 – 780, 1987.

[82] J. Cugnon and M. Lemaire, "Medium Effects in Pion Production," *Nucl.Phys.*, vol. A489, p. 781, 1988.

[83] J. Cugnon, D. L'Hote, and J. Vandermeulen, "Simple parametrization of cross-sections for nuclear transport studies up to the GeV range," *Nuclear Instruments and Methods in Physics Research Section B: Beam Interactions with Materials and Atoms*, vol. 111, no. 3–4, pp. 215 – 220, 1996.

[84] J. Cugnon, "Spallation reactions," 1996.

[85] J. Cugnon, S. Leray, E. Martinez, Y. Patin, and S. Vuillier, "New constraints on the Delta production cross-section," *Phys.Rev.*, vol. C56, pp. 2431–2439, 1997.

[86] J. Cugnon, C. Volant, and S. Vuillier, "Improved intranuclear cascade model for nucleon-nucleus interactions," *Nuclear Physics A*, vol. 620, no. 4, pp. 475 – 509, 1997.

[87] A. Boudard, J. Cugnon, S. Leray, and C. Volant, "Intranuclear cascade model for a comprehensive description of spallation reaction data," *Phys. Rev. C*, vol. 66, p. 044615, Oct 2002.

[88] S. Leray, A. Boudard, J. Cugnon, J. David, J. Ducret, *et al.*, "Validation of high-energy nuclear models: state-of-the-art and perspectives," *Nucl.Instrum.Meth.*, vol. A562, pp. 806–809, 2006.

[89] T. Aoust and J. Cugnon, "Pion physics in the Liège intranuclear cascade model," *Phys. Rev. C*, vol. 74, p. 064607, Dec 2006.

[90] S. Pedoux, J. Cugnon, A. Boudard, J. David, and S. Leray, "Extension of INCL4 between 2-GeV and 15-GeV," *Adv.Space Res.*, vol. 44, pp. 926–933, 2009.

[91] S. Leray, A. Boudard, J. Cugnon, J. David, A. Kelic-Heil, *et al.*, "Improved modelling of helium and tritium production for spallation targets," *Nucl.Instrum.Meth.*, vol. B268, pp. 581–586, 2010.

[92] D. Mancusi, A. Boudard, J. Cugnon, J.-C. David, P. Kaitaniemi, *et al.*, "Extension of the Liège intranuclear-cascade model to reactions induced by light nuclei," *Phys.Rev.*, vol. C90, no. 5, p. 054602, 2014.

[93] J. Cugnon, "A short introduction to spallation reactions," *Few Body Syst.*, vol. 53, pp. 143–149, 2012.

[94] H. D. Vries, C. D. Jager, and C. D. Vries, "Nuclear charge-density-distribution parameters from elastic electron scattering," *Atomic Data and Nuclear Data Tables*, vol. 36, no. 3, pp. 495 – 536, 1987.

[95] E. A. Uehling and G. E. Uhlenbeck, "Transport Phenomena in Einstein-Bose and Fermi-Dirac Gases. i," *Phys. Rev.*, vol. 43, pp. 552–561, Apr 1933.

[96] G. F. Bertsch, H. Kruse, and S. D. Gupta, "Boltzmann equation for heavy ion collisions," *Phys. Rev. C*, vol. 29, pp. 673–675, Feb 1984.

[97] G. Bertsch and S. D. Gupta, "A guide to microscopic models for intermediate energy heavy ion collisions," *Physics Reports*, vol. 160, no. 4, pp. 189 – 233, 1988.

[98] W. Cassing, V. Metag, U. Mosel, and K. Niita, "Production of energetic particles in heavy-ion collisions," *Physics Reports*, vol. 188, no. 6, pp. 363 – 449, 1990.

[99] Z. Rudy and A. Kowalczyk. Joint ICTP-IAEA advanced workshop on model codes for spallation reactions, in IAEA INDC (NDS)-0530, edited by D. Filges, et al., IAEA Publications, Vienna 2008, p. 53-64.

[100] K. Niita, W. Cassing, and U. Mosel, "Hard-photon production within a self-consistent transport approach to heavy-ion collisions," *Nuclear Physics A*, vol. 504, no. 2, pp. 391 – 412, 1989.

[101] J. Aichelin, ""quantum" molecular dynamics—a dynamical microscopic n-body approach to investigate fragment formation and the nuclear equation of state in heavy ion collisions," *Physics Reports*, vol. 202, no. 5–6, pp. 233 – 360, 1991.

[102] K. Niita, S. Chiba, T. Maruyama, T. Maruyama, H. Takada, T. Fukahori, Y. Nakahara, and A. Iwamoto, "Analysis of the (*N*,*xn'*) reactions by quantum molecular dynamics plus statistical decay model," *Phys. Rev. C*, vol. 52, pp. 2620–2635, Nov 1995.

[103] L. Ou, Y. Zhang, J. Tian, and Z. Li, "Analysis of intermediate energy proton-induced spallation reactions by an improved quantum molecular dynamics plus statistical decay model," *Journal of Physics G: Nuclear and Particle Physics*, vol. 34, no. 5, p. 827, 2007.

[104] J. Lukasik and Z. Majka, "Chimera microscopic approach to heavy ion collisions at intermediate energies," *Acta Physica Polonica B*, vol. 24, p. 1959, 1993.

[105] A. Gilbert and A. G. W. Cameron, "A composite nuclear-level density formula with shell corrections," *Canadian Journal of Physics*, vol. 43, no. 8, pp. 1446–1496, 1965.

[106] R. E. Prael and H. Liechtenstein. User Guide to LCS: The LAHET Code System, Los Alamos National Laboratory, (1989).

[107] R. Charity, M. McMahan, G. Wozniak, R. McDonald, L. Moretto, D. Sarantites, L. Sobotka, G. Guarino, A. Pantaleo, L. Fiore, A. Gobbi, and K. Hildenbrand, "Systematics of complex fragment emission in niobium-induced reactions," *Nuclear Physics A*, vol. 483, no. 2, pp. 371 – 405, 1988.

[108] L. G. Moretto, "Statistical emission of large fragments: A general theoretical approach," *Nuclear Physics A*, vol. 247, no. 2, pp. 211 – 230, 1975.

[109] A. J. Sierk, "Macroscopic model of rotating nuclei," *Phys. Rev. C*, vol. 33, pp. 2039–2053, Jun 1986.

[110] E. Fermi, "High energy nuclear events," *Progress of Theoretical Physics*, vol. 5, pp. 570–583, 1950.

[111] E. Gradsztajn, F. Yiou, R. Klapisch, and R. Bernas, "Intranuclear cascade and Fermi-model breakup calculations on the production of Li, Be, and B isotopes in ^{12}C by 156-MeV protons," *Phys. Rev. Lett.*, vol. 14, pp. 436–439, Mar 1965.

[112] G. Sauer, H. Chandra, and U. Mosel, "Thermal properties of nuclei," *Nuclear Physics A*, vol. 264, no. 2, pp. 221 – 243, 1976.

[113] M. Curtin, H. Toki, and D. Scott, "Liquid-gas phase instabilities in nuclear systems," *Physics Letters B*, vol. 123, no. 5, pp. 289 – 292, 1983.

[114] M. Kleine Berkenbusch, W. Bauer, K. Dillman, S. Pratt, L. Beaulieu, K. Kwiatkowski, T. Lefort, W.-c. Hsi, V. E. Viola, S. J. Yennello, R. G. Korteling, and H. Breuer, "Event-by-event analysis of proton-induced nuclear multifragmentation: Determination of the phase transition universality class in a system with extreme finite-size constraints," *Phys. Rev. Lett.*, vol. 88, p. 022701, Dec 2001.

[115] V. Viola, K. Kwiatkowski, L. Beaulieu, D. Bracken, H. Breuer, J. Brzychczyk, R. de Souza, D. Ginger, W.-C. Hsi, R. Korteling, T. Lefort, W. Lynch, K. Morley, R. Legrain, L. Pienkowski, E. Pollacco, E. Renshaw, A. Ruangma, M. Tsang, C. Volant, G. Wang, S. Yennello, and N. Yoder, "Light-ion-induced multifragmentation: The ISiS project," *Physics Reports*, vol. 434, no. 1–2, pp. 1 – 46, 2006.

[116] S. Avdeyev, V. Karnaukhov, L. Petrov, V. Rodionov, P. Rukoyatkin, V. Toneev, H. Oeschler, O. Bochkarev, L. Chulkov, E. Kuzmin, A. Budzanowski, W. Karcz, M. Janicki, E. Norbeck, A. Botvina, and K. Gudima, "Comparative study of multifragmentation of gold nuclei induced by relativistic protons, ^{4}He, and ^{12}C," *Nuclear Physics A*, vol. 709, no. 1–4, pp. 392 – 414, 2002.

[117] V. A. Karnaukhov, H. Oeschler, S. P. Avdeyev, E. V. Duginova, V. K. Rodionov, A. Budzanowski, W. Karcz, O. V. Bochkarev, E. A. Kuzmin, L. V. Chulkov, E. Norbeck, and A. S. Botvina, "Critical temperature for the nuclear liquid-gas phase transition," *Phys. Rev. C*, vol. 67, p. 011601, Jan 2003.

[118] S. D. Gupta, S. Mekjian, and M. Tsang, "Liquid-gas phase transition in nuclear multifragmentation," *Advances in the Physics of Particles and Nuclei*, vol. 26, pp. 89 – 166, 2002.

[119] B. D. Wilkins, S. B. Kaufman, E. P. Steinberg, J. A. Urbon, and D. J. Henderson, "Evidence for a new reaction mechanism in the bombardment of ^{238}U with 11.5-GeV protons," *Phys. Rev. Lett.*, vol. 43, pp. 1080–1083, Oct 1979.

[120] J. B. Cumming, R. J. Cross, J. Hudis, and A. M. Poskanzer, "Study of a fragmentation reaction by thin-target recoil techniques; production of ^{24}Na from Bismuth by 2.9-GeV protons," *Phys. Rev.*, vol. 134, pp. B167–B174, Apr 1964.

[121] K. Beg and N. T. Porile, "Energy dependence of the recoil properties of products from the interaction of ^{238}U with 0.45-11.5-GeV protons," *Phys. Rev. C*, vol. 3, pp. 1631–1645, Apr 1971.

[122] N. T. Porile, A. J. Bujak, D. D. Carmony, Y. H. Chung, L. J. Gutay, A. S. Hirsch, M. Mahi, G. L. Paderewski, T. C. Sangster, R. P. Scharenberg, and B. C. Stringfellow, "Approach to criticality in the fragmentation of xenon by 1 - 19 GeV protons," *Phys. Rev. C*, vol. 39, pp. 1914–1928, May 1989.

[123] D. R. Fortney and N. T. Porile, "Angular distributions of sc fragments from the interaction of ^{238}U with 0.8-400 GeV protons," *Phys. Rev. C*, vol. 21, pp. 2511–2518, Jun 1980.

[124] S. Bohrmann, J. Hüfner, and M. Nemes, "Cleavage: A high-energy proton can split a nucleus into pieces," *Physics Letters B*, vol. 120, no. 1–3, pp. 59 – 62, 1983.

[125] J. Hüfner and H. M. Sommermann, "Enhanced backward emission of heavy fragments in high-energy proton-nucleus collisions," *Phys. Rev. C*, vol. 27, pp. 2090–2095, May 1983.

[126] G. D. Westfall, J. Gosset, P. J. Johansen, A. M. Poskanzer, W. G. Meyer, H. H. Gutbrod, A. Sandoval, and R. Stock, "Nuclear fireball model for proton inclusive spectra from relativistic heavy-ion collisions," *Phys. Rev. Lett.*, vol. 37, pp. 1202–1205, Nov 1976.

[127] J. I. Kapusta, "Particle production in the nuclear fireball model," *Phys. Rev. C*, vol. 16, pp. 1493–1498, Oct 1977.

[128] W. D. Myers, "A model for high-energy heavy-ion collisions," *Nuclear Physics A*, vol. 296, no. 1, pp. 177 – 188, 1978.

[129] J. Gosset, J. I. Kapusta, and G. D. Westfall, "Calculations with the nuclear firestreak model," *Phys. Rev. C*, vol. 18, pp. 844–855, Aug 1978.

[130] G. D. Westfall, R. G. Sextro, A. M. Poskanzer, A. M. Zebelman, G. W. Butler, and E. K. Hyde, "Energy spectra of nuclear fragments produced by high energy protons," *Phys. Rev. C*, vol. 17, pp. 1368–1381, Apr 1978.

[131] T. Kin, F. Saiho, S. Hohara, K. Ikeda, K. Ichikawa, Y. Yamashita, M. Imamura, G. Wakabayashi, N. Ikeda, Y. Uozumi, M. Matoba, M. Nakano, and N. Koori, "Proton production cross sections for reactions by 300- and 392-MeV protons on carbon, aluminum, and niobium," *Phys. Rev. C*, vol. 72, p. 014606, Jul 2005.

[132] J. R. Letaw, R. Silberberg, and C. H. Tsao, ""proton-nucleus total inelastic cross sections-an empirical formula for E greater than 10 MeV," *Astrophys. J. Suppl. Ser.*, vol. 51, pp. 271–276, 1983.

[133] H. P. Wellisch and D. Axen, "Total reaction cross section calculations in proton-nucleus scattering," *Phys. Rev. C*, vol. 54, pp. 1329–1332, Sep 1996.

[134] L. Sihver, C. H. Tsao, R. Silberberg, T. Kanai, and A. F. Barghouty, "Total reaction and partial cross section calculations in proton-nucleus ($Z_t \leq 26$) and nucleus-nucleus reactions (Z_p and $Z_t \leq 26$)," *Phys. Rev. C*, vol. 47, pp. 1225–1236, Mar 1993.

[135] S. Kox, A. Gamp, C. Perrin, J. Arvieux, R. Bertholet, J. F. Bruandet, M. Buenerd, R. Cherkaoui, A. J. Cole, Y. El-Masri, N. Longequeue, J. Menet, F. Merchez, and J. B. Viano, "Trends of total reaction cross sections for heavy ion collisions in the intermediate energy range," *Phys. Rev. C*, vol. 35, pp. 1678–1691, May 1987.

[136] R. Tripathi, F. A. Cucinotta, and J. W. Wilson, "Accurate universal parameterization of absorption cross sections," *Nuclear Instruments and Methods in Physics Research Section B: Beam Interactions with Materials and Atoms*, vol. 117, no. 4, pp. 347 – 349, 1996.

[137] R. Tripathi, J. W. Wilson, and F. A. Cucinotta, "Nuclear absorption cross sections using medium modified nucleon–nucleon amplitudes," *Nuclear Instruments and Methods in Physics Research Section B: Beam Interactions with Materials and Atoms*, vol. 145, no. 3, pp. 277 – 282, 1998.

[138] R. Tripathi, F. Cucinotta, and J. Wilson, "Medium modified nucleon–nucleon cross sections in a nucleus," *Nuclear Instruments and Methods in Physics Research Section B: Beam Interactions with Materials and Atoms*, vol. 152, no. 4, pp. 425 – 431, 1999.

[139] D. R. F. Cochran, P. N. Dean, P. A. M. Gram, E. A. Knapp, E. R. Martin, D. E. Nagle, R. B. Perkins, W. J. Shlaer, H. A. Thiessen, and E. D. Theriot, "Production of charged pions by 730-MeV protons from hydrogen and selected nuclei," *Phys. Rev. D*, vol. 6, pp. 3085–3116, Dec 1972.

[140] J.-C. David, D. Filges, F. Gallmeier, M. Khandaker, A. Konobeyev, S. Leray, G. Mank, A. Mengoni, R. Michel, N. Otuka, and Y. Yariv, "Benchmark of spallation models," *Progress in Nuclear Science and Technology*, vol. 2, pp. 942–947, 2011.

[141] A. Magiera. "ROZPAD" A computer code for Fermi breakup simulation. Jagellonian Univeristy Cracow, Poland.

[142] J. B. Natowitz, R. Wada, K. Hagel, T. Keutgen, M. Murray, A. Makeev, L. Qin, P. Smith, and C. Hamilton, "Caloric curves and critical behavior in nuclei," *Phys. Rev. C*, vol. 65, p. 034618, Mar 2002.

[143] D. J. Fields, W. G. Lynch, T. K. Nayak, M. B. Tsang, C. B. Chitwood, C. K. Gelbke, R. Morse, J. Wilczynski, T. C. Awes, R. L. Ferguson, F. Plasil, F. E. Obenshain, and G. R. Young, "Coincidence measurements of intermediate mass fragments produced in ^{32}S induced reactions on Ag at E/A=22.5 MeV," *Phys. Rev. C*, vol. 34, pp. 536–551, Aug 1986.

[144] Z. Sosin and J. Kallunkathariyil, "Semi-classical, microscopic approach to the liquid drop model — a possible way of the description of heavy ion reactions," *Acta Physica Polonica B*, vol. 45, no. 4, pp. 925–946, 2014.

[145] G. Duda, A. Kemper, and P. Gondolo, "Model-independent form factors for spin-independent neutralino–nucleon scattering from elastic electron scattering data," *Journal of Cosmology and Astroparticle Physics*, vol. 2007, no. 04, p. 012, 2007.

[146] K. Olive *et al.*, "Review of Particle Physics," *Chin.Phys.*, vol. C38, p. 090001, 2014.

[147] K. Wildermuth and T. Kanellopoulos, "The "cluster model" of the atomic nuclei," *Nuclear Physics*, vol. 7, no. 0, pp. 150 – 162, 1958.

[148] H. Horiuchi, "Present status of nuclear cluster physics (theory)," *Journal of Physics: Conference Series*, vol. 569, no. 1, p. 012001, 2014.

[149] H. Akimune, M. Fujiwara, J. Gibelin, M. N. Harakeh, L. Achouri, S. Bagchi, B. Bastin, K. Boretzky, H. Bouzomita, L. Caceres, S. Damoy, F. Delaunay, B. Fernández-Domínguez, M. Caamano, U. Garg, G. F. Grinyer, N. Kalantar-Nayestanaki, O. Kamalou, E. Khan, A. Krasznahorkay, G. Lhoutellier, S. Lukyanov, K. Mazurek, M. Najafi, J. Pancin, Y. Penionzkhevich, L. Perrot, R. Raabe, C. E. Rigollet, T. Roger, S. Sambi, H. Savajols, M. Senoville, C. Stodel, L. Suen, J. C. Thomas, J. van de Walle, and M. Vandebrouck, "Alpha cluster structure in ^{56}Ni," *Journal of Physics: Conference Series*, vol. 436, no. 1, p. 012010, 2013.

[150] K. Morawetz, P. Lipavský, V. Špička, and N.-H. Kwong, "Duration and nonlocality of a nucleon-nucleon collision," *Phys. Rev. C*, vol. 59, pp. 3052–3059, Jun 1999.

[151] K. Morawetz, V. Špička, P. Lipavský, G. Kortemeyer, C. Kuhrts, and R. Nebauer, "Virial corrections to simulations of heavy ion reactions," *Phys. Rev. Lett.*, vol. 82, pp. 3767–3770, May 1999.

13 Glossary of abbreviations used in the monograph

A

ADS - Accelerator Driven Systems;

ARC - Adiabatic Resonance Crossing;

B

BCD - Bragg Curve Detector;

BNB - Berlin Neutron Ball - a 4π acceptance neutron detector;

BSiB- Berlin Silicon Ball - a 4π acceptance charged particle detector;

BUU - Boltzmann-Uehling-Uhlenbeck transport equations;

C

CEA - Research Center in Saclay, France;

CERN - European Organization for Nuclear Research;

CM - Center of Mass reference system;

CNO - Carbon, Nitrogen, Oxygen - group of isotopes;

COSY - COller SYnchrotron - an accelerator in Research Center Jülich (Germany);

D

DCNM - Dynamical Clustering in Nuclear Medium - an hypothetical intranuclear process postulated in this dissertation

E

ESS - European Spallation Source;

G

GCR - Galactic Cosmic Rays;

GEM, GEM2 - Generalized Evaporation Model;

GEMINI - model of statistical emission from excited nuclear system;

H

HSD - Hadron String Dynamics model;

I

IAEA - International Atomic Energy Agency;

IMF - Intermediate Mass Fragments - spallation products of $Z > 2$ and $A < A_{Target}/3$;

INCL - Intranuclear Cascade Liege - model of nuclear cascade;

ISM - Interstellar Medium;

L

LAB - Laboratory reference system;

LAHET - Los Alamos High Energy Transport code system;

LCP - Light Charged Partices - spallation products of $Z \leq 2$;

LEAR - accelerator in CERN;

LiBeB - Lithium, Beryllium, Boron - group of isotopes;

M

MCP - Micro Channel Plate;

N

NESSI - scientific collaboration and name of spallation experiment;

NN - Nucleon-Nucleon (potential, interaction);

P

PISA - Proton Induced SpAllation - scientific collaboration and name of spallation experiment;

Q

QMD - Quantum Molecular Dynamics;

S

SMC++ - Spallation Model with Cascade++;

SMM - Statistical Multifragmentation Model;

SATURNE - accelerator in CEA Research Center;

T

TOF - Time Of Flight - an experimental technique;

U

UHV - Ultra High Vacuum;